Characterisation of a newly identified family of lipid transfer proteins at membrane contact sites

Alberto Gatta

This thesis is submitted to the University College London
for the Degree of Doctor of Philosophy

First supervisor: Dr. Tim Levine
Second supervisor: Prof. Clare Futter

September 2016

UCL Institute of Ophthalmology
Department of Cell Biology
11-43 Bath Street
London
EC1V 9EL

DECLARATION

I, Alberto Gatta, confirm that the work presented in this thesis is my own. Where information has been derived from other sources, I confirm that this has been indicated.

London, September 2016

ABSTRACT

Non-vesicular intracellular lipid traffic is mediated by lipid transfer proteins (LTPs), which contain domains with an internal cavity that can solubilise and transfer lipids. One of the most widespread LTP folds is the Steroidogenic Acute Regulatory Transfer (StART) domain, which forms a hydrophobic pocket, and appears in proteins with different localisations and lipid specificities. The aim of this study was to characterise a new StART-like domain family, which we identified by a bioinformatics approach. I studied aspects of the localisations, functions and structural properties of six StART-like proteins in *S. cerevisiae*. The yeast StART-like proteins were endoplasmic reticulum (ER)-integral membrane proteins with transmembrane domains, and they localised at membrane contact sites: Lam1p/Lam3p, and Lam2p/Lam4p at junctions between ER and plasma membrane (PM); Lam5p/Lam6p at junctions between the ER and the vacuolar membrane, at nucleus-vacuole junction (NVJ) and at ER-mitochondria contacts. To study their functions, I purified the second StART-like domain of Lam4p, and I identified sterol as its lipid ligand from *in vitro* binding assays and in a spectroscopy approach with fluorescent ergosterol. We named the whole family LAM for Lipid transfer proteins Anchored at Membrane contact sites. The sterol binding property of the domains was related to a phenotype shared by LAM1, LAM2 and LAM3 delete strains, which showed an increased sensitivity to the sterol-sequestering polyene antifungal drug Amphotericin B (AmB). The two most sensitive strains (*lam1*Δ and *lam3*Δ), displayed low sphingolipid levels, which is as yet unexplained. All AmB phenotypes were rescued by StART-like domains from the human LAMa, Lam2/4p and Lam5/6p, suggesting that these domains bind sterol. Simultaneous deletion of LAM1, LAM2, and LAM3 significantly reduced the extent of cortical ER-PM contacts, implying that they create the structure of the particularly punctate contact site they target. Finally, I started structural analysis of Lam4S2 to study the mechanism of sterol binding and to confirm our structural model.

ACKNOWLEDGEMENTS

Firstly, I would like to thank Tim Levine for accepting me in his laboratory to work on such an interesting project. Tim has ideated the project, wisely supervised all of its phases, and thought me so much along the way. He has supported me every time I needed it from the very beginning of my PhD to the puzzling choices about my future in research. The originality and brightness of his scientific ideas, and the thoughtful logic behind the strong opinions he has about everything, were really inspiring and will not be forgotten.

Second, I would like to thank Louise Wong, working at her side, at the bench and in the office, was a real pleasure, and her presence was an endless reassurance against the difficulties of the lab work and the perfect companion for the achievements. Every time the royal “we” appears in this thesis, it is usually me, Tim and Louise thinking together, too often with Tim annoyingly ahead of us. Thanks to the other past and present members of the Levine lab, especially Rachel and Sarah, for bearing with me and for sharing benches, pipettes, plates and all sort of lab consumables.

Huge parts of this work would have not been possible without the substantial help and expertise of key people. Shamshad Cockcroft (UCL) and her postdoc Tim Ashlin, for teaching me all the biochemistry tricks around the radiolabelled lipid binding assays. Howard Riezman and Isabelle Riezman (University of Geneva) for the lipidomics. Matt Hayes (UCL) for electron microscopy. Anant Menon (Weill Cornell Medical College, New York) and his lab for the successive and, sometime, frustrating collaboration on this project. Thanks to all the people that helped me to plan, perform and analyse the NMR structural experiments: Anastasia Zhuravleva (University of Leeds); Steve Matthews and Andrea Sauerwein (Imperial College London). Thanks to all the investigators that sent us strains and plasmids, and sorry in advance if we lost them and we will have to ask for them again.

I would like to thank the European Commission for funding this project through the Marie Curie Initial Training Network “Sphingonet”, cleverly coordinated by Joost Holthuis (University of Osnabrück, Germany). Gathering together with all the young (and less young) scientists in the network for workshops and meetings was very helpful and a lot of fun. I am sure that collaborations and friendships will carry on in the future as well.

I still cannot believe how lucky I was to have met such wonderful people, all together in the same office. Thanks to all the members of the Futter/Levine/Moss office for all the times we spent together in the institute and, above all, outside.

Thanks to all the other friends in Italy, in the UK and all over the world for an infinite number of reasons. Knowing that there is always someone almost everywhere who is ready to share some time with you for drinks, laughs, tears, music, and holidays, is invaluable.

Thanks to Giulia, for moving with me to London for this adventure, for trying at her best to ignore my OCD, for sharing beautiful moments and for taking care of me whenever I needed. It sounds cheesy, but all this would have not been possible without you.

Finally, thanks to my parents because I know that their support will never fade.

Alberto Gatta

London, September 2016

TABLE OF CONTENTS

LIST OF FIGURES

LIST OF TABLES

LIST OF APPENDICES

LIST OF ABBREVIATIONS

1D, one-dimensional
2D, two-dimensional
25-HC, 25-hydroxycholesterol
3D, three-dimensional
aa, amino acid
ABC, ATP-binding cassette
ACAT, Acetyl-Coenzyme A acetyltransferase
AEBSF, 4-(2-aminoethyl) benzenesulfonyl fluoride hydrochloride
ALPS, Amphipathic lipid packing sensor motifs
AmB, Amphotericin B
AMP, Adenosine MonoPhosphate
ATG, AuTophaGy related
ATP, Adenosine triphosphate
BAR, Bin-Amphiphysin-Rvs domain
bp, base pair
BfA, Brefeldin A
BLAST, Basic Local Alignment Search Tool
BSA, Bovine Serum Albumin
Ca^{2+}, Calcium
CD, Cyclodextrin
CDP-, cytidine-diphosphate-;
CE, cholesterol esters
CEPT, Cho/Eth-phosphotransferase
Cer, ceramide
cER, cortical ER
CerS, ceramide synthase
CERT, Ceramide transfer protein
CFU, colony forming unit
Cho, choline
CL, Cardiolipin
CLL, Chronic Lymphocytic Leukaemia
CLS, cardiolipin synthase
CMV, cytomegalovirus
CoA, coenzyme A
COPI, Coat protein complex I
CPT, choline-phosphotransferase
CRD1, cardiolipin synthase-1
CTCF, corrected total cell fluorescence
DAG, diacylglycerol
DesK, Des Kinase
DGAT, diglyceride acyltransferase
DHC, dehydroceramide
DHPR, dihydropyridine receptor
DHS, dehydrosphingosine, sphinganine
Dm, *Drosphila melanogaster*
DNA, deoxyribonucleic Acid
DSS, 4,4-dimethyl-4-silapentane-1-sulfonic acid
DTT, Dithiothreitol
E-Syt, extended synaptotagmin
EDTA, Ethylenediaminetetraacetic acid
EE, Early Endosome
EGFP, Enhanced Green Fluorescent Protein
ER, Endoplasmic Reticulum
ERES, ER Exit Sites

ERMES, ER-mitochondria encounter structure

FA, fatty acid

FAS, FA synthase

FBS, foetal bovine serum

FFAT, two phenylalanines (FF) in an acid tract

FID, free induction decay

FL, full length

FRET, Förster Resonance Energy Transfer

FT, Fourier transform

FYVE, Fab1, YOTB, Vac1 and EEA1 zinc finger domain

GAL, galactose

GBF1, Golgi BfA-resistant GEF 1

GCS, GlcCer synthase

GDP-Man, guanosine diphosphate mannose

GEF, Guanine nucleotide exchange factor

GFP, Green Fluorescent Protein

GlcCer, glucosylceramide

GRAM, Gucosyltransferases, Rab-like GTPase activators and Myotubularins domain

GRASP, GRIP-associated proteins

GSL, glycosphingolipid

GTPase, guanosine triphosphatase

GWAS, genome-wide association study

h, hour

H_2DCF-DA, 2',7'-dichloro-dihydrofluorescein diacetate

HMG-, hydroxymethylglutaryl-

HMGCR, 3-hydroxy-3-methylglutaryl-CoA reductase

HMGCS, HMG-CoA synthase

HMM, hidden Markov model

HOPS, homotypic fusion and protein sorting complex

HPLC, High Pressure Liquid Chromatography

Hs, *Homo sapiens*

HSQC, Heteronuclear single quantum coherence spectroscopy

HT, high throughput

Hz, Hertz

IB, inclusion body

ILV, Isoleucine Leucine Valine

IMM, Inner mitochondrial membrane

Ins, inositol

IP_3, Inositol trisphosphate

IPC, inositolphosphorylceramide

KO, knock-out

LAM, Lipid Transfer Protein Anchored at Membrane Contact Site

LCB, Long Chain Base

LD, Lipid Droplet

LDL, Low Density Lipoprotein

LE/LY, Late Endosome / Lysosome

LPMC, lysosome-peroxosime membrane contacts

LTC, Lipid Transfer at Contact sites

LTP, Lipid Transfer Protein

m, minute

M_0, magnetic field

MβCD, Methyl-β-cyclodextrin

MCS, Membrane Contact Site

Mdm, Mitochondrial Distribution and Morphology
MDR, Multidrug resistance
MECA, Mitochondria ER cortex anchor
MICOS, Mitochondria contact sites
MIPC, mannosyl-inositolphosphorylceramide
mito, mitochondrion
MLN64, Metastatic lymph node 64 protein
mol%, molar fraction
MORN, Membrane Occupation and Recognition Nexus motif
MS, Mass Spectrometry
MSA, Multiple Sequence Alignment
MSP domain, Major sperm protein domain
MTMR, Myotubularin-Related protein
MW, Molecular Weight
MβCD, Methyl-β-cyclodextrin
NAC, *N*-acetylcysteine
NE, Nuclear Envelope
Ni-NTA, Nickel Nitrilotriacetic Acid
Ni, Nickel
NMR, Nuclear Magnetic Resonance
NPC, Niemann-Pick disease type C
NSF, N-ethylmaleimide sensitive fusion protein
NVJ, Nucleus-vacuole Junction
OMM, Outer mitochondrial membrane
ORAI1, Ca^{2+} release-activated Ca^{2+} channel protein 1
ORD, OSBP-related domain
ORF, Open reading frame
ORP, OSBP-related protein
OSBP, Oxysterol binding protein
Osh, OSBP homologue (yeast)
PA, Phosphatidic acid
PAGE, Polyacrylamide gel electrophoresis
PC, Phosphatidylcholine
PCD, Programmed cell death
PCR, Polymerase chain reaction
PCTP, Phosphatidylcholine Transfer Protein
PDB, Protein Data Bank
PDH, Pyruvate dehydrogenase complex
PE, Phosphatidylethanolamine
PERMIT, Peroxisomes – Mitochondria contact sites
PFO, Perfringolysin O
PG, phosphatidylglycerol
PGP, phosphatidylglycerolphosphate
PH, Pleckstrin Homology
PHC, phytoceramide
PI, Phosphatidylinositol
$PI(3,4,5)P_3$, phosphatidylinositol-(3,4,5)-trisphosphate
$PI(3,5)P_2$, phosphatidylinositol-(3,5)-bisphosphate
$PI(4,5)P_2$, phosphatidylinositol-(4,5)-bisphosphate
PI3P, phosphatidylinositol-3-phosphate
PI4P, phosphatidylinositol-4-phosphate
PIP_2, phosphatidylinositol-bisphosphate

PIPES, piperazine-N,N'-bis(2-ethanesulfonic acid)
PIS, PI synthase
PL, Phospholipid
PLC, Phospholipase C
Plin5, Perilipin 5
PM, Plasma membrane
ppm, part per million
PS, Phosphatidylserine
PSD, PS decarboxylase
PSI-BLAST, Position-specific iterated BLAST
p^{SS}, probability of shared structure
PSSM, position-specific scoring matrix
Rab, Ras-like protein in brain
RdgB, Retinal degeneration B
RF, Radio frequency
RFP, Red Fluorescent Protein
RND, resistance-nodulation-division
ROS, Reactive Oxygen Species
rpm, revolution per minute
RPMI, Roswell Park Memorial Institute medium
RT, Room Temperature
RyR, Ryanodine receptor
s, second
S1P, Sphingosine-1-phosphate
Sc, *Saccharomyces cerevisiae*
SCAP, SREBP cleavage-activating protein
SDS, Sodium Dodecyl Sulphate
SE, Sterol esters
SEC, Secretory protein
SERCA, Sarco/endoplasmic reticulum Ca^{2+} ATPase
Sip3, SNF1-Interacting Protein-3
SL, Sphingolipid
SLO, Streptolysin O
SM, Sphingomyelin
SMP, Synaptotagmin-like-mitochondrial-lipid binding protein domain
SMS, Sphingomyelin synthase
SNAP, Soluble NSF attachment protein
SNARE, SNAP receptor
SNF, Sucrose Non Fermenting
SOCE, Store operated Ca^{2+} entry
Sph, Sphingosine
SPT, serine palmitoyltransferase
SR, Sarcoplasmic reticulum
SREBP2, Sterol regulatory element-binding protein 2
SRPBCC, START/RHOαC/PITP/Bet_v1/CoxG/CalC ligand-binding domain superfamily
Sso1, Suppressor of Sec One
StAR, Steroidogenic Acute Regulatory protein
StARD, StAR-related Lipid Transfer Domain protein
StART, StAR-Related Lipid Transfer domain
STIM1, Stromal interaction molecule 1
STP, Sterol transfer protein
SUMO, Small Ubiquitin-like Modifier
Syt, Synaptotagmin
T-tubule, Transverse tubule
TAG, Triacylglycerol
Tcb1-3, Tricalbin1-3

TEV, Tobacco etch virus

TGN, trans-Golgi network

TKO, Triple knock-out

TLC, Thin Layer Chromatography

TMD, Transmembrane domain

TMH, Transmembrane helix

Tom, Translocase of the Outer Membrane

TORC, Target of Rapamycin Complex

TROSY, Transverse relaxation-optimised spectroscopy

TULIP, Tubular lipid-binding protein

UPR, Unfolded protein response

UTR, Untranslated region

VAMP, Vesicle associated membrane protein

VancE, Vacuolar non cytoplasmic ER

VAP, VAMP-associated protein

vCLAMP, vacuole and mitochondria patch

VAD, Vascular-Associated Death protein 1

Vps, Vacuolar Protein Sorting

WT, Wild type

YPD, Yeast peptone dextrose

Ypt, Yeast protein two

Ysp, Yeast suicide protei

Chapter 1

Introduction

1. INTRODUCTION

Membrane trafficking is a vital process for cell homeostasis. Eukaryotic cells are compartmentalised in different membrane-enclosed organelles, each of them characterised by specific location, resident proteins, lipid composition and overall function. To maintain this equilibrium, in parallel to protein trafficking, lipids must travel to maintain the final lipid composition of membranes, which is different and highly specific for each organelle. The endoplasmic reticulum (ER), where the majority of lipid molecules are synthesised, is the source from which the different species need to travel to their final destination. This intracellular movement is mediated by vesicular or non-vesicular pathways, and the balance between these two mechanisms is important for membrane composition and signalling. Strong evidence of the existence of non-vesicular lipid traffic were published in seminal works in the 1980s (Sleight and Pagano, 1983; Kaplan and Simoni, 1985a; Urbani and Simoni, 1990), and their importance for cellular lipid homeostasis has recently come back in the spotlight (Levine, 2004; Holthuis and Menon, 2014).

Non-vesicular traffic is mediated by lipid transfer proteins (LTPs), which are conserved throughout eukaryotes (with some families also dating back to prokaryotes) and are defined as domains with an internal cavity that can solubilise and transfer lipids *in vitro*. Based on the presence of distinct structural folds, lipid transfer domains can be classified into one of 15 families (Table 1.1, pag. 50). The common feature of all the folds is the presence of an internal cavity that evolved with the capacity to accommodate a hydrophobic molecule shielding it from the aqueous environment of the cytosol and often possessing a flexible component functioning as a lid. *In vitro* their exchange mechanisms can be divided into three steps: (i) collection of a lipid from a donor membrane, (ii) shielding of the molecule from the aqueous environment, and (iii) release to the donor membrane (Voelker, 2009; Holthuis and Levine, 2005; Holthuis and Menon, 2014; Chiapparino et al., 2015).

In this introduction I will start by discussing important aspects of lipid homeostasis and why intracellular traffic must be a highly regulated process. I will describe the strongest evidence in favour of non-vesicular lipid traffic mechanisms and I will emphasise how proteins with lipid transfer domains are responsible for these movements by preferentially targeting Membrane Contact Sites (MCS), tethered by specialised proteins.

Regarding MCSs, I will highlight the central role of the ER for these junctions, with particular interest in the known proteins acting at ER-Plasma Membrane (PM) contacts, including the LTPs operating lipid counter transport. I will briefly consider how virtually every organelle could come to close contact with each other by reporting two examples of ER-mediated three way contacts.

Next, I will describe other aspects of LTPs, such as their lipid specificities, and their implications in cellular defence mechanisms against antifungal drugs, especially the sterol-sequestering polyene antifungal Amphotericin B (AmB). Finally, I will present the importance of structural studies for the full description of the molecular mechanisms of lipid binding domains, especially focussing on biomolecular NMR applications for structural insights into LTPs interactions with lipids.

1.1. Lipids in biological membranes

The lipid bilayer is the thin boundary of every organelle and ultimately the separation between a living cell and the outside world. Biochemistry, biophysics and mass spectrometry (MS) applied to lipid research (also called Lipidomics) have given information on the detailed structure and composition of biological membranes from different organisms, cells, organelles, leaflets and domains. The eukaryotic cell contains thousands of different lipids devoting about 5% of its genome to lipid biosynthesis (van Meer et al., 2008). Even if we know the specific function of many lipids, the use of such a diverse population, the regulatory processes important for their homeostasis and the mechanisms of their intracellular transport between membranes remain elusive.

1.1.1. Biological functions of lipids

Cellular lipids in biology have three important functions: (i) energy storage molecules, (ii) amphipathic lipids as components of membrane bilayers, and (iii) signalling molecules acting as second messengers. I will discuss briefly all these three functions, and then I will focus on the second point in more detail, describing the role of intracellular lipid traffic in membrane homeostasis.

First, lipids are used as efficient energy storage molecules in lipid droplets (LD). Eukaryotic cells favour lipids to sugars as energy reservoirs because the former have a greater energy per unit of mass due to the high content of reduced hydrocarbons. LDs are universally conserved organelles whose main function is the store of lipids for energy production and as precursors for membrane building blocks (Thiam et al., 2013; Ohsaki et al., 2014). Excess lipids are buffered into neutral lipids that exclude water, mainly triacylglycerol (TAG) and sterol esters (SE), and stored in LDs, which are coated by a phospholipid (PL) monolayer. Since LDs are excluded from vesicular traffic, their growth and shrinkage depend on multiple pathways, always reliant on the exchange of lipids between LDs and other organelles, typically at MCSs (Barbosa et al., 2015a; b).

Second, membranes are the physical barriers that separate a cell from the outside world and parts of the cell from each other. They are formed by two layers of amphipathic lipids, molecules with hydrophobic and hydrophilic moieties, acyl chains and a charged head. This lipid bilayer, with an average thickness of 5-9 nm (Schneiter et al., 1999; Mitra et al., 2004), is entropically favoured by the tendency of the hydrophobic tails to self-aggregate in an aqueous environment. Each organelle is surrounded by a membrane with a specific lipid composition that also differs for its leaflets. The biochemical reason for this compartmentalisation could be explained by an overall higher efficiency of chemical reactions through physical separation of some steps, coupled with limited and controlled diffusion of products of other steps. In addition to the barrier function, different lipid species also confer different physical properties to the membranes, allowing them to bud, internalise, tubulate, shed or fuse; all these features are at the base of important cellular processes such as cell division, secretion, vesicle trafficking, and cell-cell communication.

Last, lipids can function as messengers in signalling cascades and they can be recognised by protein effectors. Amphipathic lipids can be hydrolysed by specific proteins such as lipases, so that their polar head can propagate within the cytosol, while the hydrophobic portion can transmit the signal to other membrane partners (van Meer et al., 2008). A classic example for phospholipids is the phospholipase C (PLC)-mediated cleavage of phosphatidylinositol 4,5-bisphosphate ($PI(4,5)P_2$) on PM inner leaflet with formation of diacylglycerol (DAG) and inositol 1,4,5-triphosphate (IP_3). DAG remains inside the membrane where it is a physiological activator of protein kinase C (PKC) and a critical ligand for the priming factor Munc13 (Lackner et al., 1999; Rhee et al., 2002). IP_3 diffuses in the cytosol where it binds IP_3-receptors, to mediate calcium (Ca^{2+}) responses and, in some cases, trigger secretion (Di Paolo and De Camilli, 2006).

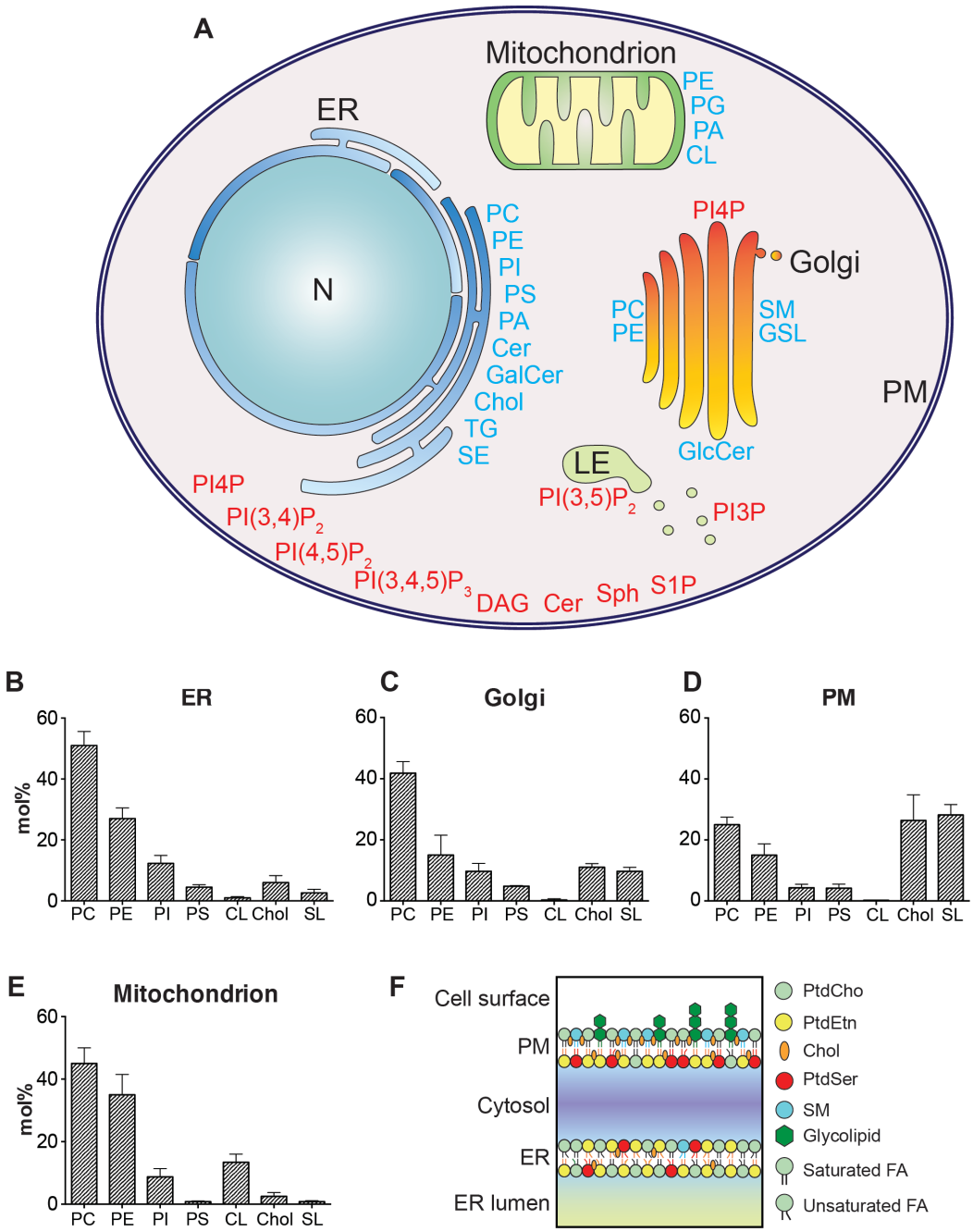

Figure 1.1 The different lipid composition of mammalian cell membranes

A. The diagram represents a simplified cell with some organelles of the secretory pathway. The lipid composition varies in the membranes of different organelles. The figure shows the place where lipids are synthesised (blue abbreviations) and the place where the lipids exert important cellular function (red abbreviations) because of their involvement in recognition pathway, signalling events, or determination of membrane physical properties. The ER is the place where the majority of lipids molecules are synthesised: phosphatidylcholine (PC), phosphatidylethanolamine (PE), phosphatidylinositol (PI), phosphatidylserine (PS), phosphatidic acid (PA), ceramide (Cer), galactosylceramide (GalCer), cholesterol (Chol), and triacylglycerol (TG) and sterol esters (both then stored in lipid droplets). Sphingomyelin (SM), and complex glycosphingolipids (GLS) are synthesised in the Golgi apparatus. PC can be

also synthesised in the Golgi. Mitochondria and other organelles such as chloroplasts and lipid droplets are excluded from vesicular traffic, nevertheless all have specific membrane composition including lipids that they cannot synthesise *in situ*. No membrane contact sites are shown. This image is a personal rendition (inspired and updated from van Meer *et al.*, 2008). Other abbreviations: CL, cardiolipin; DAG, diacylglycerol; PG, phosphatidylglycerol; PI3P, phosphatidylinositol-3-phosphate; $PI(3,5)P_2$, phosphatidylinositol-(3,5)-bisphosphate; $PI(4,5)P_2$, phosphatidylinositol-(4,5)-bisphosphate; $PI(3,4,5)P_3$, phosphatidylinositol-(3,4,5)-trisphosphate; PI4P, phosphatidylinositol-4-phosphate; S1P, sphingosine-1-phosphate; Sph, sphingosine. **B-E**. The graphs show the lipid compositional data from lipidomics analysis, presenting the molar fraction (mol%) of lipids composing the membranes of ER, Golgi, PM and mitochondrion. The mol% refers to the total lipid composition of mammalian bone marrow derived macrophages (Andreyev et al., 2010). Graphs made by mining databases of lipidomics studies on subcellular fractionations at lipidmaps.org. **F**. Schematic representation of ER and PM leaflets. The two PM leaflets have different lipid compositions. Most SL are present in the outer leaflet, while PI, PE and PS are only present on the inner leaflet (Fairn et al., 2011; Bretscher, 1973). This different distribution is actively maintained by energy-dependent transport, in fact exposure of PS on the outer leaflet is a marker of apoptosis (Fadok et al., 1992). Cholesterol has a spontaneous flipping rate ($t_{1/2}$) between leaflet of 1 second (Müller and Herrmann, 2002; Steck et al., 2002), but it is known to preferentially interact with SL (Slotte, 2013).

1.1.2. Lipid species

The main lipid species of all eukaryotic membranes are glycerolipids, sphingolipids and sterols.

Glycerolipids are the main components of the eukaryotic membranes: they are composed of a phosphate head group ester linked to a hydrophobic glycerol backbone. Their classification is based on the structure of their head group: zwitterionic in phosphatidylcholine (PC) and phosphatidyl-ethanolamine (PE), and anionic in phosphatidylserine (PS) and phosphatidylinositol (PI). Their hydrophobic moiety is DAG, a glyceride consisting of two acyl chains (also called fatty acid, FA) of varying length covalently bound to a glycerol molecule through ester linkers. The FA chains can be saturated with no double bonds, or *cis*-unsaturated. The *cis* configuration is the only one present in nature with the two hydrogen atoms adjacent to the double bond facing the same side of the chain. The rigidity of the double bond blocks its conformation and causes the chain to bend decreasing the conformational freedom of the FA. A consequence of unsaturated FAs in the lipid bilayer is the reduction of lipid packing, making the membrane more fluid (Holthuis and Menon, 2014).

Lipid packing can be defined as dependent on the ratio between unsaturated and saturated FAs and the ratio between bulky and small headgroups. This combination of PL headgroups, ratio between saturation/desaturation, and acyl chain lengths influence the properties of the membrane.

PC is the most abundant PL component of all membranes in the cell. It accounts for about 50% of the total PL in the membrane of every organelle, and because of its relatively cylindrical shape, in water it can assemble spontaneously into bilayer exposing the headgroup to the aqueous environment. The second most abundant PL is PE, with a conical shape in which the relatively small headgroup is located at the tip of the cone. It imposes negative curvature to the membrane and it is essential to phenomena of fusion and budding (Holthuis and Menon, 2014). While PC and PE have zwitterionic headgroups, PS and PI anionic headgroups are key determinants of the net surface charge of membrane. For example, anionic lipids are the cause of the

negative charge of PM inner leaflet, which is important for functional interactions of transmembrane proteins and peripheral membrane proteins with positive charge from basic residues.

The hydrophobic portion of sphingolipids (SL) is always ceramide (Cer), which is formed from a long chain base (LCB) condensed onto sphingosine (Sph). Sphingomyelin synthase (SMS) can add phosphocholine to make sphingomyelin (SM), or saccharides can be added to ceramide to form glycosphingolipids (GSL). SLs form narrower and taller cylinders than PC making the membrane denser and thicker, and they are particularly abundant in the PM. SLs have pleiotropic effects on controlling protein kinases, actin cytoskeleton, endocytosis, apoptosis, cell cycle, vesicular trafficking, cell migration and inflammation (Hannun and Obeid, 2008; Platt, 2014).

Sterols are hydrophobic lipids with an inflexible core and a very small hydrophilic domain consisting of a single hydroxyl group facing the aqueous environment. Adjacent to this hydrophilic domain there is the inflexible planar core composed of four fused rings with a short single side chain tail at the opposite end. Membranes of mammals have cholesterol with an iso-octyl side chain, while fungi have ergosterol with a 9-carbon mono-unsaturated side chain (Figure 6.4). Sterols have a major affinity for SLs, so they are also more abundant in the PM making a rigid membrane more fluid but keeping its thickness and impermeability properties (Holthuis and Menon, 2014). In fact, cholesterol has a huge impact on the physical properties of the membrane bilayer. At physiological temperatures, phospholipid bilayers exist in their fluid (or liquid) phase. This structure is profoundly altered by the presence of cholesterol: its inflexible core causes the acyl chains to become closely packed and the bilayer to be thicker in the so called liquid ordered (l_o) phase. Cholesterol arranges perpendicularly to the acyl chains so that the lipids can still diffuse on the same plane, but they cannot deform to allow movement of small molecules across the bilayer, thus decreasing its permeability to water (Munro, 2003; van Meer et al., 2008).

These lipid species populate differently the diverse organelle membranes where they confer definite physical and biological properties and they also give the specificity for signalling, trafficking and recognition events. However, even if we know in more details about their distribution and biosynthesis, the reason for so many species, the feedback mechanisms important for their equilibrium and the mechanisms of their intracellular transport that maintain the homeostasis remain elusive.

In this project, I used *Saccharomyces cerevisiae* as a model organism. Yeast has advantages and disadvantages for the study of lipid biology: (i) convenient experimental tractability, with simple and highly governable growth conditions in fully defined medium, allowing precise control of physical and biochemical parameters (lipid free media); (ii) simple genetic manipulation compared to mammalian cells; (iii) high degree of conservation of metabolic pathways between yeast and mammals; (iv) yeast has only a few hundred lipid species, mammalian cells have thousands (Santos and Riezman, 2012). A major difference between mammalian and yeast lipidome is the presence of cholesterol as opposed to yeast ergosterol (requiring distinctive enzymatic steps not present in mammals). In contrast to mammalian PS synthases, which form PS through a base-exchange mechanism, yeast PS synthase forms PS from CDP-DAG and serine (Figure 1.2). For sphingolipids, the predominant long-chain base in yeast is phytosphingosine as opposed to animal sphingosine, and *S. cerevisiae* has only three complex sphingolipids (Figure 1.2A), as opposed to the wide diversity and turnover of mammalian cells (Daum et al., 1998).

The basic pathways for the biosynthesis of the three lipid classes (Figure 1.2) were formed early in eukaryotic evolution, however individual enzyme families followed unique evolutionary developments (Lykidis, 2007). For example, the multiplicity of glycerolipid biosynthetic enzymes underwent gene expansion in a lineage-specific manner; and unicellular eukaryotes, including *Saccharomyces cerevisiae*, maintained procaryotic-like enzymes for the synthesis of phosphatidylglycerol and cardiolipin (Lykidis, 2007).

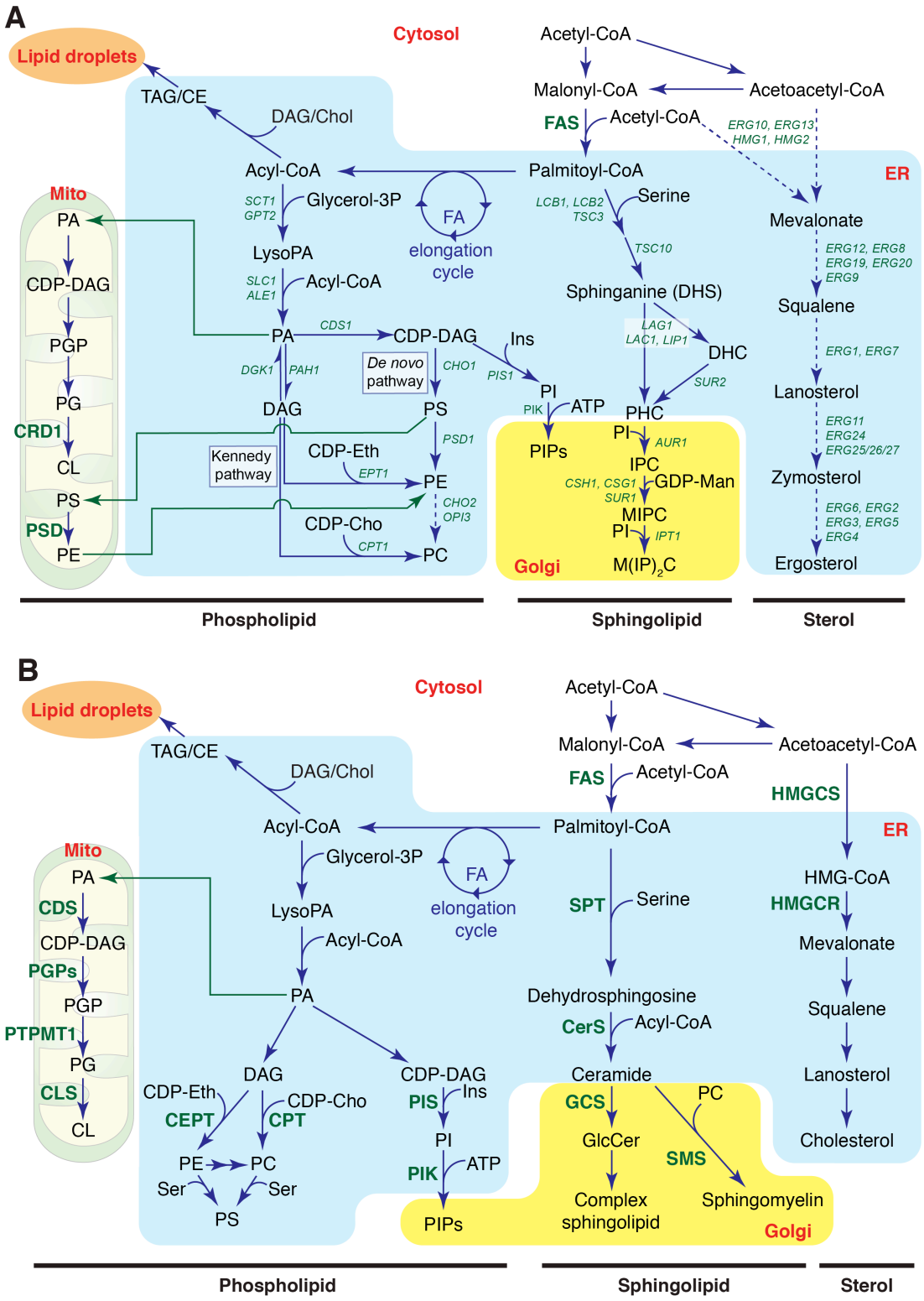

Figure 1.2 Compartmentalisation of lipid biosynthesis in yeast and mammals

Simplified view of main phospholipid, sphingolipid and sterol biosynthetic pathways in yeast (**A**) and mammalian (**B**) cells. The majority of lipids are made within the ER membrane (light blue). Other important organelles shown in the figures are Golgi (yellow), mitochondria (on the left), and lipid droplets (orange). CDP-, cytidine-diphosphate-; CEPT, Cho/Eth-phosphotransferase; CerS, ceramide synthase; Cho, choline; Chol, cholesterol; CL, cardiolipin; CLS, cardiolipin synthase; -CoA, coenzyme

A; CPT, choline-phosphotransferase; CRD1, cardiolipin synthase-1; DHC, dehydroceramide; DHS, dehydrosphingosine, sphinganine; FA, fatty acid; FAS, FA synthase; GCS, GlcCer synthase; GDP-Man, guanosine diphosphate mannose; GlcCer, glucosylceramide; IPC, inositolphosphoceramide; HMG-, hydroxymethylglutaryl-; HMGCS, HMG-CoA synthase; HMGCR, 3-hydroxy-3-methylglutaryl-CoA reductase; Ins, inositol; MIPC, mannosyl-inositolphosphoceramide; PA, phosphatidic acid; PG, phosphatidylglycerol; PGP, phosphatidylglycerolphosphate; PHC, phytoceramide; PI, phosphatidylinositol; PIPs, phosphoinositides; PC, phosphatidylcholine; PE, phosphatidylethanolamine; PIS, PI synthase; PS, phosphatidylserine; PSD, PS decarboxylase; SMS, sphingomyelin synthase; SPT, serine palmitoyltransferase; TAG/CE, triacylglycerol/cholesterol ester. Dashed arrows represent multiple enzymatic reactions. Green arrows represent lipid transfer. This figure is a personal rendition obtained by merging simplified pathways from different figures. For yeast pathways (**A**): Figure 2 (Holthuis and Menon, 2014), Scheme 1 (Riezman, 2006), Figure 1 (Carman and Han, 2009). For mammalian pathways (**B**): Figure 2 (Holthuis and Menon, 2014), Figure 1 (Choi et al., 2004), and Figure 1 (Fagone and Jackowski, 2009).

1.1.3. Lipid composition and organelle function

The ER is the largest membrane bound organelle in eukaryotic cells, the cellular main factory, and as such, the starting point of the secretory pathway. It is the principal location for the synthesis of proteins destined for secretion, the site where membrane proteins undergo insertion and folding, an organelle for Ca^{2+} storage and release, and the major place of lipid biosynthesis (Park et al., 2014; Phillips and Voeltz, 2015). In the ER, different but interconnected enzymatic pathways synthesise (i) the bulk of phospholipids and sterols, (ii) the precursor of all sphingolipids, *i.e.* Cer, and (iii) storage lipids such as TAG and sterol esters destined for LDs (Figure 1.2).

Sterols are synthesised in the ER where they are present at low concentration (5-8 mol%), and they are abundant in the *trans*-Golgi network (TGN) and PM (30-40 mol%) (van Meer et al., 2008; Radhakrishnan et al., 2008), where they interact with lipids bearing saturated acyl chains and bulky headgroups, such as sphingolipids, whose levels are also higher at the PM (Hannun and Obeid, 2008; Slotte, 2013).

According to these features, a simplistic but helpful 'two membrane territories' model has been proposed (Bigay and Antonny, 2012), interpreting lipidomics experiments and analysis of lipid probes distributions (Yeung et al., 2008; Wenk, 2010) (Figure 1.1F). The first territory is constituted of the ER and *cis*-Golgi membranes: both of them are thin and characterised by monounsaturated acyl chains (leading to loose membrane packing), uncharged lipids (low anioinic lipids on cytosolic side) and low sterols (Fairn et al., 2011; Kay et al., 2012). The second territory includes *trans*-Golgi and PM membranes which are thicker because populated by phospholipids with saturated acyl chains (leading to tighter and non-defective packing), and because richer in sterols and sphingolipids. They also have anionic lipids such as PS on their cytoplasmic leaflets.

It is useful to think about the implications of these differences across the lipid landscape in terms of just two aspects, the differences in thickness and surface charges. First, the different thickness of the membranes is also

reflected in the organelle-specific length of transmembrane domains (TMDs) of integral membrane proteins with the tendency of 4- to 8-residues longer TMDs (corresponding to a 6 to 12 Å increase for mammalian or fungal PM, respectively) in post-Golgi compartments (Levine et al., 2000; Sharpe et al., 2010). Second, the different charges between the cytoplasmic leaflets of organelles' membranes have evolved different recognition and targeting mechanisms by peripheral membrane proteins: (i) organelles in the early secretory pathway bind proteins with neutral amphipathic lipid packing sensor motifs (ALPS), containing hydrophobic residues that can insert into the loosely packed membrane (Bigay and Antonny, 2012; Vanni et al., 2013); (ii) organelles in the late secretory pathway can recruit proteins that contain positively charged motifs such as the BAR domains or the polybasic regions of Stromal Interaction Molecule 1 (STIM1) and Guanosine TriPhosphatases (GTPases) (Grinstein, 2010; Walsh et al., 2010; Wang et al., 2010).

The biological significance of the transition from a loosely packed membrane into a thick and rigid one would be to allow both the biogenic work of the ER and the barrier function of the PM. This difference is driven by sphingolipid synthesis from the precursor ceramide at *trans*-Golgi and sterol supply (Holthuis et al., 2001), but the mechanisms involved in its maintenance, including how they travel along the secretory pathway to the PM against a concentration gradient, remain elusive.

One of the limitations of the two membrane territories model is the explanation of phosphatidic acid (PA) and PI distribution: both these phospholipids are anionic but they are present into the ER. PA is at the centre of different lipid biosynthetic pathways (Figure 1.2), and its levels are kept very similar and very low in all membranes (Loewen, 2012). Contrary to PA, PI levels are higher than the ER in every other organelle in the secretory pathway (Figure 1.1), and it probably populates the ER not in an equal distribution but in specific, concentrated and highly dynamic sub-compartments (Kim et al., 2011; 2016). PI can be phosphorylated by a variety of kinases on the three, four and five hydroxyl groups of the inositol ring, giving rise to seven different combinations. The phosphorylated forms, also called phosphoinositides, can be rapidly

metabolised, are important signalling intermediates and are involved in organelle identity, (indirect) membrane shaping and vesicular traffic (Balla, 2013). Nevertheless, the fact that PI populates distinct and localised sub-regions of the ER (Kim et al., 2011), together with the fact that the localisation of PS is mainly in the luminal side of ER membrane (Fairn et al., 2011; Kay et al., 2012), would still support the general concept of a neutral ER membrane on the cytoplasmic side.

As mentioned earlier, the molecular mechanisms behind the preservation of the differences between the two territories are not completely understood. However, growing evidence is supporting the interconnected contribution of two mechanisms to maintain this homeostasis: (i) sensors of membrane lipid composition and (ii) lipid traffic.

Sensing membrane lipid composition

The ER is the main biogenic organelle of the cell for lipids and at the same time it is equipped with proteins capable of sensing perturbations in composition and physical properties of its membrane. Experiments with bacterial, yeast and mammalian cell systems characterised some of these mechanisms for the regulation of lipid homeostasis, here I will list some examples of this feedback control linking lipid sensing to wider cellular responses such as apoptosis, transcriptional events, and induction of specific enzymatic pathways. The imbalance between saturated and unsaturated PL can induce a stress response leading to cell death (Deguil et al., 2011). Bacteria have thermosensors such as Des Kinase (DesK), whose conformational changes in its transmembrane helices are induced by the levels of fluidity/rigidity of the lipid bilayer: the structural changes shift the DesK activity towards phosphatase- or kinase-dominant activity, that can start a transcriptional program ultimately resulting in phospholipid desaturation (Aguilar et al., 2001; Aguilar and de Mendoza, 2006; Inda et al., 2014).

In yeast, Opi1 possesses a FFAT motif (FF, two phenylalanines, in an acidic tract) that interacts with ER-resident Scs2, the yeast homologues of VAMP-

associated proteins (VAP), and Opi1 also has a basic motif to bind PA. When PA levels are high, Opi1p associates with the ER membrane; when PA levels decrease, Opi1p can translocate to the nucleus to repress transcription of genes involved in lipid biogenesis (Loewen et al., 2004).

In mammalian cells, a similar mechanism to modify phospholipid composition is still not known. The majority of efforts focussed on the study of sterol levels sensing for which an elegant feedback mechanism was characterised: an interplay between the sterol sensing protein Sterol regulatory element-binding protein (SREBP) cleavage-activating protein (SCAP) and the membrane-bound transcription factor SREBP2 is able to respond to variations in the 5 mol% ER sterol concentration (Radhakrishnan et al., 2008).

Intracellular lipid traffic

In the next section, I will outline more on lipid trafficking, focussing in particular on non-vesicular traffic mediated by lipid transfer proteins (LTPs). LTPs work in parallel, and sometimes against vesicular trafficking and they represent excellent controllers of lipid exchange between the two different membrane territories.

1.2. Lipid traffic

Lipids are unequally distributed along the secretory pathway and the composition of the cellular compartments is crucial for their identity and function. However, lipids do not possess targeting instructions such as localisation signals that regulate the cellular journey of a protein. How can they travel from their place of synthesis to the membrane of destination? And in relation to this question, how is the lipid composition of organelles kept at physiological levels against vesicular traffic, signalling events, extracellular stress and organelle dynamics?

A lipid molecule can be subjected to three kinds of movement: (i) lateral movement in a single membrane, (ii) transbilayer exchange (also known as flip-flop) between leaflets of the same membrane, (iii) vesicular transport, and (iv) monomeric exchange between different membranes which involves the desorption of the lipid into the aqueous phase of the cytosol and subsequent insertion into a new membrane (Lev, 2010).

1) Lateral movement is most likely not the critical step: lipids molecules move on the lateral plane of the same membrane 10-100 times faster than transmembrane proteins (Holthuis and Menon, 2014).

2) Transbilayer exchange is relatively quick for lipid with apolar headgroups such as DAG and cholesterol (with $t_{1/2}$ of seconds to minutes), but it is very slow for lipids with polar headgroups such as glycerophospholipids ($t_{1/2}$ of hours to days for PC) or glycosylated lipids (Holthuis and Levine, 2005). This movement can be energetically eased by protein flippases that mask the hydrophilic head from the hydrophobic core of the bilayer (Bretscher, 1973; Sanyal and Menon, 2009). An example is the family of the P4-ATPases, transmembrane proteins implicated in translocation of phospholipids between membrane leaflets of different organelles. Conserved in all eukaryotes, there are 14 members in the mammalian family. P4-ATPases require energy from ATP consumption to drive the re-distribution against a concentration gradient, and they coordinate various membrane trafficking events such as exocytosis, endocytosis and formation of clathrin-coated vesicles. There are also proteins

capable of dissipating lipid asymmetry, called scramblases. These proteins catalyse an ATP-independent, bidirectional and nonspecific movement of different lipid classes across the PM (Montigny et al., 2015), and some of them rely on transient activation mechanisms, such as caspase cleavage (Suzuki et al., 2014) or Ca^{2+} binding (Brunner et al., 2014).

3) Vesicles transfer proteins along the exocytic and endocytic pathways, requiring metabolic energy and the cytoskeleton. Vesicles are dominated by proteins (2:1, w/w), but their basic constituents are lipid molecules (Takamori et al., 2006). Also membrane expansion during cell growth is mainly achieved by regulated membrane vesicle fusion with the PM (Pfenninger, 2009).

4) Finally, lipids can exchange between different membranes as single molecules. *In vitro*, the rate of spontaneous movement of lipids between membranes is limited by the entropically unfavourable desorption step with $t_{1/2}$ of minutes for lyso-phospholipids, up to $t_{1/2}$ of days for lipids with two acyl chains, which would translate in incompatibility with life *in vivo* (McLean and Phillips, 1984; Bai and Pagano, 1997; Holthuis and Levine, 2005)

A priori, this intracellular movement could be mediated by vesicular and non-vesicular pathways and the balance between these two mechanisms is important for membrane composition and signalling. The presence of non-vesicular traffic is strongly supported by at least three experimental proofs:

1. lipids reach organelles excluded from vesicular pathways, in the case of mitochondria, there is an interchange of lipids from the outer mitochondria membrane (OMM) and the ER (Tatsuta et al., 2014), and some of the biosynthetic steps are catalysed on the OMM and then the new molecule is transported back to the ER (Figure 1.2),
2. the kinetics of lipid transfer from ER to PM seen for PC ($t_{1/2}$ export of 2 minutes), PE ($t_{1/2}$ export of 20 minutes), and cholesterol ($t_{1/2}$ export of 5 minutes) are faster than protein traffic in the secretory pathway (Sleight and Pagano, 1983; Kaplan and Simoni, 1985a; Urbani and Simoni, 1990; Gnamusch et al., 1992),

3. sterol and phospholipid delivery to the PM continues even when vesicular trafficking is perturbed with different methods:
    a. genetically knocked out in a *sec18* mutant. Sec18p is the *S cerevisiae* homologue of N-ethilmaleimide-sensitive fusion (NSF) protein, and it is required for every SNARE-mediated fusion step (Novick et al., 1980; Wilson et al., 1989; Graham and Emr, 1991). In yeast, the transport of newly synthesised sphingolipids (Funato and Riezman, 2001) and ergosterol (Baumann et al., 2005) from the ER to the PM is not affected at non-permissive temperatures.
    b. pharmacological blockage with Brefeldin A (BfA). The main cellular target of BfA is the guanine nucleotide exchange factor (GEF) GBF1, which mediates the formation of Golgi vesicles by recruiting COPI coat proteins. Knockdown of GBF1 activity induces the collapse of the Golgi into ER, but leaves lipid transport unaffected (Urbani and Simoni, 1990; Graham et al., 1993).

Non-vesicular traffic is largely ascribed to LTPs, whose lipid binding folds fall in one of the 15 families (Table 1.1). The common feature of all the folds is the presence of an internal cavity that evolved with the capacity to accommodate a hydrophobic molecule shielding it from the aqueous environment of the cytosol. However, their role *in vivo* has been more difficult to prove and only recently appropriate experimental design has started to discover their function in maintenance of cellular lipid homeostasis and their involvement in many other processes.

1.2.1. Lipid transfer proteins

LTPs have been originally defined as proteins able to transfer a lipid molecule *in vitro*. This description dates back to the 1960s, when the first potential LTPs were detected *in vitro* as soluble factors that increased the rate of lipid transfer between mitochondria and microsomes, vesicles resulting from the breakage of the ER isolated from cells (Wirtz and Zilversmit, 1968).

Usually they have the form of a pocket with a mobile lid shielding the lipid monomer from the surrounding aqueous environment (Holthuis and Levine, 2005). The binding domain is internally lined mostly with hydrophobic residues that stabilise the lipid. In vivo, a LTP binds and transfers a limited range of lipids for which affinity is determined by interactions with both headgroup and acyl chains.

Mining recent works of tissue-based human proteomics studies (Uhlén et al., 2015), the human genome contains ~130 LTPs, mainly expressed in all cell types with some tissue-specific enrichment only in sporadic cases (Chiapparino et al., 2015). LTPs can be grouped according to the structural fold that binds lipids: there are 15 different structural folds, characterised by the presence of mainly alpha-helices, mainly beta-sheets, or more commonly, an alternation of them (Table 1.1 and Figure 1.3). Despite the fact that they share a similar fold, LTPs in the same group show a striking variety of possible lipid ligands (Schrick et al., 2014). The characterisation of the full spectrum of LTP-lipid interaction in the protein physiological condition (for localisation and expression levels) is still an open task (see Section 1.7).

Together with the lipid binding/transfer domain, the domain organisation of a LTP may include other domains: (i) elements that mediate protein-protein interactions with downstream effectors (enzymes, nuclear receptors, transmembrane transporters, other LTPs), or (ii) domains/motifs for membrane targeting that specify their subcellular localisation. Furthermore, typically LTPs that do have targeting domains often have *two* targeting elements that allow them to bind the membranes of two different organelles. A development from this has been to determine if the two targeting elements

work at the same time, which would indicate recruitment to places called membrane contact sites (MCSs), where two organelles come close enough to be spanned by individual proteins (within 30 nm). This bivalent binding at contact sites confers the LTP with the ability to engage both donor and acceptor membrane at the same time and to shuttle the lipid in between.

The current models suggest that many steps in lipid traffic are mediated by LTPs that preferentially work at contact sites between early and late secretory organelles to bypass vesicular traffic; this appears to be a widespread phenomenon, and so it may be the basis for optimal control of lipid levels and exchange (Holthuis and Menon, 2014). The next sections focus on (i) the description of the structural fold of LTPs belonging to the Steroidogenic Acute regulatory (StART) domain family, (ii) the portrayal of known mechanisms of intracellular sterol traffic and regulation of sterol levels in the cell membranes, and (iii) membrane contact sites, first presenting proteins functioning at contacts between ER and PM, then concentrating on newly described mechanisms of lipid traffic at contact sites.

Secondary structure elements	**Families**
All α-helices	Coq9 GLTP TPSO
α-helices / β-sheets	FAD/NAD binding NPC1-N terminus* SCP-2* Sec14 (CRAL/TRIO) VAT-1 WIF
Mainly β-sheets	OSBP-related* SRPBCC* (StART, PITP, Bet_v1, LAM) TULIP
All β-sheets with short α-helices	Lipocalin/calycin
All β-sheets	FABP NPC2*

Table 1.1 Fifteen structural folds of intracellular lipid binding proteins

Lipid transfer proteins have been originally defined as proteins with a hydrophobic cavity able to transfer a lipid molecule *in vitro* (Wirtz and Zilversmit, 1968). They have the form of a pocket with a mobile lid shielding the lipid monomer from the surrounding aqueous environment. The binding domain is internally lined with hydrophobic residues that stabilise the lipid. In vivo, a LTP binds and transfers a limited range of

lipids for whose affinity is determined by its headgroup and the length of acyl chains. Their classification depends on the predominant secondary structural element in their fold. Twelve of these families were included in a previous reviews (Holthuis and Levine, 2005; Chiapparino et al., 2015), with an increasing rate of discovery of new proteins suggesting that more members are yet to be identified. * = some members of the family bind sterols.

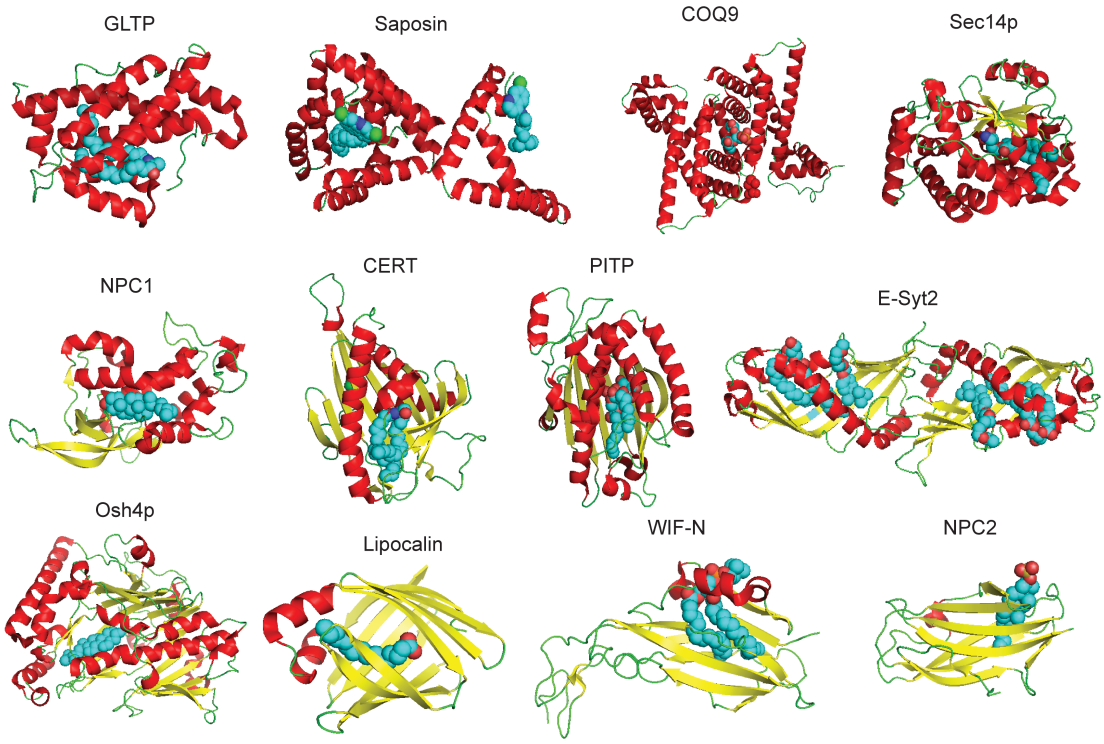

Figure 1.3 Structural folds of lipid transfer domains

The cartoons show the three-dimensional structures of some members of LTP families with their lipid ligands. The lipid transfer proteins are ordered from the all alpha-helix fold to the all beta-sheet structure. GLTP in lactosylceramide-bound form (1SX6) (Malinina et al., 2004), Saposin B in complex with chloroquine (4V2O) (Huta et al., 2016), COQ9 in complex with a PE-derived phospholipid (4RHP) (Lohman et al., 2014); yeast Sec14 homolog Sfh1p in complex with PE (3B74) (Schaaf et al., 2008), N-terminal domain of NPC1 with cholesterol (3GKI) (Kwon et al., 2009); CERT StART domain with C18-ceramide (2E3Q) (Kudo et al., 2008), StART domain of PITPα in complex with PI (1UW5) (Tilley et al., 2004), dimerised TULIP domains of E-Syt2 in complex with 1,2-dioleoyl-*sn*-glycero-3-phosphoethanolamine and Triton X-100 (4P42) (Schauder et al., 2014), yeast Osh4p in complex with cholesterol (1ZHY) (Im et al., 2005), rat lipocalin in complex with palmitic acid (2IFB) (Sacchettini et al., 1989); WIF-N in complex with 1,2-dipalmitoyl-phosphatidylcholine (2YGO) (Malinauskas et al., 2011), bovine NPC2 with cholesterol sulphate (2HKA) (Xu et al., 2007). All crystals are from the human proteins, unless otherwise stated. Cartoons were made with PyMOL: molecules were coloured by secondary structure with (red helices, yellow sheets, and green loops), lipid ligands were rendered as spheres coloured by element (CNOS). Cartoons were not drawn to scale.

1.2.2. StART domain

The cytoplasmic sterol specific LTPs are some members of the OSBP related family and some members of the StART protein family (Table 1.1). Among the fifteen human StART proteins, the founding member of the family (StARD1) transports cholesterol into mitochondria in steroidogenic cells (Clark et al., 1994), and StARD4 transports cholesterol from the late secretory pathway to the ER (Mesmin et al., 2011). The steroidogenic acute regulatory protein (StAR) transfer domain (StART), is a lipid transfer domain of 210 residues forming a “helix-grip” domain of curved beta-sheet wrapped around a long alpha-helix (Figure 1.3, CERT). The core of the domain that forms the cavity is 170 residues in the form of a pocket composed by antiparallel β-strands with a lid composed by the long C-terminal α-helix. Two Ω loops are inserted between β5 and β6 (Ω1) and strands β7 and β8 (Ω2). The resulting cleft is wide enough to accommodate a molecule (sterol, phospholipid or sphingolipid), but its two openings are too narrow to allow entrance/exit of the lipid without major structural rearrangements, such as the movement of the C-terminal helix possibly with the loop Ω1 (Thorsell et al., 2011). The fifteen members of the human StART protein family have different binding specificities, different localisations and different functions (Alpy and Tomasetto, 2014). At the beginning of this project, no StART proteins were identified in *Saccharomyces cerevisiae*.

1.3. Intracellular sterol traffic

Sterols, such as cholesterol in animal cells or ergosterol in yeast cells, are essential components of cellular membranes. As already mentioned, their concentration determines important membrane properties, such as fluidity and rigidity, and they are not uniformly distributed along the different organelles' membranes. Cells evolved sophisticated mechanisms to precisely regulate their sterol levels, which are critical both for maintenance of membrane properties and adaptation to environmental stress, but also for preventing accumulation of toxic free sterols (Goldstein and Brown, 2015).

For the purpose of my thesis, it is important to analyse in more detail what is known about intracellular cholesterol focussing on its transport.

All nucleated cells are able to synthesise cholesterol from acetyl-CoA via the mevalonate pathway (Figure 1.2). The rate-limiting step of this biosynthetic pathway is the enzyme 3-hydroxy-3-methylglutaryl-CoA reductase (HMGCR), converting of HMG-CoA to mevalonate. This enzyme and others along the pathways, including some responsible of the fatty acylation to form cholesterol esters (CE), are integral ER membrane proteins. CEs do not populate membrane bilayers but partition into lipid droplets, which function as cellular stores for neutral lipids such as cholesteryl esters and triglycerides.

Sterol synthesis is localised to the ER, but the vast majority of cellular cholesterol is found at the PM (80-90%), therefore cholesterol must be delivered from one site to the other. As already mentioned in section 1.1.3, the mechanism of transcriptional regulation for cholesterol homeostasis resides into the ER (Goldstein and Brown, 2015), therefore the ER must receive information about the sterol concentration in the PM and recycling endosomes (for mammalian cells). Furthermore, the sensing and synthetic mechanisms, both residing on the ER, must be separated not to cause a negative feedback on the sterol biosynthesis.

It has been known for some time that cholesterol is transported along vesicular and non-vesicular pathways. Specific vesicles in endocytic and exocytic routes

might be cholesterol-rich (Möbius et al., 2003), however, different studies proved that cholesterol is transported from the ER to the PM also when vesicular trafficking through the Golgi apparatus is poisoned (Urbani and Simoni, 1990; DeGrella and Simoni, 1982; Kaplan and Simoni, 1985b) or genetically disrupted (Baumann et al., 2005). In steady state conditions, the rate of exchange of sterol in and out of the PM has been estimated to range between 30-60 x 10^3 molecules per second in yeast (Li and Prinz, 2004; Maxfield and Mondal, 2006; Sullivan et al., 2006).

1.3.1. Sterol transport from ER to PM

Cholesterol is made in the ER and subsequently enriched in the PM where it accounts for 30-40% of PM total lipids. Sterol anterograde transport is Sec18-independent, BfA-insensitive, bidirectional and rapid ($t_{1/2}$ = 5 min) (Urbani and Simoni, 1990; Baumann et al., 2005; Field et al., 1998).

The candidates identified in yeast some years ago were oxysterol binding protein (OSBP) homologues (Osh) proteins. When six Osh proteins were deleted and the seventh was conditionally inactivated, sterol transport between ER and PM was significantly slower (Raychaudhuri et al., 2006). The same data also suggested that there was PIP-mediated regulation of sterol transport (Raychaudhuri et al., 2006), and the relationship between the two aspects was further elucidated with the discovery of the counter-transport of sterol for PI4P operated by Osh4p *in vitro* (de Saint-Jean et al., 2011). However, when a different group later measured anterograde transport, the deletion/inactivation of all seven Osh proteins failed to identify any difference in metabolically radiolabelled-ergosterol delivered to the PM (Georgiev et al., 2011). So it was proposed that these LTPs are not sterol transporters *in vivo*, but they influence sterol indirectly by affecting the ability of the PM to sequester sterol molecules into a second PM pool that is accessed indirectly from the ER (Georgiev et al., 2011). When accessibility is measured in mammalian cells, instead of two, three cholesterol pools can be identified in the PM (Das et al., 2014). The three cholesterol pools in the PM are identified for their different

accessibility to radiolabelled perfringolysin O (PFO): (i) the first pool binds the probe when cholesterol concentration exceed ~35 mol%, this pool is labile, (ii) the second pool is the 'SM-sequestered pool' that binds PFO only after SMase treatment to reduce the amount of SM in the PM, (iii) the third pool is remains after SMase treatment (SM-independent pool), and its depletion by a cyclodextrin causes cells to round up and lose adherence. Only the PFO-accessible pool is the 'free cholesterol' for the cell, and small variations in its concentration will regulate cellular cholesterol homeostasis (Das et al., 2014). Nevertheless, a comprehensive description of the mechanisms of ER to PM sterol transport is still missing.

1.3.2. Sterol storage

The only homeostatic mechanism that rapidly reduces free sterol levels is esterification, which is operated by acyl-CoA cholesterol acyltransferase (ACAT) in the ER. Neutral lipids are then stored into lipid droplets (LD), which arise from ER membrane (Walther and Farese, 2012).

1.3.3. Sterol transport from PM to ER

Yeast is fully autotrophic for ergosterol, but in anaerobic conditions exogenous sterol must be supplied in the medium because sterol biosynthesis requires oxygen in two enzymatic steps. Aus1p and Pdr11p belong to the ATP-binding cassette (ABC) family of membrane transporters, primarily localise to the PM and they are expressed under hypoxic or anaerobic conditions (Li and Prinz, 2004; Wilcox et al., 2002). The exact mechanism by which the ABC transporters facilitate sterol movement into the PM is unknown, mainly because sterol can flip-flop rapidly between leaflets ($t_{1/2}$ = seconds) while phospholipids need ATP-dependent pumps. In mammalian cells, ABC transporters mediate sterol excretion, but the structural basis is the same. The recent crystal structure of the human ABCG5/ABCG8 heterodimer revealed the presence of symmetrical vestibules on opposing sides of the two transmembrane domains. These vestibules face the bilayer and extend to the

centre of the dimer and possess several residues conserved throughout eukaryotes that could constitute the entryways and the sterol binding surface (Lee et al., 2016).

1.3.4. Cholesterol transport in the endocytic pathway

In contrast to yeast, mammalian cells can uptake cholesterol in the form of low density lipoprotein (LDL) via a receptor-mediated endocytosis. LDL travels along the endocytic pathway to late endosomes and lysosomes (LE/LY) (Möbius et al., 2003). Insights into the mechanisms of LDL-derived cholesterol redistribution from these organelles come from research into the human Niemann-Pick Disease Type C. The disease is caused by mutations into two sterol binding proteins NPC1 and NPC2, conserved from yeast to mammals, that induce a cholesterol accumulation in LE/LY (Liscum et al., 1989). NPC2 is localised in the lumen and binds free cholesterol liperated from LDL by esterases to transfer it to NPC1 (Infante et al., 2008). NPC1 is a LE/LY transmembrane protein with a sterol-sensing domain able to transfer LDL-derived cholesterol out of the LE/LY compartment, possibly using a lipid channel related to resistance-nodulation-division (RND) family of bacterial permeases (Kwon et al., 2009; Davies et al., 2000). On the other side of the LE-ER contact site, ORP5 is seen in co-immunoprecipitation with NPC1 and could contribute to the export of LDL-derived cholesterol to the ER (Du et al., 2011) (see also section 1.7 for contradictory observations on ORP5 role and localisation). Other LTPs known to bind sterols are present at this contact site: ORP1L (Rocha et al., 2009; van der Kant et al., 2013) and MLN64/StARD3 (Alpy et al., 2013) interact with ER-localised VAP proteins via FFAT motifs, but their role in cholesterol sensing and/or exchange has not been fully confirmed.

1.4. Membrane contact sites

A MCS occurs when membranes of different organelles come in close apposition (10 – 30 nm) to each other without fusing, but facilitating selective exchange of ions and lipids (Levine and Loewen, 2006). MCSs are not random encounters of different organelles, they are physical bridges creating a functional link between membranes. Two additional features of MCSs are (i) the presence of biochemically unique zones, typically by excluding other organelles and large protein complexes, such as ribosomes, and (ii) the enrichment of components involved in the communication (exchange of material or signal). Some of the proteins involved in the physical bridging are defined as molecular tethers. A MCS tether should create a significant proportion of the structural link, hence its knockout should create a significant loss of the contact. As I will describe for ER-PM contacts, pure tether are relatively rare.

1.4.1. Visualisations of highly specialised contact sites

Electron microscopy allowed the visualisations of ER contact sites in the late 1950s (Bernhard and Rouiller, 1956; Porter and Palade, 1957), however their importance was overlooked for the subsequent 40 years. In this paragraph, I will present two examples of the first visualisations of highly specialised MCSs: (i) the functional proximity of ER and PM in contractile cells for efficient Ca^{2+}-mediated contraction, and (ii) the inner-outer membrane contacts in most bacteria and organelles of endosymbiotic origin, such as mitochondria and chloroplasts.

The cascade of physiological events leading to muscle contraction is so responsive and efficient thanks to the specialised anatomical feature of the muscle triad with coupling of a transverse tubule (T tubule) with two terminal cisternae . The T tubule is an invagination of the sarcolemma, the PM of skeletal muscle cells, which can depolarise in response to excitatory stimulus. The terminal cisternae are specialised smooth ER, called sarcoplasmic

reticulum (SR), able to release intraluminal Ca^{2+} upon depolarisation of T tubule membrane. This contact site between PM and ER is the physiological place where the excitation is transformed in contraction thanks to the juxtaposition of the voltage-dependent channel dehydropyridine receptor (DHPR) on the sarcolemma and the Ca^{2+}-release channel Ryanodine Receptor-1 (RyR-1) on the SR, which amplifies the initial DHPR signal. In muscle cells, these contacts are maintained by junctophilins, tethering proteins with a single transmembrane helix (TMH) in the SR and a cytosolic domain that interacts with the PM via MORN motifs (Takeshima et al., 2000; Im et al., 2007). Cells with no junctophilins show significantly fewer SR-PM contacts and have defects in Ca^{2+} signalling (Takeshima et al., 2000; Hirata et al., 2006). The remaining contacts suggest that other tethering proteins are present in the same cell type. In fact, non-excitable cells have a well characterised mechanism of store operated Ca^{2+} entry (SOCE) at ER-PM contact sites with the heterotypic dimerization of STIM1-ORAI1 proteins. The depletion of Ca^{2+} from the ER store is sensed by the stromal interaction molecule STIM1 which undergoes a conformational change, repositioning to ER-PM MCSs (Liou et al., 2005; Wu et al., 2006). Here, its interaction with Orai triggers channel opening and Ca^{2+} influx (Park et al., 2009; Wang et al., 2010). The direct activation of Orai1 by STIM1 and enrichment at these contacts of the sarco-endoplasmic reticulum Ca^{2+}-ATPase (SERCA) pump, responsible for Ca^{2+} uptake into the ER, give biological significances of this juxtaposition: passing information across the contact and directing rapid and efficient restoration of ER Ca^{2+} levels from SOCE to ER lumen without significant changes in cytosolic Ca^{2+} (Jousset et al., 2007).

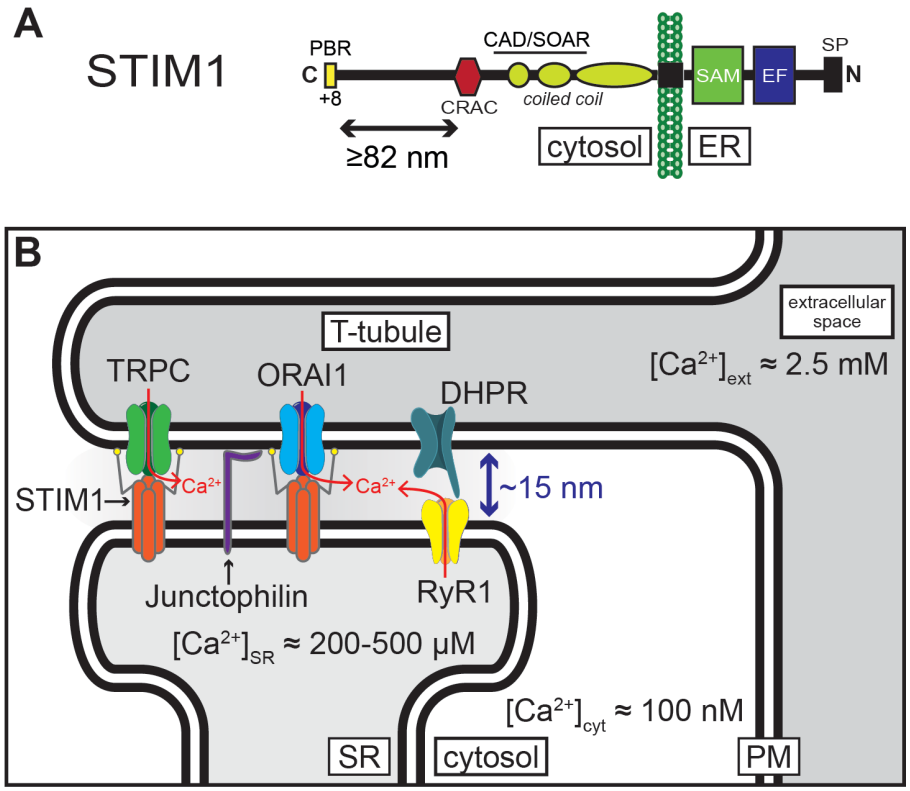

Figure 1.4 Functional organisation of T-tubule contact site

(**A**) Domain organisation of the stromal interaction molecule STIM1. The depletion of Ca^{2+} from the ER store is sensed by STIM1 which undergoes a conformational change, repositioning to 15 nm-wide ER-PM MCSs. (**B**) The different Ca^{2+} concentrations present in the extracellular space and endo-sarcoplasmic reticulum (SR) compared to cytosolic concentration are at the base of the functional activation of contractile cells. Membrane Ca^{2+}-permeable channels physically interact with protein localised to the opposite membrane, thus creating a contact site bridge.

The physiological importance of MCSs is also indicated by their conservation from prokaryotes to eukaryotes. Bacteria with double membranes have contacts at multiple points, similarly mitochondria (Rickettsial descendants) in eukaryotic cells have tethering complexes stabilising the structure of the inner membrane, organising the respiratory complex and coordinating the lipid exchange. MCSs between the inner mitochondria membrane (IMM) and the outer mitochondrial membrane (OMM) facilitate protein import, metabolite exchange in enzymatic reactions, lipid transport and organelle dynamics (Pernas and Scorrano, 2016). The molecular machinery tethering IMM and OMM is not completely known, however independent studies have described a large hetero-oligomeric complex of the IMM called mitochondrial contact site (MICOS). MICOS is conserved in plants, yeast, humans and bacteria (including members of the Rickettsia genus), and it is important for membrane architecture, cristae junctions, efficient ATP generation, membrane lipid composition and formation of intra-mitochondrial MCSs (Harner et al., 2011; Hoppins et al., 2011; Malsburg et al., 2011; Alkhaja et al., 2012; Friedman et al., 2015; Guarani et al., 2015; Michaud et al., 2016).

1.4.2. Come together: tethering organelles

As already mentioned, MCSs are not random encounters of different organelles, but they are also characterised by the presence of tethering proteins. The functions of this physical proximity relate to many aspects of cell physiology including organelle trafficking, positioning and dynamics, organelle inheritance during cell division, organelle fission, and exchange of materials (metabolites, Ca^{2+} and lipids) (Holthuis and Menon, 2014; Phillips and Voeltz, 2015; Murphy and Levine, 2016).

The exchange of materials between two organelles needs proteins associated with each side and a factor in the cytoplasm to carry the material. These proteins are either LTPs and/or specialised tethering proteins. The distinction between the two is sometimes ephemeral, in the case of LTPs, they can reversibly become structural components of the MCS by targeting both membranes to exert their function. The cytoplasmic factor is the lipid binding domain, a hydrophobic pocket within the protein organisation that is able to solubilise the lipid monomers by shielding it from the aqueous environment (see previous section).

Contacts of organelles with ER membrane does not involve exclusively these two events. MCSs are also important for signalling, membrane events such as fission of mitochondria and endosomes, and organelles trafficking along cytoskeletal structures for controlling organelle positioning (Phillips and Voeltz, 2015; Murphy and Levine, 2016; Levine and Patel, 2016).

Different elements of a protein can be responsible for targeting to MCSs, and always more than one are present at the same time to operate the double targeting to both sides of a specific contact:

a) Domains and motifs that bind lipids of the late secretory pathway
    - Pleckstrin homology (PH) domains are the 11th most common domain in the human proteome (Müller et al., 2002), they greatly differ in sequence identity but possess a significant structural conservation with the 120 residues module organised in two anti-parallel beta-sheets and a C-terminal amphipatic helix. The domain is best known for binding

phosphoinositides phosphorylated in different positions in a specific and exclusive manner (Harlan et al., 1994; Balla, 2013). However, most yeast PH domains show no evidence for membrane targeting as isolated domains and phosphoinositide binding is too weak and too promiscuous to have a physiological relevance (Yu et al., 2004).

- Polybasic regions, such as the lysine-rich area of STIM1 for facilitating the interaction with anionic lipids on the PM inner leaflet (Walsh et al., 2010).
- FYVE domains are composed by two small beta hairpins followed by an alpha helix coordinating two zinc ions. FYVE domains of ER-protein protrudin bind PI(3)P in late endosomes (Burd and Emr, 1998; Raiborg et al., 2015).
- MORN motifs of junctophilins in contracting cells connect the sarcoplasmic reticulum to the PM possibly via PA binding (Takeshima et al., 2000; Im et al., 2007).
- C2 domains of extended synaptotagmins (E-Syts), and the yeast homologue tricalbins (Tcb), interact with the PM via $PI(4,5)P_2$, in some cases following elevation of cytosolic Ca^{2+} (Giordano et al., 2013).

b) FFAT motifs (Loewen et al., 2003) or FFAT-like motifs (Mikitova and Levine, 2012) interact with VAMP-associated proteins (VAPs), which are resident on the ER (Murphy and Levine, 2016).

c) transmembrane helices (TMHs) that anchor the protein in one of the membranes, examples are Mmm1/Mdm10/Mdm34 members of ER-Mitochondria Encounter Structure (ERMES) (Kornmann et al., 2009), MLN64 (Alpy et al., 2013), and ORP5/8 (Chung et al., 2015).

d) Other protein-protein interaction, for example Mdm12 of the ERMES complex (Prinz, 2014).

The physical juxtaposition of the components of the pathway involves a donor and an acceptor compartment (the membranes of the organelles linked together) and the aqueous environment in between. In this system, some biological reasons for the juxtaposition could be hypothesised: (i) the reduced distance between the compartments which results in increased speed of the

transfer, similarly to what happens *in vitro* (Moser von Filseck et al., 2015b), (ii) the co-regulation of the mechanism that can be extended to both compartments at the same time by the same mediators, especially true for organelle remodelling (Henne, 2016), and (iii) the physical association of the second signal made in the acceptor membrane with the first coming from the donor compartment, very evident when Ca^{2+} exchange is involved (Burgoyne et al., 2015).

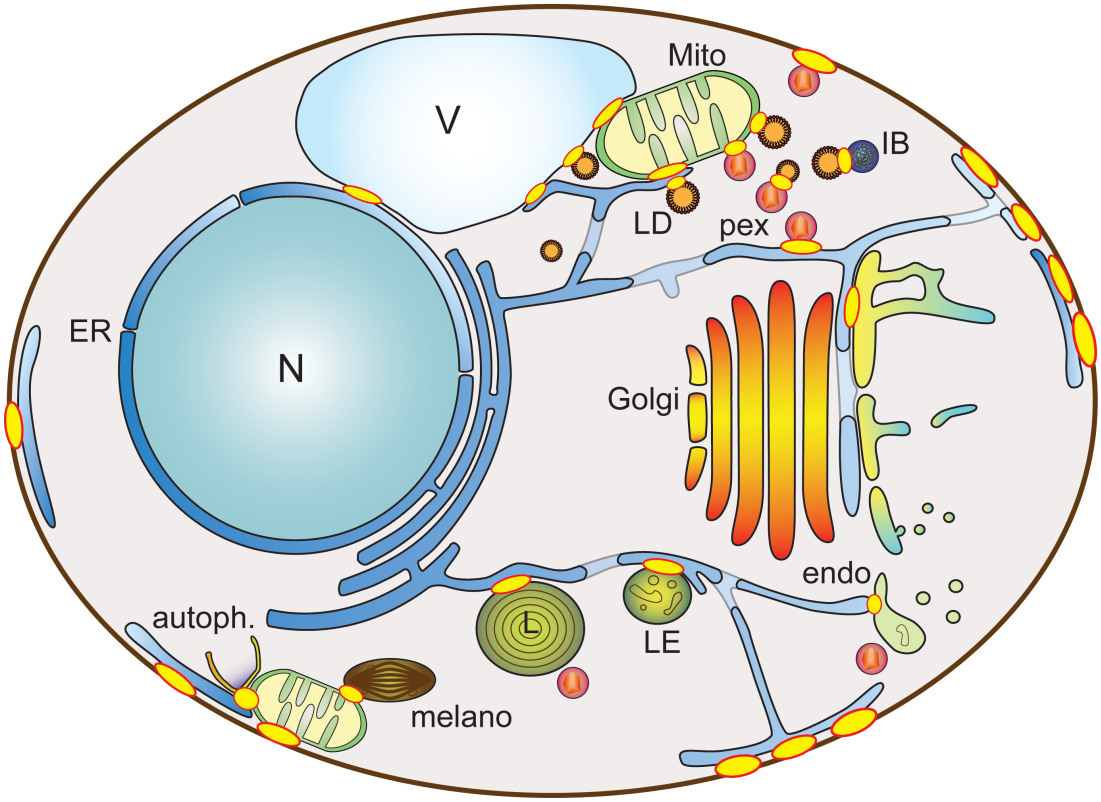

Figure 1.5 Membrane contact sites of the cell

Comprehensive representation of the identified contact sites between organelles merging discoveries in yeast and mammalian cells. The endoplasmic reticulum (ER, in blue) forms a network of membrane contact sites (MCS) with other organelles important for the exchange of ions, lipids and other solutes. Tethering proteins are present at MCSs that engage directly or indirectly with organelles' membranes involved in the contact. MCSs are an excellent platform for the activity of lipid transfer proteins (LTPs), many of which possess multiple targeting motifs to bridge the gap hence functioning as tethers. As the major site for lipid biosynthesis and calcium store, ER contacts with other organelles are important for cellular homeostasis including intracellular lipid transfer, organelle dynamics (movement, fission), ion exchange, burst of signalling events and consequent re-equilibration to steady state. Recent studies also identified new 'ER-free' MCSs. Abbreviations: autoph., autophagosome; endo, endosome; ER, endoplasmic reticulum; IB, inclusion body; L, lysosome; LD, lipid droplet; LE, late endosome; melano, melanosome; mito, mitochondrion; N, nucleus; pex, peroxisome; V, vacuole.

1.5. ER contact sites

The ER has a central role in organelle communication at contacts because it is the major cellular compartment of lipid biosynthesis, transmembrane and secretory protein translation and ion reservoir. A large portion of ER flattens around the nucleus of eukaryotic cells forming the nuclear envelope. From this core, multiple ER branches detach to reach the whole cell in a network composed by sheets and tubules. The former are a cisternae-like structures covered with ribosomes for synthesis and folding of membrane, luminal and secreted proteins; the tubules spread in all the cytosol, constitute the 'smooth ER' because they lack ribosomes, and form extensive contacts with all other organelles and the PM (Phillips and Voeltz, 2015). In yeast, 40% of the PM is reached by ER that flattens at the periphery of the cell in the compartment called cortical ER (cER). ER contact sites have been originally visualised by Bernhard and Rouillier and Porter and Palade (Porter and Palade, 1957; Bernhard and Rouiller, 1956), but generally ignored because of the ER network is widely distributed throughout the cell. Also in biochemical purification of organelles, co-purified ER was mistakenly considered ER membrane as a contaminant of purification (Holthuis and Levine, 2005; Henne et al., 2015a). In this section, first I will focus in more detail on ER-PM contact sites describing the known families of proteins which localise to these junctions and explaining their role in tethering and exchanging ions or lipids between the membranes. Secondly, I will describe mechanisms of lipid counter-transport operated by some members of the OSBP-related protein (ORP) family and Retinal degeneration B-α (RdgBα). These LTPs are localised at the contact sites of the ER with the PM in the case of ORP5/8, RdgBα and Osh3p (Tong et al., 2013; Chung et al., 2015; Yadav et al., 2015), and also the *trans*-Golgi network in the case of OSBP (de Saint-Jean et al., 2011; Mesmin et al., 2013).

1.5.1. ER – plasma membrane contacts

In the cell new contact sites are continuously being described, but the ER-PM MCSs are probably the best defined. Different protein families have been described as important components for tethering and/or functioning at ER-PM junctions (Table 1.2).

VAPs/Scs2

Vesicle associated membrane protein (VAMP)-associated proteins (VAPs) are composed of a seven beta-strand globular domain of the major sperm protein (MSP) family (120-140 aa), a linker region (about 100 aa) forming a coiled coil in some species, and an ER-anchored C-terminal TMH (Murphy and Levine, 2016). Highly conserved residues in the MSP domain are necessary for the binding of proteins containing the FFAT motif. Three families of LTPs contain FFAT motifs: oxysterol binding protein (OSBP)-related proteins (ORPs), ceramide transfer protein (CERT/StARD11), and retinal degeneration-B (RdgBα/Nir1-3/PITPNM) (Loewen et al., 2003). These interactions are necessary for VAP-mediated ER-PM tethering. In fact, in many LTPs there is a typical co-occurrence of both FFAT motifs and other PM targeting domains, such as the PH domains of OSBP and CERT. VAP has been named for its interaction with SNARE protein VAMP (Skehel et al., 1995), but the molecular basis for this interaction has not been established and, despite the name, VAPs do not seem to be involved in membrane fusion events (Murphy and Levine, 2016).

STIM1/Orai1

See Section 1.4.1 for more information on STIM1/Orai1 interaction and coupling at ER-PM contact sites for the efficient refilling of ER Ca^{2+} store.

Junctophilins

As mentioned in Section 1.4.1, the four mammalian junctophilins are sarcoplasmic reticulum integral membrane proteins with N-terminal membrane occupation and recognition nexus (MORN) domains which bind lipids such as PA. Junctophilins are necessary for functional SR-PM junctions in contractile

cells forming an extended filamentous structure of about 15 nm that extends between membranes (Bennett et al., 2013).

Ist2p

These proteins are Ca^{2+}-activated Cl^- channels with 8 TMHs anchored in the ER. Both mammalian and yeast homologues contain a C-terminal polybasic region (PBR) that directly binds anionic lipids enriched on the PM inner leaflet, such as PS and phosphoinositides (Manford et al., 2012; Wolf et al., 2012).

E-Syts/Tcb

Yeast Tricalbins (Tcb1p, Tcb2p, and Tcb3p) are highly conserved and they share the same domain organisation as the three human extended synaptotagmins (E-Syt1, E-Syt2, and E-Syt3) (Min et al., 2007; Manford et al., 2012). They all have a U-turn 'hairpin' element that anchors them into the ER membrane (Giordano et al., 2013; Chang et al., 2013), followed by a synaptotagmin-like mitochondrial lipid binding protein (SMP) domain (Toulmay and Prinz, 2012; Lee and Hong, 2006). The SMP domain is conserved throughout evolution, it appears on LTPs exclusively localised to contact sites, and it belongs to the TULIP superfamily (Table 1.2) (Kopec et al., 2010). The members of the tubular lipid-binding (TULIP) superfamily share the same structural module composed of six β-strands and three α-helices arranged to form a barrel: this hydrophobic groove is open at the extremities and allows sliding of lipid acyl chains inside with headgroup facing outside (Schauder et al., 2014; Reinisch and De Camilli, 2015). The C-terminal portions of the E-Syts/Tcbs are more similar to other synaptotagmins, possessing numerous C2 domains able to bind Ca^{2+} ions and phosphoinositides such as $PI(4,5)P_2$ (Creutz et al., 2004; Schulz et al., 2009). E-Syt1 can localise to ER-PM contacts in response of cytosolic Ca^{2+} increase (Giordano et al., 2013; Chang et al., 2013). Their tethering function is proven by the evidence that the triple knock-out (TKO) of human E-Syts impairs the Ca^{2+}-induced apposition of the ER to the PM (Saheki et al., 2016). On the contrary, yeast Tcb triple knockout is not sufficient to significantly reduce the cER, unless other ER-PM tethers are simultaneously knocked-out (Manford et al., 2012). E-Syts-mediated

contacts are also the first evidence of different sub-domains at MCSs between the same couple of organelles: at the electron microscope, STIM1-Orai1-mediated subdomains are wider and distinct from the E-Syts-mediated MCSs, which responding to Ca^{2+} activation, are able to narrow from the 15-27 nm gap to ~15 nm (Fernández-Busnadiego et al., 2015; Idevall-Hagren et al., 2015) (see also Section "RdgBα/Nir2" below). The bioinformatics prediction of the SMP domain belonging to the TULIP superfamily of LTPs (Kopec et al., 2010; 2011), has first been confirmed by the crystal structure of E-Syt2: the protein is present as a dimer, which is able to bind non-specifically four phospholipids representative of the PM inner leaflet. Only the acyl chains interact with the hydrophobic residues lining the inner cavity of the TULIP domain, with the headgroup bulging out (Schauder et al., 2014). However, the SMP domain alone is not sufficient for lipid transfer: *in vitro* lipid transfer assays from donor to acceptor liposomes show that Ca^{2+} binding operated by the C2 domains of E-Syt1 is essential for the physical tethering of the donor and acceptor compartments and for the activation of non-specific phospholipid transfer (Yu et al., 2016; Saheki et al., 2016). Consistent with the *in vitro* observations, endogenous E-Syt1 in HeLa cells is pan-localised to ER and moves to ER-PM contacts upon drug-induced cytosolic Ca^{2+} elevation (Giordano et al., 2013). The E-Syts TKO cell line does not show steady state variations in major glycerophospholipid levels, but they exhibit a prolonged presence of DAG on the cytoplasmic leaflet after PLC activation, which indicates a link of LTPs activity to rapid signalling events (Saheki et al., 2016).

Furthermore, their mechanism of action could give a clue to explain how acute changes in lipid composition in one organelle (in this case the PM) originated from different reasons (signalling responses, trafficking events), can be rapidly ($t_{1/2}$ of seconds), locally (at MCSs) and specifically (single lipid molecules or a single lipid class) brought back to equilibrium by the activity of LTPs.

ORP5/8

OSBP-related proteins are a conserved family of sterol and phospholipid binding proteins. They all share a lipid binding domain called OSBP-related

domain, which is able to bind PI4P and another lipid, often (but not always sterol). For ORP5/8 the second lipid is PS possibly with sterol as a third ligand (Du et al., 2011), in a mutually exclusive way (Mesmin et al., 2013). Yeast OSBP-homologue 6 (Osh6p), was the first to be shown to transfer PS (Maeda et al., 2013). Later, Osh6p/7p and their human homologues ORP5/8 have all been localised at ER-PM contacts where they catalyse the counter transport of PS and PI4P (Chung et al., 2015; Moser von Filseck et al., 2015a). See also Sections 1.5.2 and 1.7.

RdgBα/Nir2

Another protein localised at ER-PM contact sites is Nir2. Human Nir2 and its *Drosophila melanogaster* homologue RdgBα, have been shown to weakly transfer PA, in addition to its long known and robust ability to transfer PI, and (to a lesser extent) PC (Yadav et al., 2015). See also section 1.5.2, RdgBα/Nir2.

Contact sites sub-domains at ER-PM junctions

The same organelle pair could be tethered by different mediators so to define MCSs sub-domains. This is particularly evident for ER-PM junctions where a local difference in the proteins involved in the physical tethering and function has been shown in multiple cases.

For example, as already mentioned, Sec22b is an ER-resident SNARE closely apposed to the PM SNARE syntaxin1. Petkovic and colleagues identified a role for Sec22b in ER-PM bridging and in non-vesicular lipid transfer important for neuronal PM expansion (Petkovic et al., 2014). Just like E-Syts ER-PM contacts, also the contacts mediated by Sec22b are functionally different and structurally independent from the STIM1-Orai1-mediated (Giordano et al., 2013; Petkovic et al., 2014). Even if neither E-Syts nor Sec22b are required for SOCE, it is possible that also the contacts with these two proteins have a functional and structural independence from each other.

As these examples have shown, different contact sites between the same pair of organelles could be tethered and be the platform for the activity of different molecular events. The same concept could be extended to other MCSs

Table 1.2 Proteins at ER-PM junctions

	Protein		Tethering elements		Functions	References
	Yeast	Human	ER	PM		
Tcb/E-Syt	Tcb1p	E-Syt1	U-turn	Anionic lipid binding ($PI4,5P_2$) Multiple C2 domains (some needing Ca^{2+})	TKO human E-Syts → >50% less MCSs TULIP domain (phospholipid binding)	(Giordano et al., 2013; Yu et al., 2016; Saheki et al., 2016; Creutz et al., 2004; Manford et al., 2012)
	Tcb2p	E-Syt2				
	Tcb3p	E-Syt3				
VAPs	Scs2p	VAP-A	1 TMH	Anionic lipid binding MSP domain (FFAT motif binding)	*scs2*Δ → 50% less cER VAP-B ko → 30% less ER-mito contacts bind >100 partners (50% with FFAT motifs)	(Loewen et al., 2007; Stoica et al., 2014; Huttlin et al., 2015; Murphy and Levine, 2016)
	Scs22p	VAP-B				
	Ist2p	*Tmem16A*	8 TMHs	Anionic lipid binding (PBR binds PIP_2 on PM)	*ist2*Δ → 80% less close contacts (≤30 nm) and 0-30% less cER	(Wolf et al., 2012; Manford et al., 2012)
STIM1 Orai1	-	STIM1	1 TMH	Anionic lipid binding (C-term PBR), Orai1 binding	ER luminal Ca^{2+} sensor (EF hand domain)	(Wu et al., 2006; Zhou et al., 2013)
	-	Orai1	STIM1 binding	4 TMHs hexamers form Ca^{2+} channel	Store-operated Ca^{2+} channel	
PITP	-	Nir2	VAP binding (via FFAT motif)	DDHD domain (*PI4P interaction?*) LNS2 domain (*PA interaction?*)	PITP domain, PA/PI counter-transport	(Yadav et al., 2015; Kim et al., 2015; Peretti et al., 2008)
Junctophilin	-	Junctophilin-1	1 TMH	Multiple MORN motifs	Expressed in contractile cells Localised at triad and dyad junctions Deletion → less ER-PM contacts (in myocyte) Some overlap in function (JP-3 and JP-4)	(Ma et al., 2006; Takeshima et al., 2015; Woo et al., 2016)
	-	Junctophilin-2				
	-	Junctophilin-3				
	-	Junctophilin-4				
ORPs	Osh3p/4p	OSBP	Scs/VAP binding (via FFAT motif)	PI4P binding via PH domain	ORD domain binds PI4P and sterol	(Tong et al., 2013; Weber-Boyvat et al., 2015)
	Osh6p/7p	ORP5/8	1 TMH (ORP5/8)	PI4P binding via PH domain	PS/PI4P counter-transport	(Chung et al., 2015; Moser von Filseck et al., 2015a)
	-	Sec22b	1 TMH	Interaction with PM syntaxins	Non-fusogenic SNARE bridge (neurites PM expansion)	(Petkovic et al., 2014)

1.5.2. Lipid counterflows at ER contacts

One of the unresolved questions in lipid distribution is whether LTPs described in literature actually move the lipids or if they sense the lipids, to turn on a pathway that involves the lipid moving through some means that is physically separate from the hydrophobic pocket of the LTP. Two linked questions are (i) how LTPs ever do work, and (ii) whether LTPs are implicated in any of the asymmetric distributions of lipids that are seen in living cells. Two different families of LTPs have now produced roughly the same answer to these two questions. The two LTPs types involved bind two lipids (or more) and they are recruited to contacts where they swap their two lipid substrates in different directions. The idea is that the same domain takes one lipid cargo one way and the other cargo the other. Only one of the halves of this round trip needs to be powered energetically for both to take place. In fact, if enough energy is used up in powering one half, then the other can be forced to work even when unfavourable (*i.e.* against gradient).

The two LTPs implicated in such counter-currents are (i) the entire family of oxysterol-binding protein (OSBP)-related proteins (ORPs), and (ii) the subfamily of PI transfer proteins (PITPs) related to Retinal degeneration type B in flies (RdgB, also called Nir in mammals) (Figure 1.6).

OSBP-Related Proteins (ORPs)

All oxysterol-binding protein (OSBP) and its related proteins (ORPs) in mammals and the seven homologues in Saccharomyces cerevisiae (Osh1-7) share a conserved lipid binding domain called OSBP-related domain (ORD) (Olkkonen, 2015). The oxysterol-binding proteins is a 400 residues fold originally named after its ability to bind sterols (Dawson et al., 1989; Ridgway et al., 1992). The single specificity of the ORD domain was first questioned when Osh4p in yeast was shown to operate a counter transport of ergosterol for PI4P between ER and trans-Golgi membranes *in vitro* and in structural studies (de Saint-Jean et al., 2011). The same group also described the same four-steps cycle of counter-exchange of PI4P/sterol at ER-Golgi interface by OSBP *in vitro* and in vivo (Mesmin et al., 2013). Another evidence of a non-

sterol specificity of ORD came with the description of Osh6p/Osh7p (Maeda et al., 2013; Moser von Filseck et al., 2015b), and ORP5/ORP8 (Chung et al., 2015) localised between ER and PM contact sites in yeast and mammals, respectively. First, Osh6p was shown to have a specificity also for phosphatidylserine (PS) (Maeda et al., 2013), subsequently this unexpected specificity was further characterised with the description of the concomitant counter transport of PI4P to the ER that is believed to fuel PS transport to the PM against gradient (Moser von Filseck et al., 2015a). In mammalian cells, ORP5 and ORP8 are ER-transmembrane proteins that target contact sites via their PH domain binding PI4P on the PM (Chung et al., 2015). Similarly to yeast Osh6p/Osh7p, mammalian ORP5/ORP8 forward transport of PS would be driven by the counter transport of PI4P (generated at the PM consuming ATP) to the ER (Moser von Filseck et al., 2015a; Chung et al., 2015). PI4P would then be dephosphorylated to PI by the conserved ER-integral phosphatase Sac1 acting in *cis* (Figure 1.6), even if it has been proposed that it can also act in *trans* (Stefan et al., 2011). It is possible that the pool of PI4P that powers such mechanisms is synthesized specifically for this purpose, separate from a pool that acts as a precursor to $PI(4,5)P_2$ (Hammond et al., 2012).

RdgBα/Nir2

The PI transfer protein in *Drosophila melanogaster*, RdgBα and its human homologue Nir2, have been shown to weakly transfer PA, in addition to its long known and robust ability to transfer PI, and (to a lesser extent) PC (Figure 1.6). This is also a good example of LTPs with three lipid specificities (see Section 1.7). To explain the interplay among the transport of the three different phospholipids, PLC hydrolysis will increase PM levels of PA, and PI will be consumed at the PM for $PI(4,5)P_2$ re-synthesis. This may lead to PA going backwards to the ER where it is used by ER-resident enzymes to re-synthesise PI, which could become the preferential lipid going forward to resupply the PM pool of $PI(4,5)P_2$ precursors. In this scenario, PC could be the counter-lipid now going backward, since PA levels are normally very low. The advantage of

having this complexity could be to allow PC gradients to drive PI or PA flows under some circumstances, and to allow PC or PC-related pseudosubstrates (e.g. lysoPC, lysoPA) to inhibit PI/PA traffic completely under other circumstance, similar to the effect of 25-hydroxycholesterol (25-HC) on ORPs.

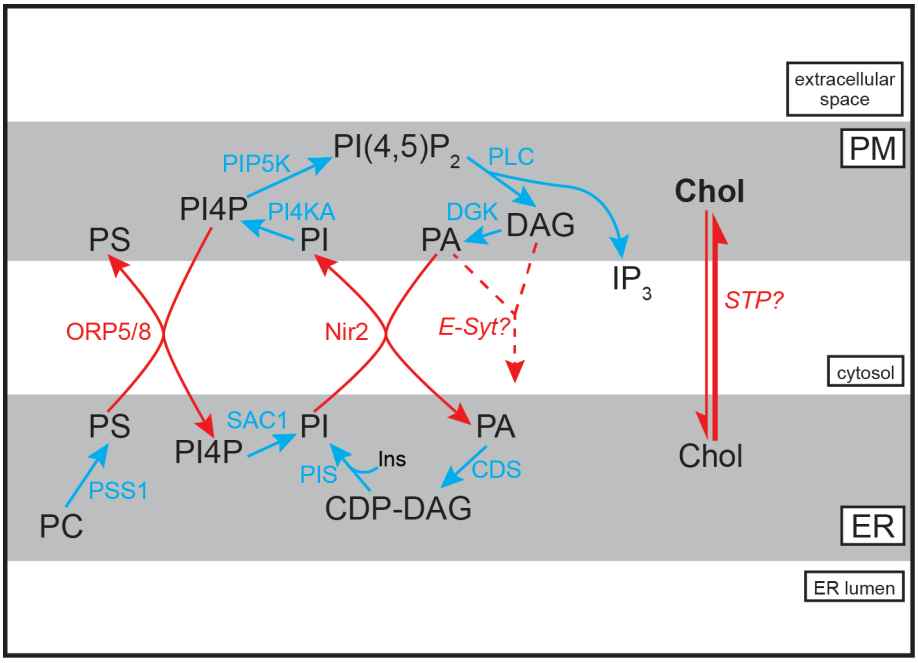

Figure 1.6 Mechanisms of lipid counterflows at ER-PM contact sites

Proposed action of lipid transfer proteins (red arrows) in enzymatic and signalling events (blue arrows) at ER-PM contact sites. The circular network is initiated by PLC-mefiated hydrolysis of $PI(4,5)P_2$ to make diacylglycerol (DAG) in the PM and release of IP_3. Rapid and intense signalling can only be maintained by resynthesis of $PI(4,5)P_2$ by the pathway DAG → PA → CDP-DAG + Ins → PI → PI4P → $PI(4,5)P_2$. Three enzymes of these five-step reaction are on the PM: DAG kinase (DGK), PI4-kinase (PI4KA), and PIP5-kinase (PIP5K). Two enzymes are in the ER: CDP-DAG synthase (CDS) and PI synthase (PIS). The lipid binding domain of Nir2 transfers both PA from PM to ER, and PI in the opposite direction. In parallel, other LTPs operate lipid transport between ER and PM. For example, ORP5/8 operate a countertransport of PS to the PM and PI4P back to the ER, where it is immediately processed by SAC1 phosphatase. Extendend synaptotagmins (E-Syts) are involved in the regulation of plasma membrane DAG dynamics during PLC activation as well, but their mechanism and (phospho)lipid specificity will have to be further clarified. The transport of sterol between ER (low concentration) and PM (high concentration) is thought to be operated by a yet unidentified sterol transfer protein (STP).

1.6. Molecular detours at contact sites

Recent studies showed that almost every organelle can contact any other organelle for functional exchange of lipids that are made and consumed asymmetrically between the donor and acceptor membranes, respectively. Virtually, all conceivable pairs could exist in nature with some of them forming or expanding only in non-physiological conditions arisen from stress, genetic knockout of tethering complexes or drug exposure. The ER is not the central hub for organelle communication: direct contacts between organelles can arise also without the ER being involved (Gatta and Levine, *submitted*).

The current section will give an example of how the cell can remodel the contacts architecture and form molecular detours in response to stress conditions as in the case of the cross-talk between ERMES and vCLAMPs (for vaCuoLe And Mitochondria Patch).

Mitochondria – vacuole/lysosome

An early review of MCSs stressed that the ER is the hub of lipid biosynthesis, and suggested that so long as all organelles form contacts with the ER, they will be indirectly in contact with each other (Levine, 2004). However, that model has now been shown to be oversimplified, because many organelle pairs form contacts. The first studies to de-emphasise the role of ER in interorganelle contacts, were related to the study of contacts called vCLAMP (for vaCuoLe And Mitochondria Patch), which form between mitochondria and the lysosome-like vacuole in yeast (Elbaz-Alon et al., 2014; Hönscher et al., 2014). Mitochondria depend on the import of lipid primarily made into the ER and sent to mitochondria even though they are not linked to the vesicular pathway. ER contacts mitochondria outer membrane via multiple protein bridges (Prinz, 2014). One such is the ERMES complex (Kornmann et al., 2009). An ERMES delete strain is still viable and it does not show a different lipid profile (Nguyen et al., 2012), although Mmm1 and Mdm12 have been shown to form a tubular structure between ER and mitochondria with a hydrophobic channel that binds phosphatidylcholine (AhYoung et al., 2015). Therefore, the cell is able to adapt to the absence of direct contacts between

ER and mitochondria by expanding the vacuole-mitochondria contacts instead, to maintain the exchange of essential ER-derived lipids between untethered organelles.

Two groups reported in parallel the presence of an alternative route for the transport of lipids to mitochondria bypassing ERMES (Elbaz-Alon et al., 2014; Hönscher et al., 2014). Using two different approaches, specifically a high-throughput screening for extended ERMES foci per cell (Elbaz-Alon et al., 2014) and a candidate gene overexpression screen (Hönscher et al., 2014), they both identified a protein of the HOmotypic fusion and vacuole Protein Sorting (HOPS) tethering machinery, Vps39 (also called Vam6). All the components of the HOPS complex are involved in vacuolar fusion, but only Vps39 and Ypt7 appeared to be important for vCLAMP formation. As I mentioned above, the apparent redundancy of ERMES and vCLAMP function could be explained by observing their complementarity in special conditions: the final aim of lipid import to mitochondria will be reached either directly via ERMES (especially during respiratory growth on glycerol when mitochondria number and activity increase) or via a detour through the vacuolar membrane (when ERMES is knocked-out).

Furthermore, lack of conservation of ERMES throughout metazoans suggests that the role of the complex in interorganelle lipid exchange, mitochondrial dynamics, and mitochondrial DNA maintenance can be bypassed by other means. The Vacuolar protein sorting 13 (Vps13) is a vacuolar membrane protein conserved in all eukaryotes, and localised at vauole-mitochondria or vacuole-nucleus, depending on growth conditions. The fact that combined loss of VPS13 and ERMES causes cell death, emphasises the redundancy of the two contacts and the growth-condition regulation of the organelle networks (Lang et al., 2015)

1.7. Multiple lipid specificities

A full understanding of the OSBP family requires detailed knowledge of their transfer specificities: OSBP itself and the most closely related homologues solubilise cholesterol (Charman et al., 2014; Liu and Ridgway, 2014), as well as its oxygenated derivative 25-HC, which is a water-soluble derivative of cholesterol that inhibits all other lipid binding. Other homologues such as Osh6p and Osh7p when extracted from yeast contain not sterol but phosphatidylserine (PS), which interacts with four key hydrophobic residues in the lid (Maeda et al., 2013). ORP5/8 are the closest human homologues to Osh6/7p, and they also solubilise PS, as does the more distant ORP10 (and presumably ORP11) (Maeda et al., 2013), ORP9 (Liu and Ridgway, 2014), and Osh4p (Raychaudhuri et al., 2006). Previously, ORP5 has been proposed to be involved with NPC1 in cholesterol transfer from lysosome to ER at these contact sites (Du et al., 2011). Consistently with Maeda et al., PS and PI4P were identified by mass spectrometry as lipid ligands in the ORD of ORP5/8 and shown to be transported at ER-PM contacts in different directions (Chung et al., 2015).

With testing of more homologues, binding to PS and PI4P appears to be universal, although PS binding is weaker when compared to cholesterol binding in ORP9 (Liu and Ridgway, 2014) and Osh4p (Raychaudhuri et al., 2006). ORP5 also bind/transfer sterol and act at other MCS. Local alignment of the lid regions of different OSBP homologues shows that the four hydrophobic residues implicated in PS binding are widely conserved; among the yeast (7 genes) and man (12 genes) at these four sites (i.e. 76 residues in total) the only non-hydrophobic amino acids are an alanine in Osh6/7p and a serine in Osh3p. Thus, variation between OSBP homologs may mostly affect affinity for sterol, which is undetectable levels in some cases (Tong et al., 2013), while PS binding is less variable (Liu and Ridgway, 2014), while all bind PI4P using the ORD conserved motif corresponding to EQVSHHPP in OSBP.

The affinities for three different membrane lipids (PI4P, cholesterol and PS) of the ORD domains is at the base of their involvement in counter-transport

mechanisms that give directionality and the energetic basis for the transfer. A three-way competition implies that there is no fixed exchange pattern, and it could be possible that the major lipid (such as sterol) can modulate the overall reaction by switching side.

A fold that has diverged considerably from a single common ancestor is the Steroidogenic acute regulatory lipid-transfer (StART) domain in plants, fungi and animals which binds sterols, sphingolipids and phospholipids (Tsujishita and Hurley, 2000; Hanada et al., 2003; Kanno et al., 2007). An important observation is that a single StART domain is capable of a broad range of interactions with previously unidentified lipid ligands (Schrick et al., 2014). For example, immunoisolated StART domain from StARD1 was found to bind cholesterol esters, ceramide, sphingomyelin, phosphatidylserine, phosphatidylcholine and diacylglycerol in a lipidomics approach (Schrick et al., 2014).

1.8. Amphotericin B

The exposure of mammalian cells to the sterol-sequestering antifungal drug AmB, allowed the discovery of the lysosome-peroxisome contact site (Chu et al., 2015). AmB is a powerful tool to disrupt sterol homeostasis and to increase cellular stress when sensitive steps in sterol biosynthesis, regulation and traffic are involved (Barker et al., 2004). In this section, I will describe the current knowledge of AmB mechanisms of action and I will direct the explanation towards their contribution in the characterization of genetic lesions that make fungi sensitive to AmB.

Evolution has produced a number of fungal species supposed to be in a range of 1.5 to 5.1 million (Blackwell, 2011). Among these, about 300 species can cause infections in humans. The most widespread human mycoses include candidiasis, produced most commonly by *C. albicans* and *C. glabrata*; aspergillosis, infections caused by a species of the genus *Aspergillus*, such as *A. terreus* and *A. fumigatus*; and cryptococcosis, caused by one of the species *C. neoformans* and *C. gattii*. Usually mycoses are opportunistic and they can successfully infect a patient only if the immune response is weakened by other factors such as viral infections (AIDS), immunosuppressive therapies (chemotherapy) or some metabolic disease (diabetes) (Monk and Goffeau, 2008).

In recent years the rise of life-threatening fungal infections has grown in parallel with the increase in fungal multidrug resistance (MDR) towards almost all antifungal drugs used in clinically (Mora-Duarte et al., 2002). Interestingly, amphotericin B (AmB), a polyene small molecule discovered in 1955 (Oura et al., 1955), is still the gold standard treatment and the last line of defence for all systemic fungal infections, with almost no development of MDR (Vincent et al., 2013). The major drawbacks of AmB therapy resides in a dose-limiting toxicity and its low therapeutic index (Mora-Duarte et al., 2002). The mechanism of antifungal action of AmB is resistance-refractory, but its pharmacodynamics is not well understood.

One of the first mechanisms to be characterised (Figure 1.7) was the capability to form transmembrane channels with consequent leakage of ions and small molecules from the cytosol (Andreoli and Monahan, 1968; Ermishkin et al., 1976). This paradigm lasted until recently when new studies synthesized analogues with functional group deletions to prove that the toxic effects are separate from the fungal membrane permeabilisation *per se* (Palacios et al., 2007; 2011). Other polyene anitifungals, such as natamycin, are still toxic despite their inability to form intermembrane channels (Welscher et al., 2010). The specific removal of hydroxyl groups important for the formation of the channel does not decrease AmB toxicity (Volmer et al., 2010). Indeed what seems essential for killing yeast is the simple binding of ergosterol (Gray et al., 2012). Another proposed mechanism involves pro-oxidative membrane damage caused by a well-documented AmB redox activity, possibly indirectly induced at the transcriptional level (Belenky et al., 2013; Mesa-Arango et al., 2014). Finally, the last mechanism to be proposed was the sterol sponge model: in this scenario, while producing intermembrane channels and causing membrane oxidative damages, AmB forms large extramembranous aggregates and kills simply by extracting ergosterol from lipid bilayers, just like a cyclodextrin (Anderson et al., 2014). This latest model does not require the others: AmB binds ergosterol and forms transmembrane channels, but the extramembranous aggregates are the main cause for the ergosterol depletion from the membrane of fungi. This explains also the lack of AmB-resistant fungi: AmB aggregates extract ergosterol from the membrane causing a perturbation on all the cellular processes that depend on membrane sterol.

AmB promiscuous mechanisms of action provide fewer routes of evasion for the emergence of resistant mutants. However, usually this comes at the costs of severe adverse effects in the patient due to strong off-target effects: the therapeutic window is related to AmB slightly higher affinity towards ergosterol of fungal cells than cholesterol of human cells. New AmB derivatives with increased sterols selectivity and still able to form the extracellular sterol sponge, show decreased dose-limiting toxicity and emergence of resistance. The few *Candida* strains developing resistance to the new AmB compounds

contained mutations into two genes involved in ergosterol synthesis ERG2 and ERG6, and in ORF19.7285, an uncharacterised WD40 repeat protein (conserved throughout fungi, YLR102c in *S. cerevisiae*). But the acquisition of resistance is always paired to a reduction of pathogenicity (Davis et al., 2015).

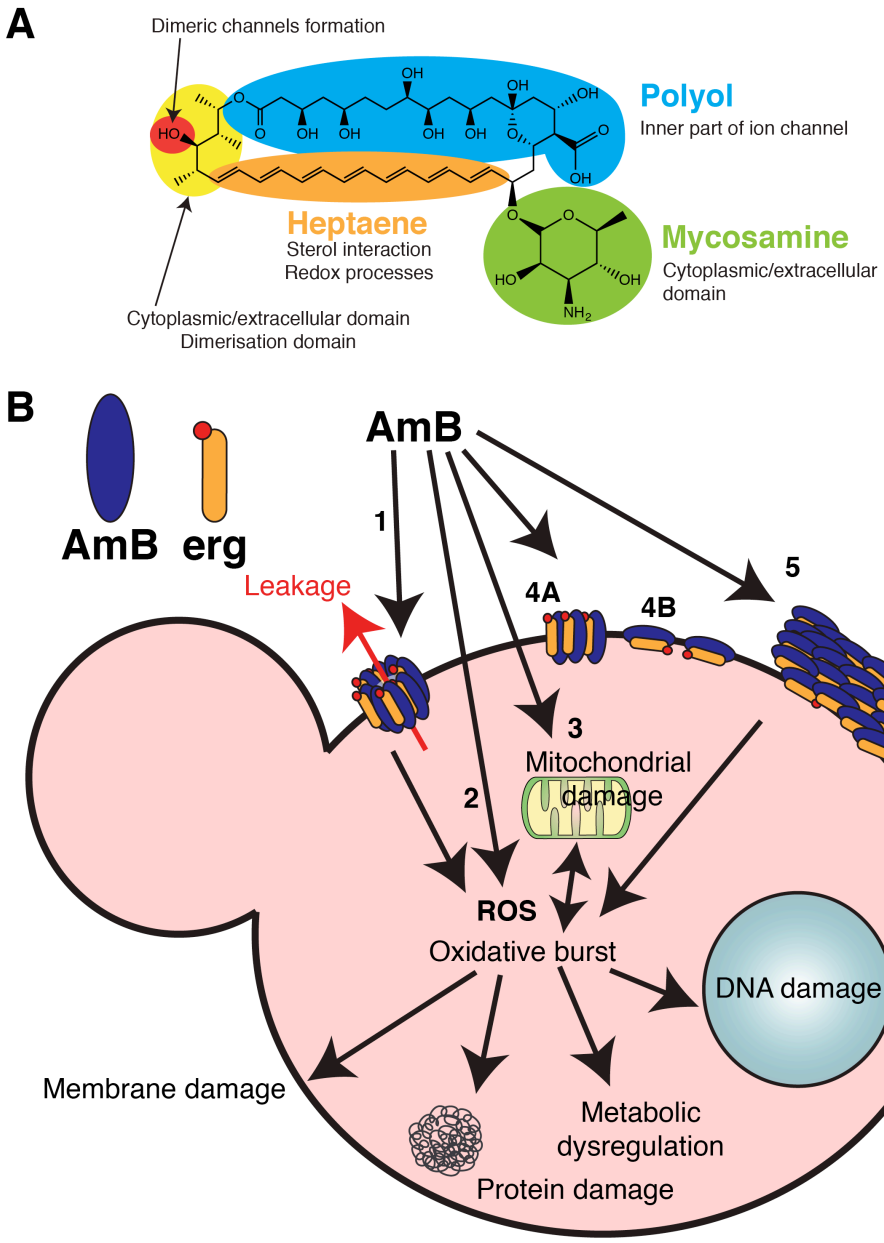

Figure 1.7 Mechanisms of action of Amphotericin B on fungal cells

(**A**) Proposed relationships between AmB structure and mechanisms of action. (**B**) Schematic representation of a yeast cell with the observed mechanisms of action of Amphotericin B (AmB) antifungal drug. AmB exerts its action at different cellular levels. (**1**) The first mechanism to be visualised was the pore-forming activity: AmB-ergosterol complexes distribute onto the PM to form transmembrane pores causing leakage of ions and other cytosolic material. (**2**) The second mechanism to be identified was the active pro-oxidant activity of AmB with increase of intracellular

reactive oxygen species (ROS) and consequent oxidative burst causing damages to membranes, proteins, and DNA in the nucleus and metabolic dysregulation. (**3**) Strictly linked to the ROS production, the mitochondrial damage could be caused also by a direct influence of AmB on mitochondrial activity again contributing to oxidative burst. (**4**) Because changes in the chemical structure of AmB to exclude the pore-forming activity, do not decrease its efficacy, ergosterol binding property alone is sufficient for the killing of the fungal cell (Gray et al., 2012). Ergosterol-binding can occur via simple ergosterol sequestration in the membrane (4A) or following the 'surface adsorption model' (4B) (Mouri et al., 2008). (**5**) In the last proposed 'sterol sponge model', AmB works in large extramembranous aggregates which extract ergosterol from lipid bilayers like cyclodextrins (Anderson et al., 2014).

1.9. Structural studies of LTPs

Structural biology merges biochemistry and molecular biology techniques to study the three dimensional structure of proteins and more specifically how their architectural features are linked to their function.

Proteins are chains of amino acids linked by a peptide bond. The conformation of this backbone depends on (i) the rotation of the chain around the C_α atom, also known as ψ (C_α-CO) and ϕ (C_α-NH) dihedral angles (Ramachandran et al., 1963), (ii) the positive and negative charges given by free CO groups (acting as hydrogen bond acceptor) and NH groups (acting as hydrogen bond donor), (iii) the specificities of the side chains. There are twenty-one amino acids all possessing different side chains: for example, glycine is the smallest residue with only a hydrogen atom as side chain and its presence increases the local flexibility. Other side chains give positive or negative charges, contributing to polarity or increasing the hydrophobicity. The protein sequence, or primary structure, determines the secondary structure: the alternation of modular structural elements (*i.e.* α-helices, β-sheets, loops), which form to neutralise the polar groups on each amino acids and to reduce the energetic state of the protein conformation (Mount, 2004).

From an evolutionary point of view, structure is more conserved than sequence for the preservation of protein function (Rychlewski et al., 1998). This concept is the foundation of protein structure prediction bioinformatics: even proteins with remote homology have similar three dimensional structure that underpins a conserved function (Kinch and Grishin, 2002). This feature can be used for homology modelling of a domain with unknown structure or for the identification of distant homologues. After the prediction of a domain and its homology model, the final conformation is confirmed with a classic technique of structural biology, such as X-ray crystallography and nuclear magnetic resonance (NMR) spectroscopy. In the field of LTPs, the use of sensitive sequence comparison tools for the prediction of remote homologues allowed the inclusion of the SMP domain, initially hypothesised to be involved in different membrane-associated functions (Lee and Hong, 2006), into the

wider TULIP superfamily of LTPs (Kopec et al., 2010). More recently, the bioinformatics prediction was confirmed by the crystal structure of one member of the human E-Syt protein family (Schauder et al., 2014).

For my project, our group attempted both techniques, but I focussed on biomolecular NMR spectroscopy to confirm the homology model and visualise the architectural differences of the protein states. In following paragraphs of this section I will compare the NMR and X-ray crystallography approaches highlighting advances and limitations of both, and I will focus on protein NMR to explain its basic principles. Next, I will describe the process of backbone assignment of protein NMR spectra using multidimensional acquisitions.

1.9.1. Biomolecular NMR

Both X-ray crystallography and nuclear magnetic resonance (NMR) spectroscopy study molecular structure at the atomic level. The former is based on the interpretation of the diffraction pattern originated by a beam of X-rays hitting a protein crystal, the latter exploits the magnetic properties of specific nuclei of a protein in solution to record their chemical kinetics and their behaviour in context with the surroundings atoms. Both techniques have advantages and disadvantages (summarised in Table 1.3).

The physical basis of the NMR method is the phenomenon of nuclear magnetic resonance[1] and it can offer detailed information about the structure and the dynamics of the protein. Broken down to its principles, the NMR spectrometer consists of different components:

- A homogeneous, intense and stable magnetic field.
- A radio frequency transmitter to deliver short pulses originated by a pulse programmer to produce precise and timely pulses.

[1] The meaning of underlined keywords in this section is presented at the end of the NMR introduction (page 92).

- A probe where the sample is placed, in the middle of the magnetic field and next to a coil that sends the pulses and record the relaxations.
- The receiver, digitizer and computer to amplify, convert, and process the NMR signals, respectively.

X-ray crystallography	NMR spectroscopy
Protein crystal	Protein in solution
Frozen structure	Dynamic structural changes are visible
Higher resolving power	Lower resolving power
Protein of any size (> 200 kDa)	Small protein (< 50 kDa)
Long screening and optimisation of sample for crystallisation	Relatively short preparation (protein requires isotopic labelling)
Systematic analysis of a good crystallised sample	Several types of information from several types of acquisition
Short time for data processing	Long time for data analysis

Table 1.3 Comparison of X-ray crystallography and biomolecular NMR.

NMR gives several types of information from many different types of experiments (the different series of radiofrequency pulses). The long analysis of the data obtained from this approach could ultimately provide angles, distances, coupling constants, chemical shifts of the different atoms related to their surroundings. The resolution of an NMR acquisition is the function of the strength of the magnetic field. All the information becomes too complicated to compute into the final structure determination for higher molecular weight molecules. This is the reason why NMR has less resolving power than X-ray crystallography. X-ray crystallography requires a short time for data processing but a long time to find the optimal conditions to obtain the protein crystal.

1.9.2. Basic NMR spectroscopy

The use of NMR is based on the recordings of the magnetic properties of atoms possessing spin, also called NMR active nuclei. When placed into a magnetic field M_0, NMR active nuclei (such as ^{1}H, ^{13}C, and ^{15}N) absorb electromagnetic radiation at an isotope-specific frequency and align themselves with the direction of the M_0 (spin polarisation). The sample is then excited with a radio frequency (RF) pulse whose parameters (power and width in μs) determine the rotation angle of the spin. The relaxation of the spin back to the direction of the M_0 gives a Free Induction Decay (FID) that is recorded by the instrument for a set acquisition time. A Fourier Transform (FT) extracts the frequency domain from the time-domain spectrum of the FID. To improve

the FID signal-to-noise ratio, the acquisitions are repeated several times and averaged. NMR-active nuclei dispose in the M_0 in two spin states, both with the same direction as M_0, but with different sense: the most populated state has the same sense as the M_0 and sets at lower energy level than the spin with the opposite sense. The energy difference between the two spin states is proportional to M_0 and the magnetic moment. Same atoms have the same magnetic moment, but for atoms in a molecule their relaxation is not identical. These differences depend on the dissimilar electron environment of the proton of interest. The electron environment differently 'shields' the protons from M_0 and these differences (chemical shift) are reported in part per million (ppm), relative to the reference signal of 4,4-dimethyl-4-silapentane-1-sulfonic acid (DSS). DSS is the accepted internal standard for calibrating NMR spectroscopy experiments because its nine identical methyl protons are highly shielded by the low electronegativity of the silicon. Different features of the chemical shift in one-dimensional (1D) spectra can provide information about the structure of simple molecules (*e.g.* small organic compounds): shape, width, area, intensity of each peak, and the observation of spin-spin coupling. The coupling originates from the interaction of different spin states of the same atom through the chemical bonds of the molecule, results in the splitting of NMR peaks, and (if undoubtedly interpretable) gives detailed insights into the connectivity (Cavanagh et al., 2010). The higher number of atoms of a protein molecule compared to a small organic compound makes these 1D spectra crowded with overlapping signals. Therefore, the first multidimensional approaches to be developed were the two-dimensional (2D) NMR techniques plotting the dimensions on two frequency axes. 2D experiments consist of four steps (Jeener et al., 1979; Wüthrich et al., 1982):

- preparation period, a series of RF pulses create magnetisation coherence,
- evolution period, time during which nuclear spins are allowed to freely precess with no RF pulses,
- mixing period, the magnetisation is manipulated by another series of RF puleses,

- detection period, recording of FID.

The two dimensions represent the two chemical shifts obtained changing the time variables of the evolution period and the detection period. Both are then converted to the frequency series using the FT. The intensity of the peak is indicated on the 2D plane using contour lines, similarly to topographic maps. A simple 2D experiment to evaluate the protein fingerprint is the Heteronuclear Single Quantum Correlation (HSQC). HSQC detects correlations between two different nuclei (typically ^{1}H and ^{15}N) separated by one chemical bond: each paired of nuclei coupled by a bond gives one peak, whose coordinates are the chemical shifts of the two atoms. The following step in structure determination requires annotation of the peaks visible in a set of spectra with the correspondent residues in the protein sequence.

1.9.3. Backbone assignment of protein NMR spectra

Before the optimisation of protocols for 2D NMR techniques in the late 1970s, the assignment process was based only on 1D NMR spectra and the assumption that the structure of the protein in solution is the same as the protein crystal (NMR experiments were mainly performed after structure determination with X-ray crystallography to study the structural changes in solution). The application of 2D NMR techniques for protein structural studies was possible thanks to the development of the sequential assignment methods (Jeener et al., 1979; Wüthrich et al., 1982), which require: (i) protein isotopic double labelling with ^{13}C and ^{15}N during protein production (Ikura et al., 1990), (ii) use of multiple programmed RF pulses to acquire different spectra (Marion et al., 1989; Messerle et al., 1989), and (iii) improved acquisition techniques, such as the Transverse Relaxation Optimised Spectroscopy (TROSY) (Pervushin et al., 1997). The TROSY experiment is designed to improve peak resolution in spectra of large protein (>15-20 kDa) by appropriate changes in the mixing period that ultimately reduce the faster relaxing resonance of the coupling (Fernández and Wider, 2003).

The protein fingerprint: two-dimensional ^{1}H-^{15}N HSQC

The first step to understand the feasibility of NMR technique for the protein of interest is the acquisition of a HSQC spectrum (Bodenhausen and Ruben, 1980). This spectrum shows the backbone amides: each peak arises from the one-bond ^{1}H-^{15}N coupling of ~95 Hz (Figure 1.8). The visible peaks represent HN correlations in the backbone amide groups and the side chains: the amide protons from all amino acids (except proline, Pro), and theoretically the side chain nitrogens of asparagine (Asn), arginine (Arg), glutamine (Gln), histidine (His), lysine (Lys) and tryptophan (Trp). However, in practice not all the side chains peaks are always visible: (i) Arg NH_{ε} and His NH_{ε} peaks have a chemical shift outside the region usually recorded (low ^{15}N chemical shift), (ii) Arg NH_{η} and Lys NH_{ζ} groups are usually folded unless the protein spectrum is recorded at pH < 5.0, (iii) Trp side chain NH_{ε} peaks have a chemical shift ~10 ppm, (iv) Asn and Gln side chain -NH_2 group peaks are generally localised in the top right quadrant of the spectrum and result in two peaks at the same nitrogen but different hydrogen ppm values.

The 2D HSQC uncovers if the protein gives NMR spectra of required quality or if further optimisation steps are required (by selecting different boundaries in the expression construct, or changing acquisition conditions such as pH, temperature, buffers) and acquisition parameters (adjustments to the instrument).

Triple resonance assignment method

The triple resonance assignment method requires uniformly (> 90%) ^{15}N and ^{13}C double-labelled protein. Different kinds of spectra can originate from this sample depending on the specific pulse sequence corresponding to the one-bond couplings between ^{1}H, ^{15}N and ^{13}C atoms and ranging from ~7 to ~140 Hz (Figure 1.8). The applied RF pulses correspond to the energy coupling to transfer the magnetisation along the chemical bond of interest (Figure 1.8). Therefore, a sequence of different pulses will be used in each 3D experiment

(Cavanagh et al., 2010). Triple resonance spectra contain the $^{1}H_{N}$, the ^{15}N, and the ^{13}C dimensions. The common way to visualise these spectra is to plot 2D $^{1}H_{N}$-^{13}C plane corresponding to a particular ^{15}N chemical shift. Each ^{15}N-plane contains only one or two peaks per residue (i.e. a specific $^{1}H_{N}$-^{13}C), so the 3D plot can be reduced to, so called, strips.

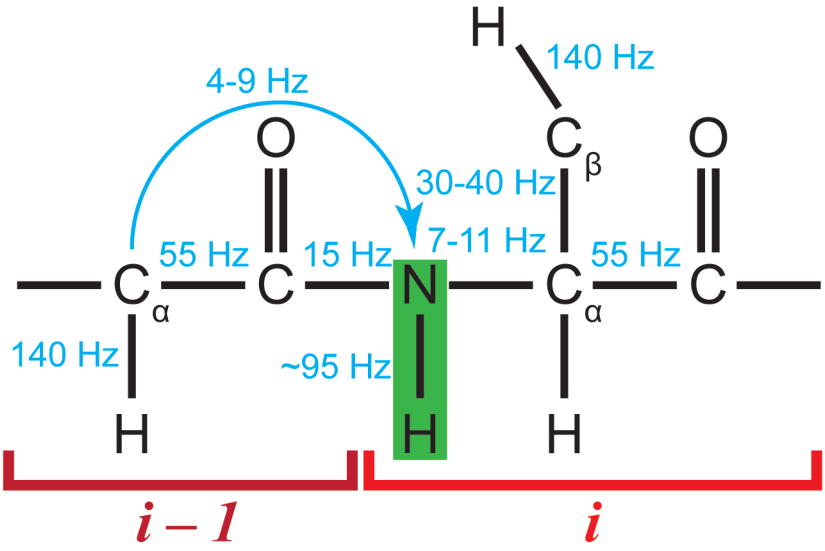

Figure 1.8 Energy couplings for triple resonance assignment

Schematic representation of the couplings between different nuclei important for triple resonance assignment. The radiofrequencies pulses (in blue) are levied to the protein solution to study the relaxation properties in many different experiments. According to the different pulses sequences, the spectra will show the recorded (i) and/or the previous (i–1) residues. The green shade is underneath the recorded NH signal. The only two-bond coupling shown is between the $C_{\alpha}(i\text{-}1)$ and the NH(i) and it falls in the range 4-9 Hz.

Triple resonance spectra correlate a backbone $^{1}H_{N}$–^{15}N pair (green shape in Figure 1.8) with one or more ^{13}C chemical shifts. The naming system for triple resonance experiments uses letters to underline correlated chemical shifts in the order they are excited during the radiofrequency pulse sequence. For example, in the 3D HNCO experiment, backbone $^{1}H_{N}$–^{15}N pairs (in i) are correlated with the carbonyl carbon (^{13}CO) of the preceding residue (i–1). In the HN(CO)CA experiment, the backbone $^{1}H_{N}$–^{15}N is correlated with the $^{13}C_{\alpha}$ of the preceding residue (whose chemical shift is measured) with coherence transfer via the preceding ^{13}CO shift (whose chemical shift is not measured).

Backbone assignments using $^{1}H_N$, ^{15}N, $^{13}C_\alpha$ and ^{13}CO

The backbone assignment of a good sample can be obtained from the analysis of a minimum of four triple resonance experiments: HNCO, HNCA, HN(CA)CO, and HN(CO)CA (Appendix 1). A mixture of automated and manual comparison of the observed peaks in these experiments from decent quality spectra should allow the identification of backbone connectivities (Kay et al., 1990; Ikura et al., 1990; Grzesiek and Bax, 1993).

Triple resonance methods with deuteration

The couplings of triple resonance experiments (Figure 1.8 and Appendix 1), allow assignment of significantly larger proteins than 2D experiments. However, as the protein molecular weight increases, short relaxation times will limit the transfer efficiency along the coupled bonds, especially when involving the transfer via C_α. The solution to this problem is protein deuteration by inducing protein production from bacteria grown in presence $^{2}H_2O$-based medium. ~75% of protein deuteration improves transfer of magnetisation along the bonds, while leaving a visible population of $^{1}H_N$.

1.9.4. NMR glossary

Chemical shift: resonant frequency of a nucleus in the magnetic field relative to the standard.

Fourier Transform (FT): mathematical integral transform to represent a time-dependent function in the frequency domain.

Nuclear Magnetic Resonance (NMR): physical phenomenon in which nuclei in a magnetic field absorb and re-emit electromagnetic radiation.

Relaxation: process by which nuclear magnetisation returns to equilibrium. It describes the time the spins require to re-align with the magnetic field.

Spin: the nuclear spin is an intrinsic form of angular momentum. Nuclei possessing spin rotate around their axis. Nuclear spin quantum number (I) is dependent on atomic mass and atomic number. NMR active nuclei have spin different from an integer number, *e.g.* $I = 1/2$ for ^{1}H and ^{13}C, $I = 3/2$ for ^{15}N.

Spin-sping coupling: indirect interaction between nuclear spins arising from small interactions between nuclei and local electrons.

Chapter 2

Aim of work

2. AIM OF WORK

Lipids are predominantly synthesised in the endoplasmic reticulum (ER) and they reach the membranes of the target organelle using vesicular and non-vesicular pathways. The balance between these two mechanisms is essential for cell homeostasis, membrane composition and signalling events. Despite the obvious involvement of vesicular routes, experiments have always shown that these only play a minor role (Pagano, 1990; Holthuis and Menon, 2014). The non-vesicular lipid trafficking mechanisms are more important, but still poorly understood. Growing evidence identifies lipid transfer proteins (LTPs) as major players in the regulated transport of lipid monomers between membranes. These proteins take the overall form of a box with a hydrophobic pocket and a lid that can open to allow a lipid to enter inside and be carried across the aqueous environment (Holthuis and Levine, 2005; Voelker, 2009). Mutations in LTPs and misregulation of their activity are linked to various human diseases including cardiovascular conditions (Tall, 1995), metabolic syndrome (Sanyal, 2005), lysosomal storage disorders (Infante et al., 2008), chronic inflammation (Simanshu et al., 2013), Alzheimer disease (Tong et al., 2015), and cancer (Vassilev et al., 2015; Keinan et al., 2014). Based on the conservation of overall 3-dimensional fold, several families of lipid transfer domains have been identified (Table 1.1). The steroidogenic acute regulatory protein-related transfer (StART) domain is a lipid transfer domain of 210 residues: a helix-grip fold composed of curved beta-sheets wraps around a long alpha-helix to form a hydrophobic pocket. The 15 members of the human StART protein family have different binding specificities, different localisations and different functions (Alpy and Tomasetto, 2014). Using bioinformatics software for remote homology prediction based on structural conservation (Soding et al., 2005), our group identified a new family of StART-like domain proteins conserved in all eukaryotes with six members in *Saccharomyces cerevisiae* and three in humans. The aim of this work was the characterisation of the members of this new family using baker's yeast *S. cerevisiae* as a

model, and also evaluating the interspecies conservation of the StART-like domain activity.

This characterisation proceeded on different fronts:

1) bioinformatics predictions,
2) localisation experiments,
3) functional studies,
4) structural visualisation.

The bioinformatics characterisation gave important information on the presence of a predicted lipid transfer domain, which is a structural homologue to the canonical StART domain. Further bioinformatics analysis was used to determine the presence of transmembrane helices and other domains. During this work additional information was collected from published high throughput experiments reporting ORFome-wide localisations, interactions and chemogenomics in yeast. Our localisation experiments were mainly carried out visualising at the confocal microscope with GFP-tagged version of the proteins of interest expressed at endogenous or high levels. The localisation effort was focussed in more detail to describe the single protein Lam2p, trying to dissect the elements responsible for its targeting. To study the function, the purification of the predicted lipid binding domains was optimised and the most soluble constructs were used in *in vitro* assays. These assays aimed first at the identification of the lipid ligands and subsequently to the dynamics of the binding. Another important arm of the functional characterisation took advantage of the sensitivity that the delete strains showed when exposed to a sterol-sequestering antifungal drug: first trying to dissect the different cellular effects of the drugs, second rescuing the phenotype using different domains of the proteins from yeast and human homologues, and lastly using a lipidomics approach to compare whole-cell lipid levels. A strain missing three of the proteins was also observed with electron microscopy to understand the role of these proteins as membrane tethers. Finally, NMR experiments were performed to visualise the three dimensional details of the dynamic changes of the domain in its apo and lipid-bound forms.

Chapter 3

Materials and methods

3. MATERIALS AND METHODS

3.1. Bioinformatics

The majority of sequence homology searches were carried out using HHpred bioinformatics toolkit at toolkit.teubingen.mpg.de (Soding et al., 2005) using optimal features to improve the probability of shared structure (p_{ss}) score: query launched against a database comprising PDB structures available the 26th of July 2014 clustered at 70% identity (pdb70_26Jul14) in the genome of different organisms (*Homo sapiens*, *Mus musculus*, *Saccharomyces cerevisiae*, *Schizosaccharomyces cerevisiae*, and *Arabidopsis thaliana*), multiple sequence alignment (MSA) built with HHblits, 5 iterations, secondary structure was scored, local alignment mode, realignment with MAC algorithm. The searches were seeded with the sequences of known StART domains in humans and plants, and the newly identified proteins in *S cerevisiae* and *H sapiens*.

3.1.1. Alignments

For the alignment, the Full Alignments from HHpred searches were exported in JalView (Waterhouse et al., 2009). The MSA was exported from HHpred results page to JalView Desktop in the form of a *.a3m* full alignment (Waterhouse et al., 2009). Then the MSA was manually processed to eliminate redundancy, delete sequences longer than 210 or shorter than 180 residues, and substitute the formal code name with the more informative names. The original file exported from HHpred results came from a search with Lam4pS2 as query. The alignments with Bet-v1A, StARD1, StARD2/PCTP, StARD3/MLN64, StARD4, StARD5, StARD6, and StARD10 were also included. The colouring scheme was added in JalView based on ClustalX algorithm, the graphical interface for ClustalW program: to each residue in the MSA was assigned a colour according to amino acid specificities weighted for conservation for all sequences. The first two lines show the predicted secondary structure calculated during HHpred search and then verified with JNetHMM algorithm in JalView. The schematic representations of the

predicted secondary structure, calculated during the search process, were exported from the HHpred result file to JalView and processed with Jnet PSSM and HMM algorithms (Cole et al., 2008).

3.1.2. Analysis of predicted transmembrane domains

For the analysis of transmembrane helices, a membrane topology prediction software based on HMM was used: TMHMM server v2.0 (http://www.cbs.dtu.dk/services/TMHMM). Currently, TMHMM server v2.0 is thought to be the best performing transmembrane prediction program, and it can model and predict the architecture (location and orientation) of alpha helices in membrane-spanning proteins with high accuracy (Krogh et al., 2001).

3.2. Yeast strains

Deletion strains were obtained from freezer stocks of the yeast deletion collection BY4741 (MATa), except when indicated. Other gene deletions were made in *S. cerevisiae* RS453c strain (MATα) (Levine and Munro, 2001) with the PCR method using the heterologous marker *Schizosaccharomyces pombe* HIS5 (Wach et al., 1994). Double knockout strains were made by mating and sporulation of BY4741 and BY4742 single delete strains on agar plates. Meiotic products were released from their asci in water with 1 mg/ml Zymolyase-20T solution overnight. Solution was sonicated twice to separate spores, pelleted, resuspended in water and plated on YPD plates. Colonies were genotyped by PCR for absence of LAM genes. Each experiment was carried out including the wild-type strain for comparison. Yeast transformations were carried out using the PLATE (PEG, lithium acetate, single strand DNA, Tris EDTA buffer solution) method (Gietz and Schiestl, 2007).

Strain	Genotype	Source
BY4741	(Euroscarf) MATa *his3Δ1 leu2Δ0 met15Δ0 ura3Δ0*	Euroscarf
BY4742	(Euroscarf) MATα *his3Δ1 leu2Δ0 lys2Δ0 ura3Δ0*	Euroscarf
Δ*lam1*	BY4741/2 *YHR155W*::*KANMX4*	Euroscarf
Δ*lam2*	BY4741/2 *YDR326C*::*KANMX4*	Euroscarf
Δ*lam3*	BY4741/2 *YNL257C*::*KANMX4*	Euroscarf
Δ*lam4*	BY4741/2 *YHR080C*::*KANMX4*	Euroscarf
Δ*lam5*	BY4741/2 *YFL042C*::*KANMX4*	Euroscarf
Δ*lam6*	BY4741/2 *YLR072W*::*KANMX4*	Euroscarf
Δ*lam1*Δ*lam2*	*LAM1*::*KANMX4 LAM2*::*KANMX4*	This work
Δ*lam1*Δ*lam3*	*LAM1*::*KANMX4 LAM3*::*KANMX4*	This work
Δ*lam2*Δ*lam3*	*LAM2*::*KANMX4 LAM3*::*KANMX4*	This work
Δ*lam2*Δ*lam4*	*LAM2*::*KANMX4 LAM4*::*KANMX4*	This work
Δ*lam1*Δ*lam2*Δ*lam3*	BY4741 *LAM2*::*KANMX4 LAM1*::*HISMX4 LAM3*::*HYGMX*	DCN
WPY361 (upc2-1)	MATa *upc2-1 ura3-1 his3-11,-15 leu2-3,-112 trp1-1*	(Li and Prinz, 2004)
Upc2-1 Δ*lam2*	WPY361 (*upc2-1*) *YDR326C*::*KanMX4*	DCN
Upc2-1 Δ*lam3*	WPY361 (*upc2-1*) *YNL257C*::*HYGROR*	DCN
RS453C	MATα *ade2-1 his3-11,15 ura3-52 leu2-3,-112 trp1-1*	(Levine and Munro, 2001)
Δ*lam1*	RS453C *YHR155W*::*HIS5 S.p.*	LHW
Δ*lam2*	RS453C *YDR326C*::*HIS5 S.p.*	LHW
Δ*lam3*	RS453C *YNL257C*::*HIS5 S.p.*	LHW
Δ*lam4*	RS453C *YHR080C*::*HIS5 S.p.*	LHW
Δ*lam5*	RS453C *YFL042C*::*HIS5 S.p.*	LHW
Δ*lam6*	RS453C *YLR072W*::*HIS5 S.p.*	LHW
SEY6210*	MATa *leu2-3,-112 ura3-52 his3Δ200 trp1Δ901 lys2-801 suc2-Δ9 GAL*	(Manford et al., 2012)
ANDY198 (Δtether)*	SEY6210 *ist2Δ::HISMX6 scs2Δ::TRP1 scs22Δ::HISMX6 tcb1Δ::KANMX4 tcb2Δ::KANMX46 tcb3Δ::HISMX6*	
RSY271 sec18-1**	MATa sec18-1 ura3-52 his4-619	(Novick et al., 1980)

Table 3.1 Yeast strains used in this study

This table lists the strains used in this study. The source is reported: Euroscarf (details); LHW, strains made by Louise H Wong in the Levine laboratory; gifts from *Chris Stefan (UCL, London, UK), **Mike Lewis (MRC-LMB, Cambridge, UK).

3.3. Plasmids

All plasmids were based on pRS vector series (Sikorski and Hieter, 1989) and contained the constitutive portion of *PHO5* promoter, unless otherwise stated.

The sequences of LAM1, LAM3, LAM4 genes were obtained with the gap repair method (Orr-Weaver et al., 1983). Briefly, the recovery of the chromosomal sequence of the genes of interest was obtained using a linearised pRS416 plasmid. The restriction site for linearisation was flanked by two PCR products containing 130 bp sequences homologous to the 3' and 5' end of the chromosome sequence. The repaired plasmids (that did not undergo crossing-over and subsequent genome integration) were purified using QIAprep Spin Miniprep Kit (Qiagen, Cat.no. 27106) with an optimised protocol for yeast plasmid recovery (Singh and Weil, 2002).

The sequence of LAM2 was built by cloning different PCR products corresponding to different domain combination of the protein (Figure 5.7). LAM5 and LAM6 were a gift from Sean Munro laboratory (MRC-LMB, Cambridge, UK). The open reading frames (ORF) of the three human genes were obtained buying commercially available I.M.A.G.E. Fully Sequenced cDNA clones. The StART-like domains of the hLAMs were cloned from these vectors by PCR.

Gene name	I.M.A.G.E. source	Clone ID	Unigene ID
GramD1a	Lifescience SourceBioscience	4126671	Hs.515351
GramD1b	ThermoScientific	40026781	Hs.144725
GramD1c	Lifescience SourceBioscience	4829130	Hs.24583

Table 3.2 IMAGE clones used as PCR source for human sequences

Cloned regions are from *S. cerevisiae* (S288c) or human I.M.A.G.E. clones; size of whole proteins/promoters are in brackets, for protein [aa] and nucleotide {bp}; promoters are regions of genome just prior to open reading frame starts; ranges within proteins are not in brackets; changes in wild type residues are written as 'X123 > Z'.

Yeast expression	Description
GFP-Lam2p	pRS416: GFP + Ydr326c/Lam2p ORF [1438], with 2 extra residues to facilitate cloning in five sections: K828 > KT and S1244 > SR
GFP-Lam1p/Lam3p/Lam4p	pRS416: GFP + whole ORFs: Yhr155w/Lam1p [1228], Ynl257c/Lam3p [1229], Yhr080cp/Lam4p [1348]
GFP-Lam5/6p*	pRS406: GFP + whole ORFs: Yfl042cp/Lam5p M1 > S [674], Ylr072wp/Lam6p M1 > S [693]
GFP-Lam1p/Lam2p/Lam3p/ Lam4p - own promoters	as above for GFP-ORF, replaced *PHO5* promoter with: *LAM1* {951}, *LAM2* {459}, *LAM3* {360}, *LAM4* {701}
RFP-ER	pRS405: dimeric DsRed TDimer2(12) [464] + RNSKP (linker) + ENESSS•MGIFILVALLILVLGWFY•R = RFP + linker[5] + Scs2p 220-244 ([6] + TMD[18] + lumen[1])
RFP-mito	as RFP-ER, but after RNSKP (linker): G + Tom6p [61]
RFP-Lam2p	pRS406: dimeric DsRed TDimer2(12) [464] + Lam2 K828 > KT and S1244 > SR
GAL > GFP-Lam2p	as for GFP-Lam2p, except pRS406, and replaced *PHO5* promoter with *GAL1* {807}
GFP-Lam2ΔN	pRS416 *LAM2* prom.: GFP + Lam2 611-1438
GFP-Lam2ΔPH	pRS416 *LAM2* prom.: GFP + Lam2 1-610 + 829-1438
GFP-Lam2S1S2CT	pRS416 *LAM2* prom.: GFP + Lam2 829-1438
GFP-Lam2S2CT	pRS416 *LAM2* prom.: GFP + Lam2 1028-1438
GFP-Lam2CT	pRS416 *LAM2* prom.: GFP + Lam2 1245-1438
GFP-Lam2ΔCT	pRS416 *LAM2* prom.: GFP + Lam2 1-1319
GFP-Lam2ΔTMD	pRS416 *LAM2* prom.: GFP + Lam2 1-1246
RFP-Lam2CT	as RFP-ER, but after RNSK: LGSAPVMSR + Lam2 1245-1438
GFP-hLAMa	pRS416: GFP + hLAMa
GFP only	pRS416: GFP + GFP
GFP-Lam1S	pRS416: GFP + Lam1 773-978
GFP-Lam3S	pRS416: GFP + Lam3 771-976
GFP-Lam2S1	pRS416: GFP + Lam2 829-1028
GFP-Lam2S2	pRS416: GFP + Lam2 1027-1244 + R
GFP-Lam4S1	pRS416: GFP + Lam2 759-929
GFP-Lam4S2	pRS416: GFP + Lam4 968-1140
GFP-Lam5S	pRS416: GFP + Lam5 381-586 + AS
GFP-Lam6S	pRS416: GFP + myc tag + Lam6 374-582 + DV
GFP-hLAMaS	pRS416: GFP + GramD1a 359-547 + DV
GFP-hLAMbS	pRS416: GFP + GramD1b 372-543 + DV
GFP-hLAMcS	pRS416: GFP + GramD1c 326-497 + DV
Pdr11p-GFP**	pWP1251. 316: *PDR11* prom.: Pdr11p-GFP
Aus1p-GFP**	pWP1220. 316: *AUS1* prom.: Aus1p-GFP
GFP-Sso1	pRS406: *GAL1* prom.: GFP + LGSAPVMSS + Sso1 1-290
GFP-TGBp3***	pRS416: *ADH1* prom..: GFP + TGBp3 1-52 + CYC1 term {80}
GFP-Lam1pS (v1)	pRS416: GFP + Lam1 754-986
GFP-Lam1pS v2	pRS416: GFP + Lam1 754-994
GFP-Lam1pS v3	pRS416: GFP + Lam1 754-881
GFP-Lam1pS v4	pRS416: GFP + Lam1 754-997
GFP-Lam1pS v5	pRS416: GFP + Lam1 754-1003
GFP-Lam1pS v6	pRS416: GFP + Lam1 754-1009

Table 3.3 Yeast expression plasmids

All plasmids from the pRS series with constitutive portion of *PHO5* promoter {168}, unless otherwise stated: pRS405 = integrating LEU2, pRS406 = integrating URA3, pRS416 = CEN-URA3. Construct with endogenous promoters do not possess terminators, unless otherwise stated. Plasmids were gifts from: *Sean Munro (MRC-LMB, Cambridge, UK), **Will Prinz (NIH, Bethesda, USA), ***Chao-Wen Wang (Academia Sinica, Taipei, Taiwan).

Bacterial expression	Details
His_{11}-Lam2S1	+ PVMT + Lam2 829-1027 + R
His_{11}-Lam2S2	+ PVMT + Lam2 1027-1244 + R
His_{11}-Lam4S1	+ M + Lam4 731-938 + DV
His_{11}-Lam4S2	+ M + Lam4 946-1155 + DV
His_{11}-Lam4S2 G>R	as His-Lam4S2, G1119R
His_{11}-Lam1S v1	+ M + Lam1 754-986
His_{11}-Lam1S v2	+ M + Lam1 754-994
His_{11}-Lam1S v3	+ M + Lam1 754-881
His_{11}-Lam1S v4	+ M + Lam1 754-997
His_{11}-Lam1S v5	+ M + Lam1 754-1003
His_{11}-Lam1S v6	+ M + Lam1 754-1009
His_{11}-SUMO-TEV-Lam1S v2	+ M + *Sc*Smt3p 2-98 + AGAENLYFQSNGAM + Lam1 754-994
His_{11}-SUMO-TEV-Lam1S v3	+ M + *Sc*Smt3p 2-98 + AGAENLYFQSNGAM + Lam1 754-881

Table 3.4 Plasmids for bacterial expression

pTrcHis$_6$ plasmid. Constructs all start: MGGSHHHHHHGMASHHHHHARA. Residues corresponding to the TEV cleavage site are in blue.

3.4. Microscopy

Yeast growing in log phase were examined with a Leica TCS SP2 Confocal Microscope (AOBS, 63×/NA1.4 objective lens) at room temperature using LCS software (Leica) for acquisition and with a Zeiss LSM700 Confocal Microscope (Plan Apochromat, 63×/NA1.4 objective lens) at room temperature using ZEN 2.1 Software. Images were processed with Photoshop CS6 (Adobe) and combined in the final figures with Illustrator CS6 (Adobe).

3.4.1. Corrected total cell fluorescence (CTCF)

For the quantification of ROS (Figure 6.11), the calculation of the corrected total cell fluorescence was used (Burgess et al., 2010). Confocal images in

grey-scale were processed in ImageJ. From the selected cells, using the “Selection tool”, measurements of the area (A), integrated density (ID) and mean grey value (MGV) were set. At least 15 cells per condition were analysed, the average of 3 circles outside the cells perimeter was used as background value. All values were exported to a Microsoft Excel worksheet, and processed following this rule (where n is the cell taken in examination):

$$CTCF = ID_n - \left(A_n \times MGV_{background}\right)$$

Graph and statistics were made with Prism 6 (Graphpad).

3.5. Protein overexpression and purification

The solubility of the eleven StART-like domains was checked observing the GFP-tagged version of the domains in competent BL21(DE3) *E. coli* cells (Invitrogen, Cat.no. C6000) at the epifluorescence microscope. The selected residues of each StART-like domain (Table 3.5) were inserted into the pTrcHis$_{11}$ vector using XmaI and Asp718I sites. Competent BL21(DE3) *E coli* cells (Invitrogen, Cat.no. C6000) expressing the 11-histidine-tagged-proteins were cultured in LB medium and induced at OD_{600} = 0.5 at different temperatures and testing a range of isopropyl-β-D-1-thiogalactopyranoside (IPTG – Sigma, Cat.no. I6758) concentrations for 4 hours (Gräslund et al., 2008). Optimal constructs, IPTG concentration and growth temperature are determined and listed in Table 3.5. GFP was then excised using the two AgeI sites flanking both sides of GFP sequence. Mutants for Lam2S2 and Lam4S2 were constructed by fusion PCR, and checked by sequencing.

StART domain	Uniprot entry	Residues	IPTG mM	Induction
Lam2S1	Q06681	829-1030	0.20	37°C, 4 h
Lam2S2	Q06681	1028-1247	0.20	37°C, 4 h
Lam4S1	P38800	731-938	0.20	37°C, 4 h
Lam4S2	P38800	946-1155	0.20	37°C, 4 h
GramD1aS	Q96CP6	359-547	0.30	25°C, 7 h
Lam1S (v1)	P38851	754-988	NS	NS
Lam1S v2		754-994	0.40	25°C, 8 h
Lam1S v3		754-881	0.40	25°C, 8 h
Lam1S v4		754-997	NS	NS
Lam1S v5		754-1003		
Lam1S v6		754-1009	0.40	18°C, O/N
SUMO-TEV-Lam1S v2	P38851	754-994	0.40	25°C, 8 h
SUMO-TEV-Lam1S v3	P38851	754-881	0.40	25°C, 8 h
Lam3S	P38717	753-985	NS	NS
Lam3S				
Lam5S	P43560	381-586	NS	NS
Lam6S	Q08001	374-582	NS	NS

Table 3.5 Recombinant StART-like domains best induction conditions

Detailed induction conditions for the different StART domains including the residues present in the pTrcHis$_{11}$ induction vector, IPTG concentration at OD_{600} = 0.5-0.6, and time of induction. NS, non-soluble in the range of conditions tested.

Knowing the best conditions for growth and induction, the protein overexpression was scaled up to 1 litre for Lam2S1, Lam2S2, Lam4S1, Lam4S2, and to up to 4 litres for the other StARTs. After induction, cells were spun down at 6,000 rpm for 10 min. Pellet was suspended in 30 ml of Lysis Buffer: 25 mM TrisHCl pH 8.0, 300 mM NaCl, 5 mM imidazole (Sigma, Cat.no. I202), 0.5 mM DTT, 1 cOmplete EDTA-free protease inhibitor cocktail tablet (Roche, Cat.no. 11-873-580-001), 0.1 mg/ml lysozyme chloride form (Sigma, Cat.no. L2879). After a freeze and thaw cycle, cell lysate was sonicated for 90 sec and clarified at 18,000 rpm for 30 min at 4°C in a Sorvall SS34 rotor. The soluble 11-his-tagged protein was captured on His-Select Nickel Affinity gel (Sigma, Cat.no. P6611), and eluted with 25 mM Tris pH 8.0, 300 mM NaCl, 300 mM imidazole. The flow-through was loaded on the Illustra NAP-10 column Sephadex G-25 DNA grade (GE Healthcare, Cat.no. 17-0854-01), pre-equilibrated with PIPES Buffer (20 mM PIPES, 137 mM NaCl, 3 mM KCl, pH 6.8) following manufacturer's instructions. Protein aliquots were snap frozen in a dry ice-ethanol bath and kept at –80°C. The protein concentration is determined by a Bradford assay and at the Nanodrop (ThermoScientific) taking consideration of each protein's molecular weight (MW) and extinction coefficient (ε). Purity was checked by SDS-PAGE gel with Coomassie staining: >90% for all preparations.

3.6. Lipids

Lipid stock solutions were prepared in chloroform at the following initial concentrations.

Lipid	Abbreviation	Producer	Cat.no.	Stock conc.
Dehydroergosterol	DHE	Sigma	E2634	5 mg/ml
Ergosterol	Erg	MP Biomedicals	02101649	10 mg/ml
Cholesterol	Chol	Avanti Polar Lipids	700000	50 mg/ml
Diacylglycerol 18:1	DAG	Avanti Polar Lipids	800811C	5 mg/ml
Triacylglycerol 18:0-18:0-18:1	TAG	Avanti Polar Lipids	111004	10 mg/ml

Table 3.6 Lipid stock solutions

List of lipid stock solutions prepared in chloroform and kept at -20ºC in a glass desiccator jar.

3.6.1. Sterol – Methyl-β-cyclodextrin complexes

Third party copyright material

Table 3.7 Cyclodectrins

Schematic representation of the three cyclodextrins with dimensions of overall structure and hydrophobic cavity (Tonelli, 2014).

The desired amount of lipid from stock solution in chloroform was transferred to a round-bottom glass vial. The lipid was dried into thin film under argon-flow and then under vacuum for 30 min. 25 mM Methyl-β-cyclodextrin (MβCD) (Sigma-Aldrich, Cat.no. 332615) in PIPES Buffer to get a lipid/MβCD ratio of 1:5. To resuspend the lipid film, the glass vial was warmed to 37° C, vortexed repeatedly, left in a sonicator for 20 min, and then shaken at 37°C overnight. After 16 hours the vial is vortexed and sonicated again for 10 min. The aliquots are made after a final centrifuge for 10 min at 21,000 × g to remove undissolved lipid, and stored at 4°C under argon. The solution was briefly

centrifuged to remove lipid crystals just before use (Maxfield and Wüstner, 2012).

3.7. DHE binding assay

Tryptophan fluorescence was measured upon excitation at 295 nm at an emission scan from 320 to 410 nm (bandwidth 0.5 nm) in a LS55 Fluorimeter (Perkin Elmer). The sample was placed in a quartz cuvette with 1 ml volume of PIPES Buffer containing 2 μM protein. The FRET signal is detected when DHE:MβCD complex was added in excess. Proper controls were performed to assess that this FRET signal did not originate from proximity between donor (protein tryptophans) and DHE, but by the DHE in the hydrophobic pocket of the StART-like domain (de Saint-Jean et al., 2011).

3.8. Amphotericin B

Amphotericin B studies were carried out according to Phillips et al. (2003). The drug was obtained from Sigma-Aldrich (Cat.no. A2942), with a stock concentration of 250 μg/ml. The working concentration was calculated on the total volume of 20 ml if on an agar plate. The concentration used in the experiments ranged from 60 ng/ml to 500 ng/ml. Cells were grown overnight in YPD or the appropriate selection medium, diluted to OD_{600}=0.1 and grown to OD_{600}=0.5. Before plating, three 1:200 serial dilutions were made so to produce 5-10 colonies in the highest dilution. The incubation time and temperature of the plates were always optimised to increase the visualisation of phenotypic differences among the control and the delete strains (Phillips et al., 2003). Generally, plates were grown for 48 hours at 30 °C. All growth assays involving serial dilutions were repeated at least three times. For some experiments, AmB was supplemented with 30 mM *N*-acetylcysteine (NAC) (Sigma, Cat.no. A7259) added to either the plate or the liquid culture (Pozniakovsky et al., 2005).

3.8.1. Colony forming units assay

To quantify colony-forming units (CFUs), colonies were counted at the end of AmB exposure. CFU/ml were calculated using the following rule:

$$CFU/_{ml} = \frac{n_{colonies} \times d_f}{V}$$

Where $n_{colonies}$ is the number of colonies, d_f is the dilution factor, and V is the volume of initial culture used.

3.8.2. AmB growth in liquid cultures

Cells were grown overnight at 30ºC, diluted back in the morning to OD_{600} = 0.1 and grown until early log-phase. At OD_{600} = 0.4 cells were treated with 250 ng/ml AmB and kept at 30ºC for additional 24 hours. OD of wild type and double delete strains were measured at the time points specified in the graph.

3.8.3. AmB binding assay

At OD_{600} = 0.5 wild type and double delete cells were incubated with 250 ng/ml AmB in solution for 1 hour at 30ºC. Cells were then centrifuged and the fluorescence in the supernatant was measured. Taking advantage of the concentration-dependant properties of AmB, the fluorescence emitted at 375 nm is measured with an excitation scan from 300 nm to 375 nm (Gruszecki et al., 2009).

3.8.4. ROS visualisation after AmB treatment

The cellular reactive oxygen species (ROS) production was visualised with 50 μM dichlorofluorescin diacetate (H_2DCF-DA) (Sigma, Cat.no. D6883). H_2DCF-DA is a cell permeable non-fluorescent compound that can be oxidised inside the cell by ROS that turn it into the cell impermeable and highly fluorescent dichlorofluorescin. This feature can be used to have a sensitive, rapid and indirect readout for quantification of oxidative metabolism. At OD_{600} = 0.5 the cells are treated with 250 ng/ml AmB in solution for 1 hour at 30°C. Then 50 μM H_2DCF-DA was added to the liquid culture for additional 30 min. The cells were imaged after multiple washing (Pozniakovsky et al., 2005). At least three experiments were performed for each condition.

3.9. Radiolabelled lipid transfer assay

HL60 cells were routinely grown in a humidified 5% CO_2 atmosphere at 37°C in RPMI medium (Gibco, Cat.no. 31985-047), containing 10% (v/v) heat-inactivated Fetal Bovine Serum (Gibco, Cat.no. 1099-141) and 1% (v/v) Pen Strep (Gibco, Cat.no. 15140-122). HL60 cells were pre-labelled with 1 μCi/ml [2-^{14}C]-acetate (American Radiolabelled Chemicals, Cat.no. ARC-0158B) for 72 hours. Proteins to be assayed were diluted in PIPES buffer supplemented with 0.1 mg/ml defatted BSA (Sigma, Cat.no. A6003) and 1 mg/ml glucose to a final 200 μg of protein in 200 μl buffer. Approximately 2 μg of protein were analysed on 12% SDS-PAGE to compare the input with the output after recapture. 10^7 HL60 cells were permeabilised at 37°C with a permeabilisation cocktail containing 0.6 i.u. recombinant Streptolysin O (SLO) and 2 mM MgATP (Sigma, Cat.no. A0770) in complete PIPES buffer. After 10 min cells were transferred on ice for 5 min and centrifuged (3,000 rpm for 5 min) to remove the cytosolic components and resuspended in a small volume of complete PIPES buffer. 400 μl of the donor compartment was then incubated with 200 μl of protein at 37°C for 20 min. Then the pellet was removed by centrifugation at 3,000 rpm for 5 min. 550 μl supernatant containing the His-tagged protein was transferred in a clean tube, centrifuged again, and incubated with 120 μl His-Select Nickel Affinity gel (Sigma, Cat.no. P6611) beads in mini-spin columns (Thermo Scientific, Cat.no. 69700) for 30 min at 4°C on a rotating wheel. After recapture on the agarose beads, the protein is washed twice with 500 μl low salt buffer (50 mM sodium phosphate, 300 mM NaCl, 10% glycerol, pH 6.0) and twice with 500 μl high salt buffer (50 mM sodium phosphate, 525 mM NaCl, 10% glycerol, pH 6.0), and then eluted with 500 μl of 500 mM imidazole in high salt buffer. The protein was desalted using buffer exchange column (PD MidiTrap G-10, GE Healthcare, Cat.no. 28-9180-11) and was eluted in 1 ml PIPES buffer. 20 μl of protein were analysed on 12% SDS-PAGE as experiment output, the remaining was processed to extract the lipid following the chloroform methanol procedure: 1 ml protein in aqueous solution + 3.75 ml $CHCl_3$:MeOH (1:2) + 1.25 ml $CHCl_3$ + 1.25 ml H_2O. The mixture was vortexed thoroughly and the organic phase was dried down

in a Savant SpeedVac. The following morning the pellet was resuspended in 50 μl chloroform and spotted on a Whatman Silica Gel 60 TLC plate, and developed using the solvent system $CHCl_3$:MeOH:acetic-acid:H_2O (75:45:3:1). The TLC plate was then dried at room temperature and was imaged using Fuji PhosphoImager screen for up to one week (Ségui et al., 2002; Garner et al., 2012; Holic et al., 2014). To better characterise the feature of the apparent cholesterol band, the area was scraped off from the TLC plate and subjected to another chloroform:methanol lipid extraction. The lipid was then resuspended in chloroform and seeded on a new Whatman Silica Gel 60 TLC plate, developed with a solvent mixture to resolve neutral lipids, hexane:diethyl-ether:acetic-acid (155:45:2).

3.10. Electron microscopy

Wild type and triple delete (Δ*lam1*Δ*lam2*Δ*lam3*) BY4741 yeast strains from a fresh patch were grown in YPD overnight at 30 °C. In the morning cells were diluted in 100 ml and grown to exponential phase to about 10^7 cells per ml of liquid culture for permanganate fixation (Stevens and White, 1979). Cells were pelleted, washed twice in distilled water, and resuspended in 1 ml of freshly prepared 1.5% $KMnO_4$ (Sigma, Cat.no. 7722-64-7) in 1.5 ml Eppendorf tubes. After vortexing, the tubes were topped up with 0.5 ml of 1.5% $KMnO_4$ to exclude air and incubated for 30 min at 4 °C. The $KMnO_4$ was then replaced with 1.5 ml of the same solution and the cells were incubated for further 30 min. Cells were then washed five times in water and further processed for dehydration, embedding, sectioning and imaging by Matt Hayes (UCL). Cells were dehydrated in gradients of ethanol by incubating them for at least 20 min in 10%, 30%, 50%, 70%, 90%, 95% and 100% at room temperature with gentle agitation, the process was repeated three times. Dehydrated cells were embedded in Spurr resin. The Spurr Low-viscosity Embedding Kit (Sigma, Cat.no. EM0300) was used for incubations of 1 hour in 33% and 66% resin, followed by 6 hours in 100% resin. The pellets were heated to 70 °C for 10 hours for resin polymerisation. Pale gold ultrathin sections were cut and stained by incubation in 5% uranyl citrate for 10 min at 60 °C, and further processed with Reynold's lead citrate for 2 min to increase contrast (Kaiser and Schekman, 1990). Sections were imaged on a transmission electron microscope (Jeol, JEM-1010). The final magnification of the micrographs was 6,000X.

For the quantification in electron microscopy images, random fields of cells were photographed and analysed (using ImageJ) to measure the cell perimeter and every identifiable section of cortical ER (cER). cER was defined as the electron-dense linear structures near and parallel to the PM (Loewen et al., 2007). For each of the 30 cells per condition examined, the length of each segment of cER was recorded. Different values were expressed as specified in Section 6.5.

3.11. Lipidomics

Lipidomics studies were carried out by Isabelle Riezman under the supervision of Howard Riezman at the University of Geneva (Switzerland) using delete strains sent from our laboratory. I prepared provided the strains, and I took part to the preparation of samples (cell growth, and lipid extraction from pellets) for one biological replicate and I analysed the data obtained from the whole study performed on BY4741 single deletes (two biological replicates) and RS453c single deletes (one biological replicate).

Solvents used were HPLC- and LC-MS-grade: chloroform, methanol and ammonium acetate were purchased from Acros (Belgium), Fluka (Germany), and Fisher Scientific (UK), respectively. Internal lipid standards were bought from Avanti Polar Lipids: 17:0/14:1 PC (LM-1004), 17:0/14:1 PE (LM-1104), 17:0/14:1 PI (LM-1504), 17:0/14:1 PS (LM-1304), C17 ceramide (860517), and C8-glucosyl-(β)-ceramide (860540).

3.11.1. Cell preparation and communal steps of lipid extraction

Yeast cells were processed as previously described (Guan et al., 2009; da Silveira Dos Santos et al., 2014). Wild type and single delete yeast strains were grown in YPD until OD_{600} = 25 in duplicate. Pellets were resuspended in 1.5 ml of extraction solvent (ethanol, water, diethyl ether, pyridine, 4.2 N ammonium hydroxide, 15:15:5:1:0.018, vol/vol). A mixture of internal lipid standards (7.5 nmol of 17:0/14:1 PC, 7.5 nmol of 17:0/14:1 PE, 6.0 nmol of 17:0/14:1 PI, 4.0 nmol of 17:0/14:1 PS, 1.2 nmol of C17:0-ceramide, and 2.0 nmol of C8-glucosylceramide) was spiked into each sample. After adding 250 *µ*l of glass beads, the samples were vortexed vigorously on a multitube vortexer (Labtek Inernational) at a maximum speed of 5 minutes and incubated at 60°C for 20 min. Samples were cleared from debris by centrifugation at 1,800 x *g* for 5 min. The duplicates were combined before drying under a stream of nitrogen under vacuum in a Centrivap (Labconco). The sample was divided into two equal aliquots: one for glycerophospholipids, the other for sphingolipid extraction.

3.11.2. Glycerophospholipid extraction

For desalting, samples were resuspended in 300 µl of water-saturated butanol and sonicated for 5 min. After addition of 150 µl of LC-MS-grade water, samples were vortexed and centrifuged at 3200 × *g* for 10 min to induce phase separation. The upper phase was collected. The lower phase was processed twice again with 300 µl of water-saturated butanol, sonicated, and centrifuged after addition of LC-MS-grade water. The three upper phases were combined, dried and stored at -80°C until analysis.

3.11.3. Sphingolipid extraction

Before desalting, the half samples for ceramide and sphingolipid analysis, were processed with a monomethylamine reagent (methanol, water, n-butanol, methylamine solution, 4:3:1:5, vol/vol). This additional step is important to deacylate glycerophospholipids and reduce ion suppression due to PL in SL detection (Cheng et al., 2001). The following steps followed the glycerophospholipids extraction protocol.

3.11.4. ESI-MS/MS analysis

Frozen lipid extracts were thawed and samples were resuspended in 500 μl of chloroform:methanol (1:1, vol/vol). Samples were diluted two times with $CHCl_3$:MeOH:H_2O (2:7:1, vol/vol/vol) for positive mode, or with $CHCl_3$:MeOH (1:2, vol/vol) containing 5 mM ammonium acetate for negative mode. Samples were infused with a gas pressure of 30 psi with a Triversa Nanomate (Advion) and a spry voltage of 1.2 kV with a TSQ Vantage (ThermoFisher Scientific). The mass spectrometer was operated with a spray voltage of 3.5 kV in positive mode and 3kV in negative mode. The temperature of the capillary was set to 190°C. Multiple-reaction monitoring mass spectrometry (MRM-MS) was used to identify and quantify the lipid species (Guan et al., 2009; da Silveira Dos Santos et al., 2014). Data were converted and quantified relative to standard curves of internal standards that had been spiked during extraction as previously mentioned. Two biological replicates, comprising several technical replicates each, were analysed. A Q Exactive Hybrid Quadrupole-Orbitrap Mass Spectrometer (Thermo Scientific) was used. Positive-ion-mode analysis

was performed using scan range m/z = 650-800 (for monitoring PC and PE species), and 540-750, using lock mass 588.4471 (for ceramides). Negative-ion-mode analysis was performed using scan range m/z = 700-850 (for monitoring PI and PS species), and 550-1150 (for complex sphingolipids). Spectra were acquired using mass resolution of 280,000 and automatic gain control at $3e^6$ for 100 scans. Lipid species were identified according to their m/z, and their abundance was calculated by their signal intensities relative to the internal standards at known concentrations.

3.11.5. Data analysis

I carried out data analysis supervised by members of the Reizman laboratory and according to their optimised procedures (Guan et al., 2009; da Silveira Dos Santos et al., 2014). The screening was conducted in one batch of lipid analysis. Each batch contained the wild-type strain and the six LAM genes single mutants from the BY4741 and the RS453c background. For each of the two biological replicates, the MS analysis was done in three sequential repetitions (technical replicates). The signal intensities from the detected lipids in each technical replicate were obtained from the raw files as previously described (Epstein et al., 2012) and quantified according to standard curves from the internal standards spiked in every sample during lipid extraction. Quality controls for frequency of lipids, variability of lipids, artifactual lipids and biological replicates were taken into consideration as previously described (da Silveira Dos Santos et al., 2014).

Values were normalised on the wild type and not on the median. Fold change on the wild type processed for hierarchical clustering in Matlab R2015a (Mathworks) using the following function:

```
CGobj = clustergram(MajorL, 'RowLabels', Table1,
'ColumnLabels', Table2, 'Cluster', 2, 'Linkage',
average, 'Colormap', redbluecmap)
```

Where MajorL is the table containing the relative abundances of measured sphingolipid and phospholipid levels for each strain; ‘Table1’ and ‘Table2’

listed the names of the lipid molecules and strains, respectively; Cluster 2, was for computing the clustering only for strain proximity (and not for lipid species); Linkage method to apply the proximity algorithm; and colour range of the heatmap.

The resulting hierarchical clusters with heatmap colours were exported to Adobe Illustrator for annotation. The fold change graph was made combining lipid of the same classes grouping values from molecules with different acyl chain lengths in Prism 6 (Graphpad).

3.12. Structural studies with NMR

3.12.1. Homology modelling

To obtain Lam4pS2 model, the core of the predicted second StART-like domain (967-1139) was used as query in HHpred against PDB structures database, with HHblits-based secondary structure prediction, 5 iterations, and global alignment mode. The three top scoring alignments with human StART domain proteins with known functions (StARD3, PCTP, and StARD5) were manually selected as “user-defined multiple templates” and used to generate a PIR-alignment for Modeller (Sali and Blundell, 1993; Webb and Sali, 2014). Modeller 9.16 was launched within the HHpred bioinformatics toolkit to make the PDB file. The resulting PDB coordinates were exported to PyMOL for three-dimensional rendition of the protein, its overlay with PCTP crystal structure, and the highlights of key residues. The quality of the model was assessed by Verify3D tool (Lüthy et al., 1992).

3.12.2. Protein expression and purification for NMR studies

The majority of the experimental structural studies were done in collaboration with Anastasia Zhuravleva (University of Leeds), who verified the feasibility of the recombinant protein for NMR experiments and decided the step required for assignment. Andrea Sauerwein (Steve Matthews group at Imperial College London) helped with suggestions, reagents, spectra acquisition, data analysis, and partial assignment of the deuterated sample. Protein production for all conditions was optimised and carried out by myself in the Levine lab.

Lam4S2 for NMR studies is produced adapting the protocol from Tugarinov et al. (2006). A single colony of BL21(DE3) cells transformed with pTrcHis$_{11}$-Lam4S2 is grown overnight at 30°C in 2 ml of LB medium. In the morning the culture is diluted 1:1,000 into 3 ml of unlabelled M9 medium (45 mM Na_2HPO_4, 20 mM KH_2PO_4, 10 mM NaCl, 1 mM $MgSO_4$, 0.1 mM $CaCl_2$, 20 mM NH_4Cl) + 2.5% LB at 37 °C. At OD_{600} = 0.5 the culture is diluted 1:120,000 in 100ml of unlabelled M9 medium + 2.5% LB and left overnight at 30 °C, so to have the cells in log phase in the morning. The following day the cells are spun down and resuspended in 500 ml of labelled M9 medium made with 45 mM

Na2HPO4, 20 mM KH2PO4, 10 mM NaCl, 1 mM MgSO4, 0.1 mM CaCl2, 20mM 15NH4Cl (Goss Scientific, Cat.No. NLM467) + 2.5% LB and transferred at 37°C. At OD600 = 0.5 the culture is diluted in 2 litres of labelled M9 medium + 2.5% LB. Protein overexpression is induced at OD600 = 0.5 with 0.2 mM IPTG for 6 hours at 37°C (Tugarinov et al., 2006).

For the protein purification the protocol described in paragraph 1.6 is followed, with the following modifications:

- Lysis buffer: 25 mM TrisHCl pH 8.0, 300 mM NaCl, 10 mM imidazole, 0.5 mM DTT, 1 cOmplete EDTA-free protease inhibitor cocktail tablet, 0.1 mg/ml lysozyme chloride form.
- Desalting buffer: 10 mM PIPES pH6.8, 50 mM L-Arginine (Sigma, Cat.no. A5006), 50 mM L-Glutamate (Sigma, Cat.no. G1626) in substitution of 140 mM salts to improve protein solubility and signal-to-noise ratio (Golovanov et al., 2004).

For 3D NMR spectroscopy studies, 2 litres of bacteria are grown in the presence of both 20 mM $^{15}NH_4Cl$ and 10mM D-[^{13}C]-glucose (Goss Scientific, Cat.No. CLM1396). The protein was purified following the same protocol.

3.12.3. ILV reverse labelling

To produce ^{15}N- and ^{13}C-labelled Lam4S2 with selective unlabelling of specific hydrophobic residues (Krishnarjuna et al., 2011), BL21(DE3) cells were grown in M9 medium as described above, with the addition of 1 g/l of the following amino acids (1 g in 50 ml of water stock solution, filter sterilised):

- Isoleucine (Sigma, Cat.no I2752)
- Leucine (Sigma, Cat.no L8000)
- Valine (Sigma, Cat.no V0500)

The same protein production protocol and buffers described above were used.

3.12.4. Protein deuteration

^2H_2O-adapted BL21(DE3) *E. coli* colonies were selected on a ^2H_2O-based M9 minimal medium agar plate grown for 2 days at 37 °C. Best fitting colonies were screen in small volume to determine the growth speed and the best induction conditions. Whole cell lysates were run on a Coomassie-stained SDS-PAGE to compare Lam4S2 levels. The best colony was chosen for the 2 litres protein production in ^2H_2O medium, performed as described above.

3.12.5. NMR spectra acquisition

300 µl of Lam4S2 (sequence) at a concentration ranging from 0.35 to 0.5 mM (12-15 mg/ml) in 10 mM PIPES pH 6.8, 50 mM L-Arg + L-Glu pH 6.8, 49 mM NaCl, 1 mM KCl, 10 % D_2O was used to record acquisitions. standard 2D (HSQC), To obtain backbone assignments, standard and transverse-relaxation optimized spectroscopy (TROSY)-modified triple-resonance experiments were recorded HNCA, HN(CO)CA, HNCO, HN(CA)CO (Ikura et al., 1990). The recordings were acquired at:

- Varian INOVA 600 MHz spectrometer at 288 K, 293 K, 298 K and 303 K (15°C to 30°C) at The Astbury Centre for Structural and Molecular Biology of the University of Leeds.
- Bruker 900 MHz spectrometer at 293 K (20°C) at the Henry Wellcome Building for NMR (HWB-NMR) of the University of Birmingham.
- Bruker Avance III HD 950 MHz at 293 K (20°C) MRC Biomolecular NMR Centre at the Francis Crick Institute - Mill Hill.
- Bruker 800 MHz NMR spectrometer equipped with BMPC2 magnet pump control system, AVANCE III HD, TXI cryoprobe and cryoplatform at 283 K (10°C) at the Cross Faculty NMR Centre (Imperial College London).

Spectra acquisition were controlled by Bruker TopSpin software. Applied pulse sequences were obtained from the software database (Sattler et al., 1999; Cavanagh et al., 2010). Spectra analysis was carried out using CcpNmr Analysis software (Skinner et al., 2015).

Results

Chapter 4
Bioinformatics predictions and data mining

4. Bioinformatics predictions and data mining

4.1. HMM homology prediction finds new StART-like domain proteins

4.1.1. Newly identified StART-like domain protein family in eukaryotes

The functional features of an unknown protein can be inferred by finding its homologues with known function. Since the early 1990s, the effort of bioinformatics focussed on the implementation of algorithms for detection of homology, *i.e.* the descent of different proteins from a common ancestor (Altschul et al., 1997). Tools based on sequence homology prediction, such as basic local alignment tool (BLAST), perform poorly when less than 30% of the sequence is conserved (Brenner et al., 1998). Their evolution produced profile-based sequence searches, such as PSI-BLAST, which increase sensitivity by making a profile that contains statistical-weighted scores of the conserved aspects of multiple sequences related to the initial query (Altschul et al., 1997). A further evolution of the profile-based tools, produced profile-profile searches which contain family-wide statistical information for both query and target sequences (Yona and Levitt, 2002; Panchenko, 2003). These tools require the creation of profiles for all members of the target library, which necessitates a substantial computational effort. Searches can also account for conservation of secondary structure, either by launching the query against Protein Data Bank (PDB) of solved structures (Shi et al., 2001; Soding, 2005), or by including in the search a specific step of secondary structure prediction (Blundell et al., 1987).

Here, we applied a profile-profile search tool to identify remote homologues of the StART domain in *Saccharomyces cerevisiae*. The steroidogenic acute regulatory protein (StAR) transfer domain (StART), is a lipid transfer domain of 210 residues forming a “helix-grip” domain of curved beta-sheet wrapped around a long alpha-helix. The resulting cleft is wide enough to accommodate a lipid molecule (either sterol, phospholipid or sphingolipid). The fifteen members of the human StART protein family have different binding specificities, different localisations and different functions (Alpy and

Tomasetto, 2014). The StART domain is highly conserved throughout evolution from vertebrates to bacteria and plants, but at the beginning of this project, the only known proteins with StART-related domain in fungi were the distantly related Coq10 and Aha1, which bind either a non-bilayer lipid (ubiquinone) or no lipid at all (Barros et al., 2005).

This bioinformatics approach has been successfully used to find remote homologues of other proteins that further molecular characterisation confirmed their role as LTPs, including TULIP domains in tricalbins/extended-synaptotagmins (Kopec et al., 2011; Schauder et al., 2014) and StART domains in Ups1-3p (Connerth et al., 2012; Miliara et al., 2015).

Our initial searches were seeded with a member of the mammalian StART family, and targets were sought within databases containing profiles of the complete proteomes of *S. cerevisiae*, *H. sapiens*, and *A. thaliana*. The use of profile-profile tools was sufficient to identify some members of the new family in *S. cerevisiae*, and the inclusion of the secondary structure conservation successfully identified six new StART-like domain proteins, which are not strongly related in terms of sequence with any of the previously identified StART-like domain families, for example those in the SRPBCC (StART/RhoαC/PITP/Bet-v1/CoxG/GalC) superfamily (Marchler-Bauer et al., 2015) (Table 4.1).

My attention focussed on the three pairs of paralogous StART-like domain proteins in budding yeast *Saccharomyces cerevisiae*, as well as on their human homologues (Figure 4.4). Out of six members in yeast, only three proteins have been previously studied and named Ysp1p (Pozniakovsky et al., 2005), Ysp2p (Sokolov et al., 2006), and Sip3p (Lesage et al., 1994). Because *S. cerevisiae* underwent a whole genome duplication about 10 million years ago (Kellis et al., 2004), it has three pairs of paralogs, Lam1p/Sip3p, Ysp2p/Lam4p and Lam5p/Lam6p, while related fungi have three members.

The multiple sequence alignment (MSA) of the StART-like domains from the six yeast and three human proteins of interest with the StART domain of human StART proteins (including CERT and MLN64) and plant Bet-v1 showed

the conservation of secondary structure (Figure 4.1). In terms of sequence identity, there are few conserved residues (some of which potentially involved in important protein functions), but first the application of profile-profile searches and secondly the inclusion of the predicted secondary structure (derived by PSI-PRED), significantly improved the alignment quality.

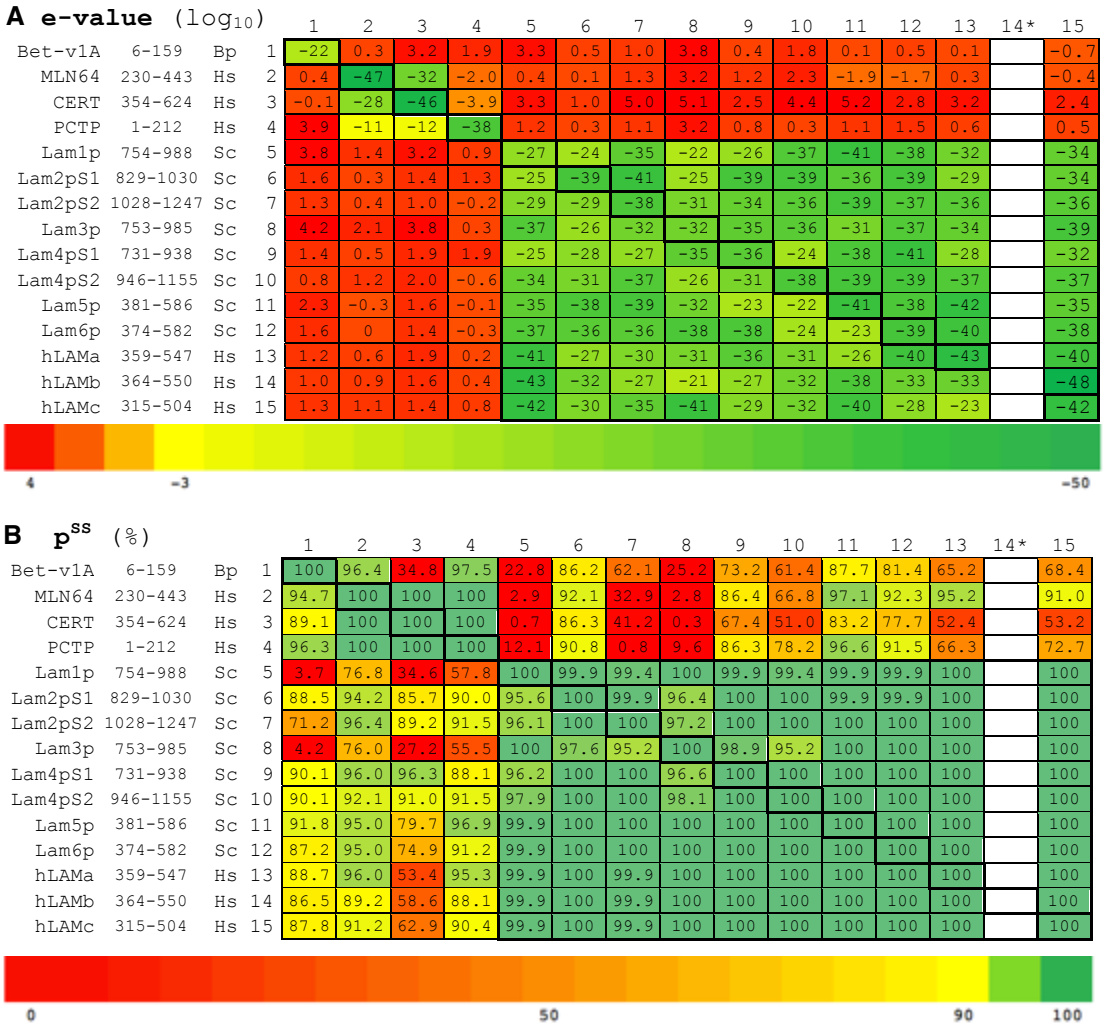

Table 4.1 Sequence and structural relationships of StART and StART-like domains

The two tables compare (**A**) the e-value calculated by sequence similarity (shown in $\log_{10}$) and (**B**) the probability of shared structure (p^{SS}) as computed by HHpred, when taking into consideration the conservation of the predicted secondary structure. Searches were initiated by seeding the sequence of the StART/StART-like domains listed on the left and performing 3 iterations of HHblits (an algorithm for building multiple sequence alignments that is faster and more sensitive than PSI-BLAST), before alignment with the targets indicated across the top, global alignment mode (MAC threshold = 0.35). The first three columns represent name of the query, residues included in the search and species. Heatmap bars at the bottom of each table represent the range of significance of the relationship: red for distant relationship, yellow for significant relationship, green for very close relationship. The use of profile-profile searches and the inclusion of structural conservation were able to identify the new family. Thick lines surrounds diagonal values (protein against itself) and the perimeter of the values corresponding to the new StART-like domain family. 14*: hLAMb is absent from the HHpred target database, only the results when it is used as query are shown. Bp, *Betula pendula*, Hs, *Homo sapiens*, Sc, *Saccharomyces cerevisiae*.

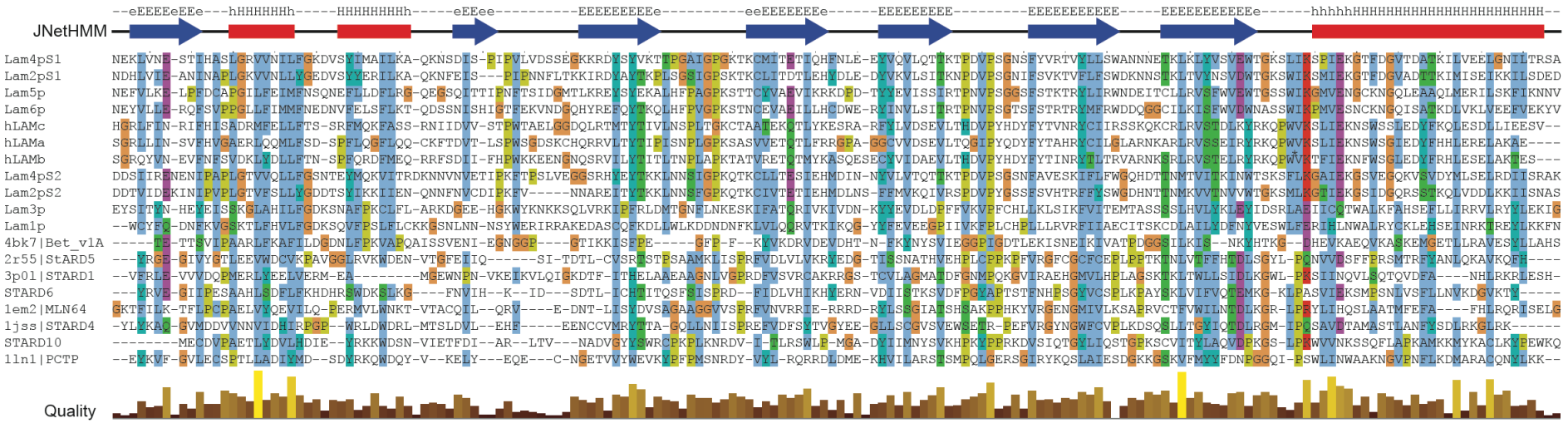

Figure 4.1 Alignment of known StART domains with newly predicted StART-like domains

Multiple sequence alignement (MSA) of HHpred search seeded with Lam4S2 sequence with 3 iterations and standard setting. MSA was analysed for 7 StARD domains (StARD1, StARD2/PCTP, StARD3/MLN64, StARD4, StARD5, StARD6, and StARD10), Bet-V1A and the members of the newly idnetified family in human and yeast. The colouring scheme was added in JalView based on ClustalX algorithm, the graphical interface for ClustalW program: to each residue in the MSA was assigned a colour according to amino acid specificities weighted for conservation for all sequences. The first two lines show the predicted secondary structure calculated by PSI-PRED 3.0 during HHpred search and then verified with JNetHMM algorithm in JalView. The alignment shows the core of the StART domains with secondary structure elements in this order β_3-α_2-α_3-β_4-β_5-β_6-β_7-β_8-β_9-α_4 (see also Figure 7.1). The top line lists β-sheets (E), and α-helices (H), capital letters indicate high prediction confidence. Second line shows blue arrows for sheets and red blocks for helices. The last line represents the quality of the alignment as calculated by JalView and gives the quantitative extent of the consensus. hLAMb sequence was added manually and two residues in the last loop were omitted (*) from the alignment.

Accessory domains

Lipid transfer proteins (LTPs) frequently also contain additional domains or motifs to the lipid binding domain. These give specificity to their subcellular localisation and function by mediating other protein-lipid or protein-protein interactions (Chiapparino et al., 2015). Membrane targeting can be mediated by transmembrane domains (such as NPC1, E-Syts/Tcb and some members of the ORP family), or by other specialised domains such as a pleckstrin homology (PH) domain. PH domains are present in several families of LTPs including StART, GLTP, OSBP, and CRAL-TRIO.

The proteins of the new StART-like domain family were already classified by the bioinformatics identification of their GRAM domain (Doerks et al., 2000). The GRAM domain is a ~70 amino acids domain found in glucosyltransferases, myotubularins and other putative membrane-associated proteins. It is thought to be capable of protein-protein or protein-lipid interactions with important function for membrane-associated events. GRAM domains are predicted to appear in ~180 human proteins with highly conserved residues in the core domain (Doerks et al., 2000). The crystal structure of Myotubularin Related protein 2 (MTM2) revealed that the GRAM domain is part of a larger motif with a pleckstrin homology (PH) fold (Begley et al., 2003).

In the case of the newly identified StART-like domain family, its members showed predicted accessory domains involved in membrane targeting including transmembrane helices, PH-like domains (including the known GRAM domains), and BAR domains. Members of the new family in plants also possess C2 domains (Wong and Levine, 2016).

In the following sections, I will summarise what is already known about the LAMs and I will analyse each of the proteins in more detail to give a schematic representation of their domain organisation.

4.1.2. Lam1p/Lam3p

Literature

Lam1p was originally named Ysp1p (Yeast Suicide Protein-1). This name was given because the *ysp1*Δ strain is insensitive to amiodarone- or pheromone-induced programmed cell death (PCD) (Pozniakovsky et al., 2005). Amiodarone, a blocker of the L-type Ca^{2+} channels, Na^{+} channels, and β-adrenergic receptors (Varbiro et al., 2003), and high levels of yeast pheromone α-factor trigger similar PCD cascades involving an increase of intracellular Ca^{2+} and fragmentation of mitochondria. The Δ*ysp1* strain does not show mitochondrial fragmentation and is resistant to amiodarone or pheromone treatments (Pozniakovsky et al., 2005). Lam1p's paralog, Lam3p was identified more than 20 years ago in yeast two hybrid screening for proteins that interact in vivo with Snf1p (Sucrose Non Fermenting-1), the yeast homologue of AMP-dependent kinase, which in yeast is necessary for release of glucose repression (Lesage et al., 1994). Neither of the individual papers on these proteins have been followed up, and their molecular functions of these proteins remain unknown.

Transmembrane domains

I manually asserted the presence of transmembrane domains using the transmembrane regions prediction TMHMM Server v. 2.0 (Krogh et al., 2001). Contrary to the manual prediction presented in UniProt database, but consistently with Pozniakovsky et al. (2005), TMHMM 2.0 predicted two transmembrane domains separated by a short hydrophilic linker of 10-11 residues for both paralogs.

Accessory domains

Extending the searches to the entire protein sequence in HHpred, other previously unknown domains can be identified (Figure 4.2). The paralogs Lam1p and Lam3p are predicted to contain a BAR domain and a second PH domain.

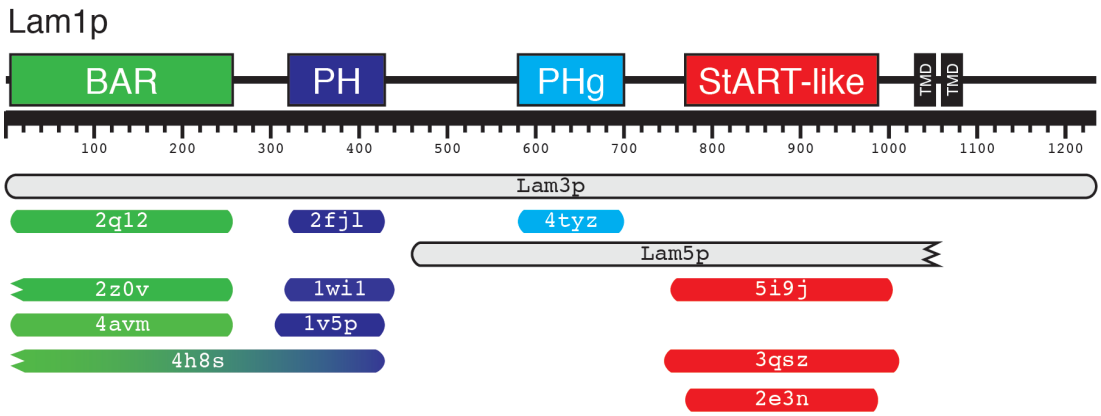

Figure 4.2 Predicted accessory domains in Lam1/3p

HHpred was able to identify new accessory domains in Lam1/3p. The diagram represents a summary of the information given by the result page of HHpred searches. Seeding the search with full length Lam1p, we looked for targets first in the yeast genome (in grey). Apart from a full alignment with itself (not shown), alignment was shown to its paralogs Lam3p (see also Table 4.1), and other LAM proteins such as Lam5p, which aligned across half of the full length protein, including one PH domain, the StART-like domain and one transmembrane helix. We also looked for targets in the Protein Data Bank (PDB) of solved proteins structures, which identified different structural components, here indicate by their PDB code. Components in green correspond to a BAR domain: 2Q12, BAR domain of human APPL1; 2Z0V, BAR domain of human Endophilin-III; 4AVM, N-BAR domain of human bridging integrator 2. Components in blue correspond to a newly identified PH domain: 2FJL, PH domain in rat PLC-gamma1; 1WI1, PH domain of human Ca^{2+}-dependent Activator Protein for Secretion (CAPS); 1V5P, N-terminal PH domain of mouse TAPP2. 4H8S, full alignment with human APPL2 BAR (green) and PH (blue) domains. Components in cyan corresponds to the PH-like domain similar to GRAM (PHg): 4TYZ, C-terminal GRAM domain of *Leishmania infantum* protein of unknown function. Components in red correspond to StART-like domain: 5I9J, cholesterol and lutein-binding domain of human STARD3 at 1.74A; 3QSZ, StART domain from fungal StARD1 (fragment 25-204); 2E3N, human CERT StART domain in complex with C6-ceramide. The higher the component is shown in the alignment, the higher is the probability of shared structure (p^{SS}) with Lam1p. Broken shapes means the structural component in the query is shorter than in the target.

4.1.3. Lam2p/Lam4p

Literature

The same group that discovered Ysp1p identified also Lam2p as a mitochondrial protein acting in the amiodarone, acetic acid, propionic acid, and nigericin-induced cell death cascade. Homology with Lam1p or higher organisms was not detected (Sokolov et al., 2006), and the newly identified protein was named Yeast Suicide Protein-2 (Ysp2p) only because it was found to act in amidoarone-induce cell death, similarly to Ysp1p/Lam1p. Its paralog, Lam4p/Yhr080cp, has never been studied in detail before. However, it was previously identified in a random transposon screen as one of 20 genes involved in sterol import (Sullivan et al., 2009).

Transmembrane helices and coiled-coil domains

Lam2p has a predicted transmembrane domain of 22 residues, while Lam4p transmembrane domain is only weakly predicted (Figure 4.3). At the extreme C-terminus of both paralogs, there is a predicted coiled coil domain of 30 residues, suggesting a possible role in protein-protein interaction of the predicted luminal domain.

Lam2/4p containing multiple StART domains

Both Lam2p and Lam4p are characterised by the presence of two predicted StART-like domains each. HHpred results showed that the sequence identity between Lam2p and Lam4p is around 40%. The two StART-like domains from the same protein have about 40% of sequence identities, while the sequence identity of these regions alone between paralogs ranges from 53% to 58%. This suggests that the duplication of the StART-like domains in evolution temporally came before the whole genome duplication occurred ~100-150 million years ago (Kellis et al., 2004). Proteins with multiple StART and StART-like domains are only present in fungi and plants.

Candidate for Ypk1-mediated phosphorylation

In response to membrane stress, the cell must undergo important lipid changes to maintain homeostasis and function. At the hub of this dynamic response, multiple groups have shown the role of Target of Rapamycin (TOR) Complex 2 (TORC2) and its downstream protein kinases Ypk1 (and its paralog Ypk2) (Roelants et al., 2011; Niles and Powers, 2012; Berchtold et al., 2012; Muir et al., 2014). In *S. cerevisiae*, Ypk1 can phosphorylate different proteins involved in the maintenance of the correct levels of different lipid classes in cell membranes. With an approach combining biochemical, genetic and bioinformatics techniques, recently a more comprehensive list of Ypk1 targets has been proposed (Muir et al., 2014). Among this potential candidates, Lam2p was bioinformatically predicted to be phosphorylatable at S326, T518, and T1237 (Muir et al., 2014).

A

```
# sp|Q06681|YSP2_YEAST Length: 1438
# sp|Q06681|YSP2_YEAST Number of predicted TMHs:  1
# sp|Q06681|YSP2_YEAST Exp number of AAs in TMHs: 23.76291
sp|Q06681|YSP2_YEAST    TMHMM2.0    outside          1  1279
sp|Q06681|YSP2_YEAST    TMHMM2.0    TMhelix       1280  1302
sp|Q06681|YSP2_YEAST    TMHMM2.0    inside        1303  1438
```

B

```
# sp|P38800|LAM4_YEAST Length: 1345
# sp|P38800|LAM4_YEAST Number of predicted TMHs:  1
# sp|P38800|LAM4_YEAST Exp number of AAs in TMHs: 19.32547
sp|P38800|LAM4_YEAST    TMHMM2.0    outside          1  1197
sp|P38800|LAM4_YEAST    TMHMM2.0    TMhelix       1204  1223
sp|P38800|LAM4_YEAST    TMHMM2.0    inside        1224  1345
```

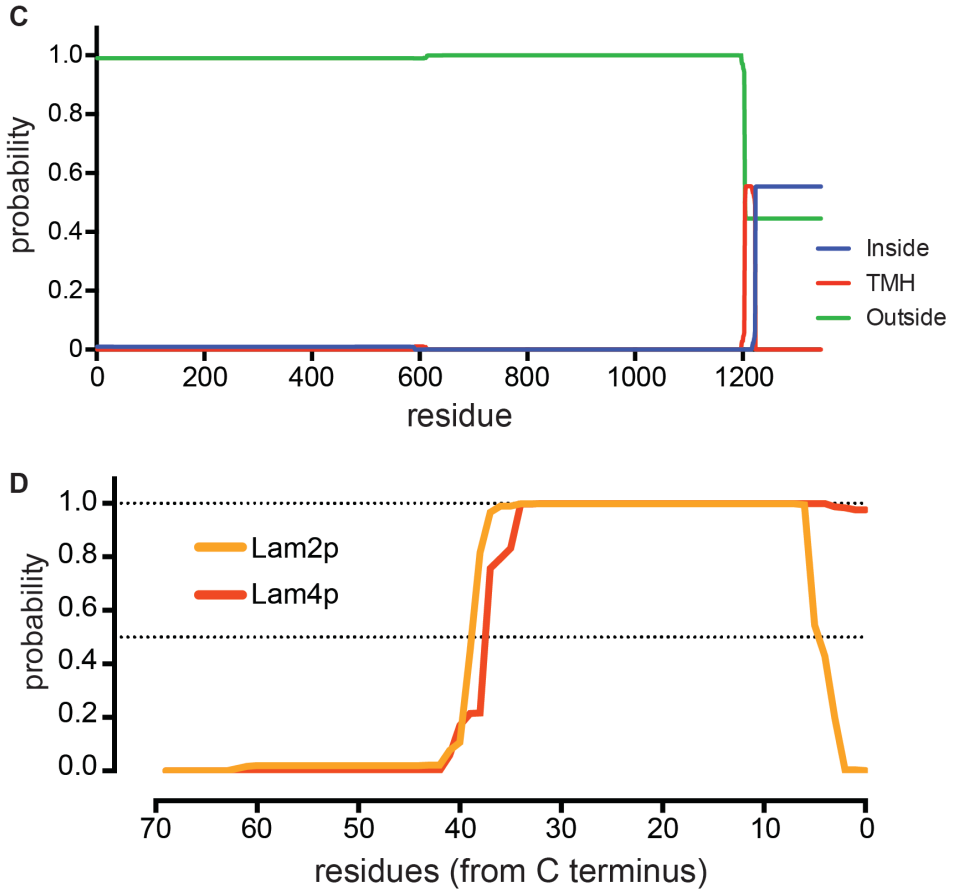

Figure 4.3 Prediction of Lam2/4p transmembrane and coiled-coil helices

(**A**) Lam2p has a predicted hydrophobic transmembrane domain of 22 residues with an 'internal' (*i.e.* cytoplasmic) C-terminal tail of 135 amino acids. (**B-C**) The transmembrane domain of Lam4p is only weakly predicted. (**D**) Both paralogs possess a coiled coil region in the extreme C-terminus, predicted in the ER lumen. Prediction and scoring were obtained by seeding COILS tool with the sequence of Lam2/4p luminal domains. Numbers indicate residues from the C-terminus.

4.1.4. Lam5p/Lam6p

At the beginning of this project, Lam5p/Yfl042cp and its paralog Lam6p/Ylr072wp had never been studied before. Both of them were known by their systematic names, and they were classified as single-pass transmembrane proteins containing a GRAM domain.

4.1.5. Human LAM proteins

Together with the three pairs of yeast paralogs, the new StART-like family in humans has three homologues: hLAMa, hLAMb, and hLAMc. None of these proteins have been previously studied. hLAMb locus appeared associated with different cancer mechanisms: variations at hLAMb 5' UTR are associated with chronic lymphocytic leukaemia (CLL) (Di Bernardo et al., 2008) and follicular lymphoma (Conde et al., 2010) in genome-wide association studies (GWAS). Furthermore, it was also shown to be associated with chemoresistance in epithelial ovarian cancer cells: the reduction of hLAMb expression increased the survival and decreased the tumour volume in the mouse model (Wu et al., 2014). According to the Human Protein Atlas (Uhlén et al., 2015), hLAMb is expressed at high levels in steroidogenic cells, in adrenal glands and in the cerebral cortex.

4.1.6. Summary

Remote homology on the basis of minimal conservation of sequence, identified a new family with a conserved and previously unidentified domain. This domain has the same arrangement of secondary structural elements of a StART-like domain, that is shared among other lipid transfer proteins (LTPs). Another constitutive feature is the presence of transmembrane domains (TMDs) that anchor all the proteins inside a cellular membrane. The presence of TMDs was a key observation for a proposed lipid transfer protein family, because if these LTPs operate lipid traffic between membranes of different organelles, they must localise at a membrane contact site (MCS) where they

could bridge the gap. Last, we emphasised the presence of diverse accessory domains generally known for their involvement in membrane targeting, such as PH, GRAM and BAR domains.

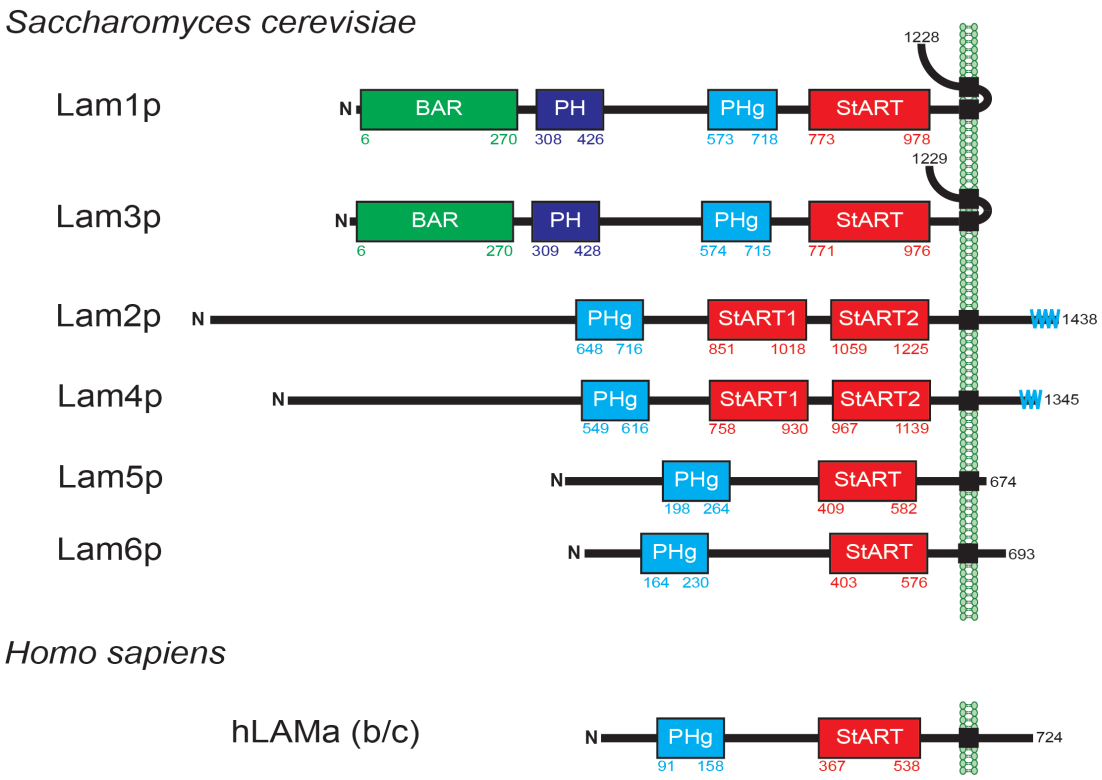

Figure 4.4 A new family of predicted StART-like domain proteins

Domain architecture organisation of the newly identified StART-like domain proteins in yeast and humans. The reasons behind the choice of the acronym LAM (Lipid transfer proteins Anchored at Membrane contact sites) are explained in Section 6.7. Transmembrane domains are represented by black squares. The PH-like domains similar to GRAM (PHg) were annotated also in the Uniprot database. Newly predicted domains are the BAR (green) and additional PH (blue) domains in Lam1/3p, and the StART-like domains (red) in all the members. Saccharomyces cerevisiae has duplicated paralogs, which arose from a whole genome duplication. Only three members are present in humans. Lam4p transmembrane domain was only weakly predicted. Lam2p and Lam4p have a predicted coiled-coil region at the extreme C-terminus (cyan).

Chapter 5

LAM proteins localise to membrane contact sites

5. LAM proteins localise to membrane contact sites

5.1. Lam2p and Lam4p localise at ER-PM contact sites

5.1.1. GFP-Lam2p localised to ER-PM contact sites

To understand the physiological function of LAM proteins, I started studying their cellular localisation in yeast. A previous study, focussing on programmed cell death induced by acidification, identified the Gram (or PHg, see above) domain and transmembrane domain of Lam2p and localised the protein at mitochondria (Sokolov et al., 2006).

To study the localisation, I cloned the full length protein tagged with GFP at its N-terminus in plasmids for yeast expression under the control of the constitutive portion of the *PHO5* promoter or under its endogenous promoter. N-terminal GFP-tagged Lam2p localised in peripheral puncta shown in high-throughput studies with C-terminal GFP-tagged protein, both in wild type and *lam2*Δ strains (Figure 5.1). Under the control of its endogenous promoter, Lam2p was still present at detectable levels by conventional confocal microscopy and it was distributed in the same numerous dots close to the PM. Higher expression levels, controlled either by the medium strong promoter *PHO5* had minor effects on Lam2p localisation (Figure 5.1). In addition to the peripheral localisation, both promoters produced occasional internal dots, usually a single GFP-positive punctum per confocal section, more intense when overexpressed. The localisation and the function of this internal GFP-Lam2p dots remain unknown.

Furthermore, it is possible to examine the localisation results obtained from high throughput (HT) experiments (Huh et al., 2003; Tkach et al., 2012). These approaches require HT tagging at the C-terminus of all ORFs via homologous recombination of the tag and a selection marker. The C-terminal tag can result in mislocalisation for some protein especially because in this case it is predicted to be in the ER lumen and to have the coiled coil domain potentially involved in the localisation. Nevertheless, C-terminally GFP-tagged Lam2p

expressed at endogenous level (Tkach et al., 2012), showed a punctate distribution at the cER similar to the N-terminal tag (Figure 5.1 E).

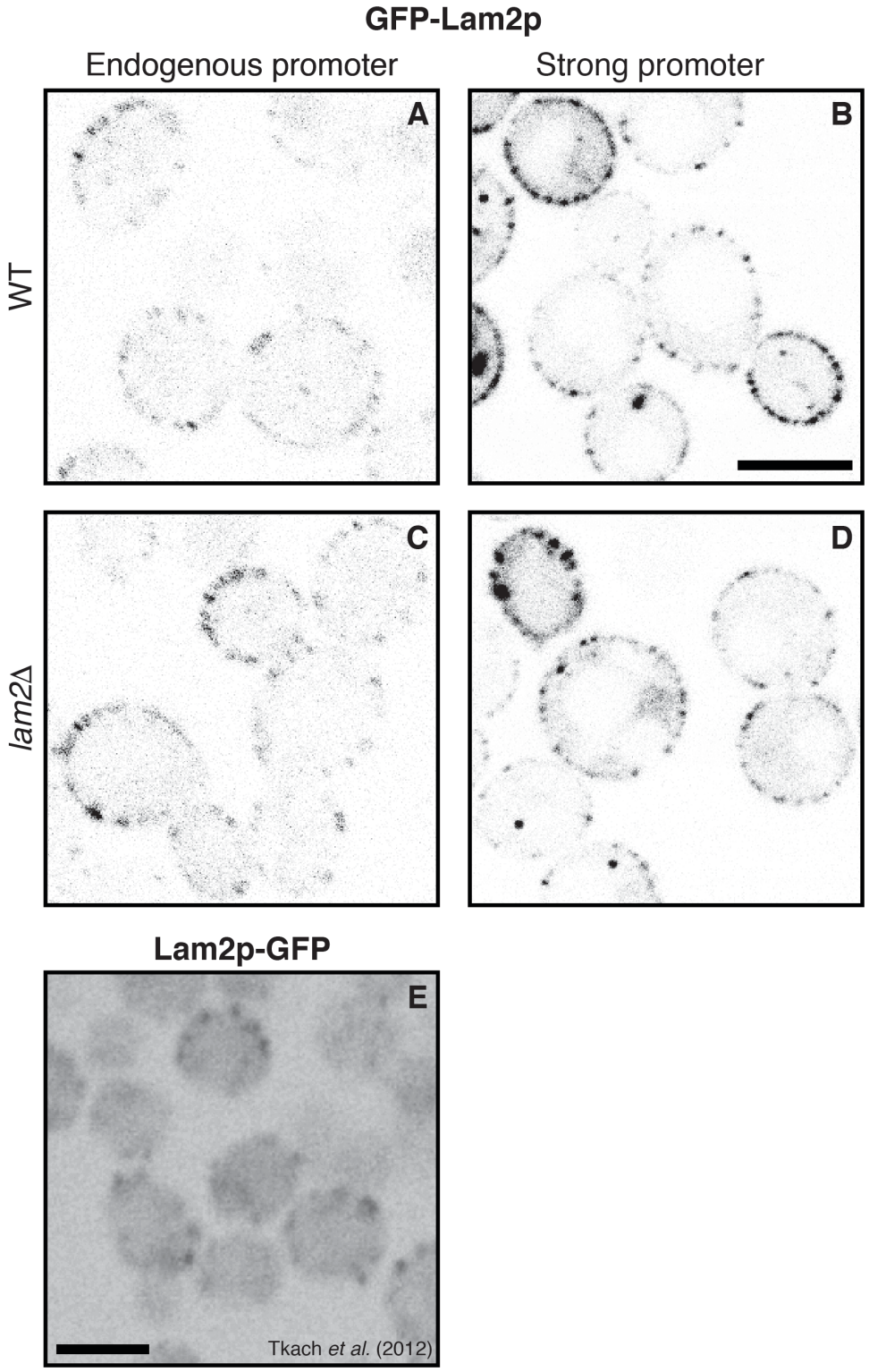

Figure 5.1 Lam2p localisation in cortical dots

GFP-Lam2p localisation in wild type (**A** and **B**) and *lam2*Δ (**C** and **D**) cells. The N-terminal tagged protein was expressed under the control of its endogenous promoter (**A** and **C**) or the constitutive portion of the moderately strong *PHO5* promoter (**B** and

D). (**E**) Lam2p was tagged in its genomic locus at the C-terminal for a high throughput screen of yeast ORFs localisation (Tkach et al., 2012). A representative section of the high-throughput image was selected. All images show the inverted grey scale of the green channel. Scale bars, 5 μm.

Observing the GFP-Lam2p dots at the resolution of the confocal microscope, one possibility is that peripheral puncta coincided with eisosomes, immobile protein assemblies at the cell cortex associated with endocytosis (Fröhlich et al., 2014). To evaluate this assumption, I studied the localisation of GFP-Lam2p in a strain lacking Pil1p, the major eisosome core component. Loss of Pil1p causes clustering of eisosome remnants and redirects endocytosis and endocytic effector proteins to these clusters (Walther et al., 2006). GFP-Lam2p localisation was not affected by the absence of eisosomes and this invalidated the hypothesis of an association between Lam2p and eisosomal structures (Figure 5.2). Consequently, Lam2p peripheral puncta might localise either on the PM or on the cortical ER (cER).

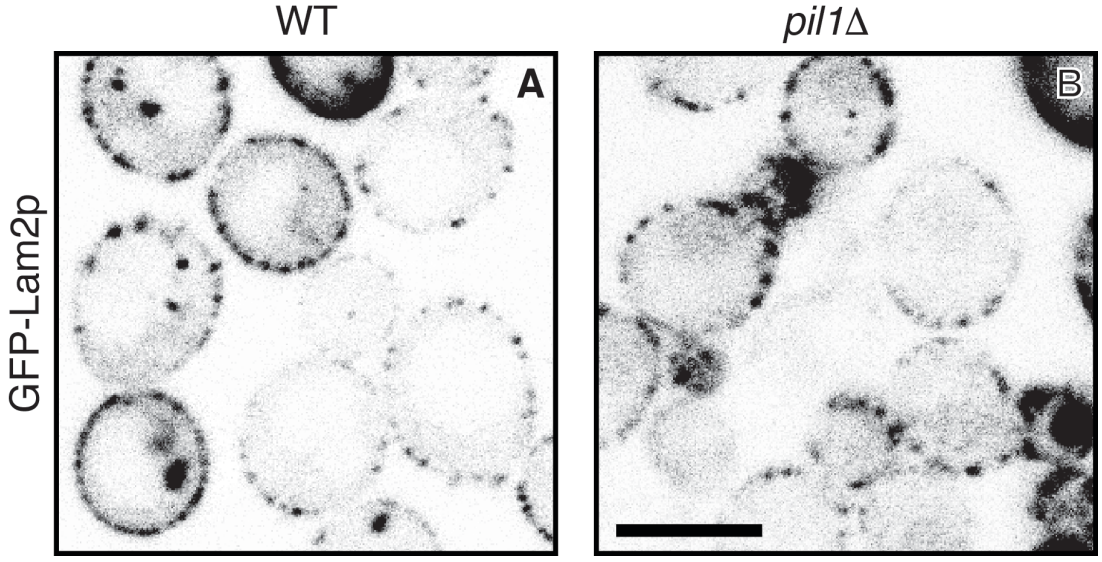

Figure 5.2 Lam2p localisation is not dependent on Pil1p

GFP-Lam2p was expressed under *PHO5* in a wild type strain and a *PIL1* delete strain, missing eisosomes. Eisosomes are immobile cell cortex structures associated with endocytosis (Frohlich et al., 2014). The deletion of the eisosomal core component Pil1p causes the lack of eisosomal compartment. Lam2p localisation was not affected when eisosomes were not present. Images shown in inverted grey scale. Scale bar, 5 μm.

Lam2p peripheral puncta have been originally identified as co-localising with mitochondria (Sokolov et al., 2006). However, a counter stain with an RFP-tagged mitochondrial marker disproved a possible association of Lam2p with mitochondria (Figure 5.3 A-C). When an RFP-tagged marker was used to counter-stain the ER, all the GFP-positive puncta localised at an RFP-positive segment of cER (Figure 5.3 D-J). This is consistent with Lam2p localisation at cER, or at the portion of the PM (about 40-50%) that is reached by the cER. However, because of the confocal image resolution, almost all the periphery of the yeast cell appears to have associated cER from out-of-focus segments. To overcome this problem, I used a yeast strain in which the amount of cER had been genetically reduced. This strain, called Δ*tether*, has 90% less cER than a wild type because six proteins responsible for the physical tethering of the cER to the PM have been deleted. The deletion of Scs2 and Scs22, the yeast orthologs of human VAMP-associated proteins (VAP), causes the most dramatic effect with 60% less cER (Loewen et al., 2003), the additional deletion of tricalbins (Tcb1, Tcb2, and Tcb3), orthologs of the extended synaptotagmins (E-Syt1-3), and Ist2, a member of the TMEM16A ion channel family (Manford et al., 2012). The concomitant deletion of these six proteins causes a dramatic but not complete collapse of the cER, about 4% of the PM is still in contact with a cER element (Figure 5.4A).

In the Δ*tether* strain, Lam2p was still localised in dots close to the PM but it was distributed in fewer and brighter GFP-positive puncta compared to wild type (Figure 5.4B-C). Furthermore, all Lam2p puncta were in close proximity to a strand of cytoplasmic ER extending to the PM (Figure 5.4D-F). The observation of adjacent sections in a Z-stack proved that every time a Lam2p-positive punctum was present, there was an ER tubule taking contact with the PM, even if the ER strand appeared in less confocal sections than the GFP-positive dot (Figure 5.5 and Figure 5.6).

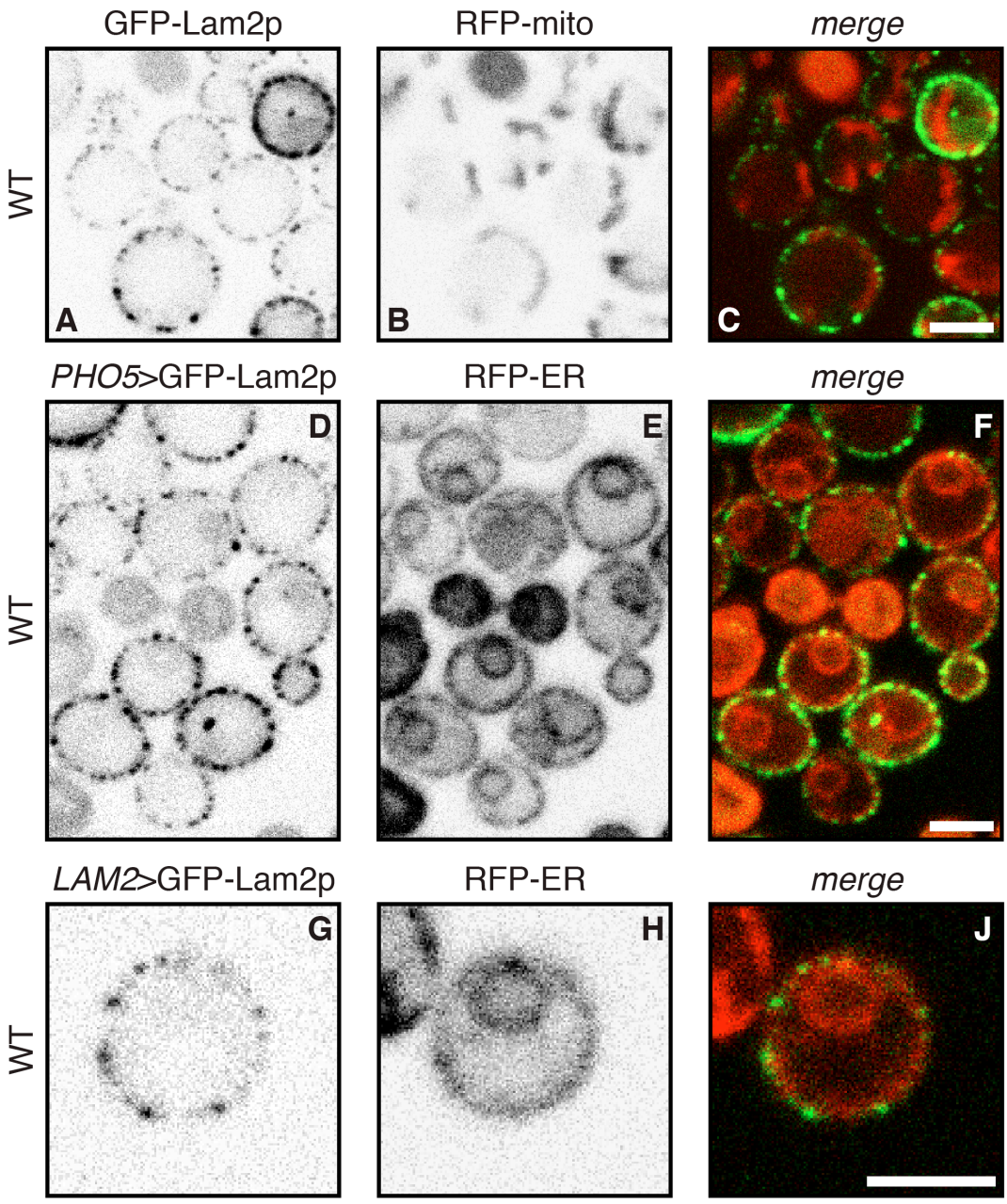

Figure 5.3 Lam2p peripheral puncta co-localise with the cER

Study of the localisation of endogenous and over-expressed GFP-Lam2p in wild type strains together with RFP-tagged counterstaining of mitochondria or ER. (**A-C**) Cells were transformed with integrating plasmids expressing RFP-tagged mitochondrial marker Tom6 under the control of *PHO5* promoter. The strain expressing this marker was then transformed with a *PHO5*-controlled GFP-Lam2p. (**D-J**) Wild type cells expressing the RFP-tagged transmembrane domain of Scs2p as ER marker, together with GFP-tagged Lam2p under *PHO5* (D-F) or its endogenous (G-J) promoters. Scale bars, 5 μm.

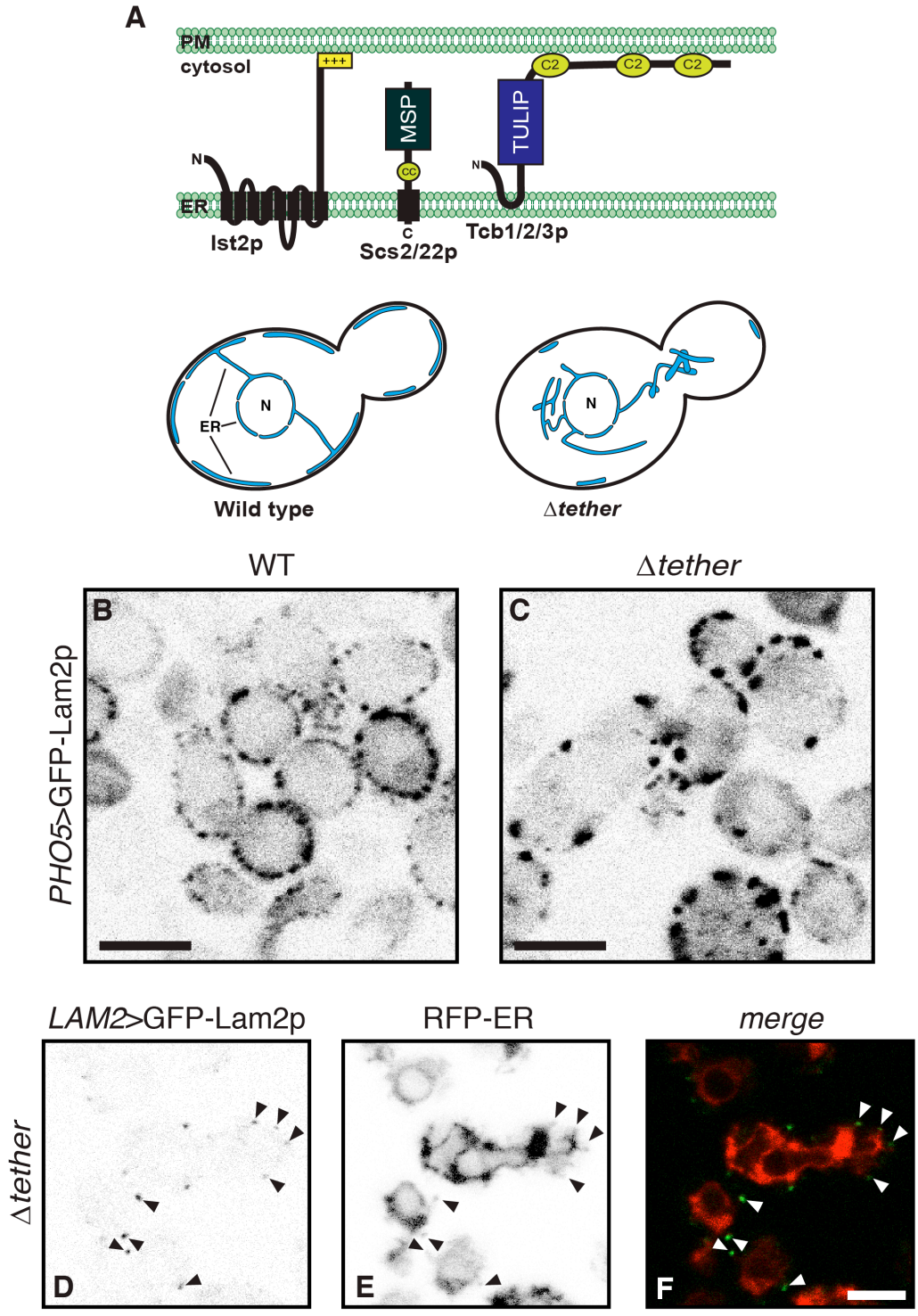

Figure 5.4 Lam2p localisation in Δ*tether* cells remains at ER-PM contacts

(**A**) Schematic representation of the ER appearance in wild type and Δ*tether* cells. The Δ*tether* strain is characterised by the knockout of six tethering proteins: Scs2/22p (homologues of human VAP-A/B), Tcb1-3 (homologues of E-Syt1-3), and Ist2p (a member of the TMEM16 ion channel family). The six-fold deletion causes a 90% loss of cER, consequent ER cytoplasmic accumulation, constitutive unfolded protein response (UPR) signalling and PI4P increase at the PM (Manford et al., 2012).

Notable elements in the tethering are: i) the polybasic region (yellow rectangle with '+' signs) in Ist2p that interacts with anionic lipids (mainly PS) on the cytosolic leaflet of the PM, ii) the MSP domain of Scs2/22p that engages in protein-protein interaction, possibly also making direct contact with PM lipids, iii) TULIP domains of Tcb1-3 (and E-Syt1-3) involved in lipid traffic in response to local perturbation of specific phospholipid levels, iv) C2 domains, whose membrane targeting activity is coordinated by PIP_2 and Ca^{2+}-binding. (**B-C**) GFP-Lam2p overexpression in wild type and Δtether cells with qualitative comparison of GFP-positive puncta in both conditions. (**D-F**) Δ*tether* strain with RFP-ER marker and GFP-Lam2p expressed at endogenous levels. Arrowheads indicate the ER tubules making contact with the PM. Scale bars, 5 μm.

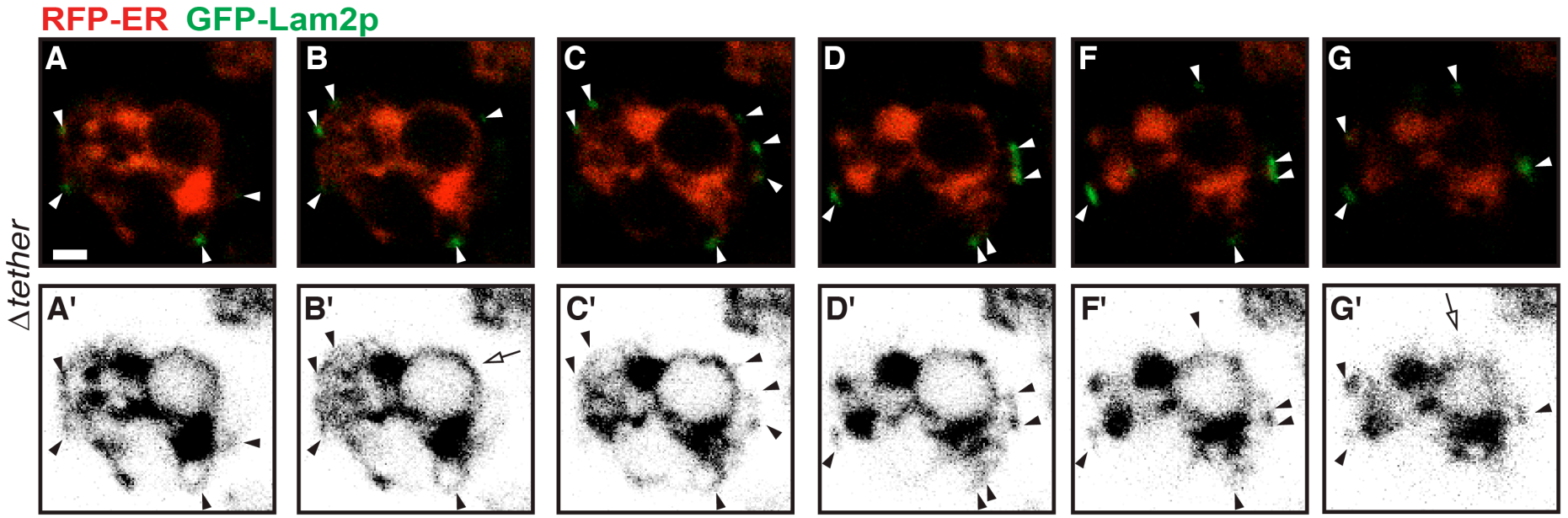

Figure 5.5 Confocal sections of a Δ*tether* expressing GFP-Lam2p

Adjacent 0.43 μm sections apart in a Z-stack of a Δ*tether* cell expressing RFP-ER under a strong promoter and GFP-Lam2p under the endogenous promoter. Every time a Lam2p-positive punctum is present (white arrowheads, panels **A-G**), an ER tubule takes contact with the PM (black arrowhead, panels **A'-G'**), even if the ER strand appeared in less confocal sections than the GFP-positive dot (arrow, panels **B'** and **G'**). Panels A-G show RFP-ER and GFP-Lam2p, panels **A'-G'** show inverted grey scale of RFP channel only. Scale bar, 1 μm.

To summarise the observations described so far:

- GFP-Lam2p localised to dots at the periphery of the cell,
- the position of the GFP-tag at the C- or N-terminus of the protein does not influence the localisation,
- expression levels played a minor role in the localisation,
- In a strain lacking 90% of cER, Lam2p localisation was maintained at close contact with the PM,
- Lam2p localisation was not related to mitochondria, but co-localised with an ER-marker.

As consequence of the last point, Lam2p must localise at ER-PM contacts different from those mediated by the six tethering proteins previously identified, so its targeting mechanisms are independent to tricalbins, Scs2/22p or Ist2p. One could speculate that Lam2p operates as a "residual tether" in the absence of the other six tethering proteins, and its role is strictly related to its localisation at these contacts. Alternatively, Lam2p could have no tethering activity, but be part of an unidentified tethering complex.

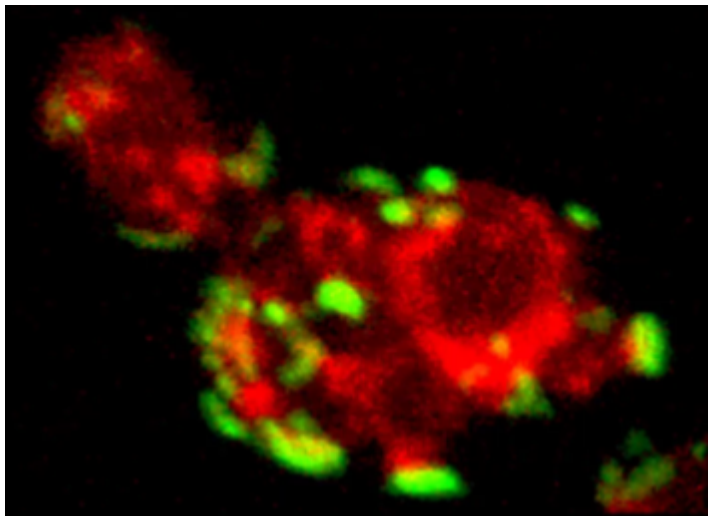

Figure 5.6 Three-dimensional reconstruction of Δ*tether* cell expressing GFP-Lam2p

Three-dimensional reconstruction of a z-stack of confocal images of Δ*tether* cells expressing an RFP-ER marker and GFP-Lam2p under the control of its endogenous promoter. Pictures were acquired using a Zeiss LS700 confocal microscope with living yeast cells blocked between slide and coverslip. The whole thickness of the cells (5.3 μm) was covered by 14 equally distanced sections so to have a 20% partial overlap. 3D image was reconstructed using ZEN Lite software (Zeiss).

5.1.2. Lam2p C-terminus is required and sufficient for targeting

Next, I determined which sequence elements were important for the right targeting at ER-PM contact sites. The sequence of full length Lam2p was modified to allow convenient clonings of different domain combinations. Some nucleotide modifications were carefully planned to insert additional restriction sites. These modifications resulted in the addition of two residues: Thr after Lys828, and Arg after Ser1244 (Figure 5.7). These insertions were made in regions with no predicted secondary structure, so to minimise structural and functional effects on the protein.

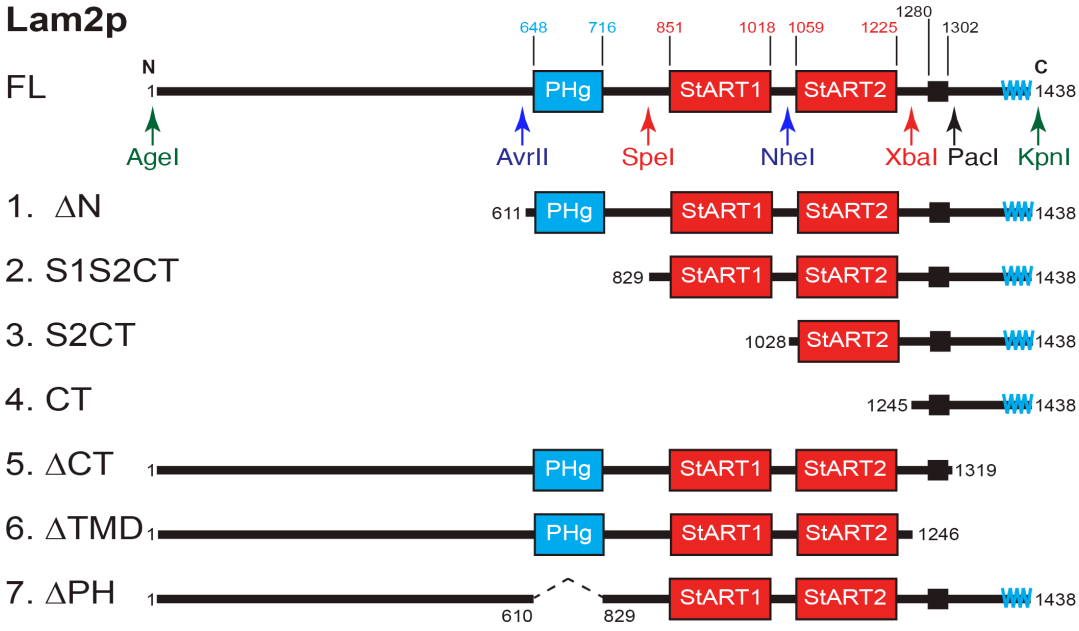

Figure 5.7 Constructs for studying Lam2p targeting

The diagram shows the domain composition of the Lam2p constructs, expressed with an N-terminal GFP-tag under both *PHO5* and *LAM2* promoters. Full length sequence contained two modifications to insert restriction sites in unstructured regions of the protein. PacI (black) is the only restriction site already present in the wild type sequence. AgeI and KpnI (green) were used to clone the full length inside the expression vector and are outside the gene sequence. AvrII and NheI (blue) were obtained by modifying the nucleotide sequence (A1829T and A1832G for AvrII; C3083T for NheI) with no effects on translation. SpeI and XbaI (red) were obtained adding the residues T after K828, and R after S1244, respectively. Structure prediction identified no ordered elements in the N-terminus (1-608). Construct 6 (ΔTMD) does not have the transmembrane domain (TMD), and the C-terminus (CT). C-terminus predicted coiled coil domain is included in the diagram (cyan).

I observed the localisation of the different constructs under *PHO5* and endogenous promoters in *lam2*Δ cells. As expected, the *PHO5* promoter induced higher expression for all constructs, however the overexpression, that resulted in cortical punctate distribution for the full length protein (Figure 5.8 FL, and Figure 5.1), induced major mislocalisation effects for selected constructs. To analyse in more details the localisation patterns (Figure 5.8):

- At endogenous levels, constructs 1, 2, 3, 4, and 7, missing increasing portions of the cytoplasmic domain, showed the expected localisation in puncta at cER-PM contacts, just like the FL protein.
- In particular, the C-terminal portion (construct 4, from the transmembrane domain to the end of the protein, the last 194 residues) was sufficient for the punctate peripheral localisation.
- Constructs 5 and 6, missing only the ER-luminal domain and the entire C-terminus including the TMD respectively, presented a nuclear GFP-staining
- When overexpressed, constructs 1 and 2, missing the N-terminus and N-terminus plus PH domain, tended to mislocalise to dots in the internal ER.
- The lack of the PH domain alone did not result in major localisation problems both at endogenous and overexpressed levels.
- Constructs 3 and 4 also lacking the StART-like domains, resulted in diffusion of the GFP-tagged proteins to the general ER, with positive dots visible both at the periphery and the nuclear envelope.
- Overexpressed construct 5, missing the ER-luminal domain, presented diffusion of GFP to the nucleus (just when expressed at endogenous levels), but also the presence of one or two noticeable cortical dots.

Figure 5.1 showed few GFP-positive internal dots per confocal section. The mechanism behind this localisation is unknown, but the behaviour of overexpressed constructs 1 and 2 to numerous internal dots suggests that the localisation could rely on the presence of the PH domain: when the protein is lacking the N-terminus and the PH domain (construct 2), the GFP-positive

internal dots remarkably increased. The localisation of Lam2p with a truncated version of the C-terminus after the TMD (construct 5, Lam2ΔCT) was very similar to the localisation of construct 6 (without the TMD). The GFP staining of the nucleus (for both 5 and 6) is not compatible with LAM cytoplasmic domains function. This observed localisation was probably due to a truncation product of the N-terminal GFP-tag, that is known to diffuse through the nuclear pore (Seibel et al., 2007). Hoewever, the overexpression of construct 5 still showed some cortical ER puncta possibly driven by (i) TMD itself, (ii) the 15 residues left in the luminal portion, (iii) elements in the cytoplasmic domains, (iv) a combination of either the former.

The part of the protein sufficient and necessary to direct the localisation to cortical ER puncta is the C-terminus including the TMD and the ER luminal domain that contains a predicted coiled-coil region (Figure 4.3). As an additional proof, I visualised the co-expression of the GFP-Lam2p (FL) and RFP-Lam2CT (RFP-tagged construct 4) in a *lam2*Δ strain. The two proteins showed significant co-localisation (Figure 5.9), suggesting the presence of an unexpected element in the luminal portion responsible for the targeting.

Looking in the literature for possible elements of cortical ER targeting in yeast and other organisms, the ER-PM localisation of Lam2p was similar to the plant viral protein TGBp3 (Wu et al., 2011). It has been shown both in plant and yeast cells, that TGBp3 partitions into puncta lying in or adjacent to tubular subdomains of cortical ER, these being characterised by highly curvature or tripartite junctions. Its localisation is controlled by a short hairpin structure in the lumen of the ER. When imaged together, Lam2CT and TGBp3 did not co-localise (Figure 5.10).

In conclusion, Lam2CT (the last 194 aa, inclusive of TMD and ER luminal domain) was sufficient for targeting to peripheral puncta. This result showed that the localisation of Lam2p is largely determined by an element present in the C-terminus of the protein, the portion predicted to be in the ER lumen.

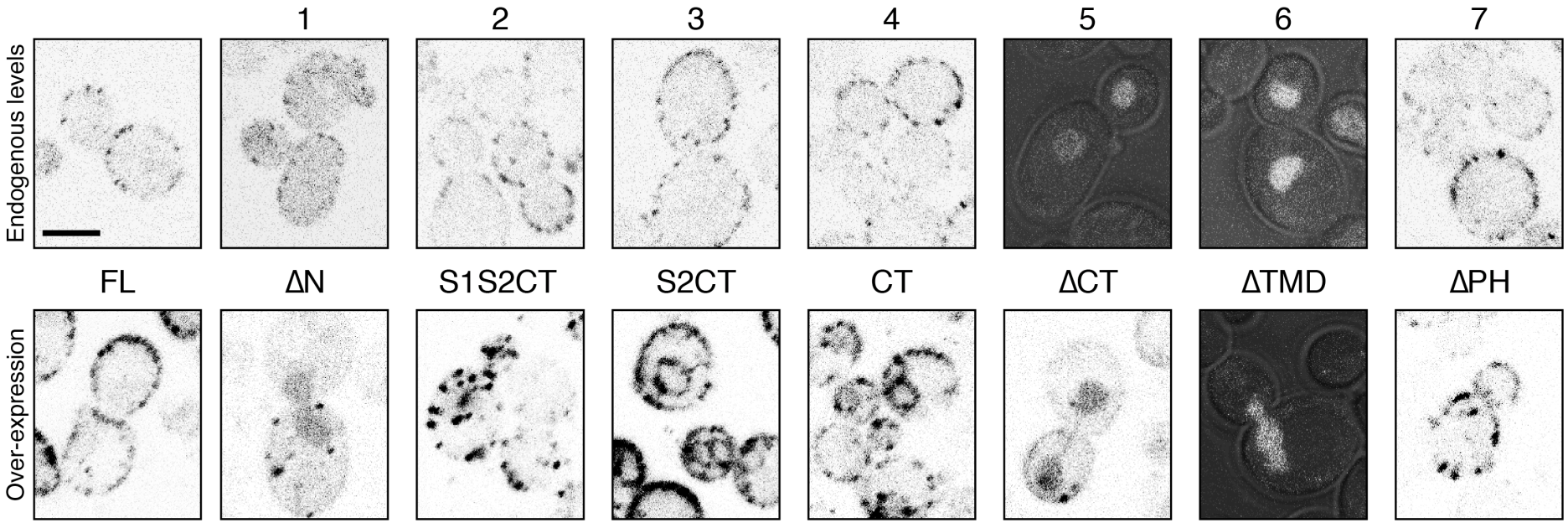

Figure 5.8 Analysis of Lam2p targeting

Analysis of the localisation of the N-terminus GFP-tagged constructs listed in the Figure 5.7. Constructs were all transformed into Δ*lam2* cells and compared to full length (FL) protein. The diagram shows the domain composition of the Lam2p constructs. No structure prediction identified ordered elements in the N-terminus (1-608). Construct n. 6 with no TMD and the CT is diffused in the nucleus and partly in the cytoplasm. Top panels show expression at endogenous levels, bottom panels show *PHO5*-driven expression. Lam2CT (the last 194 aa, inclusive of TMD and ER luminal domain) is sufficient for targeting to peripheral puncta. All images show inverted grey scale, except in construct 5 (top panel) and construct 6 (top and bottom panels) where the GFP channel is shown in grey scale overlayed to 20% opacity DIC channel. Scale bar, 5 μm.

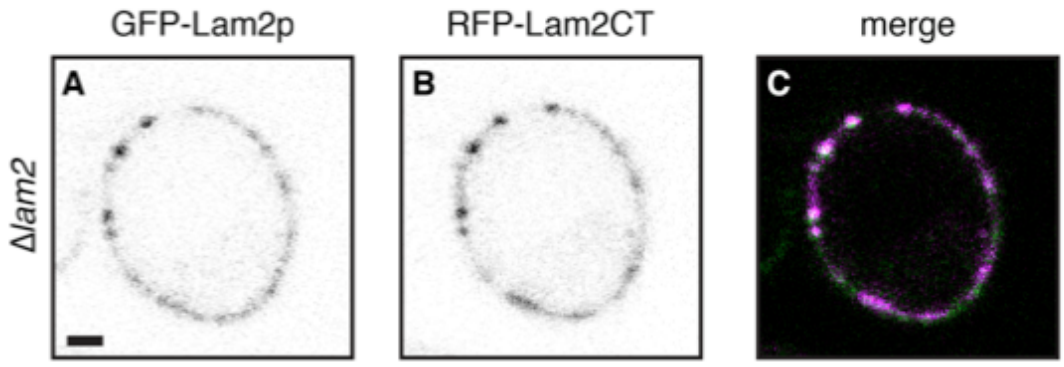

Figure 5.9 Co-localisation of Lam2p and its C-terminus

Co-expression of GFP-Lam2p with RFP-Lam2CT in Δ*lam2*. Single channels are shown in inverted grey scale, merge showing GFP in green and RFP in magenta (co-localisation in white). Scale bar, 1 μm.

Third party copyright material

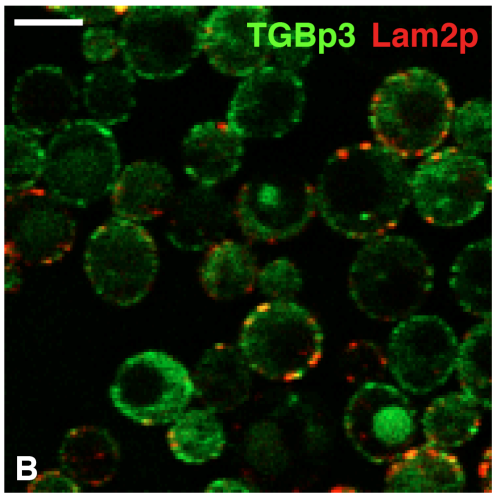

Figure 5.10 Lam2p does not co-localise with the tubular ER marker TGBp3

(**A**) In the family of plant Potexviruses, the protein TGBp3 has a localisation signal in a short ER-luminal hairpin that directs the protein to curved ER tubules. In yeast it localises to cER puncta. Image shows a 3D reconstruction of yeast cell expressing an ER marker and TGBp3 (copied from Wu et al., 2011). (**B**) Δ*lam2* strain co-expressing TGBp3-EGFP and RFP-Lam2CT. Scale bar, 5 μm.

5.1.3. GFP-Lam2p localisation is independent of vesicular traffic

Since the GFP-positive puncta are consistent with Lam2p anchoring either in the PM or in the ER, I induced expression of a portion of GFP-Lam2p from the *GAL1* promoter after inactivating *SEC18* (yeast homologue of NSF). After the block of vesicular traffic through the Golgi at non-permissive temperature, I observed the localization of the newly expressed GFP-Lam2CT (construct 4 in Figure 5.7), the part of the protein required and sufficient for correct targeting. The GFP-positive puncta were still visible at the periphery of the cell with some accumulation in the cytoplasmic ER and nuclear envelope likely due to the strong overexpression driven by the *GAL* induction and present also at permissive temperature. On the contrary, Sso1p, a PM-resident t-SNARE could only reach its final destination if expression was induced before inactivating SNARE-mediated transport through Golgi (Figure 5.11). This indicated that (i) Lam2p localisation was largely independent from vesicular traffic, (ii) it reached its final destination without leaving the ER, (iii) its TMD was embedded into the ER, and iv) its localisation in cortical dots corresponded to ER-PM contacts.

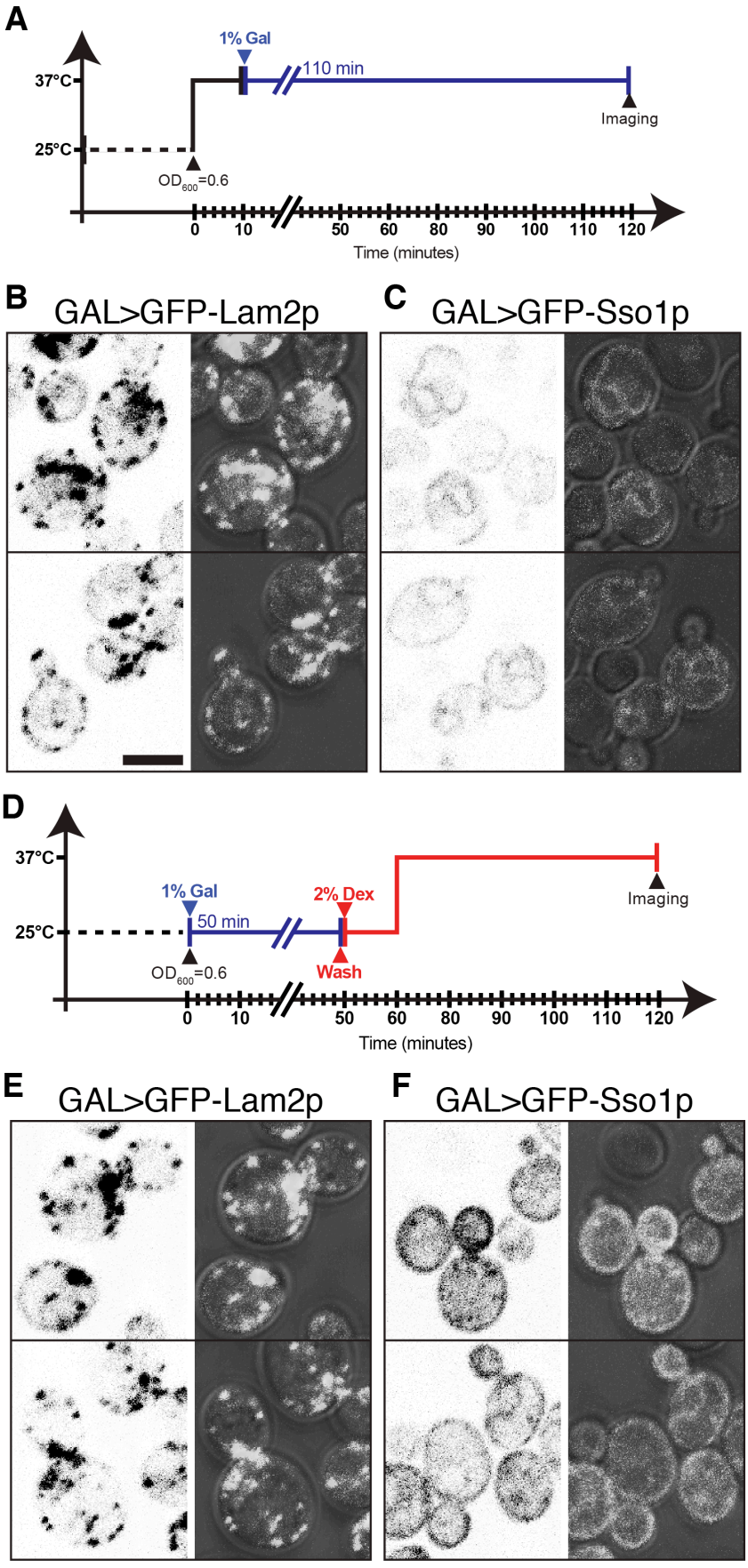

Figure 5.11 GFP-Lam2CT targeting is independent of SNARE-mediated transport through Golgi

Figure 5.11 GFP-Lam2CT targeting is independent of SNARE-mediated transport through Golgi (Previous page)

(**A-C**) *sec18-1* cells (RSY271) were grown at 25°C over-night, diluted back to OD_{600} = 0.1 and grown until OD_{600} = 0.6 (Time 0), when cells were moved to non-permissive temperature (37°C) to block Golgi transport. After an initial block of 10 minutes, GFP-tagged proteins were induced with addition of 1% galactose into the growth medium until imaging 2 hours later. (**D-F**) Cells in logarithmic phase were exposed to 1% galactose to induce transcription at permissive temperature, after 50 min cells were washed from galactose and medium was changed to dextrose to stop transcription. After 10 min cells were moved to 37°C to stop Golgi trafficking and imaged after 1 additional hour. Expression of GFP-Lam2CT (**B** and **E**, construct 5, Figure 5.7) or GFP-Sso1 (**C** and **F**), was under control of *GAL1* promoter. Two representative fields are shown for each condition with the left images displaying inverted grey scale, and on the right DIC images superimposed to the GFP channel to indicate the profile of the cells in relationship to the GFP-positive puncta. GFP-Lam2CT localised to cortical puncta also when expressed after the temperature shift (**E**). In contrast, GFP-Sso1p was found in the ER (both nuclear envelope and cER) when expressed after blocking Sec18-mediated trafficking (**C**), but otherwise reached the PM (with some punctate internal staining probably due to *GAL1*-driven overexpression, and less prominent nuclear envelope staining) and was expressed at higher levels despite the shorter induction (**F**). Scale bar, 5 μm.

5.1.5. GFP-Lam4p is localised at ER-PM contact sites

Next, I studied the localisation of Lam2p paralog, Lam4p. The GFP-tagged protein was localised in dots close to the PM both under strong and endogenous promoters (Figure 5.12 A-B). Because of this striking similarity of the localisation of Lam4p and Lam2p, I looked at the co-localisation of the two paralogs in Δ*lam2* strain. GFP-Lam4p endogenous levels were lower compared to Lam2CT, and this is consistent with GFP-based (Ghaemmaghami et al., 2003) or mass spectrometry-based (Kulak et al., 2014) high-throughput experiments, where Lam2p is about 8 fold more abundant than Lam4p. Analysing the co-localisation at a qualitative level, I identified partial, but significant overlap between the two paralogs (Figure 5.12 C-E). Also in Δ*tether* cells, GFP-Lam4p maintained its localisation at the remaining ER-PM contacts (data not shown), as we had found previously with Lam2p. This was another indication that the paralogs Lam2p and Lam4p populate a sub-class of ER-PM contacts independent from other known tethering proteins.

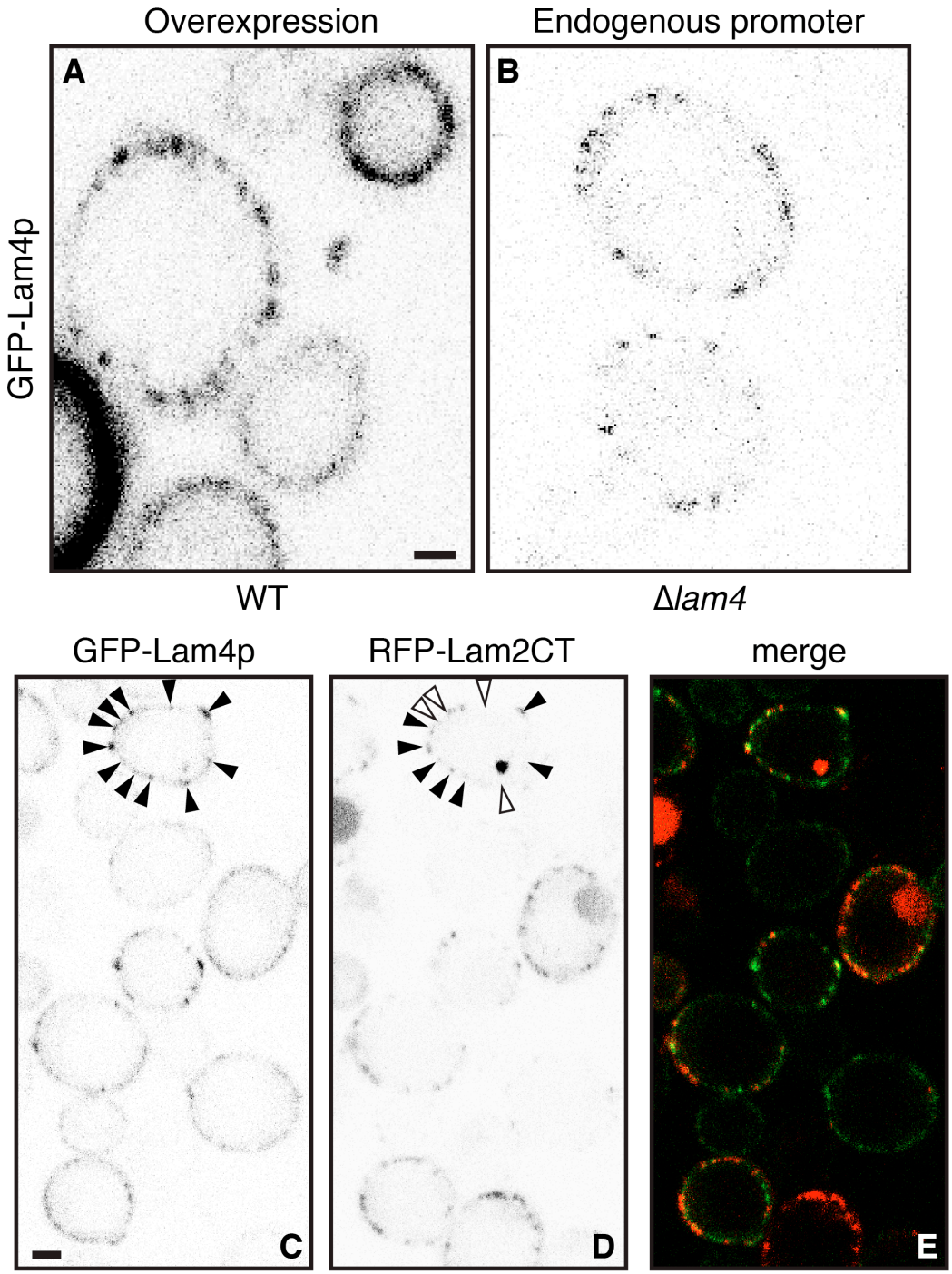

Figure 5.12 Lam4p is distributed in cortical puncta which partially co-localise with Lam2p

(**A**) GFP-Lam4p distribution under the control of *PHO5* promoter in wild type BY4741 background. (**B**) GFP-Lam4p distribution at endogenous levels in Δ*lam4* strain. (**C-E**) Co-expression of GFP-Lam4p and RFP-Lam2CT in RS453c Δ*lam2*. Single channels are presented in inverted grey scale. Qualitative analysis of the co-localisation in a single cell: arrowheads in C, indicate GFP-positive puncta corresponding to Lam4p; in **D** the black arrowheads indicate RFP-Lam2CT positivity, while white arrowheads show absence of Lam2CT. This highlights the presence of partial but significant co-localisation; also visible from the merge of the two channels (**E**). Scale bars, 1 μm.

5.2. Localisation of Lam1/3p at ER-PM contact sites

After noticing the cortical distribution and partial co-localisation of the paralogs Lam2p and Lam4p (Figure 5.12), we observed similar peripheral puncta for Lam1p and Lam3p (Louise Wong, personal communication). In Δ*tether* cells, GFP-Lam3p was still found in peripheral puncta (Louise Wong, personal communication), and similar to Lam2p, all GFP-positive puncta were in close proximity to a strand of ER extending to the periphery. While Lam2p over-expression did not cause major effect in its distribution (Figure 5.1), Lam3p expressed by a strong promoter, diffused and accumulated to the ER (Figure 5.13 B). This is consistent with the fact that Lam2p is the most expressed, while Lam4p, and Lam1/3p were only just detectable by confocal microscopy. These observations suggested that (i) LAM proteins which localised at ER-PM contacts, *i.e.* Lam2p, Lam4p, Lam1p, and Lam3p, target a sub-domain of the cER, different from the contacts mediated by the six tethering proteins missing in the Δ*tether* strain, and (ii) this sub-domain, covering 4% of the PM in the Δ*tether* strain, is saturable.

5.3. Mutual co-localisation of LAMs at ER-PM contact sites

In order to get preliminary information about the interplay of the four LAM proteins localised at ER-PM contacts, I performed two types of experiments at the confocal microscope: (i) observation of Lam2p and Lam3p co-expression, (ii) screening of the localisation of GFP-tagged LAMs in delete strains.

5.3.1. Co-localisation of Lam2p and Lam3p

I previously showed the partial overlap between Lam2p and its paralog Lam4p Figure 5.12). Next, I observed the co-localisation of Lam2p with Lam3p, a member of the other paralogous pair. This co-localisation was greater: in low expressing cells, 87% of GFP-Lam3p puncta were also RFP-Lam2p positive (observation of 20 cells, with an average of 17.2 puncta per cell, s.d. 10.7%) (Figure 5.13). Overexpression of Lam3p accumulated the protein in the general ER (as already observed), but strikingly, this overexpression caused also mislocalisation of Lam2p into internal ER puncta (Figure 5.13 B).

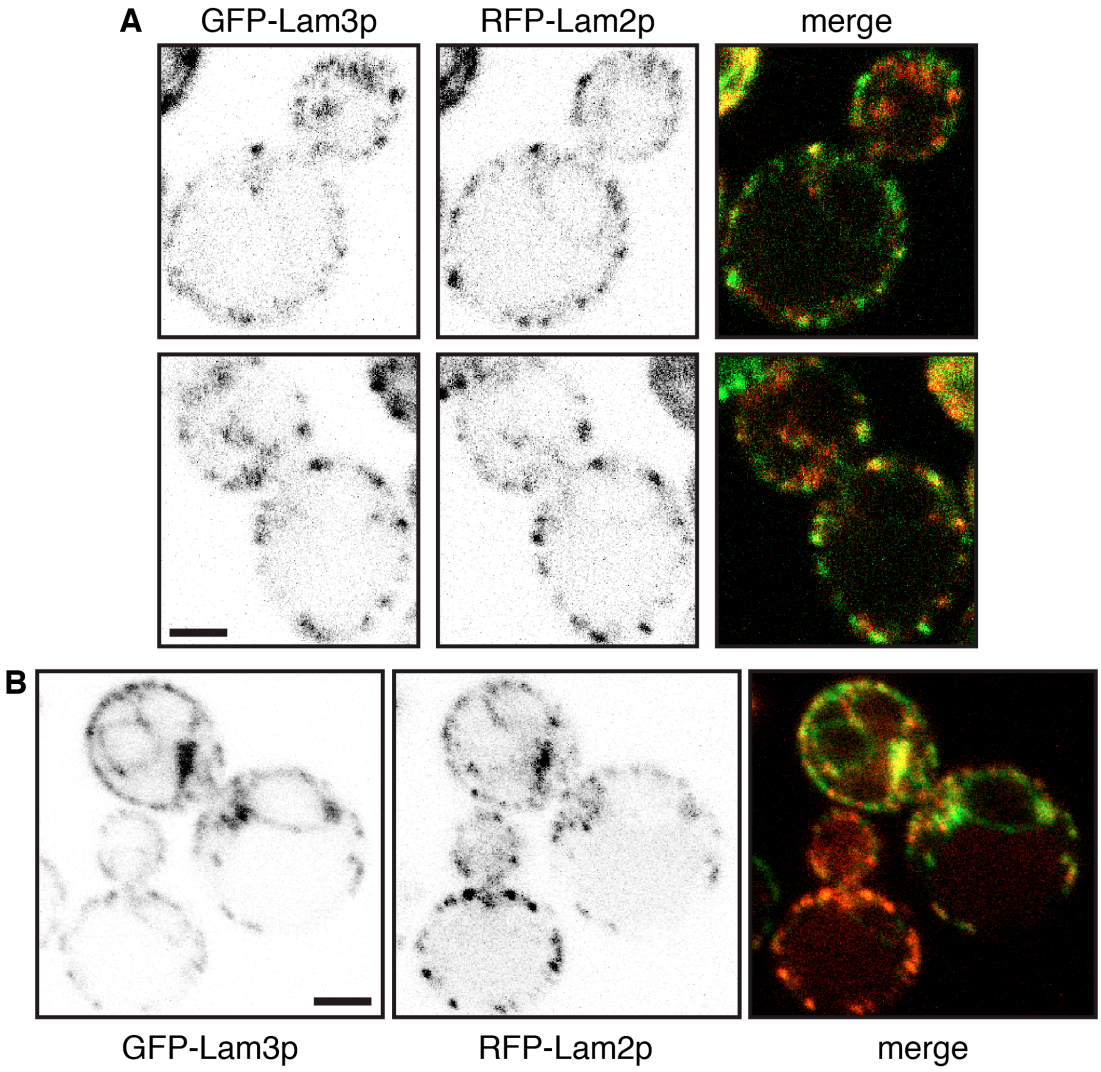

Figure 5.13 Lam2p and Lam3p co-localisation at ER-PM contact sites

Δ*lam2* cells co-expressing GFP-Lam3p and RFP-Lam2p (full length) under the control of *PHO5* promoter. (**A**) Display of cells expressing GFP-Lam3p at low levels, with separate channels as inverted grey scale. ~90% of Lam3p positive puncta co-localised with RFP-Lam2p puncta. (**B**) Display of cells with high levels of GFP-Lam3p, which diffuses into general ER and accumulates internally, associated with partial re-localisation of RFP-Lam2p to internal dots. Scale bars, 2 μm.

5.3.2. GFP-Lam2/4p are not expressed at visible levels in Δ*lam3* strain

Considering that Lam1-4p are localised at ER-PM contacts, observing the co-localisation of Lam3p and Lam2p and Lam2p mislocalisation induced by Lam3p overexpression, I wondered if the lack of Lam1/3p paralogs also caused some effects in Lam2/4p localisations. I screened the localisation of the N-terminus GFP-tagged versions of these paralogous pair expressed under endogenous promoters in the single delete strains for ER-PM LAM proteins.

First, comparing the overall expression levels of Lam2p and Lam4p, it was clear that Lam2p was expressed at more copies per cell (Table 8.2), as observed in hight hroughput studies aimed at calculating protein abundances (Ghaemmaghami et al., 2003; Huh et al., 2003). Interestingly, GFP-Lam4p levels seemed to increase in *lam2*Δ background (Figure 5.14 G). If Lam2p and Lam4p have redundant function (see following chapter), this observation could reveal a compensatory mechanism. More detailed analysis at Western blot level will be required to understand a possible co-regulation, but a promoter swap revealed that *LAM4*>GFP-Lam2p levels were comparable with *LAM2*-promoted expression, supporting a post-translation regulation of Lam2p levels (Tim Levine, personal communication). In an analogous way, Lam2p levels looked generally increased in *lam1*Δ with more intense dots at the cell periphery and continuous linear staining of the cER in some cells (Figure 5.14 B). The most interesting evidence from this screening was the disappearance of both Lam2/4p in the absence of LAM3. As observed in the previous section (5.3.1), the overexpression of Lam3p accumulated the protein in the general ER, and resulted in mislocalisation of Lam2p. Concurrently, the lack of Lam3p caused a remarkable decrease of Lam2/4p expression to levels not detectable by confocal microscopy. This could be explained by a central role of Lam3p in directing the localisation of the other paralogous pair. Lam2/4p could be rapidly degraded (*e.g.* more predisposed to ubiquitination) when Lam3p is not at ER-PM contacts. Further experiments aimed at the molecular characterisation of

LAM proteins mutual interactions should target the description of this possible complex (Discussion, Section 8.5).

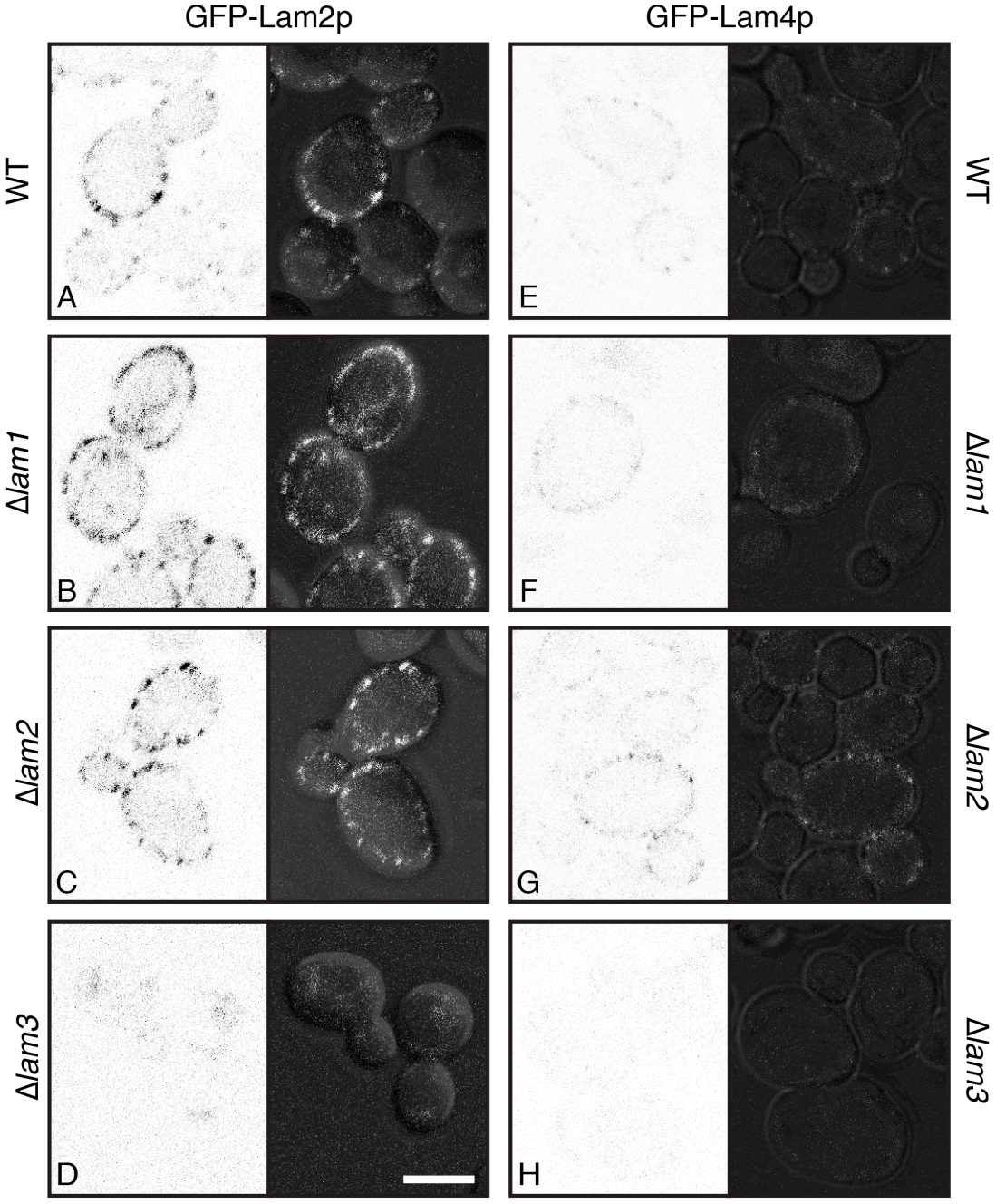

Figure 5.14 Lam2p and Lam4p localisation in LAM single delete strains

Screening of GFP-Lam2p (**A-D**) and GFP-Lam4p (**E-H**) localisation in *LAM1*, *LAM2*, and *LAM3* single delete strains compared to wild type. Cells in each conditions are presented in inverted grey scale for the GFP channel and overlayed to the DIC image on the right. Scale bar, 5 μm.

The data presented in this chapter, can be summarised in the following conclusions:

- Lam1/2/3/4p localised at a unique type of ER-PM contact sites compared with others previously known.
- Lam2p co-localised with Lam4p only partially, and also with Lam3p at a greater extent.
- The different expression levels indicate that they do not form 1:1 stoichiometric complexes.
- Overexpression of Lam3p caused strong mislocalisation of Lam2p to internal ER.
- Deletion of *LAM3* resulted in the disappearance of GFP-Lam2p and GFP-Lam4p puncta, possibly indicating a leading role of Lam3p in the localisation of Lam2/4p.

For these reasons, together with their highly punctate appearance, one speculation is that there is a “LAM complex” as formed by the two paralogous pairs, but more experiments will be required to determine the nature of their interaction and other possible components (Discussion 8.5).

5.4. Lam5 and Lam6 localise at multiple contact sites

5.4.1. GFP-Lam5p and GFP-Lam6p are localised at NVJ, ER-mitochondria, and ER-vacuole contacts

Finally, I studied the localisation of the last two members of the LAM family in yeast: Lam5p and Lam6p. I overexpressed Lam5p or Lam6p from an integrating plasmid in RS453c wild type strain co-expressing either the ER or the mitochondria marker (Figure 5.15). They co-localise with an ER marker, in accordance to their transmembrane domain being ER-embedded as I showed for their homologues Lam2/4p, and Lam1/3p. They localise at nER-vacuole junctions (NVJ), as well as at ER-mitochondrial contact sites, and with an additional punctate distribution around the vacuole. Targeting the NVJ and ER-mitochondrial contacts implies that Lam5p and Lam6p target multiple contacts that include the ER.

The pattern of distribution in puncta around the vacuole was never described previously for ER-anchored proteins. However, it is possible that these puncta represent ER-vacuolar contacts that have previously been overlooked. Indeed, close examination of cells co-expressing GFP-Lam5p and RFP-ER showed that some of the GFP-positive perivacuolar puncta also contained ER elements (Figure 5.15H, asterisks). Perivacuolar GFP-Lam5/6p puncta sometimes co-localise with mitochondria (data not shown), indicating that the puncta may be related to the newly described vCLAMP vacuolar-mitochondrial contacts (Hönscher et al., 2014; Elbaz-Alon et al., 2014), even if no ER components have been identified in vCLAMPs. The perivacuolar Lam5/6p puncta need further more detailed examination, in particular by co-localisation with vCLAMP markers, to determine if they are an ER component of vCLAMPs, or if they are a novel contact site between cytoplasmic ER elements and the vacuole, or both. Another localisation outside clearly defined contacts, includes general staining outside to the nuclear envelope or to multiple cortical patches (daughter cell in Figure 5.15A).

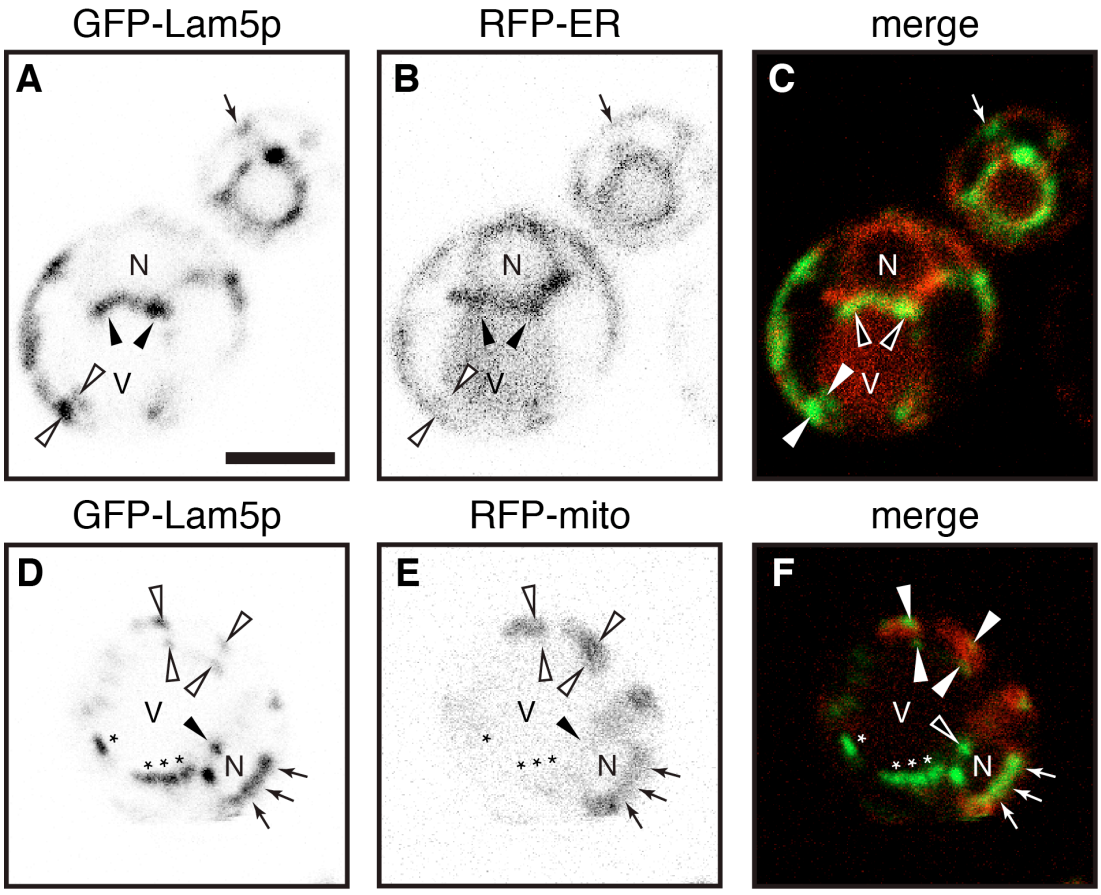

Figure 5.15 Lam5p and Lam6p target NVJ, ER-mitochondria and ER-vacuole contacts

Caption after the next part of the figure (next page).

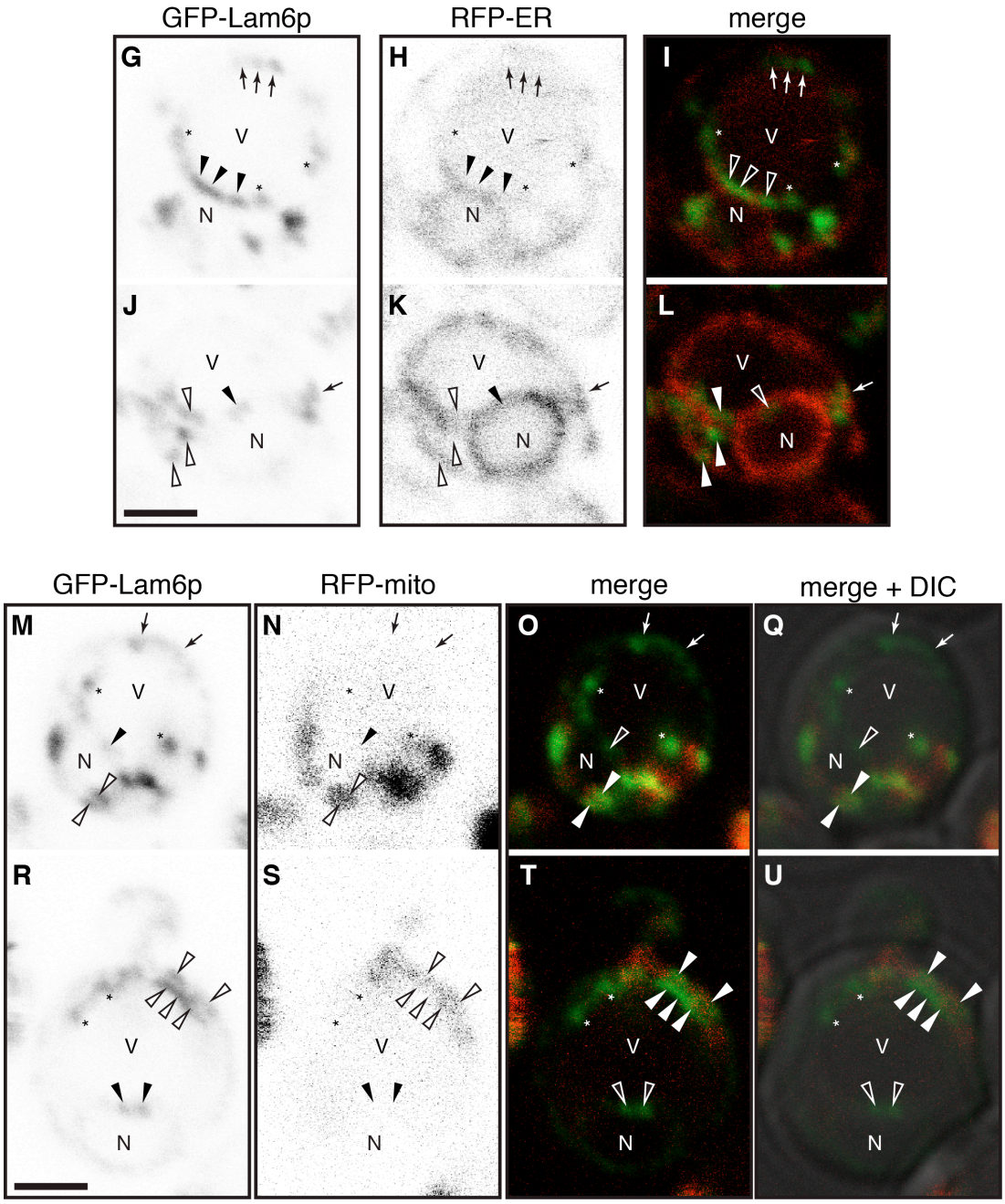

Figure 5.15 Lam5p and Lam6p target NVJ, ER-mitochondria and ER-vacuole contacts

Lam6p figure at next page. N-terminus GFP-tagged Lam5p (**A-F**) and Lam6p (**G-U**) were transformed using integrating plasmids in wild type RS453c strain. The GFP-tagged proteins were under the control of *PHO5* promoter and co-expressed with an RFP-marker for ER (**A-C** and **G-L**) or the mitochondria (**D-F** and **M-U**). Four symbols indicate the targeting: NVJ (black filled arrowheads); parallel lines (white filled arrowheads), visibly localising around mitochondria in panels **F**, **O**, and **T**; cortical ER (arrows), sometimes co-localising with mitochondria; perivacuolar dots (asterisks), possibly corresponding to new ER-vacuole junctions. Scale bars, 2 μm.

Chapter 6

LAM function at contact sites: intracellular sterol traffic

6. LAM FUNCTION AT CONTACT SITES

6.1. Lam4p sterol binding properties

LAM proteins localise to membrane contact sites between the ER and another organelle and they possess a StART-like domain whose lipid specificity and function are still unclear. Lipid transfer proteins in the StART domain family are defined by the presence of the conserved helix-grip fold of about 170–210 residues that forms the hydrophobic pocket for lipid monomer ligand binding.

To determine the lipid ligand of the region we predicted as StART-like with bioinformatics software, we tried to express the recombinant version of the yeast and human domains.

First, we had to optimise protocols for their recombinant production and purification on a sufficiently large scale. Expressing the constructs in *E. coli*, there are multiple parameters that can be changed to improve expression, solubility and stability:

- the tag for affinity purification; the tag could favour purification as well as solubility.
- the *E. coli* strain used for the production; a strain lacking specific proteases could enhance the final production yield.
- the codons of the protein sequence; optimising the sequence with codons preferred by specific bacterial strains or using a strain which has been codon-optimised for mammalian gene expression can ease/speed up protein production.
- the concentration of IPTG used to induce the production (typical concentration 0.2 mM, range 0.05 mM - 2.0 mM).
- the temperature of induction, which is linked to the time of induction, because a lower (<25°C) temperature will require more time (overnight) for the bacterial cells to produce the same amount of recombinant protein.

- changing the length of the sequence; alterations by a few residues can greatly affect the solubility maintaining the biochemical properties.
- The cellular destination; in some cases periplasmic expression improves protein solubility.

For the recombinant production of the StART-like domains of LAM proteins, I tested different conditions to record the optimal protocol. The StART-like domains that I could express as soluble proteins in bacteria were the four StART-like domains of Lam2p and Lam4p, with the second domain of Lam4p (Lam4pS2) giving the highest yield.

About Lam4pS2, I will describe here the protocols for its production and the use I made of Lam4S2 domain in two *in vitro* assays to test its lipid binding properties. Furthermore, I used this domain for structural studies using NMR due to the high yield of purification (compatible with NMR requirements) and its stability in solution (see Chapter 7. Structural studies). Also, I made several attempts to purify Lam1p and Lam3p StART-like domains (Section 6.2).

6.1.1. Production and purification of recombinant StART-like domains of Lam2p and Lam4p

To screen for the best expression conditions of the different StART domains, we selected the predicted StART-like domains and cloned them in pTrc-His bacterial expression vectors. The choice of the protein boundaries at both termini turned out to be a delicate step to obtain the soluble recombinant domain. It is known that the ability of a protein to be successfully expressed in E. coli is inversely proportional to its complexity and to the number of contiguous hydrophobic amino acids (Braun et al., 2002). There are small ranges in polypeptide space surrounding defined Pfam domains that result in expression constructs with high yield (Dyson, 2010). So the expression of the recombinant StART-like domains required a precise mapping of the domains and their boundaries by using secondary structure prediction tools, such as PSI-PRED, to make constructs spaced at five amino acid intervals for expression screening. The domains were His-tagged and GFP-tagged at the N-terminus. The original tagging vector pTrc-His-A (Invitrogen) has 6 histidines. We added five additional histidines to the His-tag, making it a His_{11}-tag to increase affinity to the Nickel-beads and decrease the background (non-specific proteins) in the elution steps.

I transformed the *E. coli* with the constructs for screening and I observed them at the epifluorescence microscope to visually check the appearances of the GFP-tagged domains after IPTG induction under different conditions and timepoints. Once the construct with optimal boundaries and the best induction conditions were determined, the His-tagged version of the protein with no GFP was produced in small volume and the whole bacterial cell lysate was run on a Coomassie gel to evaluate the presence of the band of the overexpressed protein. Finally, the culture was scaled up to 1 litre, and the protein was purified on a bench top Nickel-agarose beads affinity column.

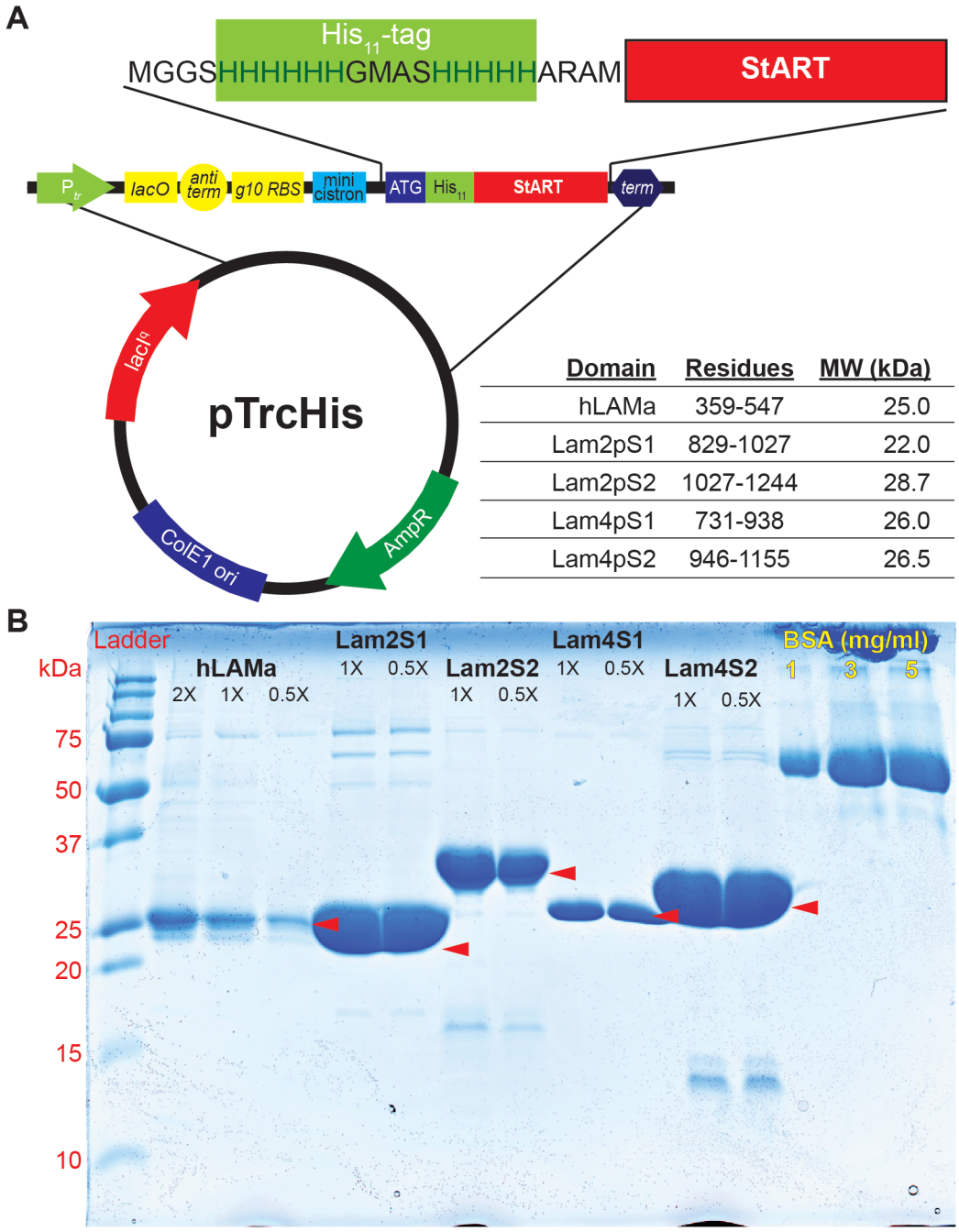

Domain	Residues	MW (kDa)
hLAMa	359-547	25.0
Lam2pS1	829-1027	22.0
Lam2pS2	1027-1244	28.7
Lam4pS1	731-938	26.0
Lam4pS2	946-1155	26.5

Figure 6.1 Recombinant StART domains production and purification

(**A**) Schematic representation of pTrcHis$_{11}$ constructs for the production of recombinant StART-like domains. The commercially available pTrcHis vectors was modified to elongate the His$_6$-tag with five more histidines to increase affinity at Ni-NTA beads and decrease the non-specific binding. The residues between His$_{11}$ and the StART domain sequence were different for each protein (ARAM residues in the drawings corresponded to Lam4S2). The table shows the residues chosen for each StART-like domain according to the prediction of the boundaries. (**B**) Coomassie stained 15% SDS-PAGE gel with samples from the different StART-like domains. Stock solution of BSA at increasing concentration and the same volume of

recombinant proteins (half the volume 0.5X, same volume 1X or twice the volume 2X) were run in parallel. 1X volume = 5 μl (corresponding to 1% of total volume of fraction).

6.1.2. Lam4pS2 binds sterol

There are multiple strategies to identify the ligand of a lipid binding protein. Usually they involve (i) the isolation of the protein or its lipid binding domain and (ii) the characterisation of the ligand within the hydrophobic region of the protein.

A recombinant lipid binding protein produced from *E. coli* can bind bacterial lipids without loosing the hydrophobic ligand during the purification process, depending on ligand affinity. Lam4S2 was processed for lipid extraction immediately after purification from *E. coli* and run on a TLC plate. A band corresponding to phosphatidylglycerol (PG), the major phospholipid of bacterial cell membrane, was identified (data not shown[2]), suggesting lipid binding properties of the recombinant domain.

In our approach, I purified Lam4S2 with the optimised protocol and I used it in radiolabelled lipid binding assay with permeabilised human cells. In this method the recombinant StART domains were incubated with HL60 cells whose lipids had been previously radiolabelled with [^{14}C]-acetate (Garner et al., 2012; Holic et al., 2014). The permeabilisation with the pore-forming toxin Streptolysin O (SLO) allows protein up to 100 kDa to enter the cell (Walev et al., 2001). In this way the protein will be able to freely get in and out of the cells and bind its lipid ligand (Figure 6.2 A). After the co-incubation, the His_{11}-tagged protein was re-captured on Ni-NTA affinity columns and lipids were extracted and analysed on a thin layer chromatography (TLC) plate. The positive controls were His-tagged proteins known for binding lipids: *Dm*RdgBα, that operates a counter transport of PA and PI at ER-PM contact sites (Yadav et al., 2015); *Hs*PITPα, that binds PI and PC in its cavity (Cockcroft, 2009); Pdr16p^{wt}, with high affinity for PI and low to sterol and its mutant Pdr16p^{E235A,}

[2] This experiment was performed by Yves Sere in Anant Menon laboratory (Weill Cornell University, NY, USA)

^{K267A}, defective for PI binding and with higher affinity for cholesterol (Holic et al., 2014); Sec14p, that has affinity for various lipid molecules, but binds PI or PC at higher affinity and it is important for vesicle formation in TGN/endosomal system (Bankaitis et al., 2010). The negative control was a His_6-GFP-tagged PH domain of OSBP[3].

The re-purified Lam4S2 was verified on a Coomassie-stained SDS-PAGE and compared to the protein input (Figure 6.2 D). The lipid extract from the re-purified protein, contained a lipid that co-migrated with cholesterol on the TLC plate (Figure 6.2 B). The solvent system used for this TLC plate was aimed at separation of lipid with polar headgroups (relatively independently from the length of their acyl chains), so I switched to another solvent system to develop neutral lipids. The lipid bands that ran near the solvent front in the TLC, were scraped and re-separated on a new TLC on a solvent system for neutral lipids, triacylglycerol (TAG) and diacylglycerol (DAG) (Figure 6.2 C). Also in this case, the lipid contained in Lam4S2 co-migrated with cholesterol, run as standard or extracted from Pdr11p (Holic et al., 2014). The experiment was repeated twice.

Lam4pS2 exclusively bound cholesterol. No other cellular lipid, including any of the major phospholipid, that all were ^{14}C-labelled, was detected in the bound fraction. This protein binding assays showed that the predicted StART-like domain has high affinity towards sterols and it is able to solubilise the hydrophobic lipid molecule similarly to other known StART domains, such as StARD1 or MLN64/StARD3.

[3] I performed the radiolabelled lipid binding assays in Shamshad Cockcroft laboratory at UCL. The recombinant proteins used as controls were gift from other laboratories: *S. cerevisiae* Sec14p, Pdr11p, and *H. sapiens* PITPα from Cockcroft laboratory, GFP-PH^{OSBP} from Olkkonen laboratory (University of Helsinki, Finland).

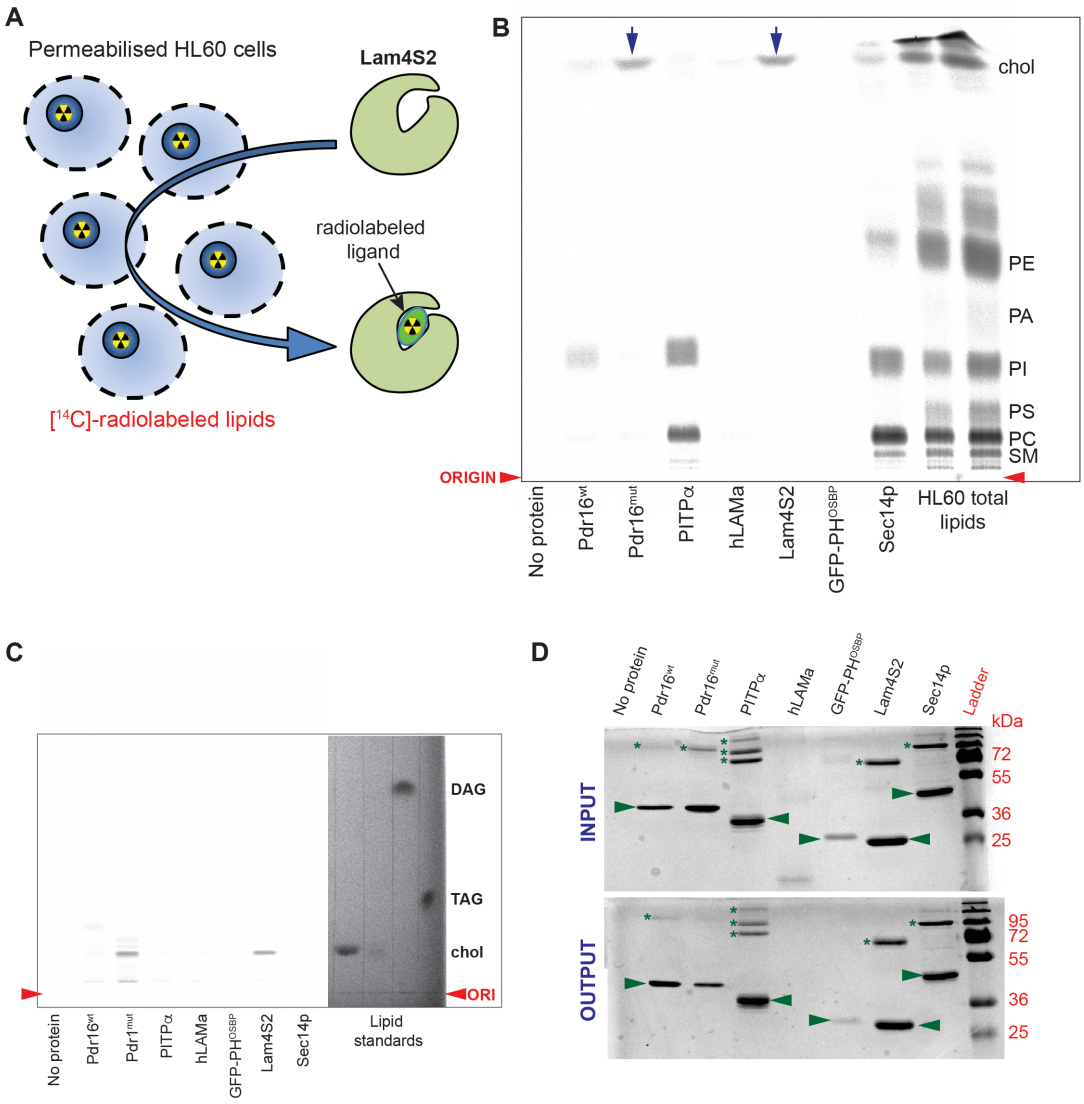

Figure 6.2 Lam4S2 binds cholesterol in *in vitro* binding assays

(**A**) Diagram showing the experimental setting of the *in vitro* binding assay: human leukemic (HL60) cells in which the majority of lipids were labelled with ^{14}C-acetate over a 48 hour period were semi-permeabilized with SLO and incubated with bacterially expressed Lam4S2 and other control proteins. After incubation, the His-tagged proteins were re-captured on Nickel beads and re-purified on small scale. The extracted protein was processed for lipid extraction, and extracts run on a TLC plate. (**B**) Lipid extracts run on a TLC plate. Controls included: incubation with no protein, Pdr16p wild type (which binds PI and cholesterol, blue arrows, very faint for Pdr16^{wt}) and its mutant (which loses the ability to bind PI, but increases the affinity for sterol) (as described in Holic et al., 2014), *Homo sapiens* PITPα or *Drosophila melanogaster* RdgBβ (included in the experiment repeat) as positive controls, and GFP-PH^{OSBP} as negative control. Lipid extracts of re-isolated proteins were separated by TLC. Positions of major identifiable lipids were ascertained from total lipids: SM, sphingomyelin; PC, phosphatidylcholine; PI, phosphatidylinositol; PA, phosphatidic acid; PS, phosphatidylserine; PE, phosphatidylethanolamine; chol, cholesterol). Red arrowheads indicate origin. (**C**) Plate shown in B was processed to recover lipids

running near the solvent front by scraping. The material obtained from the scraped bands was processed again for lipid extraction, and extracts run on a new TLC with a solvent system to separate neutral lipids. The left side with radiolabelled lipids was visible after exposure of the autoradiography, the right side was visible after copper (II) sulfate charring. Red arrowheads indicate origin. (**D**) Samples of the His-tagged proteins included in the experiment before (top) and after (bottom) the incubation and re-isolation process were separated on a 12.5% SDS-PAGE and stained by Coomassie (MW markers on the right). Asterisks indicate bacterial contaminants.

I quantified the cholesterol binding for all proteins by analysing the densitometry of the corresponding bands for the two experiments. The binding value corresponds to the fold increase in intensity of cholesterol band normalised on the GFP-tagged PH domain of OSBP (Figure 6.3). The two point mutations in Pdr16 lipid binding site increase the affinity for cholesterol (Holic et al., 2014). hLAMaS did not show cholesterol binding, but the observation of the SDS-PAGE with the proteins before and after incubation with donor compartment and recapture on Ni-NTA column (Figure 6.2 D), showed the protein to be clipped (Input) and not recovered (Output). The non-significant cholesterol signal above the background levels could be due to little amount of protein not visible by Coomassie-stained SDS-PAGE and the high sensitivity of ^{14}C detection. Lam4S2 showed significant cholesterol binding (Figure 6.3).

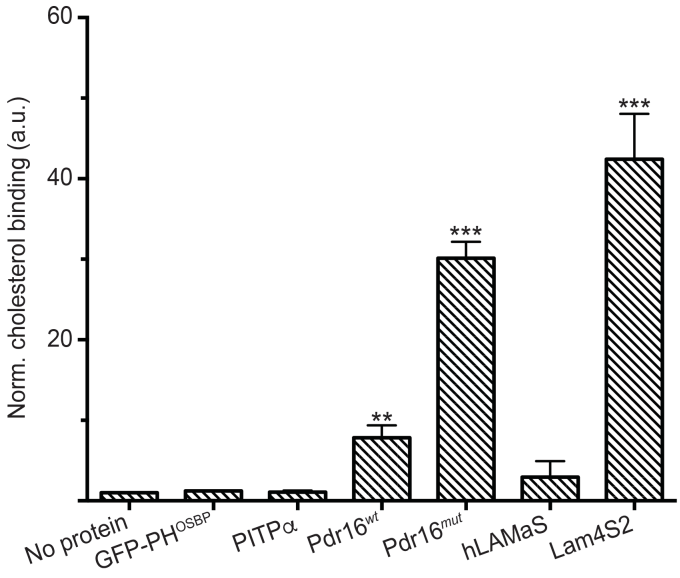

Figure 6.3 Quantification of cholesterol binding

Quantification of the cholesterol bound to lipid transfer proteins included in experiment of Figure 6.2. TLC plates were exposed to Fuji phosphorimaging screens and analysed using a Fuji BAS1000 phosphorimaging system. Both the SDS-PAGE and TLC images were analysed using AIDA software. Background level was subtracted from values, and lipid levels were weighted on recovered protein levels (from SDS-PAGE) and normalised on the negative control (GFP-PH^{OSBP}). Data represent mean ± S.E.M. Values from two independent experiments and the repeat of one experiment in another solvent system (Figure 6.2C). Two-tailed Student's *t*-test in comparison with GFP-PH^{OSBP} values, $^{**}p < 0.01$, $^{***}p < 0.001$.

6.1.3. Spectrometry of protein-lipid interaction shows the dynamic Lam4pS2 sterol binding

In the previous experiment, I showed the ability of Lam4pS2 to bind cholesterol molecules in an in vitro binding assay. The crucial step for this kind of experiments is the incubation of the donor compartment, *i.e.* the permeabilised and radiolabelled HL60 cells, with the lipid transfer proteins, followed by the separation of the two components. This separation step does not allow the determination of the kinetic and the dynamic of the protein-lipid interaction.

To overcome this limitation, previous works used a live read-out of sterol binding, switching to dehydroergosterol (DHE) as ligand (de Saint-Jean et al., 2011). DHE is a natural ergosterol analogue with fluorescent properties provided by an additional double bond in the ring structure (Figure 6.4). When excited at 300 nm wavelength light, DHE gives a specific pattern of three emission peaks at 354, 373 and 393 nm (Mukherjee et al., 1998). The other fluorophores in the assay are the tryptophans of the lipid transfer protein in solution, which emit fluorescence (peaking at 340 nm) when excited at a range between 260 and 300 nm. Excitation at 295 nm is selective for tryptophans, and gives minimal excitation of other aromatic amino acids, tyrosine and phenylalanine (Teale and Weber, 1957).

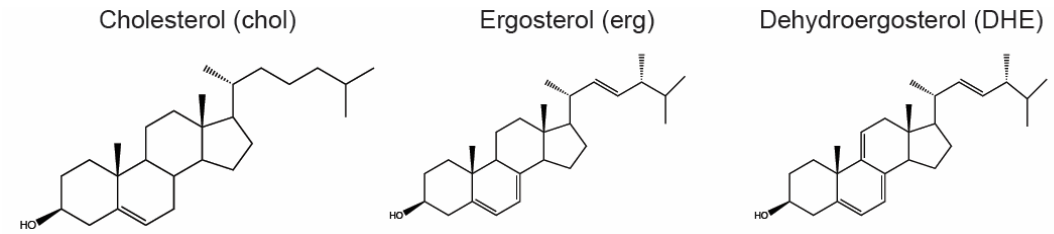

Figure 6.4 Chemical structure of sterols

Chemical structure of cholesterol (chol), the most abundant sterol in animal cells, ergosterol (erg), the most abundant sterol in fungal cells, and dehydroergosterol (DHE), a naturally occuring ergosterol analogue with fluorescent properties resulting from the additional double bond in the ring structure.

It is possible to create a new fluorescence emission from tryptophan and DHE when they are very close together. When a tryptophan residue is excited at 295 nm and the DHE is close enough to it, the Trp emission is quenched by the DHE. In place of the tryptophan emission peak at 340 nm, three peaks at 354, 373, and 393 nm will appear. These DHE peaks are caused by the Förster resonance energy transfer (FRET) from the tryptophan(s) in a protein sequence to the DHE bound in it (Schroeder et al., 1990; Liu et al., 2008; de Saint-Jean et al., 2011). To observe FRET, the distance between FRET donor (Trp) in the pocket lining and acceptor (DHE) should not exceed a Förster radius of 16 Å, and the intensity of the FRET signal decreases with an exponential decay (Loura et al., 2010; Loura and Prieto, 2011). We quantitatively studied the sterol binding properties of StART-like domains using DHE, a fluorescent sterol that mimics ergosterol (Georgiev et al., 2011). Lam4p contains two tryptophans one of which is predicted to be inside Lam4p binding pocket. To examine the binding of the domain to sterols, DHE was added to Lam4S2. DHE, added in solution in equimolar methyl-β-cyclodextrin complexes (Maxfield and Wüstner, 2012), produced a strong FRET signal (Figure 6.5). Furthermore, we observed the same event for the other StART-like domains of Lam2p and Lam4p (see Discussion, Figure 8.1). This was not the case for other control experiments in which no FRET signal was detected (Louise Wong, personal communication[4]): (i) for the equimolar concentration of a non lipid binding protein (such as soybean trypsin inhibitor); (ii) in presence of 7 M guanidinium to denature Lam4S2; (iii) emission spectra of MβCD-DHE complex only; and (iv) incubation of DHE with equimolar FRET donor only (tryptophan solution).

The FRET signal of the StART-like domain can be studied with increasing concentration of DHE to estimate the dissociation constant of the lipid with the protein (0.5 ± 0.1 μM) and the affinity of other sterols such as cholesterol,

[4] Louise Wong in the Levine lab carried out the optimisation for all StART-like domains of Lam2/4p, and the appropriate control experiments.

proven in the radiolabelled lipid binding assay (Figure 6.3) or ergosterol, the major sterol in *S. cerevisiae*.

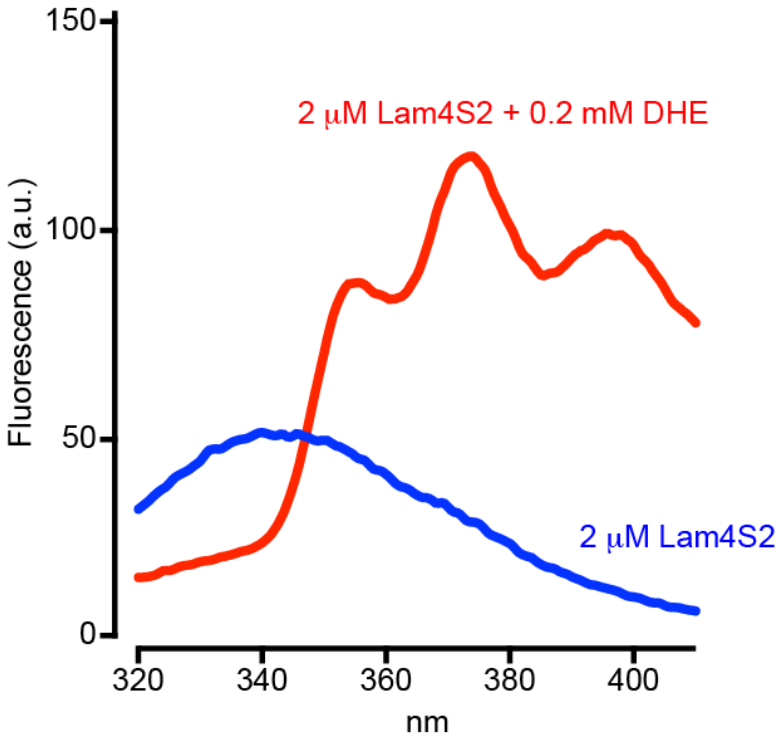

Figure 6.5 FRET between Lam4S2 and dehydroergosterol (DHE)

Emission scan of tryptophan fluorescence (excitation at 295 nm) with recombinant 2 μM Lam4S2 protein on its own (blue) or in the presence of 2 mM DHE (red) added in solution from methyl-β-cyclodextrin complexes.

6.2. Study on Lam1p StART-like domain purification

To identify the lipid ligand of the StART-like domains of the other members of the LAM family, it was necessary to have high concentration protein. Therefore, I tried to optimise protocols for the recombinant production and purification from *E. coli*. While the StART-like domains from Lam2p and Lam4p showed good production yield and stability in solution, the domains from Lam1p and Lam3p were more difficult to purify from bacteria.

To obtain these recombinant domains, I followed different strategies to optimise the expression levels and improve protein solubility and stability. These three aspects can be exploited at the same time using different changes in the expression and purification protocols.

First, StART-like domains of both Lam1p and Lam3p are divergent from the other members of the LAM family: they contain longer loops and they are evolutionary more distant from human LAM proteins and yeast Lam2/4p and Lam5/6p (Appendix 2). This could also imply that Lam1/3p have lipid ligand other than sterols. However, structural bioinformatics can predict the structural fold of an LTP, but not the lipid ligands lodged into its hydrophobic pocket. Furthermore, some StART domains have affinities for multiple lipids (Schrick et al., 2014).

Initially I tested the version 1 of the predicted StART-like domain (the plasmid called pTrcHis$_{11}$-Lam1pSv1) in *E. coli* grown in a small volume of LB and induced for different amounts of time and at different temperatures. This version was designed on the basis of the predicted core of the StART-like domain. In the whole cell protein extract run on a Coomassie gel the correspondent band was not visible, while Lam4pS2 treated in the same way showed the thickest band when induced at 37 °C for 4 hours (Chapter 6.1.1).

Next, I modified the N- and C-terminal boundaries after studying secondary structure predictions and the conservation of the residues. The resulting confidence of prediction showed a potential problem for Lam1Sv1 on the C-

terminal boundary where an additional short helix could be found after the long helix of the StART-like domain.

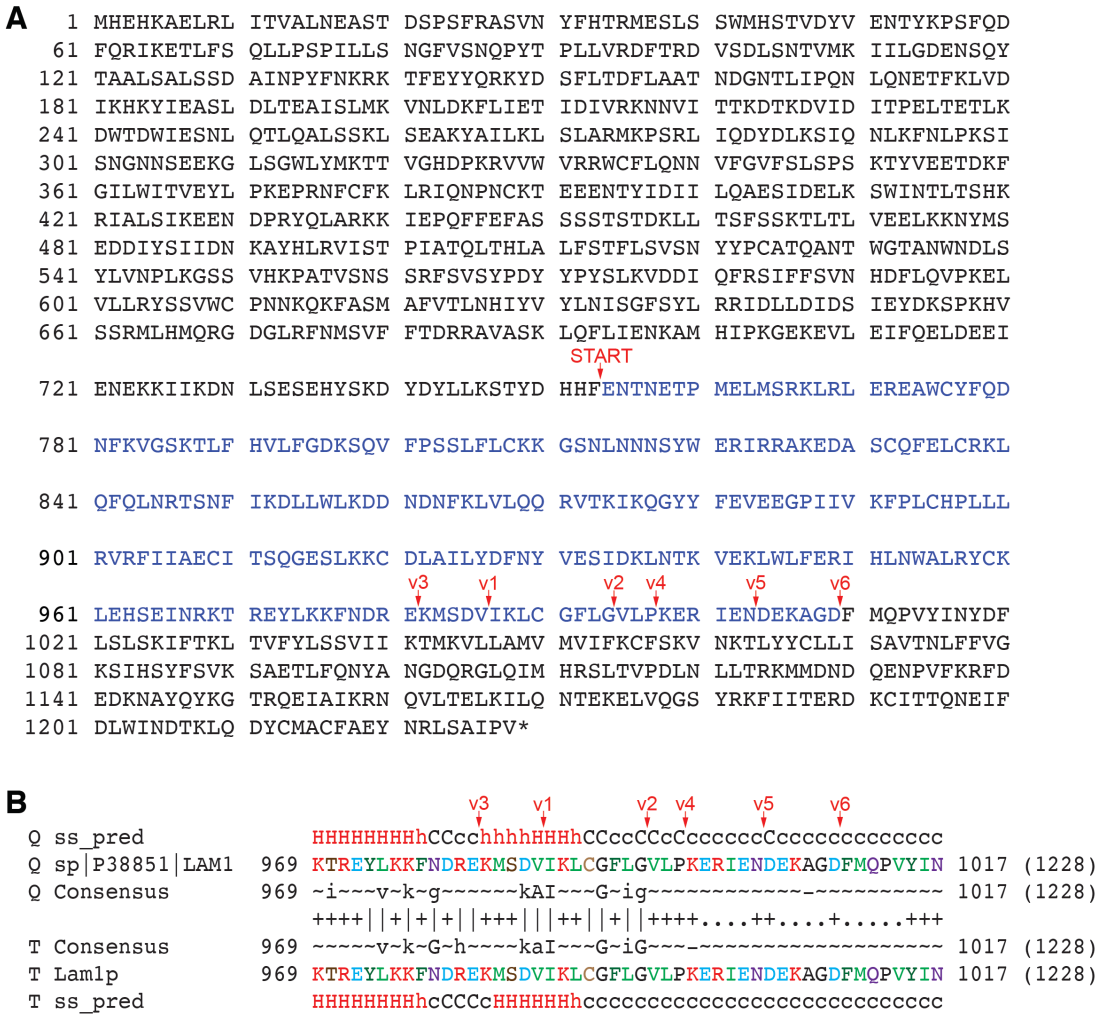

Figure 6.6 Lam1p constructs for the expression of its StART-like domain

(**A**) Full aminoacid sequence of Lam1p with predicted StART-like domain (blue residues) and different boundaries of final constructs for Lam1StART recombinant expression. Boundaries were chosen according to the predicted secondary structure given by programs such as HHpred or conserved sequence from PSI-blast. (**B**) In depth analysis of predicted ordered secondary structure (`ss_pred`, calculated using PSI-PRED 3.0) at Lam1pStART's C-terminus. Alignment is shown from the end of the long α–helix of the domain. Prediction was obtained from an HHpred search using Lam1p as query (`Q`) and observing the alignment with itself as target (`T`). The end of version 1 lies in the middle of an additional predicted short helix at the C-terminus. Residues are coloured for their characteristics.

First, I tested the solubility of the constructs with different C-terminal boundaries in yeast. We reasoned that comparing the expression of the GFP-tagged domain in the original model organism could give important information about the construct solubility *in vivo*, especially because Lam4S2, the StART-like domain with higher solubility and yield from *E. coli*, resulted in strong GFP expression in the cytosol of yeast cell. I sub-cloned them from a pTrcHis$_{11}$ vector to a pRS416 vector for yeast expression and checked the fluorescence at the confocal microscope: using Lam4S2 as positive control, the comparison suggested that some versions were more soluble than others (Figure 6.7 A).

Another way to test the solubility of the best constructs, identified screening the expression in yeast, is to observe a Coomassie gel with the bands from a small volume whole bacterial cell lysate (Figure 6.7 C). The second step involved protein production from *E. coli* at different conditions of the most promising constructs (n. 2, 3, and 6) in small volume cultures. The presence of the band corresponding to the Lam1S was compared to purified Lam4S2, and lysate of un-induced *E. coli* (Figure 6.7 B). Lam1Sv2, that gave the most intense band, was also made as a Small Ubiquitin-like Modifier (SUMO)-tag version. SUMO is known to enhance the solubility of difficult target protein (Panavas et al., 2009). The SUMO-tagged version of Lam1Sv2 gave apparent higher protein yield, but the Coomassie-stained SDS-PAGE revealed the presence of unidentified bands at lower MW than expected, possibly corresponding to proteolytic product (Figure 6.7 C).

Considering the difficulties in finding the optimal conditions for the purification of the StART-like domains of Lam1p and its paralog Lam3p, we decided to take advantage of indirect ways to uncover the lipid ligands of the predicted StART domains. First, we studied the phenotype of some LAM deleted strains when exposed to the sterol-sequestering fungal drug, Amphotericin B (AmB).

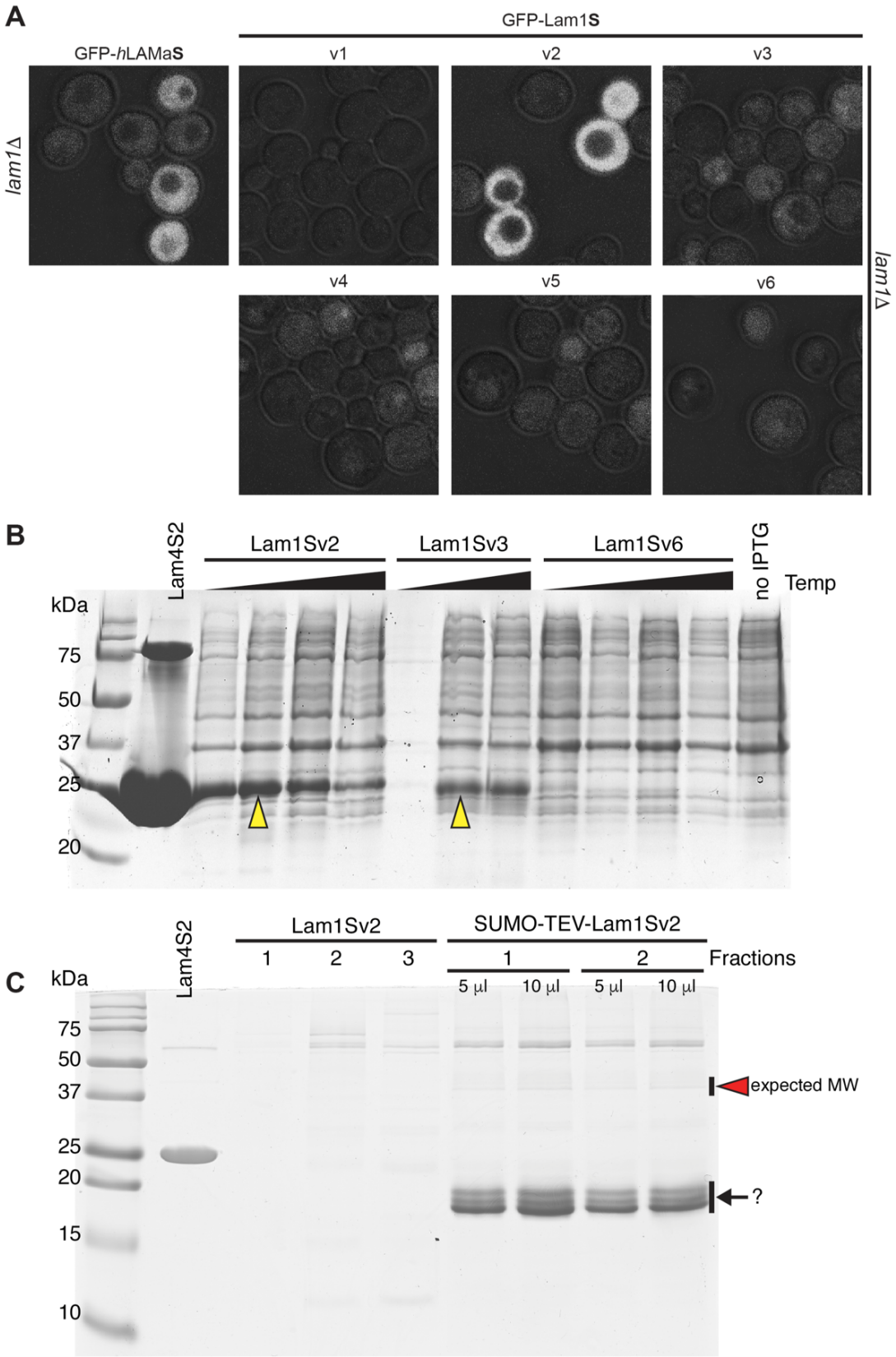

Figure 6.7 Optimisation of Lam1S purification

(**A**) Construct for bacterial production were sub-cloned into the yeast expression vector pRS416 under the control of *PHO5* promoter and N-terminally tagged with GFP. GFP-fluorescence was evaluated at the confocal microscope and compared to

Lam4S2 fluorescence. (**B**) SDS-PAGE with Coomassie staining of the whole BL21 lysates after IPTG induction at increasing temperatures (black triangles): v2 and v6 at 18°C over night, 25°C for 8 hours, 30°C for 6 hours, 37°C for 4.5 hours; v3 was induced at 18°C over night, 25°C for 8 hours, 37°C for 4.5 hours. Lam4S2 was used as comparison, lysate of un-induced BL21 was run as comparison. (**C**) Full purification of the SUMO-tagged most promising Lam1S version. SUMO tag added 12 kDa. Cells were induced at the best conditions identified in B. Fractions were not processed with recombinant proteases (SUMO or TEV proteases). Fractions were compared to un-tagged Lam1Sv2. Unexpected proteolytic bands appeared in the range 15-20 kDa.

6.3. *lam1*Δ, *lam2*Δ, and *lam3*Δ show increased sensitivity to amphotericin B at sub-lethal doses

Hillenmeyer *et al*. (2008) used small molecules libraries and different environmental conditions as powerful tools to infer protein functionality and cell physiology. In a high-throughput effort to "uncover a phenotype for all genes", they tested the growth response of *Saccharomyces cerevisiae* single delete strains for more than 400 small molecules from diverse sources and libraries (including drugs used in clinics) as well as diverse environmental conditions and stresses (including changes in pH or temperature)[5] (Hillenmeyer et al., 2008).

Looking at the most dramatic phenotypes of the single delete strains for LAM genes, Amphotericin B (AmB) is one of the most toxic drugs in the haploid knockout strains (Figure 6.8). Out of 4130 single delete strains *lam3*Δ, *lam1*Δ, and *lam2*Δ score 4th, 13th and 23rd most sensitive homozygous deletions, respectively. *lam4*Δ, *lam5*Δ and *lam6*Δ are not sensitive to the treatment.

AmB is an antifungal drug known since the mid 1950s (Oura et al., 1955) and used in the clinic for the treatment of late stage opportunistic fungal infections (Mora-Duarte et al., 2002; Vincent et al., 2013). Its mechanism of action is poorly understood, but it is ergosterol-related:

- the channel-forming property of AmB has been historically considered the main reason of its toxicity, with AmB-sterol complexes forming pores in the PM of fungal cells causing leakage of cytosolic content (Oura et al., 1955) ;
- AmB is able to bind sterols and form complexes, the narrow therapeutic window of AmB is related to the slightly increased affinity for ergosterol, the main sterol in fungal cells, compared to cholesterol, the most abundant sterol in mammalian cells (Gray et al., 2012);

[5] All the results are publicly available in a database managed by two different university servers: chemogenomics.med.utoronto.ca /fitdb/fitdb.cgi

- AmB is also able to induce an oxidative stress, overloading mitochondria with reactive oxygen species (Mesa-Arango et al., 2014);
- more recently a “sterol sponge model” was proposed, with AmB cytotoxic activity residing mainly in extramembranous aggregates that extract ergosterol from lipid bilayers (Anderson et al., 2014).

Since the *in vitro* lipid ligands of LAM proteins are sterols, it was interesting to understand how LAM function can be linked to the function of a sterol sequestering antifungal drug, such as AmB. To study the function of LAM proteins it is possible to formulate experiments observing the AmB sensitivity (AmB^S) on two fronts:

- Sensitivity of *LAM1*, *LAM2* and *LAM3* delete strains and the effects of double or triple deletes,
- Rescue of AmB phenotype of *lam*Δ strains with tuned re-expression of entire LAM proteins, shorter fragments, or StART-like domains.

6.3.1. LAM deleted strains show increased sensitivity to AmB exposure

All fungi, including *Saccharomyces cerevisiae*, can be killed by a sufficient dose of AmB (lethal dose), especially because the promiscuity of its cytotoxic effects make this drug surprisingly resistance-refractory (Monk and Goffeau, 2008). However, *LAM1*, *LAM2* and *LAM3* deletes show enhanced toxicity in the high throughput screening of a chemogenomic study (Hillenmeyer et al., 2008) (Figure 6.8). In addition to LAM genes, also other hits were intersting. Scs2p, the yeast homologue of VAP, is the main physical tether between ER and PM, and many LTPs with FFAT motifs, target contact sites via its MSP domain (Murphy and Levine, 2016), suggesting an important role of this contact sites for the increased AmB-related phenotype (see Discussion, Section 8.4).

A

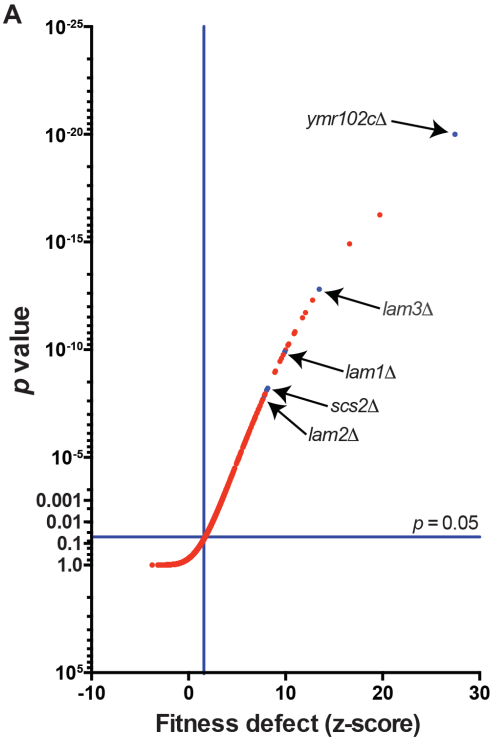

B

Gene	Fitness defect	*p* value
YMR102C	27.4651	$1.00\ 10^{-20}$
RIT1	19.7111	$5.55\ 10^{-17}$
MCK1	16.5862	$1.2212\ 10^{-15}$
LAM3/SIP3	13.4704	$1.5515\ 10^{-13}$
CAJ1	12.7969	$4.9744\ 10^{-13}$
RPL15B	12.0498	$1.912\ 10^{-12}$
GAL1	11.7572	$3.2924\ 10^{-12}$
BRE2	10.9715	$1.4862\ 10^{-11}$
YDR020C	10.9192	$1.6471\ 10^{-11}$
ITC1	10.8766	$1.7915\ 10^{-11}$
SIF2	10.3271	$5.4008\ 10^{-11}$
IES5	10.2523	$6.2933\ 10^{-11}$
LAM1/YSP1	10.0070	$1.0448\ 10^{-10}$
BMH1	9.9009	$1.3037\ 10^{-10}$
JID1	9.7587	$1.7584\ 10^{-10}$
MYO5	9.5903	$2.5141\ 10^{-10}$
SET5	8.9630	$9.8417\ 10^{-10}$
BRE2	8.9026	$1.1253\ 10^{-9}$
SCS2	8.1525	$6.195\ 10^{-9}$
YER119C-A	8.0624	$7.6431\ 10^{-9}$
HOM6	7.8994	$1.1203\ 10^{-8}$
LAM2/YSP2	7.8341	$1.307\ 10^{-8}$
HPC2	7.8328	$1.3111\ 10^{-8}$
HOS2	7.6251	$2.149\ 10^{-8}$
NHP10	7.5244	$2.7363\ 10^{-8}$

Figure 6.8 *LAM1*, *LAM2* and *LAM3* deletes show increased AmB sensitivity in high throughput screening

Adapted graphic representation of AmB sensitivity score (**A**) using data calculated and published by Hillenmeyer *et al*. (2008). The table (**B**) was reproduced from the supplementary data of the same paper. Lam3, Lam1 and Lam2 (bold in the table) score significantly high in the sensitivity defect score and they are in the top 23 most

sensitive genetic deletions out of more than 4,130. Highlighted in blue are *ymr102*Δ, *scs2*Δ and *yer119c-a*Δ (another SCS deletion) (see Discussion, Section 8.4).

LAM knockout strains from the BY4741 collection showed the expected AmB^S phenotype with *lam1*Δ and *lam3*Δ displaying the strongest defect, *lam2*Δ an intermediate sensitivity, and *lam4*Δ, *lam5*Δ and *lam6*Δ being non-sensitive to the treatment (Figure 6.9 A and B).

The strains with multiple deletions are defective in growth accordingly to the single deletes: any combination of double delete involving a sensitive strain maintains increased its sensitivity, even though not in a proportional manner, the triple delete resulted in super-sensitivity. The same phenotypic pattern was observed in a liquid culture as shown by the growth bars of two double delete strains compared to the wild type (Figure 6.9 A and C).

I repeated the same AmB sensitivity assay with the single LAM deletion strains made for this study in the RS453c background. The phenotype was faithfully reproduced, with the difference that this strain showed an overall higher toxicity to the drug, both wild-type and mutants (Figure 6.10).

These observations on *lam2*Δ phenotype are concordant with its likely involvement in sterol transfer at the interface between ER and PM and may suggest an even stronger contribution of Lam1p and Lam3p in PM sterol homeostasis. In contrast, *lam4*Δ did not increase sensitivity to AmB and this could be due to a redundant function with Lam2p, that in *lam2*Δ Lam4p expression levels cannot compensate for.

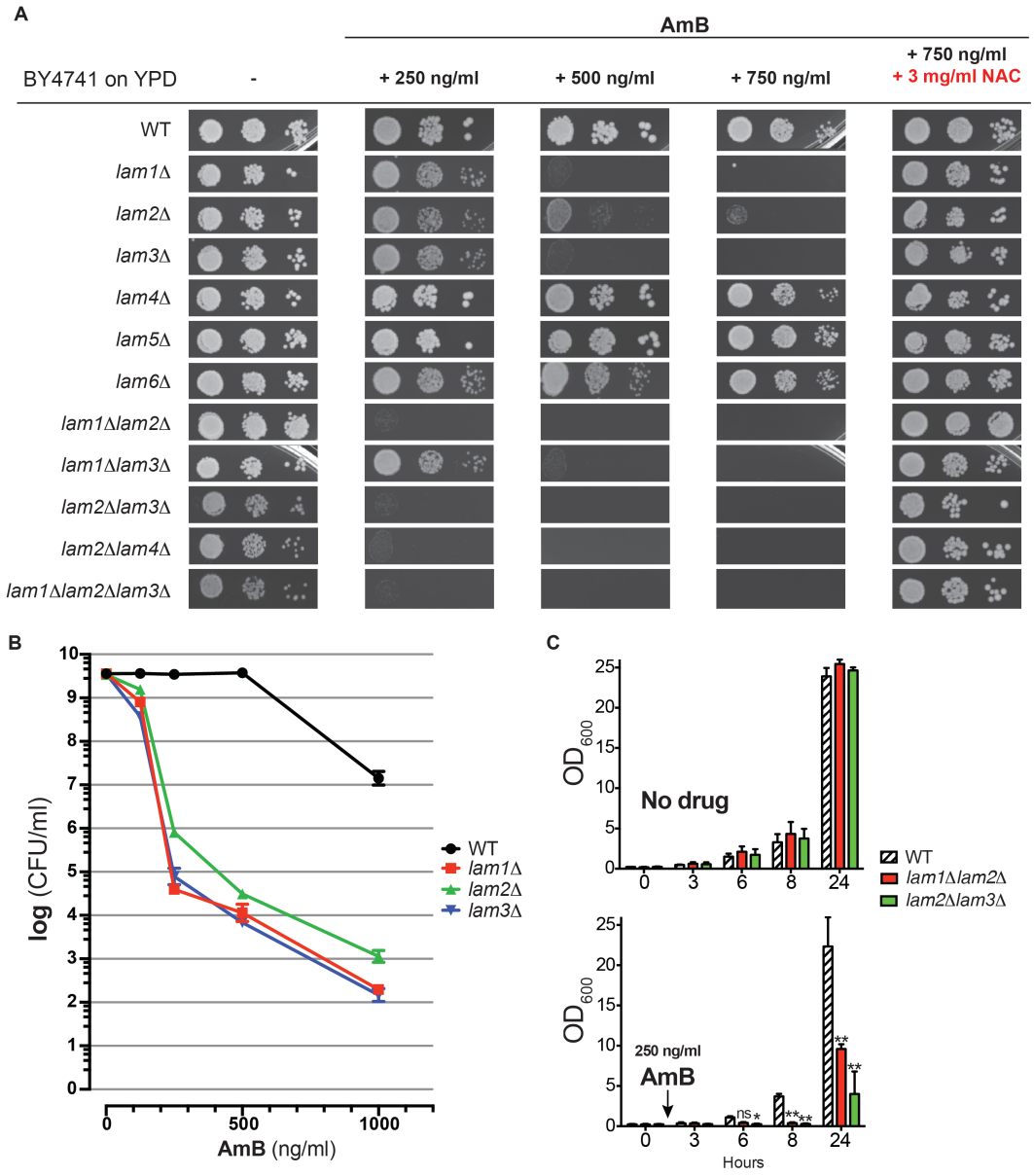

Figure 6.9 LAM1, LAM2 and LAM3 single, double and triple deletes show increased sensitivity to the antifungal drug AmB

(**A**) Dilutions of cells with single, double or triple LAM gene deletions were compared with the wild-type parental strain (WT) for ability to grow at three concentrations of AmB, or on AmB supplemented with *N*-acetylcysteine. 'No AmB' sample to control for cell number. Cells were grown in YPD liquid cultures to late exponential phase, serially diluted in three subsequent 1:200 passages in a MW96 plate, and spotted on plates supplemented with the drug using a Replica Plater. Plates were grown at 30°C for 48 hours. Addition of NAC masks the phenotype. (**B**) Quantification of colony forming units (CFUs) of single LAM deletion strains compared to wild type at the end of AmB exposure. (**C**) Comparison of growth of double delete strains in liquid cultures. Details of the growth are given in Materials and Methods (Section 3.8.2). Two-tailed Student's t-test versus WT for each time point, *ns*, not significant, **p* <0.05, ***p* <0.01.

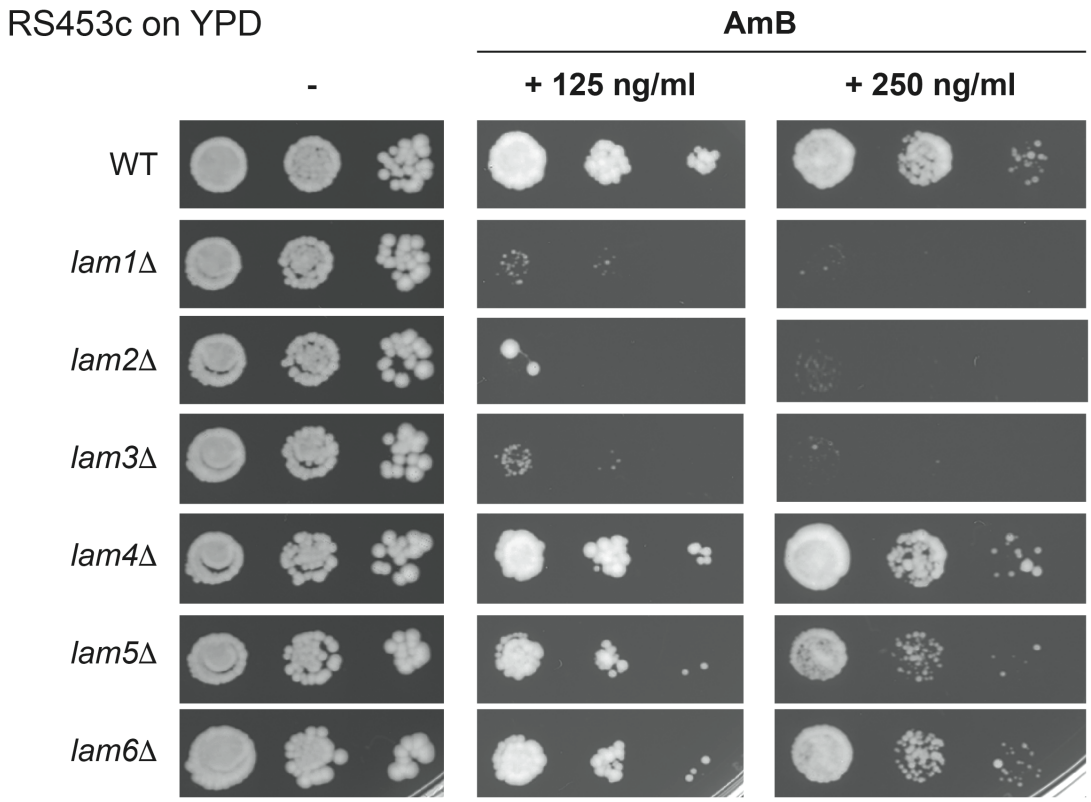

Figure 6.10 LAM knockout strain in RS453c background show the same AmB phenotype

AmB phenotype (at a lower LD_{50}) was also shown by LAM1, LAM2, and LAM3 single deletes in RS453c background. *lam2*Δ confirmed the milder phenotype.

One of the proposed mechanisms of AmB action involves the change in the cellular redox status that promotes the generation of high levels of reactive oxygen species (ROS) (Mesa-Arango et al., 2014; Belenky et al., 2013). To study the importance of this mechanism in the LAM genes knockouts, I evaluated (i) the effect of AmB toxicity in the presence of the antioxidant *N*-acetylcysteine (NAC), and (ii) the quantification of ROS induced by the acute AmB treatment using the fluorescent chemical 2',7'-dichloro-dihydro-fluorescein diacetate (H_2DCF-DA) as readout.

NAC is an antioxidant that inside the cell serves as a pro-drug to L-cysteine, the precursor of L-glutathione, a biological reducing agent. Consistently with the increased amount of ROS reported in LAM deletion strains (Sokolov et al., 2006 and Figure 6.11), a high concentration of NAC is able to cancel the toxic effect of AmB (Figure 6.9 A). Interestingly, the fitness of particularly sensitive strains, such as the double (*lam2*Δ*lam3*Δ and *lam2*Δ*lam4*Δ) and triple (*lam1*Δ*lam2*Δ*lam3*Δ) deletes, was better in the presence of NAC than on YPD alone (Figure 6.9 A). But these subtleties will require further investigation with more biological repeats and inclusion of data from liquid culture.

This result suggests that the pleiotropic effects of AmB converge on ROS induction that ultimately kill the fungal cell. Multiple mechanisms for the link between AmB and ROS have been suggested and they include both direct (on lipid or protein targets) effects and indirect responses (involving translational changes). Turning off ROS induction with high concentrations of NAC is sufficient to make the strains AmB-resistant. In the literature, there are no interactions between AmB and NAC described. When AmB in different formulations is used in the clinic for the treatment of opportunistic fungal infections, one of the major problems is the AmB-induced nephrotoxicity. The mechanisms of renal tubular damage have not been fully elucidated, however among the several approaches to treat this side effect and prevent tubular damage, a concomitant treatment of AmB and NAC has been proposed (Odabasi et al., 2009). It is possible that NAC could counteract AmB effects in the renal tubular cells with the same mechanism that turns the LAM deletions AmB-resistant. However, from these results it is likely that NAC would also be

beneficial on the fungal cells, preventing AmB from killing the invasive pathogenic fungus.

H_2DCF-DA is the cell permeable and chemically reduced form of fluorescein. Upon cleavage of the acetate groups (-DA) by intracellular esterases and oxidation, the non-fluorescent compound is converted into dichloro-fluorescein (DCF) which is highly fluorescent and it has a better cellular retention. To visualise the oxidative metabolism induced by AmB, I added H_2DCF-DA to cells growing in log phase immediately after the antifungal drug treatment (Pozniakovsky et al., 2005). AmB treatment induced a significant increase in ROS levels both for wild type and *lam2*Δ*lam3*Δ cells, suggesting that the effects of an acute exposure to sub-lethal AmB doses could be similar, but largely amplified (and/or not buffered) in the absence of the two LAM proteins. Even in control condition with no drug, the base line ROS levels resulted significantly higher in double delete cells, but further experiments are required to correlate the fluorescence levels with the ROS levels that results in cell toxicity to establish a 'CTCF toxicity threshold'. In the AmB-sensitive strains fluorescein was greatly accumulated inside the cells, and the fluorescence was reduced to untreated levels after NAC exposure, even if in contrast to the 'No drug' condition, it was concentrated in intracellular compartments and less diffused (Figure 6.11 B).

In conclusion, AmB effects are pleiotropic but results in increase of ROS levels that ultimately kill the fungal cell (Belenky et al., 2013). High concentrations of the antioxidant NAC were successful in reducing the acute ROS induction, suggesting that the AmB effects due to LAM deletion were non-transcriptional. However, some fast transcriptional responses (from signal to phenotype) take about 20 minutes. To exclude the involvement of a transcriptional mechanism in *lam2*Δ*lam3*Δ increased sensitivity, AmB treatment should be done in the presence of the ribosomal inhibitor cycloheximide.

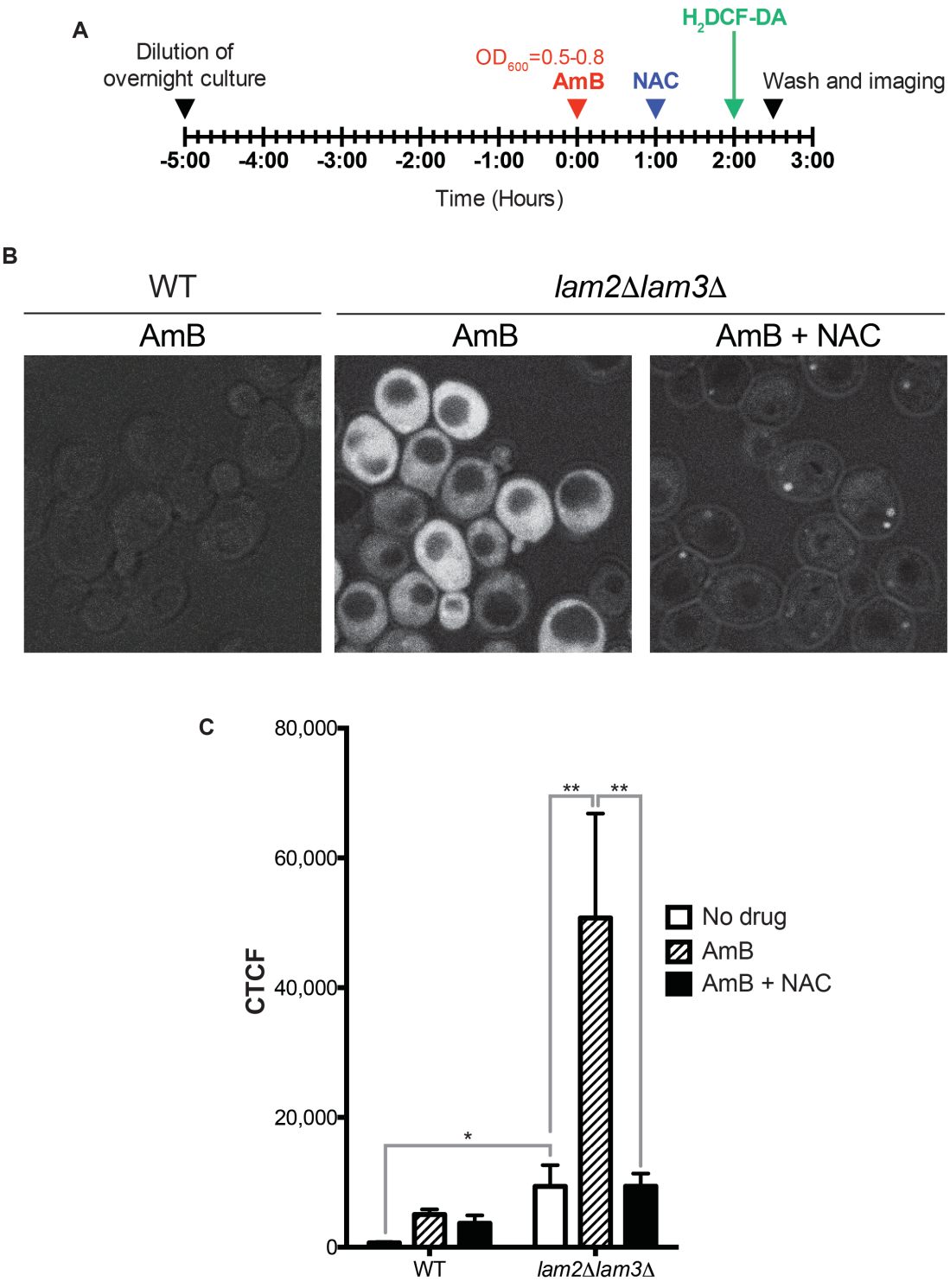

Figure 6.11 Visualisation of AmB-induced reactive oxygen species

(**A**) Timeline of the ROS visualisation experiment. Overnight culture was diluted in fresh medium, at OD_{600} = 0.5 AmB was added into the cell suspension, some samples were treated with NAC after one hour, and all the samples were treated with H_2DCF-DA to check intracellular ROS levels after an additional hour. 20-30 minutes of treatment were sufficient to visualise the differences at the confocal microscope after washes in PBS. (**B**) Qualitative comparison of wild type and *lam2Δlam3Δ* double delete strains. The same acquisition settings were kept for all conditions. (**C**)

Quantification of the corrected total cell fluorescence (CTCF) was performed processing confocal figures with ImageJ. n = 15-17 cells. Two-tailed Student's t-test, *p <0.05, **p <0.01.

Next, I wondered if the different toxicity was due to the differential binding affinity of AmB to the cells lacking *LAM1*, *LAM2* or *LAM3*. Taking advantage of the intrinsic fluorescence of AmB (Gruszecki et al., 2009), after incubating for 1 hour the wild type and two AmB-sensitive double delete strains with the same amount of AmB, I measured the fluorescence left in the medium to indirectly estimate the drug bound to the yeast cells (Figure 6.12). The difference in fluorescence intensity of the medium between the control sample with no cells and the samples with wild type and double delete corresponds to the amount of AmB taken up by the cells (Gruszecki et al., 2009). There is a significant difference between the fluorescence left in the supernatant in the presence or absence of cells, but the wild type and mutants took up and bound the same amount of AmB from the medium.

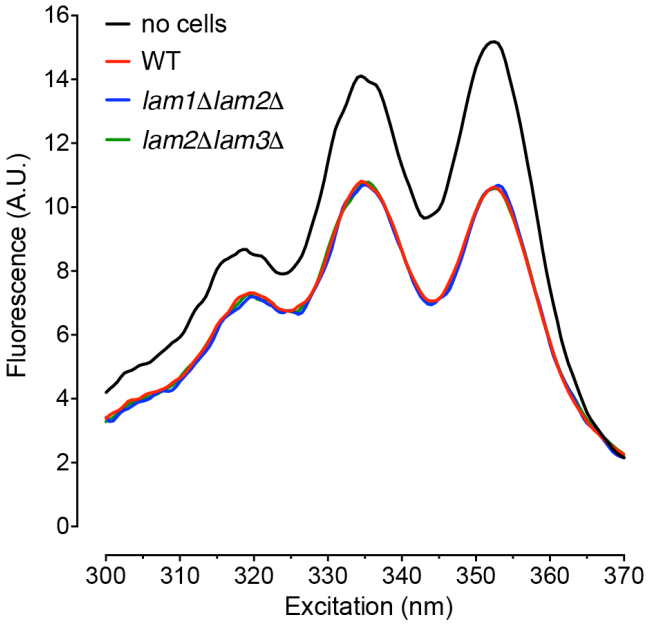

Figure 6.12 AmB does not show a different PM binding affinity to wild type compared to LAM double delete cells

Wild type and double delete cells at OD_{600} = 0.5 were treated with 250 ng/ml AmB for 1 hour at 30°C. After centrifugation of the cells, the remaining fluorescence of AmB in the supernatant is measured at 375 nm after excitation scan ranging from 300 nm to 370 nm. The control sample has been incubated with no cells. The fluorescence levels are normalised on the number of cells right before their centrifugation.

6.3.2. Sterol-binding StART-like domains rescue AmB sensitivity

Another way to take advantage of the AmB^S shown by the LAM strains, is to re-express the whole proteins or their active domain to study how and which domains are essential for the sterol-related growth defect. The expression can be regulated under a constitutive and moderately strong promoter such as *PHO5* or can be under the control of the endogenous promoter sequence.

First, I tried to re-express the N-terminally GFP-tagged version of the deleted protein. In many cases the GFP-tag can inhibit the protein activity so I also wanted to test if the presence of the tag was compatible with the phenotype rescue. As expected, in the presence of an empty plasmid expressing *PHO5*>GFP, the sensitivity of *lam1*Δ and *lam3*Δ was higher than *lam2*Δ. At standard confocal microscopy, endogenous GFP-tagged Lam1p showed a faint dotted localisation at the periphery of the cell (Section 5.2), and *lam1*Δ strong AmB phenotype was rescued to wild type levels with the endogenous promoter and to an improved fitness when overexpressed. *lam3*Δ phenotype could be equally rescued with both promoters with an increased fitness compared to the wild type. *lam2*Δ milder phenotype could be rescued by re-expression of Lam2p or Lam4p, but their levels required a more careful fine tuning for a correct rescue/toxicity balance:

- GFP-Lam2p re-expression under endogenous promoter was more effective than the *PHO5*-promoted version in rescuing the phenotype, also improving the fitness compared to the wild type.
- Expression of Lam4p on a LAM2 single delete strain (endogenous Lam4p was present in the genome) was more effective in the overexpressed conditions.
- The rescue of *lam2*Δ sensitivity by Lam2/4p supported a shared sterol-related function at ER-PM contact sites, but the rescue levels were different among the two paralogs.
- The *LAM4*-promoted version of GFP-Lam2p (promoter swap) showed similar levels to the *LAM2*-driven expression at confocal microscopy

(Section 5.3.2), it could be interesting to check any subtleties in AmB rescue as well.

- Lam2p prolonged overexpression by the inducible promoter *GAL1* caused cell toxicity (Tim Levine, personal communication).

The AmB^S phenotype of *lam1*Δ, *lam2*Δ, and *lam3*Δ can successfully be rescued by the re-expression of the full length GFP-tagged proteins with different subtleties regarding their expression levels. *lam2*Δ could be rescued by the re-expression of itself or Lam4p, suggesting an overlapping role of the two paralogs.

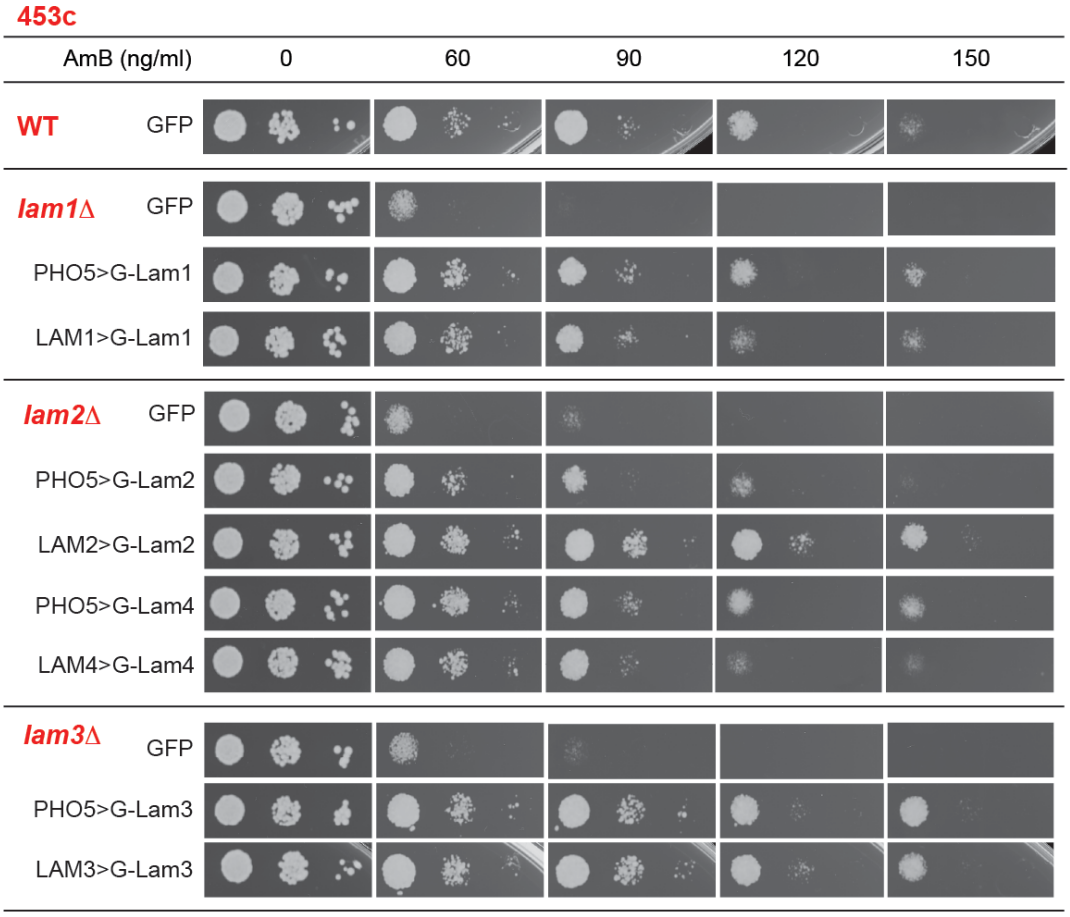

Figure 6.13 Rescue of AmB phenotype upon expression of GFP-LAM proteins

Growth assays of yeast cells with a single gene deletion in the RS453c background compared to its wild type. For each of the single deletes the strain was transformed with a *PHO5*-promoted GFP-expressing empty plasmid for comparison. The rescue was evaluated when the deleted protein was re-expressed under the moderately strong promoter *PHO5* or its endogenous promoter. Cells were grown for 48 hours at 30°C on SDD supplemented with increasing amount of AmB.

AmB sensitivity resulted increased for all yeast strains growing on minimal media (SDD), compared to complete rich medium (YPD). When wild type and mutant strains were tested on a minimal medium, the range of drug concentrations was reduced accordingly (compare ranges in Figure 6.9 and Figure 6.13).

Next, I tried to evaluate the rescuing ability of the part of the LAM proteins hypothesised to have the major lipid-related function: their StART-like domains. Overall, when the soluble StART-like domains of Lam2/4p, Lam5/6p, and hLAMa were overexpressed in the cytoplasm of the sensitive strains, the AmB phenotype could be rescued effectively (Figure 6.14). The two StART-like domains in Lam4p had distinct rescue ability with the first one, closer to the N-terminus and more distant from the TMD, was not as efficient in rescuing AmB phenotype. Using different approaches, we proved that the predicted StART-like domains of Lam2p and Lam4p can bind (Figure 6.2) and transfer (Louise Wong, personal communication, and Discussion Figure 8.2) sterols. According to the most recent explanations, AmB works mainly as an extramembranous sterol sponge that is able to extract PM ergosterol (Anderson et al., 2014). The ability of Lam2p and Lam4p StART-like domains to counteract this AmB mechanism of action can be explained considering their ergosterol binding and transfer features (Discussion, Section 8.4). In the same way, it is likely that the predicted StART-like domains of Lam5p and Lam6p that are able to rescue the AmB phenotype, but whose lipid ligand is unknown, are sterol binding domains.

Interestingly, also the cytoplasmic StART-like domain from the human LAMa could rescue the AmB phenotype of all the sensitive yeast single deletes (Figure 6.14), suggesting a sterol (ergosterol and cholesterol are structurally very similar, Figure 6.4) binding affinity for all members of the Lam2/4/4/6p branch of the phylogenetic tree of the newly identified family (Appendix 2).

To better understand the overlapping functions of yeast and human LAM proteins, I studied the rescue ability of the human StART-like domains on yeast AmB phenotype (Figure 6.15). Single and double delete strains sensitive to

amphotericin were transformed with *PHO5*-promoted human LAMs, either with the full length protein or only the soluble StART-like domain. Human LAMa StART-like domain was successful in rescuing the phenotype (Figure 6.15 A) and also improving the fitness of the wild type (Figure 6.15A, top panel). The full length human protein was successfully expressed in yeast cells where it localised in GFP-positive dots in general ER including cell periphery, nuclear envelope, and internal ER including some perivacuolar staining (Figure 6.15 C). However, the AmB-rescue function was not observed. The soluble human StART-like domains alone had different effects on *lam1*Δ and *lam2*Δ (Figure 6.15 B) with the major rescue effect showed by hLAMaS, followed by hLAMbS that showed improved fitness compared to the empty plasmid. hLAMc resulted ineffective, but the experiment should be repeated using other strains, other growth temperatures, or another drug concentration to confirm the actual ineffectiveness of the hLAMb/c StART-like domains and reveal subtler mechanisms. Importantly, even if the expression of single StART-like domains and full length proteins was visualised at the confocal microscope (example in Figure 6.15C, other not shown), the protein levels should be checked using a Western blot approach as well.

In conclusion, the sterol-related activity from yeast (Lam2-6p) to humans (hLAMa) is strongly conserved and their StART-like domains are the active parts of this protein family. The fact that the same constructs can rescue the AmB phenotype of *lam1*Δ, *lam2*Δ and *lam3*Δ in all the sensitive strains indicates a possible overlap in their function.

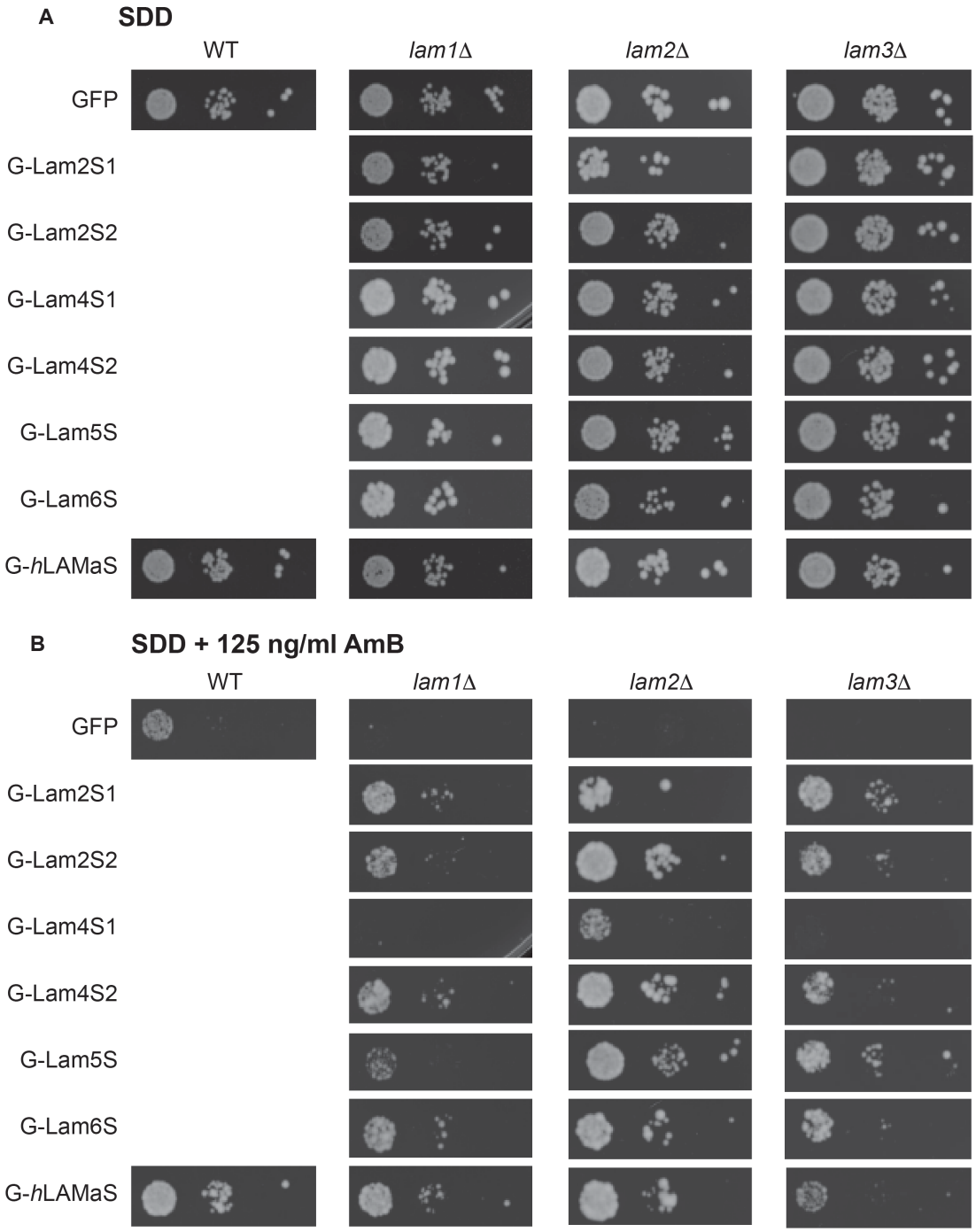

Figure 6.14 Rescue of AmB sensitive strains by expression of sterol binding StART-like domains

*lam1*Δ, *lam2*Δ and *lam3*Δ from BY4741 background were rescued by the re-expression of the proven sterol binding StART-like domains of Lam2p and Lam4p, or by the probable sterol binding StART-like domains of Lam5p, Lam6p and human LAMa. All the plasmids had the *PHO5* promoter for moderately high expression and contained the GFP-tag at the protein N-terminus. The top of the figure shows the dilutions of cells growing in the absence of antifungal drug for comparison. *H sapiens* LAMa improved the fitness of the wild type strain. Cells were grown for 36 hours at 30°C on SDD supplemented with 125 ng/ml AmB.

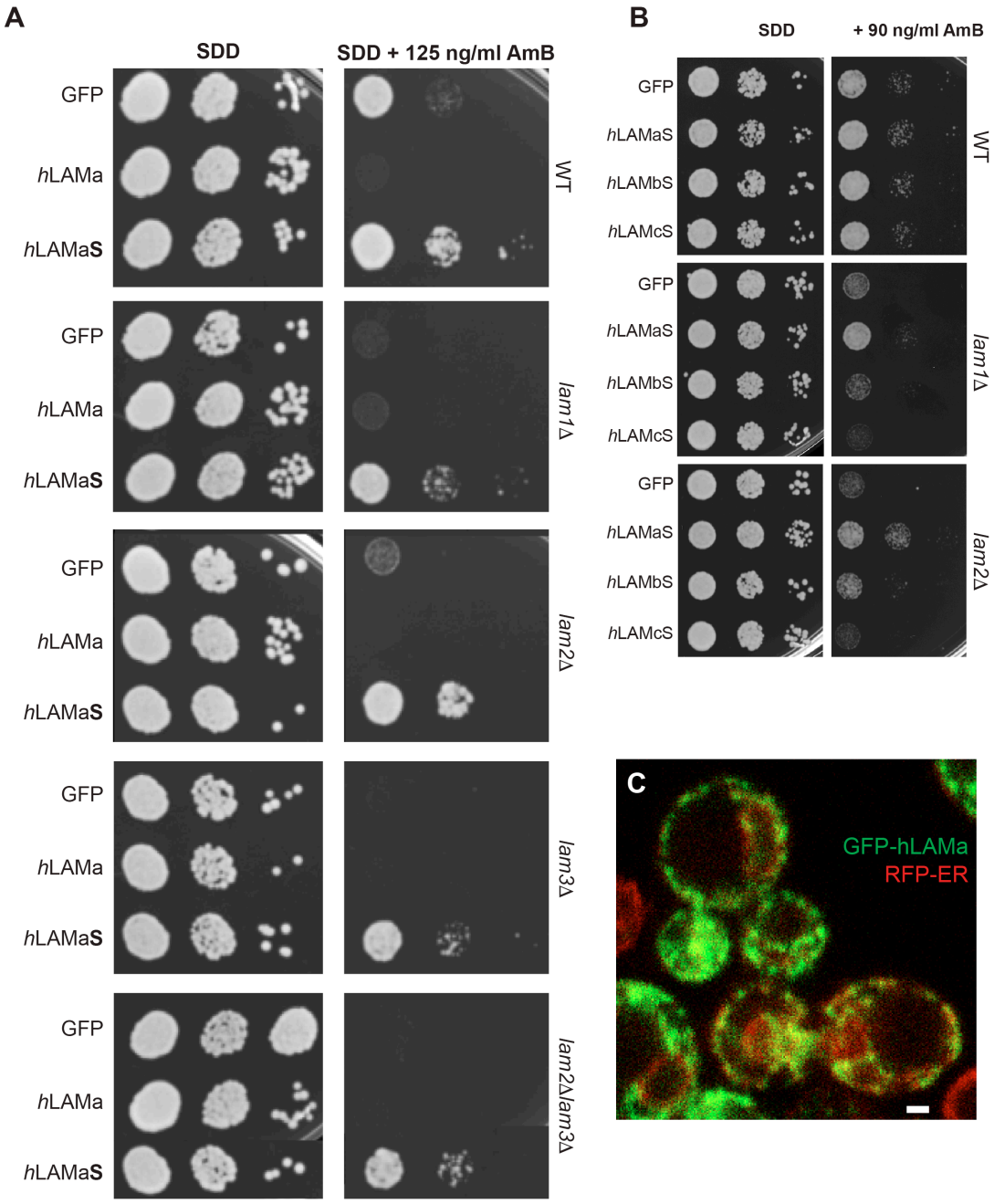

Figure 6.15 StART-like domains of human LAMa rescued AmB phenotype of sensitive strains

(**A**) BY4741 single and double deletes were transfromed with constructs expressing whole hLAMa or its StART-like domain alone under the control of the *PHO5* promoter. Each strain was also transformed with an empty GFP-expressing plasmid for comparison. (**B**) Wild type, *lam1*Δ, *lam2*Δ and *lam3*Δ were transformed with the empty plasmid or with a StART-like domain from the human LAMa, LAMb or LAMc. Cells were grown for 36 hours at 30°C on SDD plates supplemented with the reported amount of AmB. (**C**) Expression of GFP-hLAMa full length in wild type yeast cells and counterstaining of RFP-ER marker. Scale bar, 1 μm.

6.3.3. Lam1p and Lam3p StART-like domains do not rescue AmB^S

The two strains with the highest sensitivity to AmB, *lam1*Δ and *lam3*Δ were rescued by the re-expression of the missing proteins (Figure 6.13) and by the expression of StART-like domains that bind sterol, Lam2p, Lam4p, Lam5p, Lam6p and hLAMa (Figure 6.16). However, the expression of the cytoplasmic forms of the predicted StART-like domains from Lam1p or Lam3p failed to rescue AmB^S. Figure 6.16 A shows different aspects of this:

- both Lam1S and Lam3S domains slightly reduced the fitness of the wild type strain, while the human StART from hLAMa (used here as positive control) increased it,
- in contrast, in both *lam1*Δ and *lam3*Δ there was a minor improvement of the fitness compared to the empty plasmid upon moderate high expression of both StART-like domains from Lam1p and Lam3p,
- *lam2*Δ was rescued only by the domain from Lam3p, and not by Lam1S.
- *lam3*Δ sensitivity was only restored by the human StART-like domain.

All these phenotypes could be useful for the understanding of Lam1p and Lam3p functions. However, they could be explained in different ways:

- the chosen sequences of the two StART domains could translate in poorly soluble or highly unstable proteins (Figure 6.7),
- the two StART-like domains do not bind or transfer sterols, but another lipid highly important for PM sterol homeostasis,
- in this scenario, the failure in rescuing could be due to the fact that Lam1p and Lam3p differ from Lam2StARTs in that their expression needs to be finely tuned and specifically localised at ER-PM contacts; while a random, fully cytoplasmic, high level expression of these particular StART-like domains only, does not restore activity,
- Lam1p and Lam3p do not have transfer activity but are involved in Lam2p regulation (stability, localisation, integration with signalling from other proteins in a complex), and their StART-like domains alone fail to recapitulate these activities of the full-length proteins.

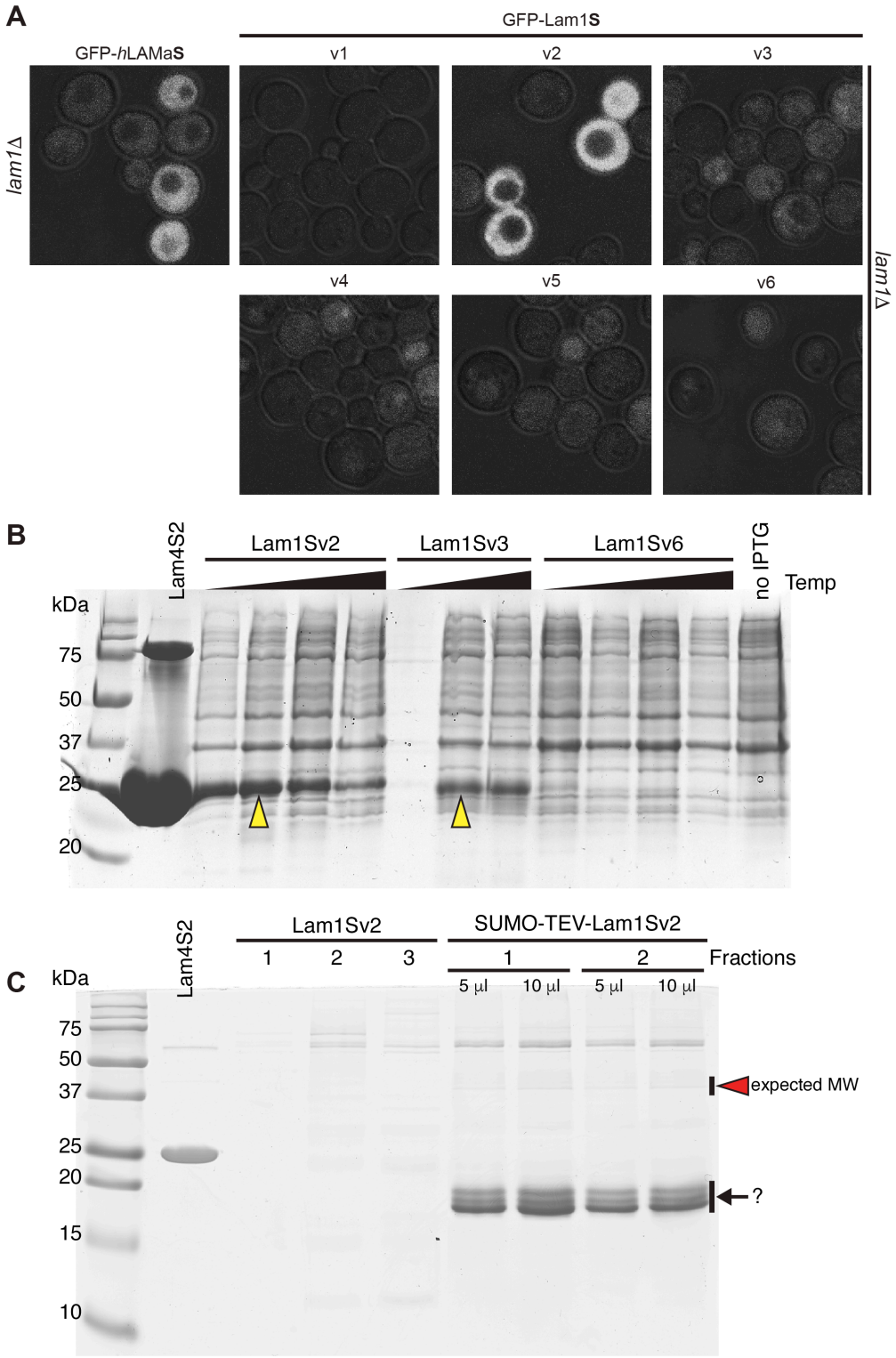

Figure 6.16 Lam1p and Lam3p StART-like domains do not rescue AmB phenotype

(**A**) Extent of AmB^S rescue by Lam1/3p StART-like domains; controls were either an empty plasmid or the StART-like domain of hLAMa (used as positive control). (**B**) Study of rescue ability of the six Lam1p-StART constructs attempted for recombinant purification (Figure 6.6 and Discussion 8.4.1).

6.4. Aus1p and Pdr11p are not mislocalised in the knockout strains

Aus1p and its paralog Pdr11p are plasma membrane sterol transporters belonging to the ATP-binding cassette family. Their activity is essential for the uptake of exogenous sterols via their incorporation into the plasma membrane. Here, I expressed Aus1-GFP and Pdr11-GFP as C-terminal fusion proteins under the control of their endogenous promoter (Li and Prinz, 2004). I determined if the absence of LAM genes could have an indirect effect on sterol transporters (Sullivan et al., 2009). Figure 6.17 shows that the strains missing each member of the new yeast StART family did not have defect in Aus1p and Pdr11p localisation. Any lipid-related defects shown by these strains are not caused by problems in sterol uptake, and that the knocked out proteins are not involved in Aus1p and Pdr11p localisation. This also suggested that the defects in sterol homeostasis shown by these cells are not in the sterol uptake at the PM level, but rather in the step of sterol transport between the ER and PM, concordantly for the role we proposed for these StART-like domain proteins in sterol transport at ER-PM contact sites.

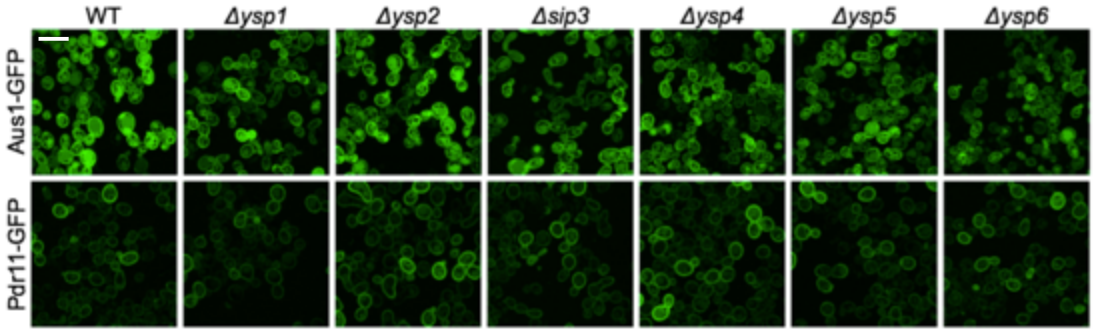

Figure 6.17 Aus1p and Pdr11p are not mislocalised by LAM deletion

Knockout strains for LAM proteins were transformed with vectors bearing either Aus1-GFP or Pdr11-GFP under the control of their endogenous promoters. Localisation of the two sterol transported were observed at the confocal microscope and compared to the wild type. Scale bar, 10 μm.

6.5. Lam1, Lam2 and Lam3 triple delete has decreased ER-PM contacts

Proteins localised at membrane contact sites can regulate the physical tethering of the organelles. If the protein is involved in tethering directly or in the regulation of tethering, its knockdown or overexpression may tend to cause the extent of the contact site to reduce or expand, respectively.

Considering ER-PM contact sites, in a wild type strain about 40% of the PM is associated with cER (0.4 cER/PM ratio) (West et al., 2011). The cER/PM ratio of *scs2*Δ*scs22*Δ mutant, the yeast homologues of human VAP proteins, decreases to 24% (Loewen et al., 2003; Manford et al., 2012). A more extreme example is the Δ*tether* strain obtained by deleting six proteins at ER-PM contact sites: at the electron microscope, it is possible to observe the cER structures to decrease to ~4% in the deletion of the ER tether proteins Scs2p, Scs22p, Tcb1p, Tcb2p, Tcb3p and Ist2p. Interestingly, a hierarchy among the cER-PM tethers can be observed: with Scs2/22p contributing more than Ist2p and followed by the three tricalbins (Manford et al., 2012). More recently, the further deletion of a seventh gene encoding Ice2p, a protein involved in the inheritance of cER (Loewen et al., 2007; Tavassoli et al., 2013), has produced a new strain called Δ-super-tether, in which the extent of ER-PM contact sites is reduced to 1.4% of PM (YY Sere and AK Menon, personal communication).

In some cases, proteins that regulate the contact site extent might be involved in other functions other than only the physical tethering of the two membranes. The StART-like domain of Lam6p is able to transfer sterols between membranes (Murley et al., 2015) and its knockdown does not affect the extent of ER-mitochondria and NVJ contacts. However, its overexpression causes 1.5- to 6-fold expansion: at ER-mitochondria contact sites N-terminally GFP-tagged Lam6 showed the strongest phenotype with elongation of the ER tubules contacting (Elbaz-Alon et al., 2015) and embracing (Figure 5.15) mitochondria.

To assess whether Lam1p, Lam2p and Lam3p are involved in the regulation of ER-PM contacts, we performed ultrastructural analysis using transmission

electron microscopy of the triple delete *lam1*Δ*lam2*Δ*lam3*Δ in two different strains BY4741 and upc2-1. Cells were grown to early exponential phase and fixed with potassium permanganate before processing for EM.

I quantified the cER segment length, frequency and overall ratio of cER over the total cell perimeter taking into consideration the following parameters (Tavassoli et al., 2013):

$$cER{:}\,PM\ ratio = \frac{\sum(contacts\ lenght)}{PM\ perimeter}$$

$$Length\ (nm) = average\ length\ of\ contacts$$

$$Frequency\ (per\ \mu m) = \frac{number\ of\ contacts}{PM\ perimeter}$$

$$Tubules = \frac{number\ of\ tubules}{number\ of\ total\ contacts}$$

Where tubules were defined as segments of cER shorter than 60 nm (Phillips and Voeltz, 2015). The triple knockout of LAM1, LAM2 and LAM3 in BY4741 caused a <10% average decrease in the amount of cER-PM contact. In wild type cells cER covered 42% of the PM, but in the triple delete this ratio was down to 37% (Figure 6.18). The role of Lam1p, Lam2p, and Lam3p is therefore not as important as Scs/22p for physical tethering, but they do contribute a minor amount of the overall tethering. This is in consistent with their localisation at enduring ER-PM contacts in Δ*tether* strain (Figure 5.4).

During the blind quantification, we noticed that some cells possessed more tubular structures in the cortical ER. This could suggest a phenotype that does not visibly decrease the number of cER segments or their length, but is effective in inducing tubulation of the cER instead of keeping the wide cisternae-like structures that usually make contact with the PM (Shibata et al., 2006). To test this (Figure 6.18, Panel E), I set a threshold for tubules being any cER contact equal or shorter than 60 nm in length. The percentage shown takes into consideration only the tubules at the cortex, tubular structures in the cytoplasm (the arrowheads in Panel E show all the tubules visible in the

magnification) are ignored because in an endogenous setting the three LAM proteins are localised only at cER. This work showed that there was no tubular phenotype, either in terms of frequency or average length of contacts in the triple deletion.

Another possibility is that the overexpression of one of the LAM proteins changes the extent of the contacts. This is the case of Lam6p overexpression (Elbaz-Alon et al., 2015), and many other contact sites components. For Lam2p, not only we did not see this by fluorescent microscopy (Figure 5.1-5.5), but by electron microscopy, overexpression of GFP-tagged Lam2p did not have visible effects on the contacts extent (Matt Hayes and Tim Levine, personal communication). While the overexpression of Lam1p and Lam3p caused a major mislocalisation to internal ER that would weaken other conclusions (Tim Levine, personal communication).

In conclusion, the lack of LAM1, LAM2, and LAM3 caused a significant reduction of ER-PM contacts of ~5% which is consistent with their role as residual tether when other proteins are missing. In the future, it will be interesting to analyse the effect of single LAM deletion or the simultaneous knock out of one LAM with other known ER-PM tethers to weight LAM tethering activity in more details.

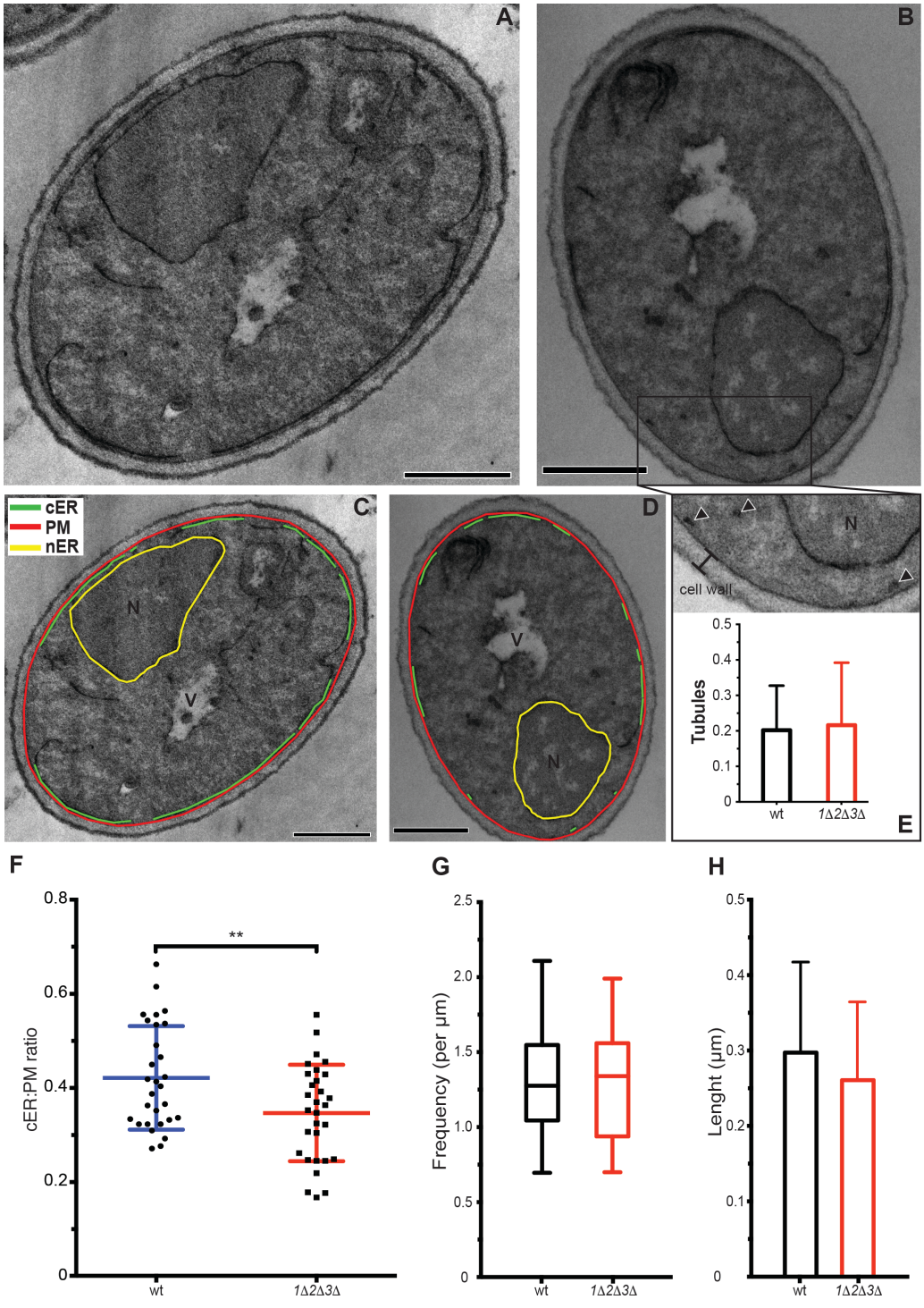

Figure 6.18 LAM1-LAM2-LAM3 triple knockout has an absolute reduction of 5% in ER-PM contact sites

(**A-B**) Representative transmission electron microscopy images of BY4741 strain wild type (A) and *lam1Δlam2Δlam3Δ* triple delete (B). (**C-D**) Superimposition of analysis method performed in blind condition using ImageJ software. Red, PM. Green, cortical ER. Yellow, nuclear ER. (**E**) Magnification of representative area from cell in panel B.

Graph indicates the percentage of contacts shorter than 60 nm (defined as tubules). Error bars, SD. (**F**) Scattered dot plot of ratio of ER-PM contacts to PM perimeter. Two-tailed unpaired Student's *t*-test, $^{**}p < 0.01$ versus WT. Mean with SD. (**G**) Frequency of ER-PM contacts: number of contacts per μm of PM. Box and whisker plot showing median value with the two central quartiles (box) and the min-max range (whiskers, or error bars). (**I**) Average length of ER-PM contact (in μm). Error bars, SD. $n = 30$ cells for all quantifications, which were carried out after random coding of images so that the scorer was blinded for genotype.

6.6. Lipidomics analysis showed low sphingolipid levels in LAM1 and LAM3 delete strains

To investigate if the single deletion of each of the six LAM genes affects the overall membrane lipid composition, we performed lipidomics analyses. Cells use linked and coordinated metabolic and catabolic lipid pathways to synthesise and degrade phospholipids, sphingolipids and sterols (Daum et al., 1998). This network allows both cell adaptability to environmental stresses (such as nutrient availability, osmotic stress or heat shock) and also the sensing of the different lipid levels for the preservation of lipid homeostasis and overall cellular functions (Zaman et al., 2008; Ejsing et al., 2009; Guan et al., 2009; Young et al., 2010; De Smet et al., 2012; Frechin et al., 2015). For these reasons, the deletion of a single gene involved in lipid biosynthesis (and/or lipid traffic), could be rescued by a parallel step in a linked pathway that could compensate for cell viability with no visible changes in overall lipid levels. Nevertheless, at the epidemiological base of some diseases there are single genes involved in lipid homeostasis on the metabolic (Hotamisligil, 2006; Holland and Summers, 2008; Fu et al., 2011), trafficking (Simanshu et al., 2013; Tong et al., 2015) or catabolic side (Futerman and van Meer, 2004; Vitner et al., 2010; Platt, 2014). Lipidomics profiling, the application of lipidomics for the study of single gene deletion or overexpression, has proven successful in identifying overall changes in the lipidome (Serhan:2003wc; Klose et al., 2012).

I investigated the effect of a missing LAM protein on the lipid profiles. Strains were grown in rich complete medium until early exponential phase, then lipids were extracted using a phospholipid-specific or sphingolipid-specific method. The high throughput analysis was carried out by electrospray ionization mass spectrometry (ESI-MS) using the multiple reaction monitoring (MRM-MS) technique (Guan et al., 2010; da Silveira Dos Santos et al., 2014). We identified the signals of hundreds of lipids with different headgroups and fatty acid adducts, and we obtained their relative quantification adding internal standards into the samples.

I analysed the six LAM deleted strains and the wild type from the BY4741 collection (two biological repeats) and the RS453c strains made in this project (one biological repeat). For each biological repeat we obtained measurements from two different assays from a single set of cultures experiments: for phospholipids or sphingolipids (Figure 6.19).

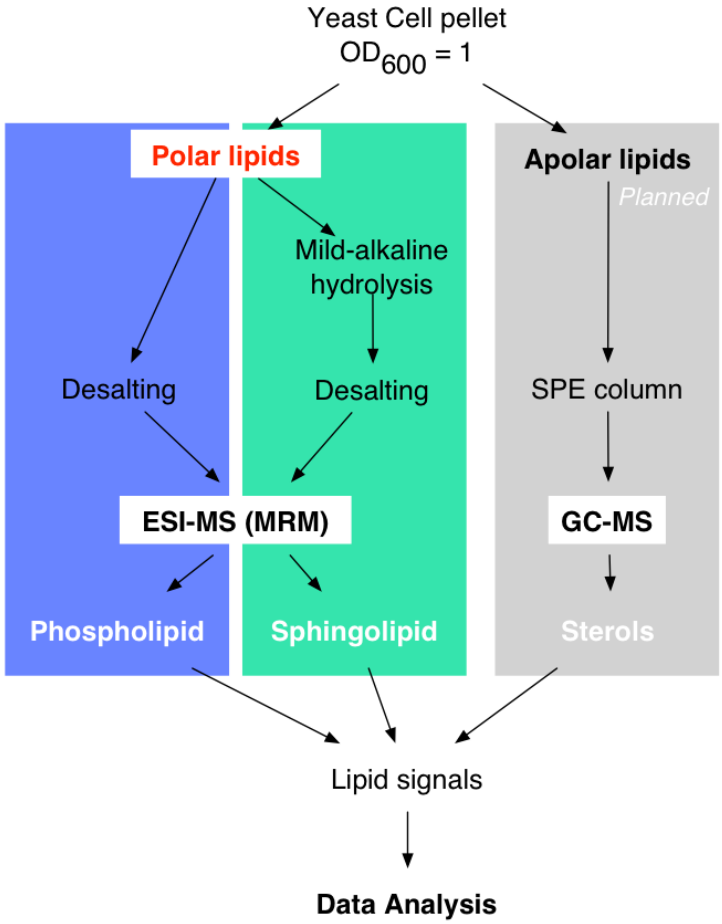

Figure 6.19 Workflow of lipidomics protocols for different lipid classes

In this work we studied only the changes in levels of polar lipids. We compared the levels of wild type BY4741 or RS453c with their correspondent single LAM deleted strains. Each strain was grown until early log phase and lipids were extracted using different methods for phospholipids or sphingolipids. Lipid extracts were analysed using by electrospray ionisation mass spectrometry (ESI-MS) coupled to a multiple reaction monitoring (MRM). Relative concentrations could be estimated by considering the standard curves of internal standards spiked in the samples before lipid extraction. Data were analysed as described in Materials and Methods. SPE, solid phase extraction; ESI-MS, Electrospray Ionisation Mass Spectrometry; MRM, multiple reaction monitoring; GC-MS, Gas-Chromatography Mass Spectrometry.

The entire list of analysed lipids included 392 molecules observed in the ESI-MS experiment. They are classified for lipid class (PC, PE, PI, PS, Cer, SL) and subclass (lyso-phospholipids, or complex SL), chain length of the fatty acid, unsaturation index and hydroxylation. Apparent quantities were calculated from the raw data considering the known amount of standard lipids spiked in the lipid extractions. The analysis for the BY4741 strains was obtained comparing each wild type with the correspondent six LAM deletions. Of the initial 392 molecules, 79 were excluded from the analysis because data were not robust enough according to previously determined evaluation methods and quality control criteria (da Silveira Dos Santos et al., 2014). Only results from BY4741 delete strains were used for the analysis.

I included the most abundant molecules for each class of lipids taking into consideration fatty acid chain length (for phospholipids), and hydroxylation position (for sphingolipids). Lipids included in the clustering and the statistical analysis. From other high-throughput studies, it is clear that the ceramide-sphingolipid pathway is overall more easily affected by single knockout genes (da Silveira Dos Santos et al., 2014). The main reasons for this are (i) the single entry point of sphingolipid biosynthesis (Figure 6.21), as well as (ii) the single mechanism of degradation via Dpl1p that regulates and intracellular levels of sphingolipid long-chain base phosphates and degrades phosphorylated long chain bases, and (iii) the multiple entry, recycling and degradation pathways of glycerophospholipids. On the other hand, usually sterol levels in yeast are the least affected with most of the genes involved in its synthesis being essential for cell viability (da Silveira Dos Santos et al., 2014). No mass spectrometry analysis of sterols was performed in this study.

6.6.1. Phospholipids are not perturbed by deletion of LAM proteins

In *S. cerevisiae*, the most common phospholipids are PC, PE, PI, PS, PG and cardiolipins (CL). The pathways of synthesis, degradation and recycling of phospholipids are numerous, complex and interconnected. These mechanisms are highly regulated both from a genetic and from a biochemical side (Henry et al., 2012). Two important aspects are often overlooked when studying the biosynthetic pathways of phospholipids: the chain length and the unsaturation index of their fatty acid moieties. In budding yeast, Elo1p/Elo2p and Elo3p are the elongases localised in the ER controlling the length. The four most abundant fatty acids esterified to the glycerol-3-phosphate backbone are palmitic acid (16:0), palmitoleic acid (16:1), stearic acid (18:0) and oleic acid (18:1). The combination of fatty acids in the *sn-1* and *sn-2* positions of the backbone is different for each class: the major PC is PC32:2, the major PS is PE34:1 (da Silveira Dos Santos et al., 2014). The mechanism and the players underneath the precise regulation of this equilibrium is unknown (Boumann et al., 2003; 2004).

To visualise if the single deletes of the LAM proteins have some effects on the phospholipid homeostasis, I summarised the crude numbers of the apparent lipid quantities in a hierarchical clustering heatmap for the major phospholipids showing the fold increase values compared to the wild type levels (Figure 6.20).

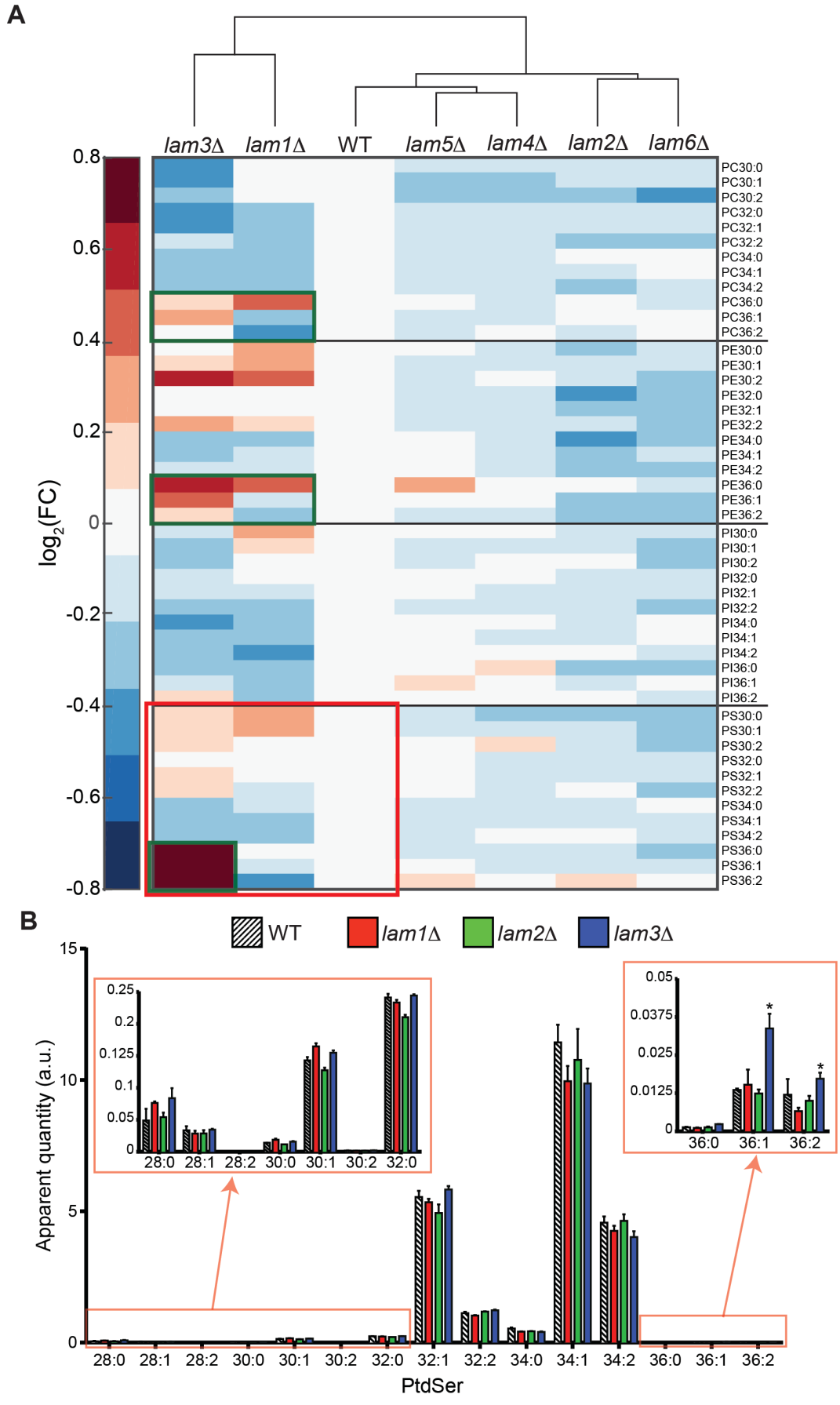

Figure 6.20 Phospholipids levels are not perturbed in LAM deleted strains

Figure 6.20 Phospholipids levels are not perturbed in LAM deleted strains (Previous page)

(**A**) Hierarchical clustering of phospholipid profiles from BY4741 and RS453C strains. Raw values for the major classes of sphingolipids were normalised to the wild type levels. This fold change was transformed with a base 2 logarithmic equation to obtain a range from –1 to +1 compared to wild type. The hierarchy, clustering and their visual rendition were obtained using Matlab. The green squares highlight the trend of increased long chain phospholipids in *lam3*Δ and *lam1*Δ. The red box contains the apparent PtdSer quantities shown in detail in part C. (**B**) Apparent quantities of PtdSer species. The quantities are related to the levels of PS31:1, one of the artificial internal standards spiked into the samples before lipid extraction. *LAM1* and *LAM3* knockout have statistically significant increased levels of two of the most abundant species PS34:1 and PS34:2. *lam3*Δ has increased levels of very long fatty acid chains (PS36:1 and PS 36:2). **p* <0.05, two-tailed Student's *t*-test. PtdSer, phosphatidylserine.

Situated in a range from -0.8 to +0.8 fold change to the wild type, overall phospholipid levels did not change significantly in LAM deleted strains. In a hierarchical clustering representing the fold change (FC) normalised on the wild type, LAM1 and LAM3 single delete strains clustered together indicating a closely related phospholipid profile (Figure 6.20). From the statistical analysis, the only remarkable feature seemed that both of them, but especially *lam3*Δ, had the propensity of increased phospholipids with long fatty acid chains >C18 (Figure 6.20; A, green squares; B, box on the right). The ratio between long and short FAs chains, relatively conserved throughout the different species, could be important to understand the activity of different biosynthetic routes. The increase of low abundance PS species with long FA chains was not sufficient to cause significant differences in the total ratio between long and short acyl chains.

6.6.2. Low levels of complex sphingolipids in *lam1*Δ and *lam3*Δ

The role of sphingolipids is not limited to their importance as structural membrane components, but they are also involved in significant cellular processes such as endocytosis, trafficking, cell cycle, apoptosis, inflammatory responses, and cell migration ((Hannun and Obeid, 2008). The study of sphingolipids in *Saccharomyces cerevisiae* has the potential to advance the general knowledge of the field and uncover important mechanisms of biosynthesis, catabolism, regulation and traffic (Montefusco et al., 2014).

As mentioned earlier, sphingolipid levels tend to be more variable than glycerophospholipids in lipidomics analysis. This is due to the reduced elasticity in their biosynthetic pathway, *i.e.* limited entry points and one main catabolic route via the lyase Dpl1p (da Silveira Dos Santos et al., 2014).

To understand if LAM proteins are involved in sphingolipid homeostasis, we studied the ceramide and complex sphingolipid profiles of the single deletes focussing on ceramides and complex sphingolipids. Whereas in mammalian cells, after the steps of ceramide synthesis, there are numerous species of complex sphingolipids with many possible combinations of different headgroups, in budding yeast the system is simpler but can nonetheless be useful to understand their mechanisms of biosynthesis, degradation and traffic. In *S. cerevisiae* there are only three complex sphingolipids (Funato and Riezman, 2001):

- inositolphosphoryl-ceramide, IPC;
- mannose-inositolphosphoryl-ceramide, MIPC;
- mannose-di-inositolphosphoryl-ceramide, $M(IP)_2C$.

The phosphoinositol containing sphingolipids and the pathways for their synthesis, regulation and intracellular transfer are unique to fungi and they are considered a useful and effective target for antifungal drugs (Nagiec et al., 1997; Mor et al., 2015).

LAM1 and LAM3 deletes cluster together to the left side of the wild type with an overall decrease in sphingolipid levels. It is also clear that the decreased

fold change is more dramatic for more complex sphingolipids towards the bottom of the heatmap, which relates to the more terminally modified lipids, in particular $M(IP)_2C$ (Figure 6.21A).

Next I compared the relative levels of ceramides and sphingolipids in the wild type cells with LAM1, LAM3, LAM2 and LAM4 knockout strains. For *lam3*Δ the trend in decreased levels is visible also for phytoceramides (PHC), but not statistically significant (and not for dihydroceramides, DHC). On the other hand, both *lam1*Δ and *lam3*Δ have reduced levels of the complex sphingolipids IPC and MIPC (Figure 6.21C). No deletes affected the levels of $M(IP)_2C$, but this is consistent with previous lipidomics studies (Bodenmiller et al., 2010; Berchtold et al., 2012; da Silveira Dos Santos et al., 2014). $M(IP)_2C$ is the most abundant sphingolipid, it is synthesised on the Golgi from MIPC and it is the end product of the complex sphingolipid synthetic pathway. This could leave the cells with time to adapt to pharmacological or genetic stresses:

- exposure to myriocin (myr) or aurobasidin A (AbA) does not cause changes in $M(IP)_2C$ levels (Berchtold et al., 2012),
- the absence of Ipt1 itself (Figure 6.21B; (Figure 6.21B; Nakase et al., 2010) causes some increased sensitivity towards environmental stress, but the cell maintains its viability.

Therefore, Lam1p or Lam3p could be involved in important steps for sphingolipid homeostasis even if the levels of $M(IP)_2C$ are not affected. Here, I entertain two main possibilities: (i) Lam1p and Lam3 primarily affect sphingolipids, or (ii) they are required for multiple activities including regulation of Lam2p, and that compensation for their deletion affects sphingolipid cross-regulation.

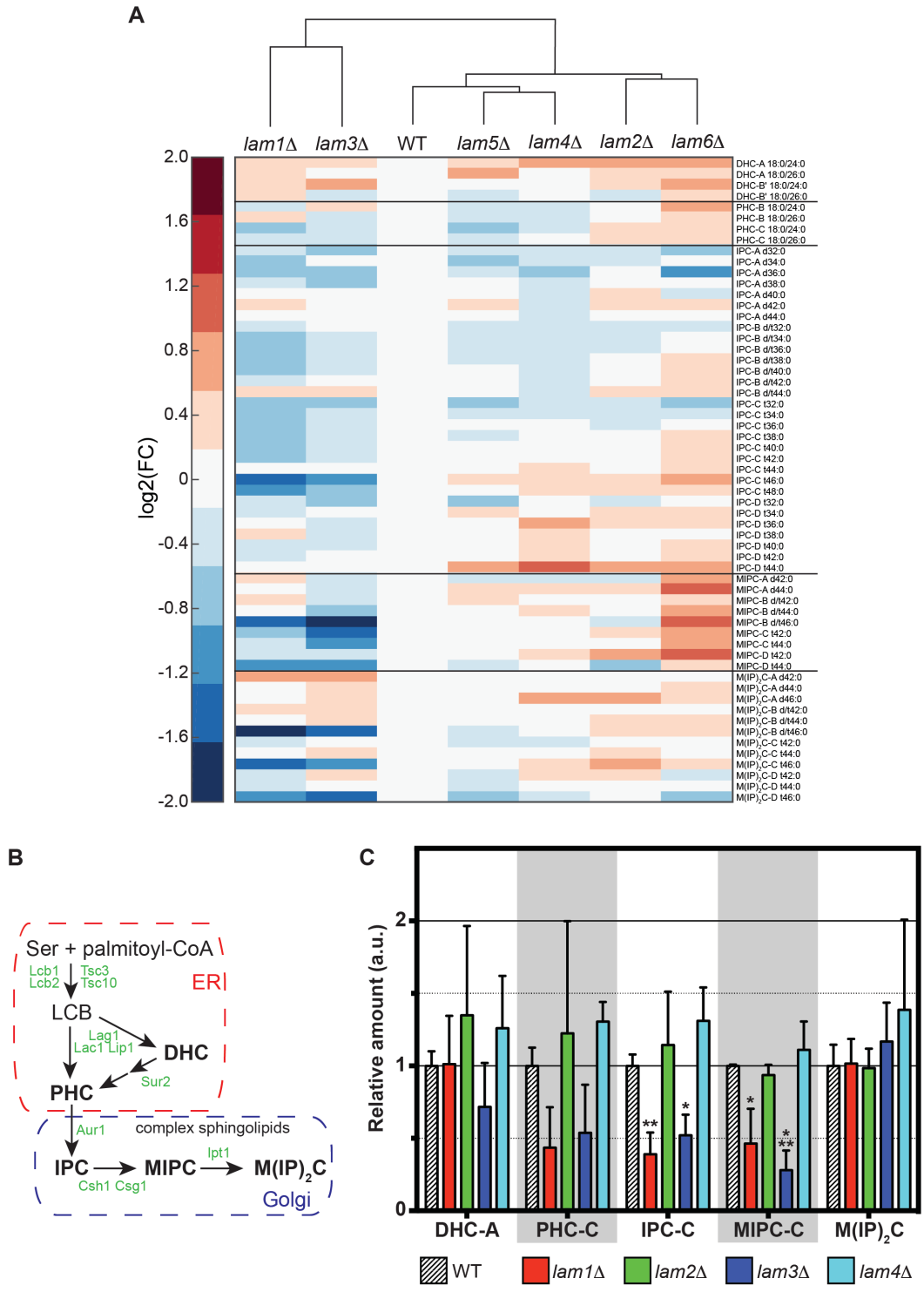

Figure 6.21 Complex sphingolipid levels are reduced in *lam1*Δ and *lam3*Δ strains

(**A**) Hierarchical clustering of sphingolipid profiles. Raw values for the major classes of sphingolipids were normalised on the wild type levels. This fold change was transformed with a base 2 logarithmic equation to obtain a range from –2 to +2 compared to wild type. The hierarchy, clustering and their visual rendition were made with Matlab. (**B**) Simplified overview of sphingolipid biosynthesis in yeast *S cerevisiae*. Known proteins involved in enzymatic steps (green), ER (red), Golgi (blue).

Intermediates observed in the lipidomics study (bold). (**C**) Relative amounts of ceramides and sphingolipids levels. Cells were grown to early log phase, lipids were extracted and their relative levels were measured by mass spectrometry. The mean values and s.d. shown derive from monomers with different length of the same lipid class. IPC-C and MIPC-C levels are significantly lower in *lam1*Δ and *lam3*Δ strains (*p <0.05, **p <0.01, ***p <0.001, two-tailed Student's *t*-test). DHC, dehydroceramide; PHC, phytoceramide.

6.6.3. Correlations between lipidomes of LAM deleted strains

Both the hierarchical clusterings centred on sphingolipids and phospholipids clustered lam1Δ and lam3Δ on the same side of the tree compared to the wild type. lam2Δ lipid profile was closely related to lam4Δ/5Δ/6Δ than the lam1Δ/3Δ (Figure 6.20 and Figure 6.21), implying that the latter two paralogs must have more functions than just stabilising Lam2p. Another observation is that lam4Δ and lam5Δ clustered very closely to the WT, which is consistent with the lack of AmB phenotypes of Δlam4 (Figure 6.8) and lack of protein-protein interactions of Lam5p (Murley et al., 2015). Overall, the lipid profile clustering is also highly similar to the phylogenetic tree of sequence distances (Appendix 2) that clustered Lam1/3p sequences in another branch of the tree, suggesting related functions among Lam2/4p and Lam5/6p (such as sterol transport at ER contact sites with other organelles); in contrast, Lam1/3p are also localised at ER-PM contacts (with Lam2/4p), but they could also be involved in other functions for lipid homeostasis. For example, the accumulation of long chain phospholipids in lam3Δ, and less importantly in lam1Δ, could denote some of the membrane lipid changes that the cell has to make to adapt to the lack of physiological sphingolipid levels.

6.7. Give it a name: LAMs

During the course of this project, we gave a name to the previously unknown members of the newly identified family and we suggested to extend the same name to the entire family. The abbreviation we proposed took into consideration the functional and localisation experiments we performed and it was LAM, for Lipid transfer proteins Anchored at Membrane contact sites (Gatta et al., 2015). In this thesis, I used the abbreviation LAM for naming the members of the newly identified family. We named the uncharacterised proteins as Lam4p (Yhr080cp), Lam5p (Yfl042cp) and Lam6p (Ylr072wp), but unanimous decisions to extend the LAM acronym across all the *S. cerevisiae* family members have not yet been forthcoming (Table 6.1). Nevertheless, for simplicity and clarity, in this thesis I called all the proteins LAMs. In this naming system, the pairs of paralogs are Lam1p/Lam3p, Lam2p/Lam4p and Lam5p/Lam6p as described throughout the result chapters.

Name As used in this work	**Standard name** yeastgenome.org	**Systematic name** ORF	**Alias** Other names
Lam1 (1)	Lam1 (1)	YHR155W	Ysp1 (2)
Lam2 (1)	Ysp2 (3)	YDR326C	Lam2 (1), Ltc4 (4)
Lam3 (1)	Sip3 (5)	YNL257C	Lam3 (1)
Lam4 (1)	Lam4 (1)	YHR080C	Ltc3 (4)
Lam5 (1)	Lam5 (1)	YFL042C	Ltc2 (4)
Lam6 (1)	Lam6 (1)	YLR072W	Ltc1 (4)

Table 6.1 Naming a new yeast protein family: LAMs

For clarity and simplicity, throughout this thesis I used the Lipid transfer protein Anchored at Membrane contact sites (LAM) acronym as listed in the first column. However, the standard name has not been agreed by the scientific community for Lam2 and Lam3 which keep their previous names, Ysp2 and Sip3, respectively. For completeness, the table also lists the systematic names of the nuclear open reading frame (ORF). Aliases are listed in the yeast yeastgenome.org database as “any other associated names”. Numbers in brackets correspond to the original reference where the name was proposed: (1) (Gatta et al., 2015), (2) (Pozniakovsky et al., 2005), (3) (Sokolov et al., 2006), (4) (Murley et al., 2015), (5) (Lesage et al., 1994).

We also suggested changing the name of the human proteins to human Lipid transfer proteins Anchored at Membrane contact sites (hLAMs).

Name (as used in this work)	**Gene name**	**Protein name**
hLAMa	GRAMD1A	GRAM domain-containing protein 1A
hLAMb	GRAMD1B	GRAM domain-containing protein 1B
hLAMc	GRAMD1C	GRAM domain-containing protein 1C

Table 6.2 Proposed names for the human LAMs

GramD proteins were named after the Gram domain present in their sequences. There are four GramD proteins with the longest members in the GramD1 subfamily, whose three proteins (GramD1a/b/c) have also the StART-like domain. We proposed to change their names to hLAM (hLAMa/b/c).

Chapter 7

Structural studies

7. Structural studies

LTPs are defined as structural folds with a pocket internally lined with hydrophobic residues able to accommodate a lipid molecule shielding its hydrophobic moieties from the aqueous environment. The application of profile-profile bioinformatics software for remote homology prediction, showed the presence of a new StART-like domain family (Figure 4.1). At the experimental level, Lam4S2 showed *in vitro* sterol binding (Figure 6.2 and Figure 6.5), and the AmB rescue abilities of the StART-like domains suggested conserved sterol-binding properties shared by Lam2/4/5/6p and the hLAMs (Figure 6.14). The final confirmation of the prediction involved the study of the structure of the predicted StART-like domain and its conformational dynamics upon lipid binding.

Our approach focussed on two complimentary techniques X-ray crystallography and biomolecular NMR spectroscopy to study the most soluble StART-like domain of the new yeast family, Lam4S2 (Figure 6.1). The objectives of biomolecular NMR approach were to (i) obtain a first confirmation of Lam4S2 structure calculated from homology modelling, (ii) study the conformational dynamics of the StART-like domain in the presence of its ligand, and (iii) get the structure of a member of the newly identified family at a reasonable resolution to model the others.

7.1. Lam4S2 homology model

In general, protein domains are divided into families of structural folds with limited energetically favourable conformations (Chothia, 1992). Structural similarity between two homologous proteins can be inferred from their sequence alignment by calculating their spatial constraints (Sali and Blundell, 1993). There is a direct correlation between the sequence identity and the accuracy of the new model (deviation of the Cα of their backbone) (Chothia and Lesk, 1986). Nevertheless, the profile-profile searches we used for the identification of the new StART-like family, incorporate data that can be used for the determination of 3D homology models (Yan et al., 2013).

Here, initial structural information of the Lam4S2 domain was obtained by generating a homology model for the core region of the second StART domain of Lam4p (residues 948-1120). I used a HHpred search based on PDB database to build an MSA with many remote homologues with solved structure, including PCTP, StARD10, StART4 and StARD3. The best alignment was used to make the homology model with Modeller 9 (Sali and Blundell, 1993; Webb and Sali, 2014). The resulting structure, largely based on its alignment with PCTP, showed a typical StART domain conformation (Figure 7.1). The second StART-like domain of Lam4p formed a core 170 residues "helix grip" fold of seven antiparallel β-sheets wrapped around a long C-terminal α-helix, that in other StART domains works as a mobile lid (Kudo et al., 2008). The quality of the model scored an overall 44.68% accuracy rate using Verify3D (Lüthy et al., 1992), with disordered loops showing lower scores than secondary structure elements such sheets and helices. This model was based on StART domains that have an amino terminal extension of some structural elements not involved in lipid binding. These elements include α_1, β_1 and β_2, which were absent from predicted StART-like domains of LAMs and other members of the SRPBCC superfamily (including Bet-v1). The numbering system of the model was based on the long version of the StART domain. The loops between β_3 and β_4, and between β_7 and β_8 (corresponding to the Ω_2) were omitted from the model. The two openings of

the cavity at its top and bottom (Figure 7.1 C) are too narrow for the loading/unloading of the sterol ligand, so it is possible that the long C-terminal α-helix is part of a mobile lid with the Ω_1 loop between β_5 and β_6. A conserved glycine residue in the α_4 helix could also be important for the dynamics of the structural changes required for lipid binding. Indeed, a Gly to Lys mutation impeded sterol binding in DHE-FRET assays (Louise Wong). This Gly is also conserved in human LAMs and it could be involved in interaction with the α_1-β_3 loop (close to the N-terminus in Figure 7.1 D). Hydrophobic residues in the centre of four antiparallel β_6-β_7- β_8-β_9 and on the residues on the three α-helices are predicted to face the inner cavity (Figure 7.1 E). The position of their side chains will allow a more detailed determination of the residues involved in sterol binding.

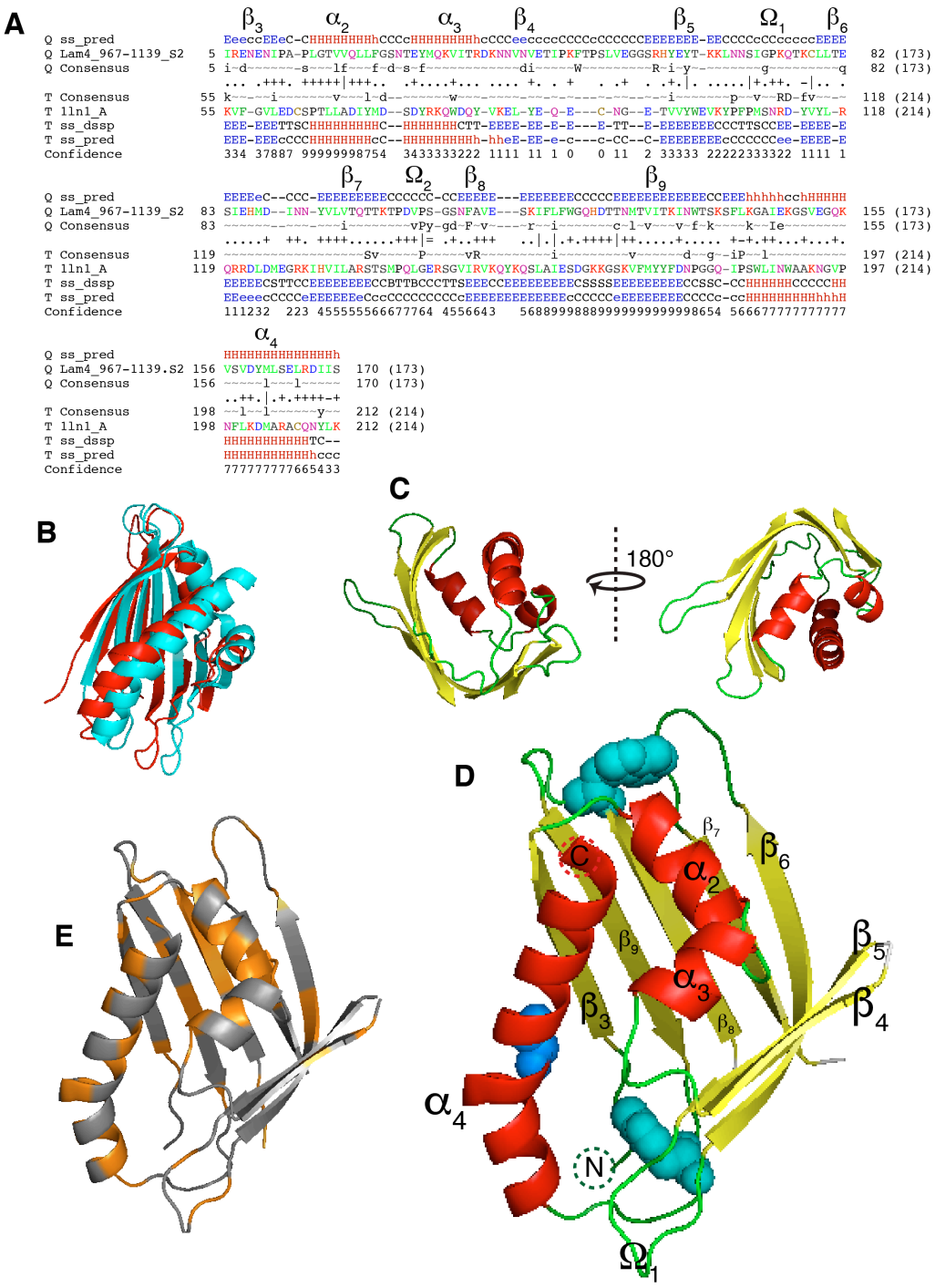

Figure 7.1 Homology model of Lam4pS2

(**A**) Detailed alignment of Lam4S2 with PCTP showing consensus, confidence and secondary structure prediction. The query alignment from HHpred MSA showed the top score with PCTP (PDB: 1LN1). (**B**) Superimposition of Lam4S2 (red) and PCTP (cyan). The homology model of Lam4S2 was obtained by exporting HHpred MSA (containing the 3 best alignments of the query with PDB repositories) to the tertiary structure prediction software Modeller 9.16 (Sali and Blundell, 1993; Webb and Sali, 2014). Both domains are represented as cartoons for β-strands and α-helices. Structures and superimposition processed with PyMol. (**C-E**) Lam4S2 (968-1136) is

represented with cartoons showing α-helices (red), β-sheets (yellow) and loops (green). Loops between β_4 and β_5, and loop between β_7 and β_8 (Ω_2) were omitted from the model. (**C**) View of Lam4S2 domain from top and bottom of the binding pocket to show the antiparallel β-sheets wrapping the long C-terminal α-helix (positioned perpendicularly to the observer). (**D**) Domain with long C-terminal α-helix working as mobile lid of the domain on the left. Also shown: N and C termini; two conserved tryptophans (cyan), one inside (bottom) and the other outside (top) of the pocket; and a conserved glycine in the C-terminal helix (blue, G1119 in Lam4p, G1205 in Lam2p). (**E**) Lam4S2 model (same as D) with highlighted (orange) hydrophobic residues (Ala, Gly, Val, Ile, Leu, Phe, Met).

7.2. The NMR fingerprint of Lam4S2

The first experiments aimed at validating the feasibility of the NMR approach to observe Lam4S2 structure in solution. Initial tests were conducted on a sample of ^{15}N-labelled Lam4S2 in the buffer used for *in vitro* binding assays. Sample conditions were enhanced for the NMR experiments by improving the buffer. First, the buffer concentration was reduced by 50% (final 10 mM PIPES), and tested in Heteronuclear Single Quantum Coherence (HSQC) experiments: these conditions required long RF pulses, incompatible with more complex experiments. Subsequently, also the concentration of salt was reduced by reducing it to a third and supplementing the buffer with 50 mM L-Arginine/L-Glutamate solution to improve signal-to-noise ratio and increase protein solubility (Golovanov et al., 2004). These conditions resulted in more feasible for NMR experiments. The Lam4S2 construct contains 235 amino acids. In the HSQC spectrum, all amino acids, except prolines and the N-terminus, should produce a peak at the chemical shifts of their backbone amides yielding the characteristic fingerprint of a protein: each peak has the chemical shift on the ^{1}H axis corresponding to the H_N-proton and the nitrogen chemical shift corresponding to the nitrogen directly bonded to the amide proton. In this case 222 backbone amide peaks were expected. The two-dimensional ^{1}H-^{15}N HSQC of ^{15}N-labelled Lam4S2 at 25 °C showed 172 peaks corresponding to 77% of expected backbone amide peaks (Figure 7.2). The ^{1}H dispersion indicates that the protein was stable and correctly folded, and the absence of doublets suggested a single conformation for the time of the experiments (22 min at 25 °C). HPLC analyses before and after the acquisition revealed that the protein remained monomeric (Anastasia Zhuravleva, personal communication). Several strong peaks with proton chemical shifts around 8 ppm were likely to correspond to the unfolded 11-histidine tag. Also visible were the amides of the two tryptophan side chains on the bottom left side of the spectrum (Figure 7.2, circle).

The NMR approach at the optimised conditions seemed a feasible technique to study Lam4S2 structural features. The initial NMR fingerprint of Lam4S2

suggested that further optimisation (*i.e.* relaxation properties by means of deuteration) of sample conditions would allow for a full backbone assignment of the protein.

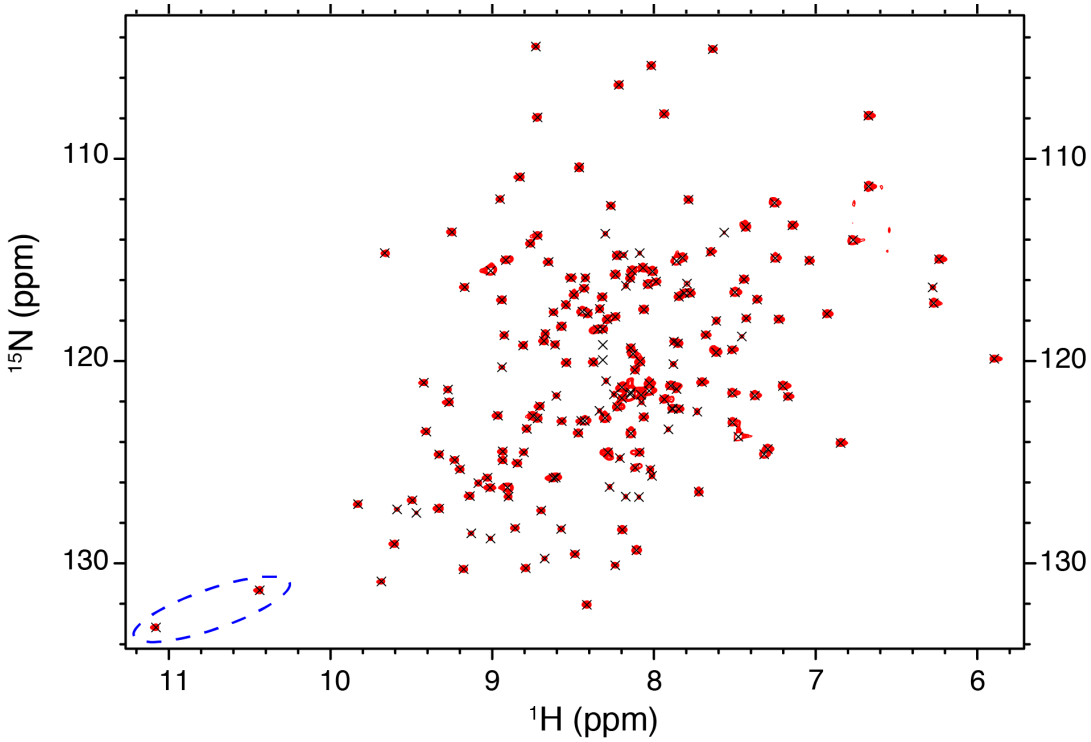

Figure 7.2 2D ^{1}H-^{15}N HSQC of 15N-Lam4S2

Two-dimensional ^{1}H-^{15}N HSQC spectrum of the ^{15}N-labelled second StART-like domain from Lam4p (0.4 mM in NMR buffer at pH 6.8). Spectra were analysed using CcpNmr Analysis software (Skinner et al., 2015). 2D peaks were selected automatically by the software using the optimal contours function in CcpNmr (Skinner et al., 2015). The peaks correspond to the backbone amide, with the chemical shift on the ^{1}H axis corresponding to the H_N-proton and the nitrogen chemical shift corresponding to the nitrogen directly bonded to the amide proton. Some side chains amides are also visible: H_N of the indole tryptophan side chains are visible at the bottom left corner of the 2D spectrum (blue dashed-line circle).

7.3. Backbone assignment of Lam4S2

To achieve a complete backbone assignment a full set of backbone assignment experiments (Material and Methods, Section 3.12.5) was recorded and analysed on (i) a uniformly labelled ^{1}H-^{13}C-^{15}N-Lam4S2 sample and (ii) a uniformly labelled ^{2}H-^{13}C-^{15}N-Lam4S2 sample. These standard experiments were underpinned by Isoleucine Leucine and Valine (ILV)-reverse labelled samples to identify the I, L and V residues in the sequence. As explained in the introduction, triple resonance experiments correlate a backbone $^{1}H_{N}$-^{15}N pair with one or more ^{13}C chemical shifts (Figure 1.8 and Appendix 1).

I used the peak list from the 2D HSQC experiments to manually pick the corresponding peaks in triple resonance spectra in CcpNmr Analysis software (Skinner et al., 2015). For the assignment, the analysis of the triple resonance peaks obtained with the uniformly labelled ^{1}H-^{15}N-^{13}C-Lam4S2 was performed in a semi-automated calculation by Anastasia Zhuravleva (University of Leeds) using CcpNMR Analysis software, and only 56 connectivities were identified (out of the 222 expected peaks to be assigned). Figure 7.3 illustrates local connectivity among the residues . The strips represent the peaks seen along a ^{13}C and ^{15}N dimension each centred on the corresponding amide proton chemical shift. Each strip represents the superimposition of 3D HNCA-HN(CO)CA (top) and HNCO-HN(CA)CO acquisitions (Appendix 1). Together these two pairs of experiments should reveal the Cα and CO, respectively, chemical shift for each amino acid residue in a protein sequence. Each strip presents two peaks of the HNCA correlating Cα_{i} and Cα_{i-1} peaks and a single HN(CO)CA peak corresponding to the Cα_{i-1} peak. In the bottom panels, HNCO showed only one peak of the CO_{i-1} and HN(CA)CO should show both CO_{i} and CO_{i-1} (expected to be waker). However, some of the CO_{i-1} peaks (D39 and D43 in the figure, grey crosses) are not detectable. ~60% of CO_{i-1} in HNCO spectra were masked by the background noise. This high level of ambiguity, when extended to multiple adjacent residues, did not allow a successful run of the algorithm for the automated sequential assignment. The ambiguity was

hypothesised to be due to the protein MW >20 kDa and that gives a poor signal-to-noise ratio and signal overlap.

The lack of signal in the protonated spectra and the size of the protein led us to adopt another assignment strategy. First of all, the protein was deuterated which changes the relaxation properties of the sample and thus improves the sensitivity of the assignment experiments. A further improvement in spectral resolution and sensitivity could be obtained by moving to higher magnetic fields (from 600 MHz to >800 MHz). Lastly, we recorded the experiments in TROSY rather than HSQC based triple resonance experiments, which added to our chances of success because of improved coupling detection and increased peak resolution.

The selective unlabelling of the aliphatic amino acids ILV reverse labelling, allowed the identification of these three residues from the spectra and it reduced crowding of the spectrum making it easier to distinguish peaks in crowded regions (McIntosh and Dahlquist, 1990). Triple resonance experiments were performed with the ILV-reverse labelled protein and compared to the fully labelled Lam4S2: the missing peaks identified aliphatic residues (Figure 7.4). Lam4S2 contained a total of 45 residues that should disappear from the spectrum: 15 Ile, 13 Leu, and 17 Val. The ILV-reverse labelled spectrum allowed the identification of the 38 peaks that disappeared. The three hydrophobic amino acids have the tendency to be buried in the core of the protein with low water accessibility and it will be helpful also for the side chains assignment at later stages. The seven residues difference (38 out of the 45 ILV residues disappeared) might be caused by isotopic scrambling during the labelling (incorporation of ^{15}N- and/or ^{13}C- isotopic-labelled source into the nascent protein).

Finally, the additional experiments involved random fractional (~75%) protein deuteration, obtained by inducing protein production from BL21 cells growing in $^{2}H_2O$. Deuteration removes external contributions of spin relaxation, and gives improved signal-to-noise ratio and better resolution (Nietlispach et al., 2002). For the expression on the deuterated sample, expression conditions

had to had to be re-evaluated because of $^{2}H_2O$ toxicity on BL21 *E. coli*. A screening of BL21 cells was necessary to select the colonies best fit for growth in deuterated conditions. The best performing colonies from a $^{2}H_2O$-agar plate were used for small scale protein production prior to induction in full volume (Figure 7.5). The rate of exponential growth was reduced to ~3h30m doubling time for the best performing colonies.

Data collection and analysis of deuterated sample were performed with the help of Andrea Sauerwein (Imperial College London). All the information obtained with these approaches were integrated with the previous experiments and the secondary structure prediction for the computational assignment. The increased quality of the spectra confirmed and expanded the 56 connectivities already obtained to a total of 124. This partial assignment covered 56% of peaks (Figure 7.6 and Appendix 3).

The unassignable portions included the core regions of predicted secondary structures, while unexpectedly the residues corresponding to unstructured loops were assigned more easily. The unassignable peaks were due to poor or absent signals recorded in the most sensitive 3D acquisitions. The specific reasons for this behaviour were not known. In particular, the signals corresponding to the core residues of the β-sheets forming the hydrophobic cavity were lost in the noise for the most sensitive acquisition.

Therefore, in summary, the assignment of peaks, and hence the determination of Lam4S2 structure, failed using the construct I have been working with. Similar loss of core signals from NMR assignments is said to be uncommon, and is caused by factors such as transient weak homotypic interaction in solution, or instability of unstructured regions at either ends of the construct, as discussed in Section 8.6.

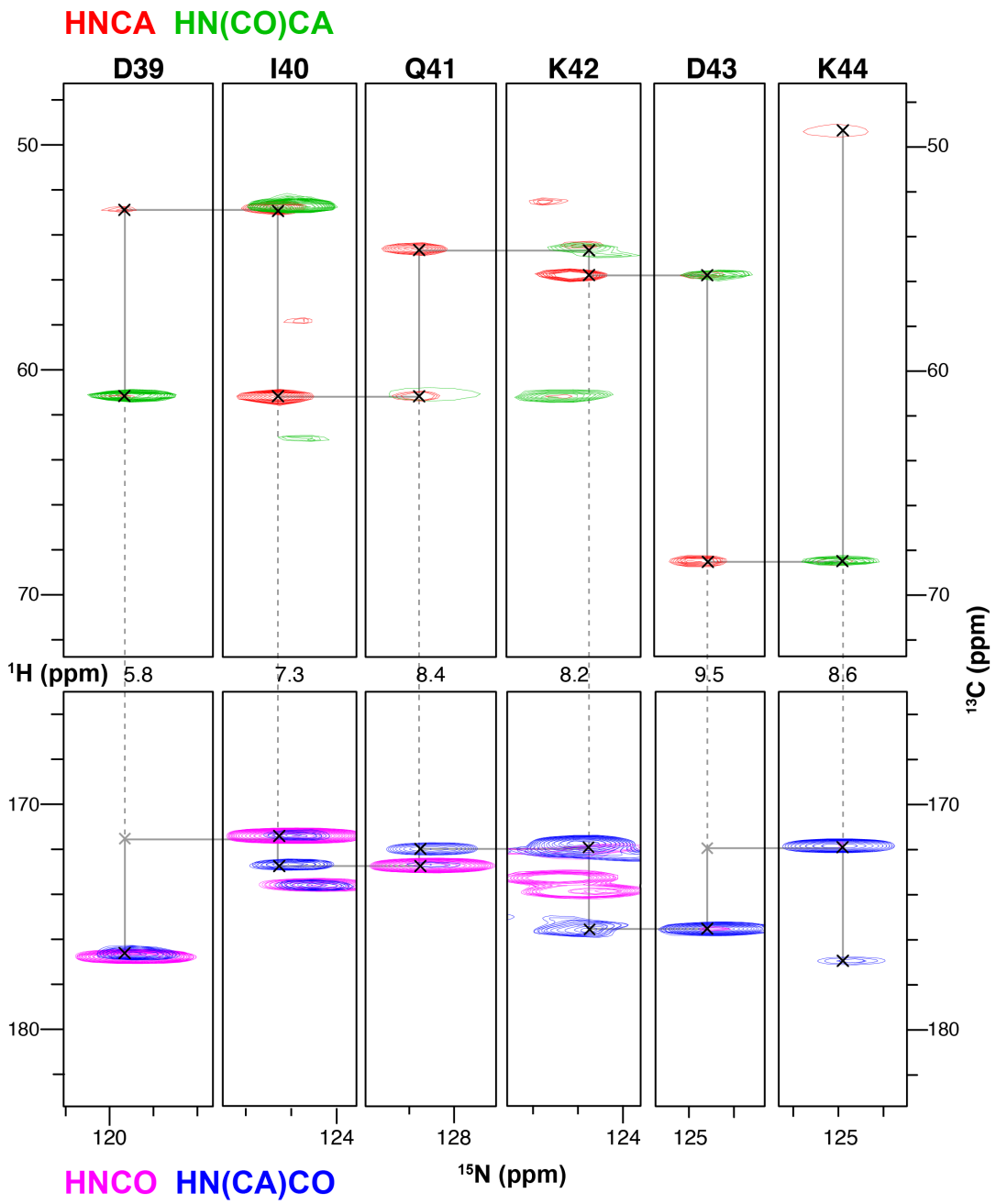

Figure 7.3 Representative peaks connectivity in triple resonance experiments

Stripes of triple resonance NMR spectra showing the connectivity of Lam4S2 residues in the range 39-44 of the His-tagged construct. (Top) Strips derived from HNCA (red) and HN(CO)CA (green) spectra. (Bottom) Strips derived from the HNCO (blue) and HN(CA)CO (magenta) spectra. Strips are presented along ^{13}C (y axis) and ^{15}N (x axis) chemical shifts, and are centred on the corresponding amide proton chemical shift (indicated between top and bottom panels). Horizontal and vertical lines demonstrate the connectivities. Dashed lines connect top and bottom panels. Spectra were processed with CcpNmr Analysis for semi-automated assignment and visualisation of local connectivity.

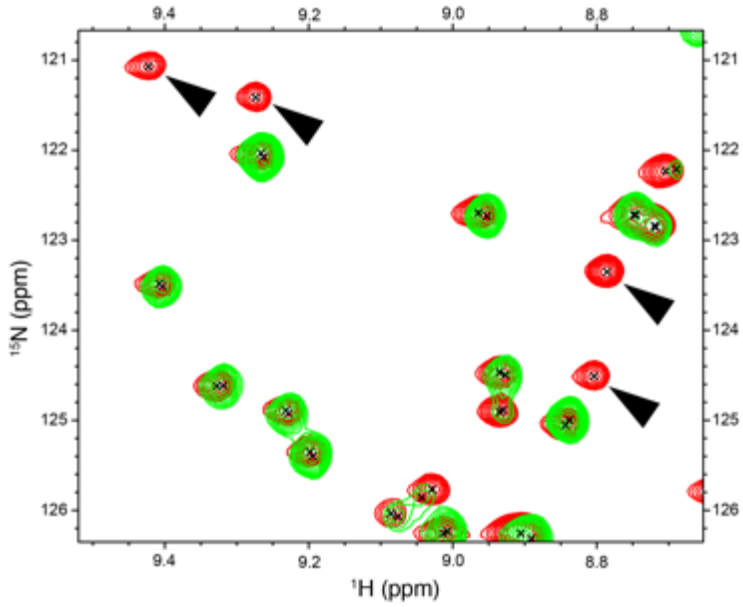

Figure 7.4 ^{1}H-^{15}N-^{13}C-TROSY of ILV reverse labelled Lam4S2

Lam4S2 production was induced in M9 minimal medium containing $^{15}NH_4Cl$, ^{13}C-glucose and excess isoleucine, leucine and valine for ILV reverse labelling. The figure shows a detail of the HSQC spectrum with peaks of ILV reverse labelled protein (green) overlayed to the uniformly labelled sample (red). The peaks that disappear (arrowheads) are Ile, Leu or Val. This information was considered for the semi-automatic sequential assignment of CcpNmr software.

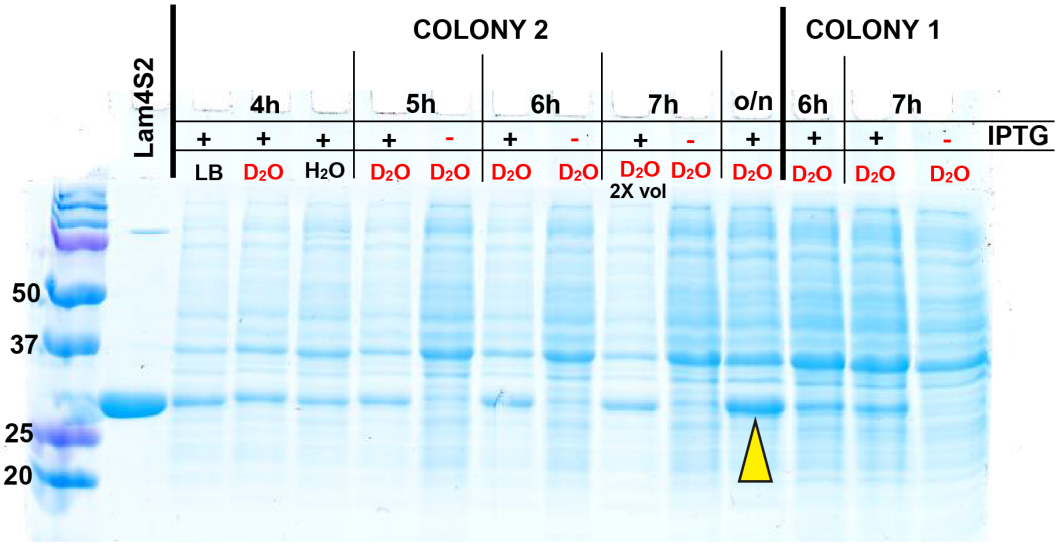

Figure 7.5 Test of optimal induction conditions for $^{2}H_2O$-fit colony

Coomassie-stained SDS-PAGE of whole cell lysate from different induction conditions. BL21 cells expressing were transformed with His_{11}-Lam4S2 and plated on standard LB plates. Colonies were replicated on M9 minimal medium $^{2}H_2O$-agar plate to select the best fitting for deuterium growth. Five colonies were screened for different induction conditions in $^{2}H_2O$. The best two (presented in this figure) were further processed for more detailed evaluation. Colony number 2 was chosen for 22 hours induction at 37°C (yellow arrowhead).

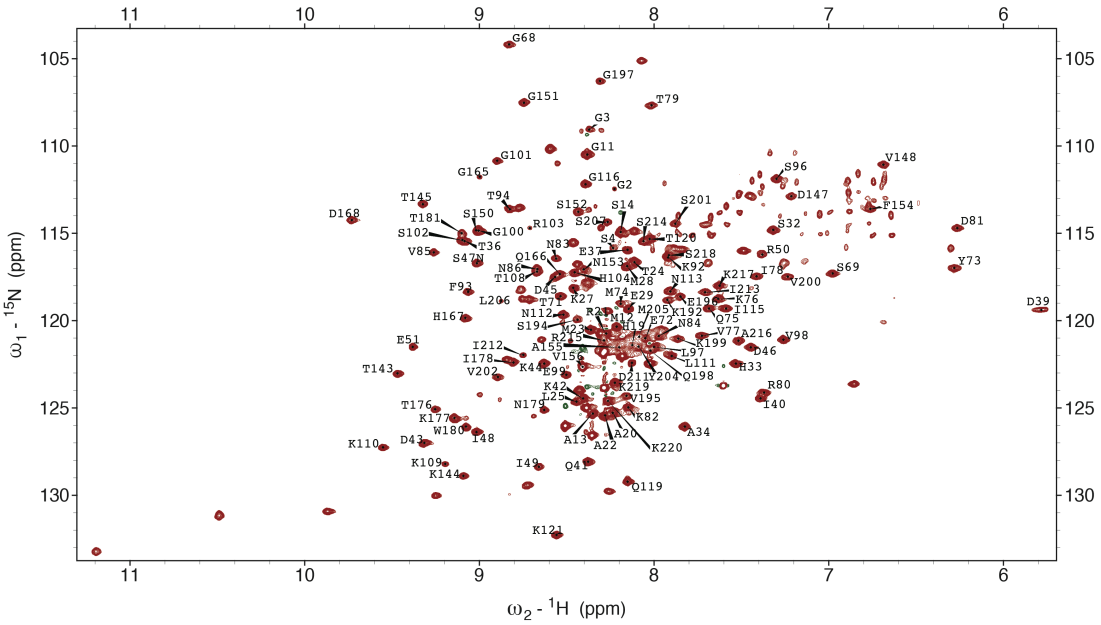

Figure 7.6 ^{1}H-^{15}N-TROSY spectrum with the partial backbone assignment of Lam4S2

HSQC spectrum with partial backbone peak assignment. Backbone chemical shifts for the assigned/all observed residues are listed in Appendix 3. The assignment was done on a ^{2}H-^{13}C-^{15}N-sample of Lam4S2 in NMR buffer. The assignment is shown on a TROSY and all backbone experiments were recorded in a TROSY fashion. TROSY-HNCO, TROSY-HN(CA)CO, TROSY-HNCA, TROSY-HN(CO)CA, TROSY-HNCACB, TROSY-HN(CO)CACB. The experiments were repeated twice and recorded at 800 MHz. The assignment was computed using NMFRAM-Sparky (Kreishman-Deitrick et al., 2003).

7.4. Sterol binding to Lam4S2

One of the advantages of NMR spectroscopy, is the possibility to study the three dimensional conformation of a protein in solution very similar to its physiological conditions. Furthermore, also in the case of lipid transfer proteins, it is possible to observe the dynamic conformational changes upon the addition of the ligand involving only specific peaks. The lack of complete assignment (56% partial assignment) does not prevent a determination of the role of these residues in sterol binding.

The addition of cholesterol excess, presented to Lam4S2 in solution using methyl-β-cyclodextrin:sterol complexes, resulted in selective and significant changes in the NMR spectrum (Figure 7.7). Some peaks disappeared and shifted to a new set of peaks likely corresponding to the lipid-bound state of the protein as opposed to the 'apo' form as purified from *E. coli*. Selective peaks broadened and their intensity decreased, a typical effect on NMR spectra of chemical exchange (Cavanagh et al., 2010). Considering the average broadening and relative weakening of the peaks involved in the binding, the exchange rate of cholesterol appeared to be in the μs-ms range. Assigned peaks were correlated with the peaks shifting upon sterol binding, revealing residues belonging to the N-terminus loop (S32, A34, D43), β_3 (I49 and E51), α_3 (T79 and R80), β_4 (E85), β_5 (S96), and others in the loops between the antiparallel β-sheets (S96, T145, G151, and H167).

If the full peak assignment could be completed, it would be possible to identify all residues involved in the conformational changes required to accommodate the sterol molecule. Nevertheless, the current experiment was sufficient to observe the behaviour of the peaks corresponding to the two tryptophan side chains (Figure 7.7 B): one peak, likely corresponding to W1086 and predicted to face outside the binding pocket (Figure 7.1), did not move; the second peak, likely corresponding to W1102 facing inside the binding pocket, shifted position. This observation was the first confirmation of at least one part of the Lam4S2 homology model. Future experiments for full peak assignment will

allow the identification of all the peaks involved in the binding and the calculation of the extent of the shift (Δppm).

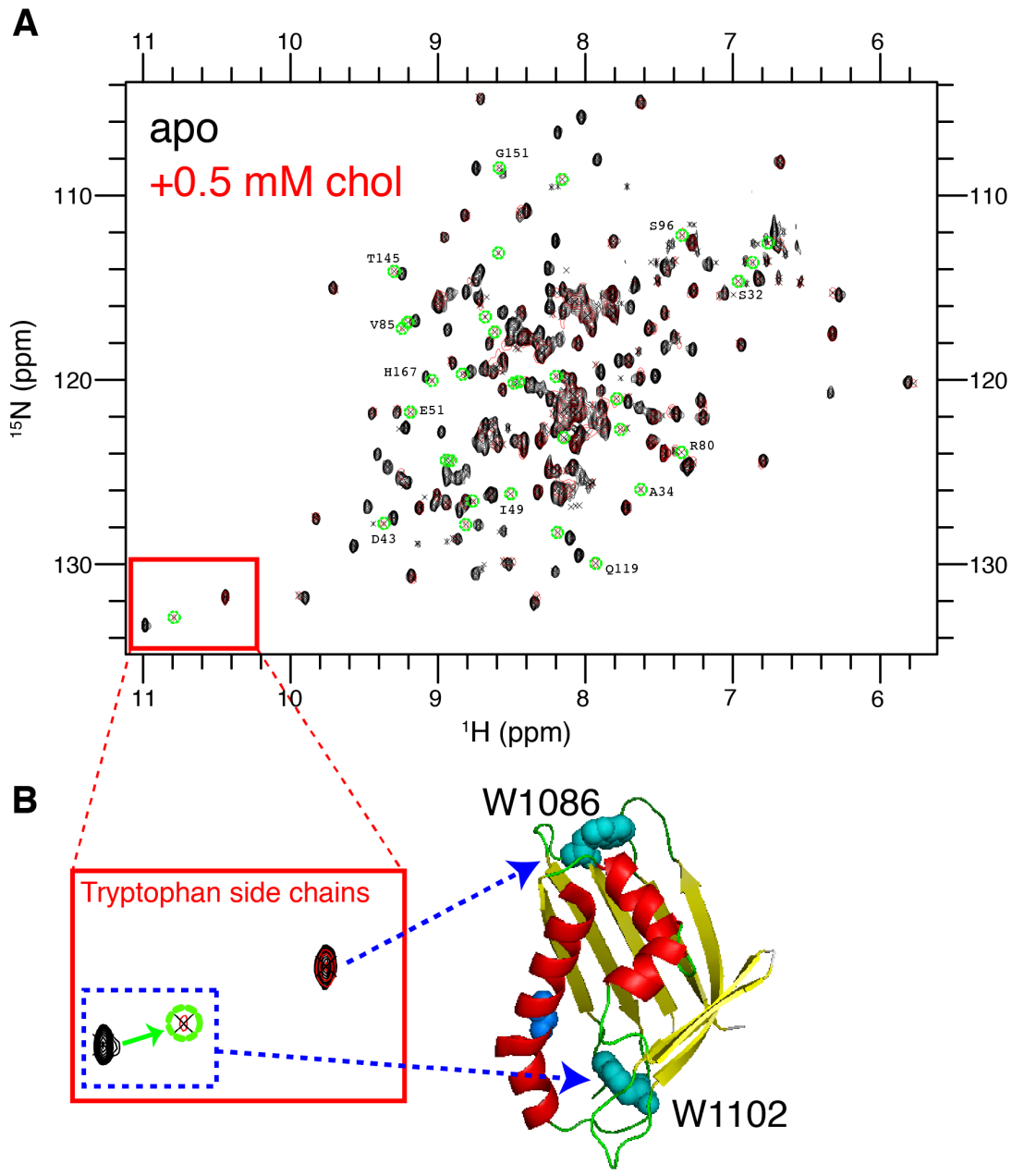

Figure 7.7 Lam4S2 changes upon sterol binding

(**A**) Superimposition of ^{1}H–^{15}N HSQC spectra of Lam4S2 (0.3 mM in NMR buffer at pH 6.8) alone (black) and in the presence of excess cholesterol (red). 0.5 mM cholesterol was presented in MβCD:chol complexes). Acquisitions were performed at 35°C. Dashed green circles represent the peaks significantly shifting of the cholesterol-bound protein. 'apo' corresponds to the His-tagged protein as purified by BL21 cells. The name of the assigned peaks is shown. (**B**) Zoom on tryptophan side

chains different behaviour. Trp Nε-Hε amide groups of the aromatic ring usually fall in the bottom left side of the HSQC spectrum. Lam4S2 sequence contains two tryptophans (cyan), W1086 and W1102, predicted to face outside and inside the binding pocket, respectively (Figure 7.1). The peak shifting upon sterol addition (green arrow and dashed circle) is likely corresponding to the tryptophan involved in the conformational changes required for the binding.

Chapter 8

Discussion

8. DISCUSSION

In this work, I describe the identification of a new family of StART-like membrane-anchored proteins conserved throughout eukaryotes, and I present the experiments I performed for their characterisation by studying localisation, functional aspects in lipid homeostasis, and preliminary structural details (Table 8.1).

Almost all members of the family possess transmembrane domains. The six members in *Saccharomyces cerevisiae* localise at membrane contact sites. Lam1p, Lam2p, Lam3p, and Lam4p resided in puncta at ER-PM contact sites structurally different from the ones mediated by the yeast homologues of VAPs and extended synaptotagmins. Lam1p, Lam2p, and Lam3p could operate as residual ER-PM tethers: I showed with electron microscopy that their triple knockout caused a statistically significant although minor loss of 5% of cER contacts, but their tethering role could be masked by the presence of other dominant tethers, such as VAPs. Lam5p and Lam6p targeted internal membrane contact sites, including nucleus-vacuole junctions (NVJ), ER-mitochondrial encounters, and perivacuolar ER.

Among the six yeast members, the second StART domain of Lam4p (Lam4S2) has sterol binding properties. These were demonstrated by two different *in vitro* approaches: (i) cholesterol was identified as the only lipid ligand in binding assays using human radiolabelled cells donors, and (ii) DHE functioned as FRET acceptor upon excitation of Lam4S2 tryptophans and subsequent energy transfer. Moreover, an involvement of LAM proteins in sterol homeostasis was also demonstrated *in vivo*. Knockout strains for LAM1, LAM2 or LAM3 showed increased sensitivity to the sterol-sequestering antifungal drug AmB. The StART-like domains from Lam2/4p, Lam5/6p and hLAMa were able to rescue the phenotype when expressed in the cytoplasm, indicating a conserved sterol binding property. Despite the effort for their recombinant purification, I was not able to identify the lipid ligands of the StART-like

domains of Lam1p and Lam3p. However, strong evidence suggests that Lam1/3p have sterol-related functions as well: (i) the higher toxicity to AmB showed by *lam1*Δ and *lam3*Δ (compared to *lam2*Δ) correlated with low sphingolipid levels, and (ii) this phenotype could be rescued by other sterol-specific StART-like domains. The structure of Lam4S2 was obtained by homology modelling based on related human StART domains. I used biomolecular NMR spectroscopy to give the first, albeit partial, confirmation of the predicted fold, and I showed some structural and dynamic changes following sterol binding.

In the following sections, I will discuss these aspects in more detail including associations with other published works, further experiments required to better delineate the function of LAMs, and implications for intracellular lipid traffic and sterol homeostasis.

Protein	Gene	Localisation	Lipid ligand	Evidence
Lam1p	YHR155w	ER-PM contact sites	*sphingolipid?*	microscopy AmB phenotype lipidomics
Lam2p	YDR326c	ER-PM contact sites	sterols	microscopy AmB phenotype/rescue spectroscopy
Lam3p	YNL257c	ER-PM contact sites	*sphingolipid?*	microscopy AmB phenotype lipidomics
Lam4p	YHR080c	ER-PM contact sites	sterols	microscopy AmB rescuing *in vitro* lipid binding spectroscopy, NMR
Lam5p	YFL042c	NVJ, ER-mitochondria, ER-vacuole	sterols	microscopy AmB rescuing
Lam6p	YLR072w	NVJ, ER-mitochondria, ER-vacuole	sterols	microscopy AmB rescuing

Table 8.1 Summary of yeast LAMs characterisation

Proofs of the localisation have been collected mainly observing the GFP-tagged version of the proteins at the confocal microscope (microscopy). AmB phenotype means the sensitivity of the correspondent knock-out strain to sub-lethal drug exposure. AmB rescuing is the ability of the protein StART domain(s) to rescue the phenotype of a sensitive strain. The open points about the lipid ligands of Lam1p and Lam3p should be proven. *Some of the open points are listed in italic.*

8.1. Discovery of a new family of StART-like domain proteins

This work stemmed from the application of profile-profile remote homology searches for the discovery of remote homologues of StART domains, on the basis that sterol transport had not yet been identified in fungi. The same approach was previously used to determine that the SMP domain of extended synaptotagmins and other contact site proteins belonged to the TULIP superfamily (Kopec et al., 2010; Schauder et al., 2014) and to show that Ups/PRELI proteins are related to StARTs (Connerth et al., 2012). During the course of this project, a bioinformatics search for domains in the plant Vascular-Associated Death protein 1 (VAD-1) performed with I-TASSER (Roy et al., 2010), found the same region that we found as being structurally related to mammalian StART and Bet_v1 superfamily (Khafif et al., 2014). All the members of this family contain the helix-grip fold formed by seven β-strands wrapped around two short and one long α-helices. Thousands of proteins with this hydrophobic cavity, identified in invertebrates, bacteria and plants have been included into the SRPBCC (START/RHOαC/PITP/Bet v1/CoxG/CalC) superfamily. Different families within this superfamily are lipid transfer proteins known to bind different lipid ligands including sterols, phospholipid, and sphingolipid (Schrick et al., 2014).

In this thesis, I described the same approach applied in the opposite direction: we used HHpred, which works exploiting profile-profile comparison that includes structural conservation scoring, to search remote homologues of known StART domains. Most eukaryotes, including fungi, have several members of the new StART-like family (Appendix 2). The human family has three members, while Saccharomyces cerevisiae has six, in three paralogous, originating from a whole genome duplication (Kellis et al., 2004). The paralogs are Lam1p/Lam3p, Lam2p/Lam4p and Lam5p/Lam6p (Figure 4.4). The phylogenetic tree of the new family () showed that Lam1/3p-like proteins are more conserved throughout fungi, while Lam2/4p and Lam5/6p appear to have arisen in fungi from a common ancestor more closely related to the metazoal form than Lam1/3p.

Apart from the StART-like domain, the other defining feature of the proteins in the family was the presence of TMDs, indicating permanent anchoring to a cell membrane. How can proteins with TMDs operate lipid transfer between membranes? Their function must be strictly linked to their localisation at MCSs, as this is the only place where they could reach both membranes. This feature has already been demonstrated for other LTPs with TMDs, such as MLN64/StARD3 (Alpy et al., 2013) and ORP5/8 (Chung et al., 2015). Importantly, these two examples represent only few exceptions in their respective families, while the presence of TMDs is one of the defining features of LAM family (Wong and Levine, 2016).

The accompanying elements of LAM proteins are other membrane targeting domains, including GRAM and BAR domains. GRAM are domains closely related related to PH domains (Figure 4.4), and the association of PH-like and StART-like domain is universal in eukaryotic evolution (Khafif et al., 2014). PH domains in mammalian LTPs are known to specifically target membrane lipids, such as phosphoinositides (Balla, 2013). However, most yeast PH domains do not show membrane targeting when isolated (Yu et al., 2004). Indeed, the deletion of Lam2p PH domain did not result in mislocalisation (Figure 5.8) and its GFP-tagged PH domain alone did not indicate specific targeting (Tim Levine, personal communication). Instead, Lam6p is found at ERMES because it interacts with Tom70/71p (Murley et al., 2015; Elbaz-Alon et al., 2015) via its PH-like domain (Murley et al., 2015), and also with Vac8p, a peripheral membrane protein that binds Nvj1p, among others (Tang et al., 2006). So, it is likely that the PH-like domains of other LAMs, rather that targeting membrane lipids, are also involved in protein-protein interactions, thus forming a complex (see Section 8.5). Future studies should be aimed at uncovering the other components. BAR are banana-shaped lipid binding domains targeting highly curved membranes in reversible and weak protein-lipid interactions (McMahon and Gallop, 2005). Thus, the simultaneous presence of TMDs and other protein-protein or protein-lipid membrane targeting domains (PH or BAR, respectively) grants the members of the new

family with double targeting features typical of proteins localised at contact sites.

8.2. Localisation at contact sites

The family is conserved from yeast to humans, but their localisation was studied only in yeast both for this thesis and in other published papers (Murley et al., 2015; Elbaz-Alon et al., 2015). I observed the localisation of yeast LAM proteins GFP-tagged at their N-terminus and under the control of either a moderately strong or their endogenous promoter. At endogenous levels, Lam2p is the most highly expressed, while Lam1p, Lam3p and Lam4p are barely detectable by conventional confocal microscopy. This is in contrast to previous high-throughput screening of C-terminal GFP-tagged yeast ORF that quantify Lam1p as the most abundant per cell (Table 8.2). However, in high-throughput studies proteins are tagged at the C-terminus. This is due to the need of including a selection marker in the PCR product containing the tag and undergoing homologous recombination. Different studies showed important variances both in expression levels and localisation (Ghaemmaghami et al., 2003; Huh et al., 2003; Tkach et al., 2012). Thus suggesting that the C-terminus tag might affect the correct sorting of LAM proteins. Indeed, Lam2p localisation is determined by its C-terminal ER-luminal region (Figure 5.8). For this reason we opted for an N-terminus tag to avoid artefacts in LAM localisation.

Protein	**Length** (aa)	**TMD**	**Abundance** (copies/cell)
Lam1p	1,228	2	1,170
Lam3p	1,229	2	432
Lam2p	1,438	1	200
Lam4p	1,345	1	57
Lam5p	674	1	408
Lam6p	693	1	672

Table 8.2 Yeast LAM abundance

Yeast LAM proteins abundance with list of protein copies per viable cell as calculated from a single high-throughput study (Tkach et al., 2012). All values were obtained from Tkach et al., 2012; number of transmembrane domain as predicted with TMHMM.

8.2.1. Lam2p localisation and targeting

I studied GFP-Lam2p more extensively because of its higher expression and detectability at usual confocal microscopy. Its peripheral punctate distribution was largely Sec18-independent, so it was concluded that its transmembrane domain is embedded into the ER (Figure 5.11). In the SEC18 block experiment, a portion of GFP-Lam2p accumulated into the internal ER, but this was probably due to the strong overexpression induced by the *GAL1* promoter. However, Lam2p could also be a PM protein that follows a Sec18-independent pathway. Indeed, Golgi-bypass routes were described for proteins reaching the PM by the use of classical or peripheral ER Exit Sites (ERES) (Grieve and Rabouille, 2011). Bypassing the Golgi grants proteins with faster trafficking (Baldwin and Ostergaard, 2002), avoidance of Golgi post-translation modifications (Abbott et al., 2008), and prevention of disruption of homeostatic Golgi processes (Yoo et al., 2002).

Despite previous description of C-terminal GFP-tagged Lam2p at mitochondria (Sokolov et al., 2006), a remarkable and robust co-localisation with cortical ER was displayed both in wild type cells and in Δ*tether* cells. The Δ*tether* strains was made by simultaneous deletion of the six ER-PM tethering proteins Scs2/22p, homologues of human VAPs, Ist2p, and the three tricalbins (Tcb1-3), homologues of extended synaptotagmyns (Manford et al., 2012). Lam2p localisation was studied with an ER-marker and remained at the few segments of cER left (Figure 5.4-5.6). Lam2p could populate a subdomain of the ER-PM contacts: the deletion of the known tethers was not sufficient to completely disrupt cortical puncta. This is also confirmed by the fact that the wild type strain missing LAM1, LAM2 and LAM3 had a minor (5%) but statistically significant reduction of cER (Figure 6.18). Their tethering abilities could be masked by other major tethers such as VAP, that could be overexpressed in response to LAM1/2/3 deletion.

Furthermore, I dissected the requirements for the correct targeting at these ER-PM subdomains: the C-terminus (Lam2CT) alone, including ER-embedded transmembrane domain with the predicted luminal domain,

produced a cortical distribution similar to the full length Lam2p (Figure 5.8). I have not identified the exact mechanism of the targeting, but it is possible to speculate about:

- A structural element reminiscent to the viral protein TGBp3 (Wu et al., 2011). Its targeting to curved ER tubules works via a luminal short β-hairpin that homo-oligomerises. PSI-PRED 3.0 also predicted two short β-strands before the coiled-coil region in the luminal domain of Lam2p (Tim Levine, personal communication), which might form a β-hairpin similar to TGBp3. However, TGBp3 is not an ER-shaping protein and it did not co-localise significantly with Lam2p (Figure 5.10).
- The predicted coiled-coil at the extreme C-terminus of Lam2/4p (Figure 4.4) could also play a role in self-assembly. However, the ΔCT construct, missing the luminal portion almost completely, still showed some cortical localisation in few GFP-positive puncta per cell, suggesting the presence of another element in the luminal portion able to target the PM (Panel n. 5 in Figure 5.8).

8.2.2. Lam1/3/4p co-localisation with Lam2p

Endogenous levels of GFP-Lam4p showed a similar punctate cortical distribution, barely detectable by standard confocal microscopy (Table 8.2), but significantly co-localising with Lam2p (Figure 5.12). The same localisation was maintained in Δ*tether* cells, where both paralogs populated the remaining 4% of the ER-PM contacts. These data, together with a similar localisation pattern of the paralogs Lam1/3p, generated the speculation of the "LAM complex", populating a sub-class of ER-PM contacts important for sterol traffic (discussed below in Section 8.5).

8.2.3. Lam5/6p localisation at multiple internal contacts

The other two members of the yeast family, the paralogs Lam5p and Lam6p, did not target ER-PM contact sites, but localised at other internal contacts.

Their transmembrane domain is embedded into the ER, as shown both in Murley et al. (2015) and by their co-localisation with an ER marker (Figure 5.15). Data from this thesis and other published studies showed two clear localisations: (i) ER-mitochondrial contacts, with co-localisation of Lam6p and mitochondria, both at the confocal microscope with a GFP-tagged protein (Figure 5.15) and by protein-protein interactions with members of ERMES (Elbaz-Alon et al., 2015); and (ii) the nucleus vacuole junction (NVJ) (Figure 5.15 and Murley et al., 2015). The third observed localisation was typically peri-vacuolar and hence not easy to explain. Lam6p was found in a "similar distribution to Vps39p" (Elbaz-Alon et al., 2015), which localises to vCLAMPs (Elbaz-Alon et al., 2014; Hönscher et al., 2014). However, the TMD of Lam6p, and all LAM proteins in yeast, is ER-embedded, so it is not clear how the protein could be found on the vacuolar membrane next to vCLAMPs. The distribution of overexpressed Cherry-Lam6p and Lam6p-Cherry (Figure 2 from Elabz-Alon et al., 2015) is compatible with the presence of tubules of ER forming contacts with the vacuole, especially because GFP-Lam6p was only present together with ER elements (Figure 5.15). These new contacts between ER and vacuole are distinct from the NVJ and could also be populated by Vac8p (Murley et al., 2015), and other ER-resident proteins such as Mdm1p and Nvj3p (Henne et al., 2015b). Therefore, our group suggested naming them Vacuolar non-NVJ cytoplasmic ER (VancE) contacts (Wong and Levine, 2016). VancE and vCLAMPs could also populate strictly linked areas forming another three way contact between nuclear envelope, vacuole and mitochondria.

8.3. Function in sterol homeostasis

8.3.1. Lipid specificity

The bioinformatics prediction of the StART-like domains was tested *in vitro* using the recombinant soluble domains. The approach I used in this thesis to identify the lipid ligand had advantages and problems. Among the advantages, the donor compartment was made using semi-intact cells displaying the full availability of lipid molecules, and the radiolabelling with ^{14}C allowed a substantial increase of sensitivity. Thanks to the additional purification step using the His-tag of the protein on new Ni-NTA beads, it was possible to completely abolish the background, but on the negative side, the additional washing, elution, and desalting steps after exposure to the donor compartment could disrupt some relatively weak protein-lipid interactions. The desalting step was required because high salt concentrations can disturb the lipid extraction (Bligh and Dyer, 1959). However, the positive controls used in the experiments (PITPα, RdgBβ and Pdr16p) showed the full spectrum of lipid ligands (Figure 6.2). In this assay, the second StART domain of Lam4p showed cholesterol binding. Once the sterol affinity was identified, we visualised the domain-lipid interaction with FRET (Figure 6.5). The binding of all StART-like domains from Lam2/4p was studied by measuring the FRET signal from the protein tryptophans and DHE and resulted in a specific affinity with a k_d ~0.5 µM (Figure 8.1 A and B). Other sterols, such as cholesterol and ergosterol, could compete with DHE binding (Figure 8.1 C). Within these two experimental settings (Figure 6.2 and Figure 8.1), and in other *in vitro* experiments (Murley et al., 2015), no binding with other lipids was identified, but more testing is needed considering that StART domains show promiscuous lipid binding (Schrick et al., 2014) and other LTPs are capable of sterol and PI4P binding in counter-transport mechanisms (de Saint-Jean et al., 2011). The lipid ligand of other LAM proteins was determined indirectly looking at the rescuing abilities of AmB^S strains (Section 8.4).

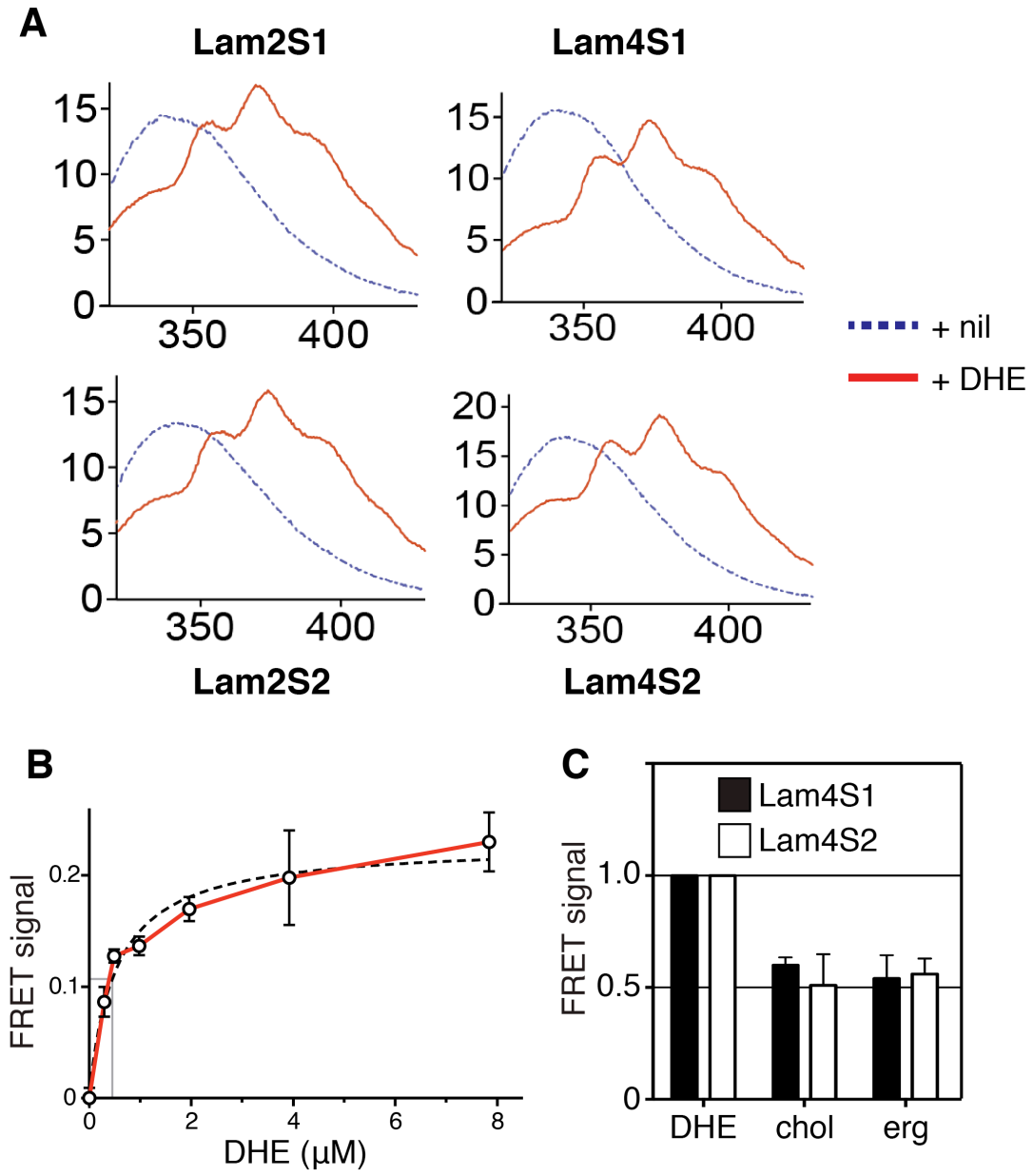

Figure 8.1 StART-like domains of Lam2/4p specifically bind sterols

(**A**) FRET between Lam2S1/S2 or Lam4S1/S2 and dehydroergosterol (DHE). Tryptophan fluorescence (excitation at 295 nm) with purified protein either on its own (nil) or in the presence of DHE presented in MβCD complexes. (**B**) Tryptophan-DHE FRET of 1 μM Lam4S2 incubated with increasing concentrations of liposomes containing 30% DHE at the final concentrations shown on the x axis. The best fitting binding curve (dashed line) indicates thatk k_d for DHE binding is ~0.5 μM. (**C**) Changes in DHE FRET signals upon competition with non-fluorescent sterols added at 1:1 ratio to Lam4p StART-like domains. Lipids added from methanol stock. All these experiments were performed by Louise Wong.

8.3.2. *In vitro* sterol transfer

Lam4S2 was also tested for *in vitro* transfer assays from donor to acceptor liposomes. *In vitro* it operates a fast, specific and passive transport of DHE between liposomes (Figure 8.2). The transfer rate was calculated as 15 times faster than the non specific and low affinity movement operated by MβCD with 2 DHE molecules moved per protein per second. The physiological in/out rate of sterol from the PM is ~30-60 10^3 molecules per second (Section 1.3). If all the sterol trafficked would be moved by Lam2p, considering its abundance (~1,000 molecules per cell), it should operate at a rate of at least 30 molecules protein^{-1} sec^{-1} (at least 15 times faster). The fast *in vitro* rate reported here can only be achieved by presenting the protein with anionic lipids on both donor and acceptor liposomes (Louise Wong, personal communication), possibly involved in an interaction with a polybasic region present between the StART-like domain and the transmembrane helix of all ER-PM localised yeast proteins, Lam1/2/3/4p, and the human LAMa/b/c (Wong and Levine, 2016). The localisation at MCSs could play an additional role: artificially anchoring the domains to both compartments, via protein-based tags (for example with a nickel-chelating lipid on one side, and a PI4P-specific PH domain on the other) or DNA-based zippers could speed up the sterol transfer rate even further (Moser von Filseck et al., 2015b; Xu et al., 2015; Mesmin et al., 2013). In fact, Lam4S2 *in vitro* transfer activity was faster than any other sterol-specific LTPs:

- StARD4 $\rightarrow$ 0.1 sec^{-1} (Mesmin et al., 2011)
- OSBP $\rightarrow$ 0.5 sec^{-1}, when tethered to donor and acceptor by PH + FFAT-VAP-A (Mesmin et al., 2013),
- Lam4S2 $\rightarrow$ 2 sec^{-1} (Louise Wong, personal communication).

Showing that LAM proteins are capable of transferring sterols fast enough, could prove that they are the long sought major sterol transfer proteins, alongside Osh proteins and vesicular transport, which account for a minor part (Georgiev et al., 2011) and it is too slow (see below, Section 8.3.3).

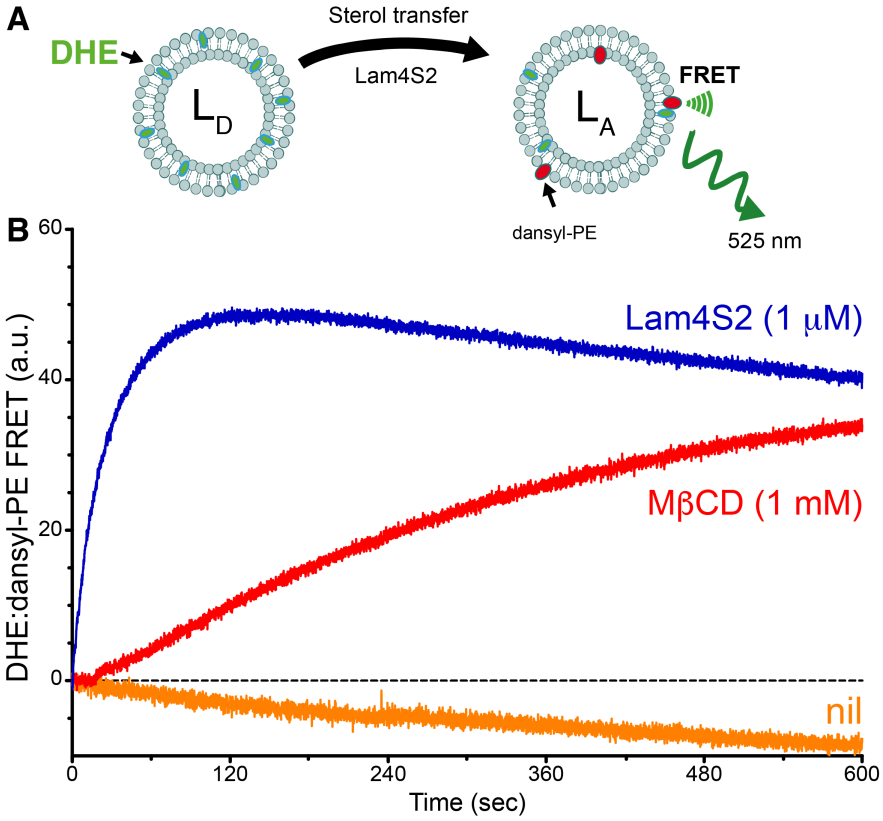

Figure 8.2 In vitro DHE transfer from donor to acceptor liposomes

(**A**) Transfer assays were set up with the FRET pair DHE and dansyl-PE. Donor liposome (L_D) contained 30% DHE and acceptor liposome (L_A) contained 3% dansyl-PE. (**B**) Initial take-off rate of 1 μM Lam4S2 is ~20 times the rate of MβCD, approximately moving 2 DHE molecules protein^{-1} sec^{-1}. The transfer experiments were optimised and performed by Louise Wong.

8.3.3. *In vivo* sterol transport

The majority of the sterol biosynthesis steps are localised in the ER, from this compartment the lipid is sent to all other membranes including the PM where is enriched to 30-40% of total lipids. Sterol moves in the cells in both directions, forward (from ER to PM) and backwards (PM to ER). We assayed single LAM deleted strains for differences in sterol traffic in both directions. The experimental setting consisted of a pulse with ^{3}H-methyl-methionine to radiolabel newly synthesised ergosterol, and chase at different time points (the first of which after 15 min) to measure radioactivity in subcellular fractions (Georgiev et al., 2011). Only *lam2*Δ was tested for forward transport, but it never changed (Anant Menon, personal communication). Probably the experimental setting did not allow the detection of any difference due to the time required for the first time point of the chase: during the first 15 minutes, the transport could be compensated by (i) minor activities of Osh proteins, (ii) vesicular traffic, and (iii) other LAM proteins. The readout of the retrograde transport experiment was the amount of DHE esterificatid in lipid droplets at a given time. First we verified that sterol uptake was not altered, and there were no differences in its distribution into the PM (no differences in its extractability), or in the activity of ACAT enzymes. Retrograde sterol traffic was reduced by 50% in strains lacking LAM1, LAM2 or LAM3 (Figure 8.3), at a similar rate of the simultaneous inactivation of all seven Osh proteins (Georgiev et al., 2011). These results showed the importance of LAM proteins for sterol traffic between ER and PM, but multiple interpretations are possible:

- LAM proteins work only for the retrograde transfer of sterol from PM to ER. Only a few asymmetric mechanisms have been described, but they involve the counter transport of two different lipids (Moser von Filseck et al., 2015b; a; Chung et al., 2015). However, no other lipids were identified in LAMs other than sterols.
- As already mentioned, the forward traffic assay could be intrinsically flawed to identify fast events such as sterol exchange between ER and PM. Especially because no negative controls were ever identified.

- Another possibility is that LAM proteins are indeed sterol-specific LTPs *in vitro*, but only indirectly affecting sterol traffic *in vivo*. For example, they could affect the size of different sterol pools (Das et al., 2014).

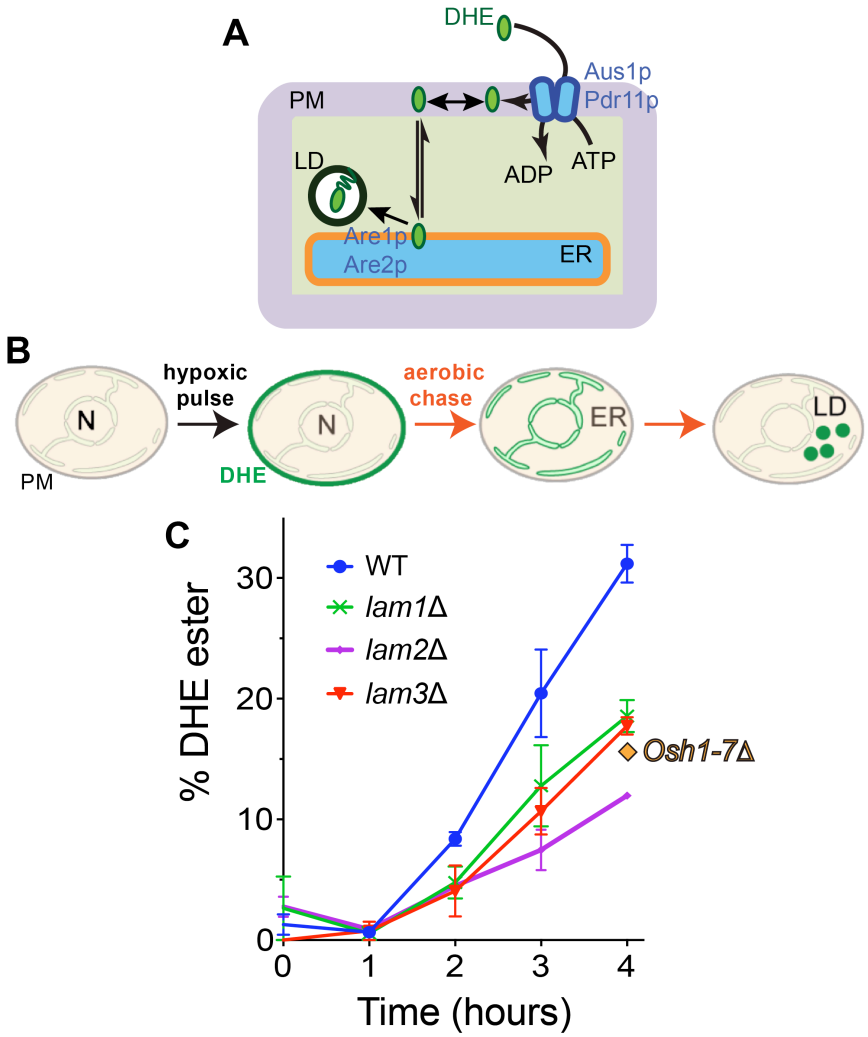

Figure 8.3 Retrograde sterol traffic is slower in strains lacking Lam1/2/3p

(**A**) Diagram of retrograde traffic pathway for exogenously supplied sterol. Steps include uptake into the PM by the ABC transporters Aus1p and Pdr11p, movement into different sterol pools at the PM, transfer by hypothetical LTPs from PM to ER through the cytosol (double arrows), esterification in the ER by ACAT enzymes Are1p and Are2p prior to storage in lipid droplets (LD). (**B**) DHE uptake into the PM was induced by exposing the strains to hypoxic conditions; reverting the cells to aerobic conditions resulted in transfer of DHE to the ER where it is esterified and stored in LD DHE ester formation was quantified by HPLC during redistribution of DHE away from the PM. (**C**) Retrograde traffic of DHE in four single delete strains of the yeast StART-like family were compared to wildtype controls and all OSH1-7 delete strains. All experiments were performed by Yves Sere and Diana Calderón-Noreña in Anant Menon laboratory (Weill Cornell University, New York, USA).

8.4. Understanding the amphotericin B phenotype

An indirect way to identify the lipid specificity is looking at the phenotype of some LAM deleted strains when exposed to the sterol sequestering antifungal drug Amphotericin (AmB). The knockout strains for Lam1/2/3p showed an increased sensitivity to AmB at sub-lethal doses (Section 6.3), with *lam1*Δ and *lam3*Δ being the most sensitive. The effects of AmB on the fungal cell are centred around its ergosterol-binding properties (Figure 1.7), but pleiotropic enough to render the resistant mutants highly susceptible to external stresses and almost non-pathogenic in the animal model (Vincent et al., 2013). In Figure 6.8, I highlighted also *scs2*Δ and *ymr102c*Δ. Scs2p is the yeast homologue of VAP, the main physical tether between ER and PM, suggesting an important role of this contact site for the increased AmB sensitivity, and consequently hinting at problems at ergosterol homeostasis. Ymr102p is an uncharacterised protein conserved throughout fungi (Davis et al., 2015). The single delete for YMR102c is the most sensitive strain to AmB over the whole yeast genome (Davis et al., 2015). There is no evidence about its interaction with LAM proteins, but it will be interesting to identify eventual relationships between the most AmB sensitive genes with the LAM genes.

The AmB phenotype could be rescued by the corresponding full length protein expressed at endogenous levels, but also by the soluble StART-like domain of any of Lam2/4/5/6p and of the human homologue hLAMb, although these domains had to be expressed at higher levels (*PHO5* promoter). This result was an indication that all these domains may have the same sterol specificity, conserved through species. Furthermore, this rescue was activated by anchoring the StART-like domains at ER-PM contacts with a linker long enough to reach both membranes across the 15 nm gap. Under these conditions, the domain rescued even off the endogenous *LAM2* promoter (Figure 5, Gatta et al., 2015). Thus, the sensitivity to AmB in LAM1/2/3 deleted strains could arise from the cell inability to compensate for the ergosterol extracted from the PM by the drug.

The AmB phenotype is a strong evidence for LAM involvement in ergosterol homeostasis, however one limitation of using this drug is related to its pleiotropic effects on the cell and the lack of a univocal mechanism of action. LAM function could be assessed *in vivo* by examining growth of deleted mutants or strains with overexpressed LAM proteins in other conditions: (i) other polyene antifungal drugs (such as nystatin), (ii) at different temperatures, (iii) exposing yeast cells to different carbon sources, (iv) exposure to poisonous drugs for specific steps in lipid biosynthesis, such as myriocin, a selective inhibitor of serine palmitoyltransferase (SPT), the first step in sphingosine biosynthesis.

8.4.1. Speculation on Lam1/3p lipid ligand

Lam1/3p StART-like domains did not rescue the phenotype, and this could be due to different reasons: (i) these two StART-like domains are longer than the rest of the family, and however I tried, in both yeast and bacterial expression they were not soluble on their own (Figure 6.6 and Figure 6.16); (ii) they could regulate Lam2p localisation (see Section 8.5), (iii) their lipid ligand is not ergosterol, but another lipid that influences ergosterol homeostasis indirectly.

Ultimately, we did not establish the molecular basis of increased AmB sensitivity in cells lacking the StART-like proteins. However, lipidomics revealed significantly lower complex sphingolipid levels for the two most sensitive strains, *lam1*Δ/*3*Δ (Figure 6.21); and the same results were obtained in an independent lipidomics experiment (Anant Menon, personal communication). Altering sphingolipid homeostasis can affect sterol traffic (Li and Prinz, 2004) and AmB sensitivity (Sharma et al., 2014; Bari et al., 2015), so one appealing possibility is that Lam1/3p are involved in intracellular sphingolipid traffic. Ceramide transfer protein (CERT) was discovered in a screening to complement the MβCD-sensitivity shown by the sphingomylin-deficient cell line LY-A, and no CERT homologues were ever identified in yeast (Hanada et al., 2003). These data, together with the fact that the sterol sponge model of AmB action has the same effect as MβCD treatment (Anderson et

al., 2014), and the low sphingolipid levels in LAM1/3 deleted strains (Figure 6.21), supports a sphingolipid affinity of the StART-like domain of Lam1/3p, but further characterisation will be required. Another possibility is that they could have a multiple lipid specificity (Section 1.7): to identify other lipid ligands, I am currently performing additional experiments to purify the TAP-tagged full-length Lam1p (Gavin et al., 2002; Maeda et al., 2013) with different combination of detergents to identify its lipid interactors using HPTLC and lipidomics.

8.5. Speculation on the LAM super-complex

LAM proteins have transmembrane helices that anchor them into ER membrane and all six yeast members target contact sites. Lam5/6p at multiple inner contact sites of the ER with mitochondria, VancE and NVJ, and Lam1-4p between ER and PM. These target a unique type of ER-PM contacts because they were independent from other known tethers and because they localised in a punctate distribution at the periphery of the cell. Wild-type cells co-expressing Tcb2-GFP and RFP-Lam2CT were also tested for co-localisation (Figure 3 – Figure Supplement 6 in Gatta et al., 2015): ~33% of Lam2CT positive puncta also contained Tcb2-GFP; and the proportion of the periphery overall that contained Tcb2-GFP was ≥25%, so the co-localisation between the two proteins was not significant (Gatta et al., 2015). The co-localisation of Lam2p with Lam4p and with Lam3p (Figure 5.13) suggest they they may target peripheral puncta in a complex. Furthermore, despite the different expression levels, Lam3p seemed to guide Lam2/4p localisation: (i) GFP-Lam3p overexpression resulted in its localisation redirected towards the internal and nuclear ER that misguided also RFP-Lam2p; (ii) the lack of LAM3 resulted in reduced levels of both Lam2/4p paralogs (Figure 5.14). We speculate that all four proteins target the same LAM super-complex, although the different expression levels suggest a non stoichiometric interaction, and other components are not known. Further studies will be required, especially to understand if other players are contributing to LAM localisation and/or

activation. Furthermore, they could also have a tethering role. Rapid over-expression of Lam2p did not increase the amount of cER found close to the PM (Matt Hayes and Tim Levine, personal communication), but I proved that the simultaneous deletion of LAM1, LAM2 and LAM3 significantly reduced the percentage of PM in contact with cER (Figure 6.18).

Lam1-4p super-complex could be a lipid transfer hub at ER-PM contacts involved in sterol homeostasis. Its regulation could depend on Slm1/2p dynamic partition from eisosomes to TORC2 membrane domain compartments upon stress conditions, such as disruption of membrane lipid homeostasis or mechanical insult (Berchtold et al., 2012; Niles and Powers, 2012). In turn, TORC2-mediated activation of Ypk1p could result in phosphorylation of Lam2p on one of its three predicted Ypk1p phosphorylation sites (Muir et al., 2015). Indeed, Lam2p was previously identified as a Slm1p interactor in a yeast two-hybrid high HT screening (Uetz et al., 2000). These studies support a role of LAM super-complex in the TORC2-mediated response to cellular stress that requires changes in membrane lipid composition. Future experiments should address the LAM super-complex interactome and its role in response to disruption of lipid homeostasis, and AmB-mediated sterol extraction. Membrane stress activates TORC2 also in mammalian cells (Kippenberger et al., 2005), it is possible that the human LAMs could be phosphorylation targets for TORC2-mediated cell responses to disruption of membrane lipid homeostasis.

8.5.1. LAM proteins regulation

Understanding the super-complex composition would also give new insights into the regulation of LAM activity. In Lam2p sequence, for example, there are multiple phosphorylation sites. As hypothesised in the previous paragraph, Ypk1 can target three sites in Lam2p, thus potentially causing activation or inactivation of its lipid transfer domains. In a similar way, it is possible that other sites could be modified by kinases/phosphatases for a fine modulation of LAM localisation and/or lipid transfer activity.

8.6. Structural studies

The structural experiments using NMR spectroscopy gave the first confirmation of Lam4S2 homology model by showing only specific peaks shifting position upon sterol binding. The behaviour of the two peaks corresponding to the amide proton of tryptophans side chains could be a strong evidence supporting the homology model: one tryptophan, facing outside the binding pocket, did not move; while the peaks corresponding to the tryptophan inside the binding pocket did shift upon cholesterol binding (Figure 7.7). The final confirmation will be obtained when all the protein peaks will be assigned. Although different strategies for peak assignment were attempted, the completion of this process in still ongoing: the signals of peaks corresponding to the predicted β-sheet of the helix grip domain were masked in the noise for the most sensitive acquisitions. This ambiguity could be consequence of domain-domain interactions. Lam4S2 did not form dimers in solution as shown in Coomassie gel (Figure 6.1) and as tested by high pressure liquid chromatography (HPLC) (Anastasia Zhuravleva, personal communication). However, both Lam2p and Lam4p have two conserved StART-like domains in their sequence, and in the proteins they could act weak and transient interactions for co-regulatory purposes. Next, we will try to obtain structural data from a construct including both StART-like domains.

Anyway, unpublished data showed that Lam2S1 crystal structure is highly similar to the predicted homology model: the crystal was obtained both for the apo and for sterol-bound form and showed minor structural changes only for an unstructured loop involved in the binding (Karin Reinisch, personal communication). NMR is more useful than crystallography to study dynamic structural changes such as lipid binding, when the full Lam4S2 peak assignment will be available, it will be possible to identify the shift (Δppm) for each of the residues involved not only in the binding, but in the dynamic process of lipid loading/exchange with the donor. The donor, i.e. how to present the ligand to the protein in solution is another issue that can be optimised: in the experiment I presented, sterol was added in solution using

MβCD complexes (Figure 7.7), but cyclodextrin has an important affinity for sterol that could unbalance the sterol exchange process. Liposomes containing sterols could be a valid alternative both to study sterol binding dynamics, and the role of the polybasic region for membrane interaction and/or sterol loading (see Section 8.3.2).

8.7. Human LAM proteins

The physiological role of human LAM proteins remains to be fully elucidated. The locus of hLAMb is strongly linked to chronic lymphocytic leukaemia (Di Bernardo et al., 2008), and the protein is involved in chemoresistance in ovarian cancer (Wu et al., 2014). While hLAMa/c are poorly expressed in all human tissues, hLAMb has a tissue-specific enrichment in the brain and in steroidogenic cells, both at transcript and protein level (data mined from Uhlén *et al.*, 2015).

The strong evidence I obtained, when the StART-like domain of hLAMa successfully rescued the AmB phenotype of sensitive LAM deleted strains, indicates a sterol-specific activity conserved from yeast to humans. I have presented data to prove a role of yeast LAM proteins in sterol trafficking between the ER and the PM, so also the human homologues are promising candidates for further studies into intracellular sterol traffic in mammalian cells. hLAMb involvement in some pathogenic processes could be explained by recent evidence that genes involved in cholesterol biosynthesis, metabolism and trafficking have indeed been implied in various disorders from atherosclerosis to cancer (Goldstein and Brown, 2015; Mohankumar et al., 2015).

APPENDICES

Appendix 1. NMR spectra magnetisation

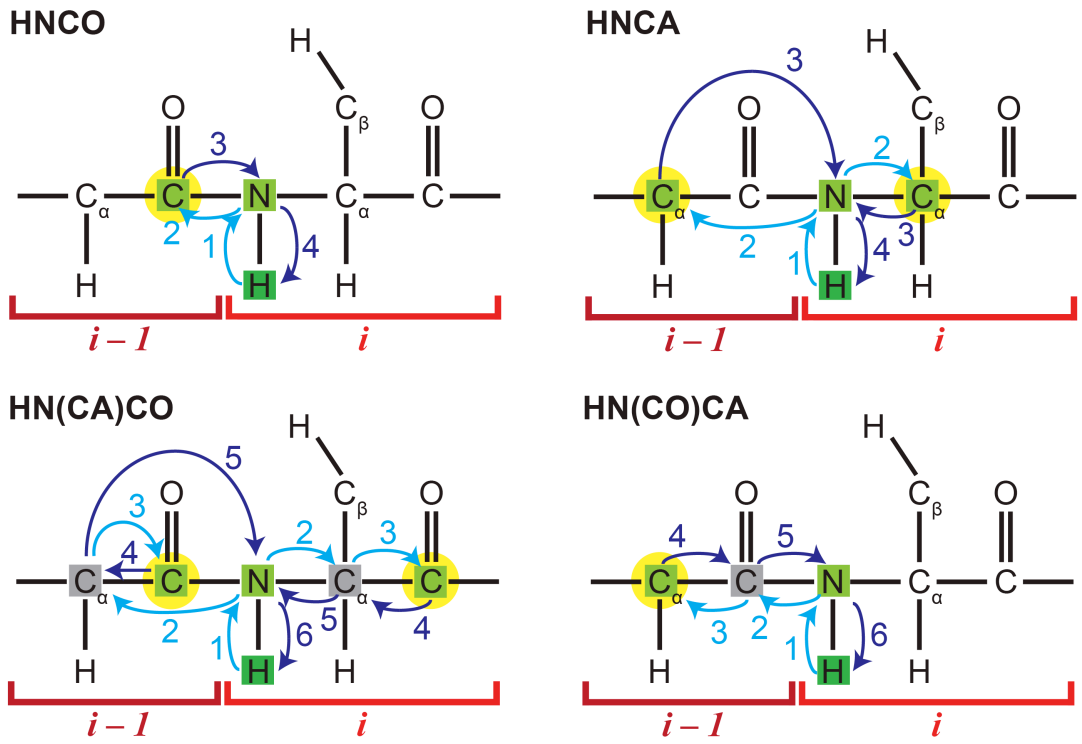

Schematic representation of the ^{1}H-^{13}C-^{15}N correlation of HNCO, HNCA, HN(CA)CO, and HN(CO)CA triple resonance experiments. These experiments are also defined as 'out-and-back' because the magnetisation starts from the $^{1}H_N$, evolves along the different nuclei couplings (light blue arrows), and is transferred back the same way (blue arrows). Starting and ending nucleus is always $^{1}H_N$ (dark green), the chemical shift of some nuclei is evolved (light green), others are involved in the magnetisation, but their chemical shift is not measured (grey). The HNCO experiment correlates $^{1}H^{N}$ -^{15}N of residue i with CO of residue $i-1$. HNCA correlates $^{1}H_N$ -^{15}N of residue i with Cα of both residues i and $i-1$. HN(CA)CO correlates the $^{1}H_N$ -^{15}N of residues i with CO of both residues i and $i-1$ via magnetisation transfer from $^{1}H_N$ -^{15}N of i to Cα of both residue and subsequent transfer to CO(i) and CO($i-1$). HN(CO)CA correlates $^{1}H_N$ -^{15}N of residue i with Cα of only residue $i-1$ because of the transfer via the CO of $i-1$ (at 15 Hz). Yellow circles correspond to the ^{13}C chemical shift peaks visible for each experiments. See also Figure 1.8.

Appendix 2. A new family of StART-like domains in all eukaryotes

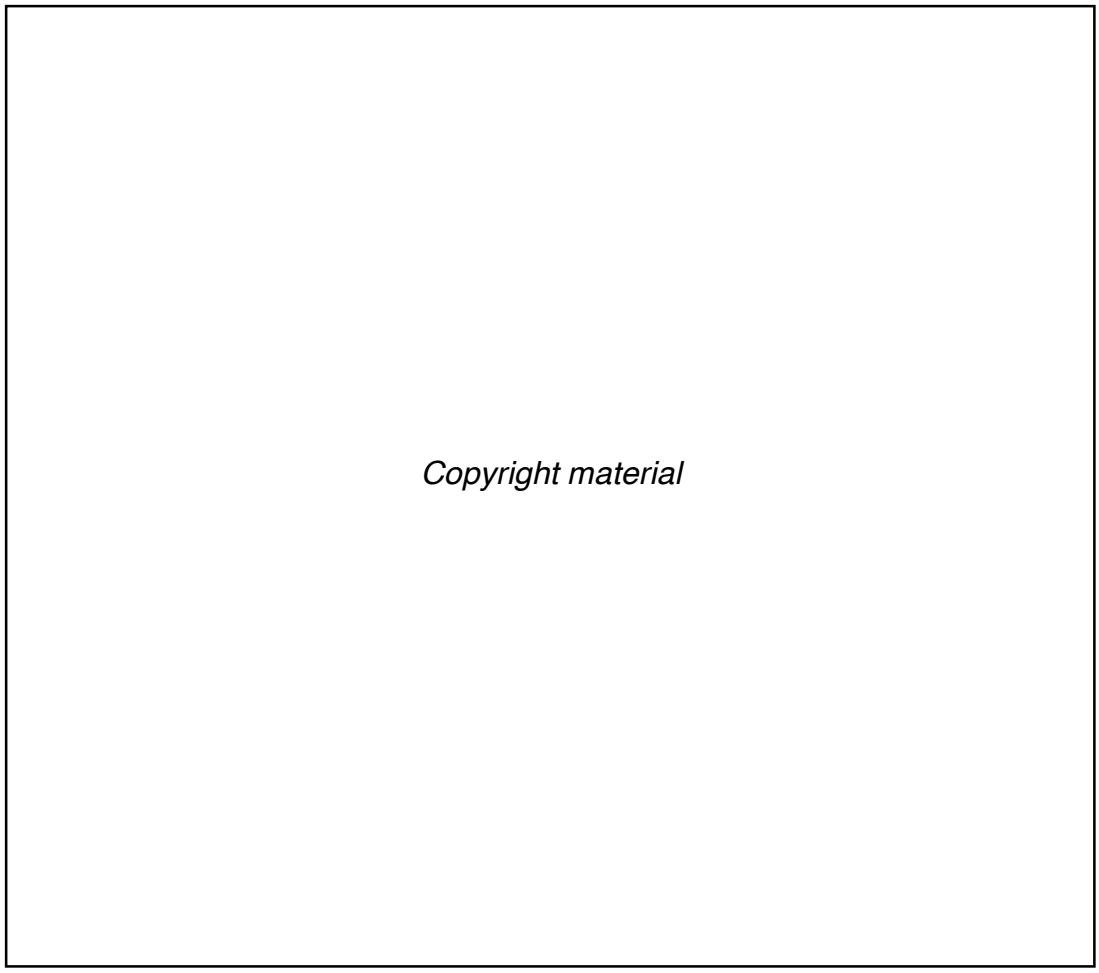

The unrooted phylogenetic tree of 143 highly diverse StART-like sequences (redundancy was reduced using a non-redundancy filter PISCES at dunbrack.fccc.edu) was inferred by PHYML at trex.uqam.ca (Guindon and Gascuel, 2003). The branches show species and Uniprot accession numbers. 10 sequence groups are bracketed (red) to show the mixture of taxa in different parts of the tree. Four parts of the tree include yeast or human sequences discussed in this thesis (black background), showing that Lam1p/Ysp1p and Lam3p/Sip3p are more distant from Ysp2p/Lam4-6p than are human LAMs, GramD1a/b/c. This figure appears as Figure 1-Figure supplement 1 in Gatta et al., 2015 and it was made by Tim Levine.

Appendix 3. Lam4p peak assignment from NMR experiments

A	B	#	aa	Peak	CA	CAm1	CB	CBa	CBb	CBm1	CBm1a	CBm1b	CO	COm1	H	N
	C	1	M													
	C	2	G	PR027	41.98	57.72	-	-	-	-	-	-	172.3	178.7	8.23	112.5
	C	3	G	PR007	41.77	42.06	-	-	-	-	-	-	171.5	172.3	8.38	109.1
	C	4	S	PR081	55.06	41.73	-	-	-	-	-	-	-	171.5	8.24	115.9
	C	5	H													
	C	6	H													
	C	7	H													
	C	8	H													
	C	9	H													
	C	10	H													
	C	11	G	R009	41.96	53.33	-	-	-	27.14	-	-	171.4	173.2	8.39	110.5
	C	12	M	PR130	52.1	41.96	29.14	-	-	-	-	-	173.4	171.4	8.22	120.4
	C	13	A	PR188	49.32	52.11	15.32	-	-	29.15	-	-	175	173.4	8.36	125.3
	C	14	S	PR068a	55.17	49.32	60.13	-	-	15.32	-	-	171.6	175	8.2	114.9
	C	15	H													
	C	16	H													
	C	17	H													
	C	18	H													
	C	19	H	PR150	53	53.24	27.26	-	-	27.31	-	-	172.3	172.5	8.13	121.4
	C	20	A	PR187	49.2	52.97	27.34	-	-	27.34	-	-	174.8	172.3	8.242	125.3
	C	21	R	PR134	52.59	49.2	15.39	-	-	15.39	-	-	173.2	174.8	8.279	120.7
	C	22	A	PR189	49.03	52.62	27.04	-	-	27.04	-	-	174.6	173.2	8.286	125.4
	C	23	M	PR132	52	49.02	15.47	-	-	15.47	-	-	173	174.7	8.37	120.5
C	C	24	T	PR091	57.94	52.01	29.46	-	-	29.46	-	-	171.4	173	8.12	116.7
C	C	25	L	PR181	49.39	57.99	66.62	-	-	66.62	-	-	171.9	171.4	8.45	124.6
C	C	26	P													
C	C	27	K	PR109	51.78	59.03	32.66	-	-	29.24	-	-	172.7	172	8.47	118.1
C	C	28	M	PR094	52.06	51.8	33.95	-	-	32.67	-	-	170.4	172.7	8.16	116.9
C	C	29	E	PR122	50.5	52.1	26.5	-	-	33.95	-	-	171.7	170.4	8.15	119.3
C	C	30	P													
C	C	31	S													
C	C	32	S	PR066	53.1	56.48	-	61.79	62.32	60.83	60.46	61.1	169.5	169.9	7.32	114.8
C	C	33	H	PR165	53.26	53.13	-	-	-	-	-	-	168.4	169.5	7.53	122.5
C	C	34	A	PR194	48	53.3	13.96	-	-	25.42	-	-	172	168	7.83	126.1
C	C	35	P													
C	C	36	T	PR077b	56.21	60.75	69.49	-	-	28.41	-	-	169.7	173.8	9.09	115.5
C	C	37	E	PR084	49.23	56.24	27.83	-	-	69.48	-	-	170.4	169.7	8.16	116
C	C	38	P													
C	C	39	D	PR125	49.56	57.91	36.03	-	-	27.23	-	-	171.2	171.6	5.77	119.4
C	C	40	I	PR178	57.78	49.56	34.4	-	-	36.03	-	-	172.7	171.2	7.39	124.5
C	C	41	Q	PR199	51.32	57.81	24.89	-	-	34.39	-	-	172	172.7	8.38	128.1
C	C	42	K	PR177	52.62	51.32	29.59	-	-	24.89	-	-	172.8	172	8.41	124.4
C	C	43	D	PR197	49.75	52.64	39.82	-	-	29.6	-	-	174.8	172.8	9.32	127
C	C	44	K	PR162	55.62	49.76	28.19	-	-	39.82	-	-	174	174.8	8.64	122.5
C	C	45	D	PR106	51.31	55.64	37.44	-	-	28.19	-	-	172.8	174	8.57	117.5
C	C	46	D	PR154	51.62	51.34	39.1	-	-	37.45	-	-	174.3	172.8	7.45	121.5
C	C	47	S	PR092	54.78	51.64	-	61.31	61.82	39.11	-	-	170.7	174.3	9.02	116.7
C	E	48	I	PR195	58.65	54.81	33.32	-	-	-	61.36	61.8	173.2	170.7	9.02	126.4
C	E	49	I	PR201	57.84	58.69	33.1	-	-	33.33	-	-	173.4	173.2	8.67	128.4
C	E	50	R	PR089	50.12	57.9	31.61	-	-	32.85	-	-	171.3	173.4	7.39	116.2
C	E	51	E	PR146	51.31	50.11	28.83	-	-	31.62	-	-	170.7	171.4	9.39	121.5
C	C	52	N													
C	E	53	E													
C	E	54	N													
C	E	55	I													
C	E	56	P													
C	C	57	A													
C	C	58	P													
H	H	59	L													
H	H	60	G													
H	H	61	T													
H	H	62	V													
H	H	63	V													
H	H	64	Q													
H	H	65	L													
C	H	66	L													
C	C	67	F													
C	C	68	G	PR001	44.08	53.95	-	-	-	37.47	-	-	173.3	174.7	8.84	104.2
C	C	69	S	PR103	62.8	44.07	65.64	-	-	-	-	-	171.8	173.3	6.98	117.3
C	C	70	N													
H	C	71	T	PR114	58.4	48.58	64.84	-	-	33.11	-	-	171.6	174.5	8.54	118.6
H	H	72	E	PR139b	54.98	58.46	25.36	-	-	64.82	-	-	175	171.6	8.05	121
H	H	73	Y	PR097	57.06	55	32	-	-	25.36	-	-	175	1	6.28	117
H	H	74	M	PR121	53.83	57.08	27.82	-	-	31.98	-	-	-	175	8.2	119.1
H	H	75	Q	PR123	56.78	53.84	24.57	-	-	27.79	-	-	175.3	175	7.69	119.3
H	H	76	K	PR119	54.9	56.81	27.94	-	-	24.55	-	-	176.2	175.3	7.64	118.8
H	H	77	V	PR137	63.45	54.92	27.23	-	-	27.95	-	-	174.6	176.2	7.73	120.9
H	H	78	I	PR104	60.99	63.48	34.38	-	-	27.24	-	-	176.6	174.6	7.42	117.5
H	H	79	T	PR005	59.8	61.01	65.76	-	-	34.4	-	-	172.8	176.6	8.02	107.7
H	H	80	R	PR175	54.41	59.83	25.46	-	-	65.75	-	-	173.6	172.8	7.37	124.1
H	H	81	D	PR063	48.95	54.43	37.49	-	-	25.44	-	-	173.5	173.6	6.27	114.7
C	C	82	K	PR184	53.85	48.94	27.3	-	-	37.49	-	-	174.4	173.5	8.15	125

C	C	83	N	PR090	50.93	53.87	34.93	-	-	27.31	-	-	171.2	174.4	8.57	116.4
C	C	84	N	PR136	48.42	50.93	34.17	-	-	34.88	-	-	171	171.2	7.98	120.9
E	C	85	V	PR087	55.42	48.41	32.21	-	-	34.19	-	-	171.5	171	9.27	116.1
E	C	86	N	PR099a	50.61	55.45	33.87	-	-	32.19	-	-	171.7	171.5	8.68	117.1
E	C	87	V													
E	E	88	E													
E	E	89	T													
C	C	90	I													
C	C	91	P													
C	C	92	K	PR088b	52.22	59.08	-	-	-	29.31	-	-	174.1	172.4	7.92	116.4
C	C	93	F	PR111	57.9	52.24	36.21	-	-	29.41	-	-	173.2	174.1	9.07	118.4
C	C	94	T	PR041	54.95	57.94	7.09	-	-	36.22	-	-	171	173.2	8.83	113.6
C	C	95	P													
C	C	96	S	PR018	53.67	61.49	58.82	-	-	30.22	-	-	169.4	173.2	7.3	111.9
C	C	97	L	PR153	50.99	53.67	35.69	-	-	-	58.81	59.27	169.7	169.3	8	121.5
C	C	98	V	PR144	55.54	50.97	32.21	-	-	35.67	-	-	171	169.7	7.26	121.1
C	C	99	E	PR168	55.69	55.59	25.13	-	-	32.22	-	-	174	171	8.51	123.1
C	C	100	G	PR264b	41.39	55.76	-	-	-	25.16	-	-	-	-	9	114.9
C	C	101	G	PR010	41.79	41.37	-	-	-	-	-	-	169.7	172.7	8.9	110.9
E	E	102	S	PR077a	54.35	41.78	-	63.8	64.32	-	-	-	170.7	169.7	9.11	115.4
E	E	103	R	PR062	51.82	54.39	30.2	-	-	63.77	-	-	169.8	170.8	8.72	114.7
E	E	104	H	PR101	51	51.76	28.75	-	-	30.22	-	-	170.2	-	8.46	117.2
E	E	105	Y													
E	E	106	E													
E	E	107	Y													
E	E	108	T	PR099b	59.16	53.44	67.31	-	-	36.16	-	-	168	169.9	8.68	117.2
E	E	109	K	PR200	50.72	59.21	31.93	-	-	67.28	-	-	173.4	168.1	9.2	128.2
E	E	110	K	PR198	53.7	50.7	28.49	-	-	31.92	-	-	172.5	173.4	9.56	127.3
C	C	111	L	PR159	50.15	53.73	39.69	-	-	28.47	-	-	173.6	172.5	7.9	122
C	C	112	N	PR127	49.38	50.15	35.3	-	-	39.66	-	-	171.7	173.6	8.52	119.7
C	C	113	N	PR112	49.3	49.37	36.38	-	-	35.3	-	-	172.7	171.7	7.91	118.3
C	C	114	S													
C	C	115	I	PR124	56.96	56.56	36.23	-	-	-	59.98	60.47	173	171.3	7.59	119.3
C	C	116	G	PR024	40.74	56.99	-	-	-	36.22	-	-	168.6	173	8.4	112.2
C	C	117	P													
C	C	118	K													
E	E	119	Q	PR203	52.57	59	27.1	-	-	27.16	-	-	172.4	173.6	8.15	129.2
E	E	120	T	PR078	60.4	52.59	65.91	-	-	27.11	-	-	171.5	172.4	8.03	115.3
E	E	121	K	PR209	54.5	60.46	33.92	-	-	65.92	-	-	-	171.5	8.56	132.3
E	E	122	C													
E	E	123	L													
E	E	124	L													
E	E	125	T													
E	E	126	E													
E	E	127	S													
E	E	128	I													
E	E	129	E													
E	E	130	H													
E	E	131	M													
C	C	132	D													
C	C	133	I													
C	C	134	N													
C	C	135	N													
E	E	136	Y													
E	E	137	V													
E	E	138	L													
E	E	139	V													
E	E	140	T													
E	E	141	Q													
E	E	142	T													
E	E	143	T	PR167	59.04	58.2	-	-	-	-	-	-	171.6	172.2	9.47	123
E	E	144	K	PR202	51.69	59.08	31.68	-	-	67	-	-	172	171.6	9.1	128.9
C	C	145	T	PR038	51.57	51.72	66.92	-	-	31.7	-	-	172.4	172	9.33	113.3
C	C	146	P													
C	C	147	D	PR035	52.3	60.73	38.1	-	-	29.02	-	-	173.6	173.7	7.22	112.9
C	C	148	V	PR014	56.3	52.31	25.73	-	-	38.07	-	-	171.2	173.6	6.69	111.1
C	C	149	P													
C	C	150	S	PR264a	58.17	61.33	60.34	-	-	27.68	-	-	-	-	9.02	114.8
C	C	151	G	PR004	44.17	58.2	-	-	-	60.6	-	-	172.7	173.3	8.75	107.5
C	C	152	S	PR050	56.44	44.16	59.64	-	-	60.14	-	-	172.7	172.7	8.44	113.8
C	C	153	N	PR100	50.45	56.49	36.88	-	-	-	-	-	170.3	172.5	8.41	117.1
E	E	154	F	PR043a	51.71	50.44	36.98	-	-	36.88	-	-	170.1	170.3	6.76	113.6
E	E	155	A	PR148	47.46	51.72	19.06	-	-	36.98	-	-	172.1	170.1	8.21	121.6
E	E	156	V	PR166	51.32	47.48	29.34	-	-	19.06	-	-	172.3	172.7	8.42	122.6
E	E	157	E													
E	E	158	S													
E	E	159	K													
E	E	160	I													
E	E	161	F													
E	E	162	L													
E	E	163	F													
E	E	164	W													
C	C	165	G	PR015	39.54	55.75	-	-	-	-	-	-	170.8	175.5	9	111.8
C	C	166	Q	PR102	52.59	39.5	25.66	-	-	-	-	-	174.1	170.8	8.54	117.3
C	C	167	H	PR128	53.11	52.6	23.7	-	-	25.65	-	-	171.2	174.1	9.09	119.9
C	C	168	D	PR056	52.93	53.14	35.81	-	-	23.76	-	-	172.6	171.2	9.74	114.2
C	C	169	T													
E	C	170	T													
E	E	171	N													
E	E	172	M													

E	E	173	T													
E	E	174	V													
E	E	175	I													
E	E	176	T	PR185	59.32	55.79	69.08	-	-	37.28	-	-	169.4	172.2	9.26	125.1
E	E	177	K	PR190a	51.65	59.4	32.04	-	-	69.05	-	-	170.2	169.5	9.14	125.6
E	E	178	I	PR161	57.16	51.64	34.12	-	-	32.06	-	-	171.8	170.2	8.81	122.4
E	E	179	N	PR186	48.41	57.19	36.35	-	-	34.12	-	-	172.1	171.8	8.63	125.1
E	E	180	W	PR193	53.47	48.4	27.66	-	-	36.36	-	-	175.3	172.1	9.08	126.1
E	C	181	T	PR067	59.25	53.5	65.46	-	-	-	-	-	175.3	175.3	9.11	115
C	C	182	S													
C	C	183	K													
C	C	184	S													
E	C	185	F													
E	H	186	L													
E	H	187	K													
C	H	188	G													
H	H	189	A													
H	H	190	I													
H	H	191	E													
C	C	192	K	PR118	56.24	57.75	28.65	-	-	24.77	-	-	177	175.1	7.93	118.8
C	C	193	G	PR002	43.48	56.26	-	-	-	28.64	-	-	174.7	177	8.08	105.1
C	H	194	S	PR129	59.22	43.46	-	-	-	-	-	-	-	174.7	8.44	119.9
H	H	195	V	PR179	64.37	59.24	27.89	-	-	-	-	-	175.1	174	8.16	124.3
H	H	196	E	PR115	56.08	64.41	25.08	-	-	27.89	-	-	177.1	175.1	7.85	118.6
H	H	197	G	PR003	43.52	56.09	-	-	-	25.08	-	-	174.3	177.1	8.31	106.3
H	H	198	Q	PR156	54.28	43.52	24.73	-	-	-	-	-	174.8	174.3	8.02	121.7
H	H	199	K	PR140	57.66	54.28	28.52	-	-	24.73	-	-	174.5	174.8	7.87	121
H	H	200	V	PR105	62.58	57.69	-	-	-	28.55	-	-	175.9	174.5	7.24	117.5
H	H	201	S	PR256	58.66	62.61	-	59.42	59.92	28.51	-	-	175.9	175.9	7.88	114.5
H	H	202	V	PR169	62.93	58.73	27.41	-	-	-	-	-	174.6	174.9	8.9	123.2
H	H	203	D													
H	H	204	Y	PR151	58.2	54.58	34.24	-	-	35.37	-	-	175	178.1	8.09	121.5
H	H	205	M	PR139a	56.45	58.23	29.4	-	-	34.28	-	-	174.7	175	8.09	120.9
H	H	206	L	PR120	54.77	56.41	38.28	-	-	29.34	-	-	176.1	174.7	8.88	118.9
H	H	207	S	PR057	58.62	54.72	-	59.07	59.54	38.25	-	-	176.2	176.2	8.27	114.4
H	H	208	E				-									
H	H	209	L													
H	H	210	R													
H	H	211	D	PR163	54.31	56.79	37.49	-	-	25.44	-	-	175.3	176.3	8.13	122.4
H	H	212	I	PR157	62.14	54.3	34.7	-	-	37.48	-	-	176.3	175.3	8.76	122
H	H	213	I	PR113	61.16	62.17	33.92	-	-	34.66	-	-	175.2	176.3	7.71	118.4
H	H	214	S	PR080	58.19	61.17	-	59.29	59.77	33.94	-	-	175.2	175.2	8.06	115.5
H	H	215	R	PR142	55.51	58.22	-	-	-	59.63	-	-	175.4	175	8.29	121.1
C	C	216	A	PR143	50.22	55.51	15.07	-	-	26.63	-	-	175.7	175.5	7.52	121.2
C	C	217	K	PR108	53.6	50.21	29.08	-	-	15.08	-	-	174.1	175.7	7.63	118
C	C	218	S	PR088a	55.48	53.61	-	60.27	60.78	29.07	-	-	171.6	174.1	7.92	116.2
C	C	219	K	PR170	52.65	55.52	-	-	-	-	-	-	173.5	171.6	8.23	123.6
C	C	220	K	PR182	50.89	52.65	28.52	-	-	29.03	-	-	171.6	173.5	8.27	124.6
C	C	221	P													
C	C	222	V													
C	C	223	K													
C	C	224	K													
C	C	225	V													
C	C	226	M													
C	C	227	K													
C	C	228	S													
C	C	229	H													
C	C	230	D													
C	C	231	K													
C	C	232	H													
C	C	233	R													
	C	234	D													
	C	235	V													

This table shows the details of the partial assignment of Lam4S2 at NMR acquisitions. The table lists the predicted secondary structure according to PSI-PRED 3.3 considering only the recombinant domain (A) or the domain in the full length protein (B); residue number from N- to C-terminus (#), residue (aa), peak reference (Peak, PR) chosen by CcpNMR; chemical shifts of Cα (CA, CAm1), Cβ (CB, CBa, CBm1, CBm1a, CBm1b), CO (CO, COm1), H_N and N. Residues are colour-coded according to their chemical properties. This table was made by Andrea Sauerwein in Steve Matthews lab (Imperial College London).

REFERENCES

Abbott, K.L., R.T. Matthews, and M. Pierce. 2008. Receptor tyrosine phosphatase beta (RPTPbeta) activity and signaling are attenuated by glycosylation and subsequent cell surface galectin-1 binding. *J. Biol. Chem.* 283:33026–33035. doi:10.1074/jbc.M803646200.

Aguilar, P.S., A.M. Hernandez-Arriaga, L.E. Cybulski, A.C. Erazo, and D. de Mendoza. 2001. Molecular basis of thermosensing: a two-component signal transduction thermometer in Bacillus subtilis. *EMBO J.* 20:1681–1691. doi:10.1093/emboj/20.7.1681.

Aguilar, P.S., and D. de Mendoza. 2006. Control of fatty acid desaturation: a mechanism conserved from bacteria to humans. *Mol. Microbiol.* 62:1507–1514. doi:10.1111/j.1365-2958.2006.05484.x.

AhYoung, A.P., J. Jiang, J. Zhang, X. Khoi Dang, J.A. Loo, Z.H. Zhou, and P.F. Egea. 2015. Conserved SMP domains of the ERMES complex bind phospholipids and mediate tether assembly. *Proc. Natl. Acad. Sci. U.S.A.* 112:E3179–88. doi:10.1073/pnas.1422363112.

Alkhaja, A.K., D.C. Jans, M. Nikolov, M. Vukotic, O. Lytovchenko, F. Ludewig, W. Schliebs, D. Riedel, H. Urlaub, S. Jakobs, and M. Deckers. 2012. MINOS1 is a conserved component of mitofilin complexes and required for mitochondrial function and cristae organization. *Mol. Biol. Cell.* 23:247–257. doi:10.1091/mbc.E11-09-0774.

Alpy, F., A. Rousseau, Y. Schwab, F. Legueux, I. Stoll, C. Wendling, C. Spiegelhalter, P. Kessler, C. Mathelin, M.C. Rio, T.P. Levine, and C. Tomasetto. 2013. STARD3 or STARD3NL and VAP form a novel molecular tether between late endosomes and the ER. *Journal of Cell Science*. 126:5500–5512. doi:10.1242/jcs.139295.

Alpy, F., and C. Tomasetto. 2014. START ships lipids across interorganelle space. *Biochimie*. 96:85–95. doi:10.1016/j.biochi.2013.09.015.

Altschul, S.F., T.L. Madden, A.A. Schäffer, J. Zhang, Z. Zhang, W. Miller, and D.J. Lipman. 1997. Gapped BLAST and PSI-BLAST: a new generation of protein database search programs. *Nucleic Acids Res.* 25:3389–3402.

Anderson, T.M., M.C. Clay, A.G. Cioffi, K.A. Diaz, G.S. Hisao, M.D. Tuttle, A.J. Nieuwkoop, G. Comellas, N. Maryum, S. Wang, B.E. Uno, E.L. Wildeman, T. Gonen, C.M. Rienstra, and M.D. Burke. 2014. Amphotericin forms an extramembranous and fungicidal sterol sponge. *Nat. Chem. Biol.* 10:400–406. doi:10.1038/nchembio.1496.

Andreoli, T.E., and M. Monahan. 1968. The interaction of polyene antibiotics with thin lipid membranes. *J. Gen. Physiol.* 52:300–325.

Andreyev, A.Y., E. Fahy, Z. Guan, S. Kelly, X. Li, J.G. McDonald, S. Milne, D. Myers, H. Park, A. Ryan, B.M. Thompson, E. Wang, Y. Zhao, H.A. Brown, A.H. Merrill, C.R.H. Raetz, D.W. Russell, S. Subramaniam, and E.A. Dennis. 2010. Subcellular organelle lipidomics in TLR-4-activated macrophages. *J. Lipid Res.* 51:2785–2797. doi:10.1194/jlr.M008748.

Bai, J., and R.E. Pagano. 1997. Measurement of spontaneous transfer and transbilayer movement of BODIPY-labeled lipids in lipid vesicles. *Biochemistry*. 36:8840–8848. doi:10.1021/bi970145r.

Baldwin, T.A., and H.L. Ostergaard. 2002. The protein-tyrosine phosphatase CD45 reaches the cell surface via golgi-dependent and -independent pathways. *J. Biol. Chem.* 277:50333–50340. doi:10.1074/jbc.M209075200.

Balla, T. 2013. Phosphoinositides: tiny lipids with giant impact on cell regulation. *Physiol. Rev.* 93:1019–1137. doi:10.1152/physrev.00028.2012.

Bankaitis, V.A., C.J. Mousley, and G. Schaaf. 2010. The Sec14 superfamily and mechanisms for crosstalk between lipid metabolism and lipid signaling. *Trends in Biochemical Sciences*. 35:150–160. doi:10.1016/j.tibs.2009.10.008.

Barbosa, A.D., D.B. Savage, and S. Siniossoglou. 2015a. Lipid droplet-organelle interactions: emerging roles in lipid metabolism. *Current Opinion in Cell Biology*. 35:91–97. doi:10.1016/j.ceb.2015.04.017.

Barbosa, A.D., H. Sembongi, W.-M. Su, S. Abreu, F. Reggiori, G.M. Carman, and S. Siniossoglou. 2015b. Lipid partitioning at the nuclear envelope controls membrane biogenesis. *Mol. Biol. Cell.* 26:3641–3657. doi:10.1091/mbc.E15-03-0173.

Bari, V.K., S. Sharma, M. Alfatah, A.K. Mondal, and K. Ganesan. 2015. Plasma Membrane Proteolipid 3 Protein Modulates Amphotericin B Resistance through Sphingolipid Biosynthetic Pathway. *Sci Rep*. 5:9685. doi:10.1038/srep09685.

Barker, K.S., S. Crisp, N. Wiederhold, R.E. Lewis, B. Bareither, J. Eckstein, R. Barbuch, M. Bard, and P.D. Rogers. 2004. Genome-wide expression profiling reveals genes associated with amphotericin B and fluconazole resistance in experimentally induced antifungal resistant isolates of Candida albicans. *J. Antimicrob. Chemother.* 54:376–385. doi:10.1093/jac/dkh336.

Barros, M.H., A. Johnson, P. Gin, B.N. Marbois, C.F. Clarke, and A. Tzagoloff. 2005. The Saccharomyces cerevisiae COQ10 gene encodes a START domain protein required for function of coenzyme Q in respiration. *J. Biol. Chem.* 280:42627–42635. doi:10.1074/jbc.M510768200.

Baumann, N.A., D.P. Sullivan, H. Ohvo-Rekilä, C. Simonot, A. Pottekat, Z. Klaassen, C.T. Beh, and A.K. Menon. 2005. Transport of Newly Synthesized Sterol to the Sterol-Enriched Plasma Membrane Occurs via Nonvesicular Equilibration †. *Biochemistry*. 44:5816–5826. doi:10.1021/bi048296z.

Begley, M.J., G.S. Taylor, S.-A. Kim, D.M. Veine, J.E. Dixon, and J.A. Stuckey. 2003. Crystal structure of a phosphoinositide phosphatase, MTMR2: insights into myotubular myopathy and Charcot-Marie-Tooth syndrome. *Molecular Cell*. 12:1391–1402.

Belenky, P., D. Camacho, and J.J. Collins. 2013. Fungicidal drugs induce a common oxidative-damage cellular death pathway. *Cell Rep*. 3:350–358. doi:10.1016/j.celrep.2012.12.021.

Bennett, H.J., J.B. Davenport, R.F. Collins, A.W. Trafford, C. Pinali, and A. Kitmitto. 2013. Human junctophilin-2 undergoes a structural rearrangement upon binding PtdIns(3,4,5)P3 and the S101R mutation identified in hypertrophic cardiomyopathy obviates this response. *Biochem. J.* 456:205–217. doi:10.1042/BJ20130591.

Berchtold, D., M. Piccolis, N. Chiaruttini, I. Riezman, H. Riezman, A. Roux, T.C. Walther, and R. Loewith. 2012. Plasma membrane stress induces relocalization of Slm proteins and activation of TORC2 to promote sphingolipid synthesis. *Nat Cell Biol*. 14:542–547. doi:10.1038/ncb2480.

Bernhard, W., and C. Rouiller. 1956. Close topographical relationship between mitochondria and ergastoplasm of liver cells in a definite phase of cellular activity. *J Biophys Biochem Cytol*. 2:73–78.

Bigay, J., and B. Antonny. 2012. Curvature, lipid packing, and electrostatics of membrane organelles: defining cellular territories in determining specificity. *Developmental Cell*. 23:886–895. doi:10.1016/j.devcel.2012.10.009.

Blackwell, M. 2011. The fungi: 1, 2, 3 ... 5.1 million species? *American Journal of Botany*. 98:426–438. doi:10.3732/ajb.1000298.

Bligh, E.G., and W.J. Dyer. 1959. A rapid method of total lipid extraction and purification. *Can J Biochem Physiol*. 37:911–917. doi:10.1139/o59-099.

Blundell, T.L., B.L. Sibanda, M.J. Sternberg, and J.M. Thornton. 1987. Knowledge-based prediction of protein structures and the design of novel molecules. *Nature*. 326:347–352. doi:10.1038/326347a0.

Bodenhausen, G., and D.J. Ruben. 1980. Natural abundance nitrogen-15 NMR by enhanced heteronuclear spectroscopy. *Chemical Physics Letters*. 69:185–190.

Bodenmiller, B., S. Wanka, C. Kraft, J. Urban, D. Campbell, P.G. Pedrioli, B. Gerrits, P. Picotti, H. Lam, O. Vitek, M.-Y. Brusniak, B. Roschitzki, C. Zhang, K.M. Shokat, R. Schlapbach, A. Colman-Lerner, G.P. Nolan, A.I. Nesvizhskii, M. Peter, R. Loewith, C. von Mering, and R. Aebersold. 2010. Phosphoproteomic analysis reveals interconnected system-wide responses to perturbations of kinases and phosphatases in yeast. *Sci Signal*. 3:rs4–rs4. doi:10.1126/scisignal.2001182.

Boumann, H.A., B. de Kruijff, A.J.R. Heck, and A.I.P.M. de Kroon. 2004. The selective utilization of substrates in vivo by the phosphatidylethanolamine and phosphatidylcholine biosynthetic enzymes Ept1p and Cpt1p in yeast. *FEBS Letters*. 569:173–177. doi:10.1016/j.febslet.2004.05.043.

Boumann, H.A., M.J.A. Damen, C. Versluis, A.J.R. Heck, B. de Kruijff, and A.I.P.M. de Kroon. 2003. The two biosynthetic routes leading to phosphatidylcholine in yeast produce different sets of molecular species. Evidence for lipid remodeling. *Biochemistry*. 42:3054–3059. doi:10.1021/bi026801r.

Braun, P., Y. Hu, B. Shen, A. Halleck, M. Koundinya, E. Harlow, and J. LaBaer. 2002. Proteome-scale purification of human proteins from bacteria. *Proc. Natl. Acad. Sci. U.S.A.* 99:2654–2659. doi:10.1073/pnas.042684199.

Brenner, S.E., C. Chothia, and T.J. Hubbard. 1998. Assessing sequence comparison methods with reliable structurally identified distant evolutionary relationships. *Proc. Natl. Acad. Sci. U.S.A.* 95:6073–6078.

Bretscher, M.S. 1973. Membrane structure: some general principles. *Science*. 181:622–629.

Brunner, J.D., N.K. Lim, S. Schenck, A. Duerst, and R. Dutzler. 2014. X-ray structure of a calcium-activated TMEM16 lipid scramblase. *Nature*. 516:207–212. doi:10.1038/nature13984.

Burd, C.G., and S.D. Emr. 1998. Phosphatidylinositol(3)-phosphate signaling mediated by specific binding to RING FYVE domains. *Molecular Cell*. 2:157–162.

Burgess, A., S. Vigneron, E. Brioudes, J.-C. Labbé, T. Lorca, and A. Castro. 2010. Loss of human Greatwall results in G2 arrest and multiple mitotic defects due to deregulation of the cyclin B-Cdc2/PP2A balance. *Proc. Natl. Acad. Sci. U.S.A.* 107:12564–12569. doi:10.1073/pnas.0914191107.

Burgoyne, T., S. Patel, and E.R. Eden. 2015. Calcium signaling at ER membrane contact sites. *Biochim. Biophys. Acta*. 1853:2012–2017. doi:10.1016/j.bbamcr.2015.01.022.

Carman, G.M., and G.-S. Han. 2009. Regulation of phospholipid synthesis in yeast. *The Journal of Lipid Research*. 50 Suppl:S69–73. doi:10.1194/jlr.R800043-JLR200.

Cavanagh, J., W.J. Fairbrother, I. Arthur G Palmer, N.J. Skelton, and M. Rance. 2010. Protein NMR Spectroscopy. Academic Press. 1 pp.

Chang, C.-L., T.-S. Hsieh, T.T. Yang, K.G. Rothberg, D.B. Azizoglu, E. Volk, J.-C. Liao, and J. Liou. 2013. Feedback regulation of receptor-induced Ca2+ signaling mediated by E-Syt1 and Nir2 at endoplasmic reticulum-plasma membrane junctions. *Cell Rep.* 5:813–825. doi:10.1016/j.celrep.2013.09.038.

Charman, M., T.R. Colbourne, A. Pietrangelo, L. Kreplak, and N.D. Ridgway. 2014. Oxysterol-binding protein (OSBP)-related protein 4 (ORP4) is essential for cell proliferation and survival. *J. Biol. Chem.* 289:15705–15717. doi:10.1074/jbc.M114.571216.

Cheng, J., T.S. Park, A.S. Fischl, and X.S. Ye. 2001. Cell cycle progression and cell polarity require sphingolipid biosynthesis in Aspergillus nidulans. *Mol. Cell. Biol.* 21:6198–6209. doi:10.1128/MCB.21.18.6198-6209.2001.

Chiapparino, A., K. Maeda, D. Turei, J. Saez- Rodriguez, and A.-C. Gavin. 2015. The orchestra of lipid-transfer proteins at the crossroads between metabolism and signaling. *Progress in Lipid Research*. doi:10.1016/j.plipres.2015.10.004.

Choi, H.-S., A. Sreenivas, G.-S. Han, and G.M. Carman. 2004. Regulation of phospholipid synthesis in the yeast cki1Delta eki1Delta mutant defective in the Kennedy pathway. The Cho1-encoded phosphatidylserine synthase is regulated by mRNA stability. *J. Biol. Chem.* 279:12081–12087. doi:10.1074/jbc.M400297200.

Chothia, C. 1992. Proteins. One thousand families for the molecular biologist. *Nature*. 357:543–544. doi:10.1038/357543a0.

Chothia, C., and A.M. Lesk. 1986. The relation between the divergence of sequence and structure in proteins. *EMBO J.* 5:823–826.

Chu, B.-B., Y.-C. Liao, W. Qi, C. Xie, X. Du, J. Wang, H. Yang, H.-H. Miao, B.-L. Li, and B.-L. Song. 2015. Cholesterol transport through lysosome-peroxisome membrane contacts. *Cell*. 161:291–306. doi:10.1016/j.cell.2015.02.019.

Chung, J., F. Torta, K. Masai, L. Lucast, H. Czapla, L.B. Tanner, P. Narayanaswamy, M.R. Wenk, F. Nakatsu, and P. De Camilli. 2015. INTRACELLULAR TRANSPORT. PI4P/phosphatidylserine countertransport at ORP5- and ORP8-mediated ER-plasma membrane contacts. *Science*. 349:428–432. doi:10.1126/science.aab1370.

Clark, B.J., J. Wells, S.R. King, and D.M. Stocco. 1994. The purification, cloning, and expression of a novel luteinizing hormone-induced mitochondrial protein in MA-10 mouse Leydig tumor cells. Characterization of the steroidogenic acute regulatory protein (StAR). *J. Biol. Chem.* 269:28314–28322.

Cockcroft, S. 2009. Measurement of phosphatidylinositol and phosphatidylcholine binding and transfer activity of the lipid transport protein PITP. *Methods Mol. Biol.* 462:363–377. doi:10.1007/978-1-60327-115-8_23.

Cole, C., J.D. Barber, and G.J. Barton. 2008. The Jpred 3 secondary structure prediction server. *Nucleic Acids Res.* 36:W197–W201. doi:10.1093/nar/gkn238.

Conde, L., E. Halperin, N.K. Akers, K.M. Brown, K.E. Smedby, N. Rothman, A. Nieters, S.L. Slager, A. Brooks-Wilson, L. Agana, J. Riby, J. Liu, H.-O. Adami, H. Darabi, H. Hjalgrim, H.-Q. Low, K. Humphreys, M. Melbye, E.T. Chang, B. Glimelius, W. Cozen, S. Davis, P. Hartge, L.M. Morton, M. Schenk, S.S. Wang, B. Armstrong, A. Kricker, S. Milliken, M.P. Purdue, C.M. Vajdic, P. Boyle, Q. Lan, S.H. Zahm, Y. Zhang, T. Zheng, N. Becker, Y. Benavente, P. Boffetta, P. Brennan, K. Butterbach, P. Cocco, L. Foretova, M. Maynadié, S. de Sanjosé, A. Staines, J.J. Spinelli, S.J. Achenbach, T.G. Call, N.J. Camp, M. Glenn, N.E. Caporaso, J.R. Cerhan, J.M. Cunningham, L.R. Goldin, C.A. Hanson, N.E. Kay, M.C. Lanasa, J.F. Leis, G.E. Marti, K.G. Rabe, L.Z. Rassenti, L.G. Spector, S.S. Strom, C.M. Vachon, J.B. Weinberg, E.A. Holly, S. Chanock, M.T. Smith, P.M. Bracci, and C.F. Skibola. 2010. Genome-wide association study of follicular lymphoma identifies a risk locus at 6p21.32. *Nat Genet*. 42:661–664. doi:10.1038/ng.626.

Connerth, M., T. Tatsuta, M. Haag, T. Klecker, B. Westermann, and T. Langer. 2012. Intramitochondrial Transport of Phosphatidic Acid in Yeast by a Lipid Transfer Protein. *Science*. 338:815–818. doi:10.1126/science.1225625.

Creutz, C.E., S.L. Snyder, and T.A. Schulz. 2004. Characterization of the yeast tricalbins: membrane-bound multi-C2-domain proteins that form complexes involved in membrane trafficking. *Cell. Mol.*

Life Sci. 61:1208–1220. doi:10.1007/s00018-004-4029-8.

da Silveira Dos Santos, A.X., I. Riezman, M.-A. Aguilera-Romero, F. David, M. Piccolis, R. Loewith, O. Schaad, and H. Riezman. 2014. Systematic lipidomic analysis of yeast protein kinase and phosphatase mutants reveals novel insights into regulation of lipid homeostasis. *Mol. Biol. Cell*. 25:3234–3246. doi:10.1091/mbc.E14-03-0851.

Das, A., M.S. Brown, D.D. Anderson, J.L. Goldstein, and A. Radhakrishnan. 2014. Three pools of plasma membrane cholesterol and their relation to cholesterol homeostasis. *Elife*. 3:e02882. doi:10.7554/eLife.02882.

Daum, G., N.D. Lees, M. Bard, and R. Dickson. 1998. Biochemistry, cell biology and molecular biology of lipids of Saccharomyces cerevisiae. *Yeast*. 14:1471–1510. doi:10.1002/(SICI)1097-0061(199812)14:16<1471::AID-YEA353>3.0.CO;2-Y.

Davies, J.P., F.W. Chen, and Y.A. Ioannou. 2000. Transmembrane molecular pump activity of Niemann-Pick C1 protein. *Science*. 290:2295–2298. doi:10.1126/science.290.5500.2295.

Davis, S.A., B.M. Vincent, M.M. Endo, L. Whitesell, K. Marchillo, D.R. Andes, S. Lindquist, and M.D. Burke. 2015. Nontoxic antimicrobials that evade drug resistance. *Nat. Chem. Biol.* 11:481–487. doi:10.1038/nchembio.1821.

Dawson, P.A., N.D. Ridgway, C.A. Slaughter, M.S. Brown, and J.L. Goldstein. 1989. cDNA cloning and expression of oxysterol-binding protein, an oligomer with a potential leucine zipper. *J. Biol. Chem.* 264:16798–16803.

de Saint-Jean, M., V. Delfosse, D. Douguet, G. Chicanne, B. Payrastre, W. Bourguet, B. Antonny, and G. Drin. 2011. Osh4p exchanges sterols for phosphatidylinositol 4-phosphate between lipid bilayers. *The Journal of Cell Biology*. 195:965–978. doi:10.1083/jcb.201104062.

De Smet, C.H., E. Vittone, M. Scherer, M. Houweling, G. Liebisch, J.F. Brouwers, and A.I.P.M. de Kroon. 2012. The yeast acyltransferase Sct1p regulates fatty acid desaturation by competing with the desaturase Ole1p. *Mol. Biol. Cell*. 23:1146–1156. doi:10.1091/mbc.E11-07-0624.

DeGrella, R.F., and R.D. Simoni. 1982. Intracellular transport of cholesterol to the plasma membrane. *J. Biol. Chem.* 257:14256–14262.

Deguil, J., L. Pineau, E.C. Rowland Snyder, S. Dupont, L. Beney, A. Gil, G. Frapper, and T. Ferreira. 2011. Modulation of lipid-induced ER stress by fatty acid shape. *Traffic*. 12:349–362. doi:10.1111/j.1600-0854.2010.01150.x.

Di Bernardo, M.C., D. Crowther-Swanepoel, P. Broderick, E. Webb, G. Sellick, R. Wild, K. Sullivan, J. Vijayakrishnan, Y. Wang, A.M. Pittman, N.J. Sunter, A.G. Hall, M.J.S. Dyer, E. Matutes, C. Dearden, T. Mainou-Fowler, G.H. Jackson, G. Summerfield, R.J. Harris, A.R. Pettitt, P. Hillmen, D.J. Allsup, J.R. Bailey, G. Pratt, C. Pepper, C. Fegan, J.M. Allan, D. Catovsky, and R.S. Houlston. 2008. A genome-wide association study identifies six susceptibility loci for chronic lymphocytic leukemia. *Nat Genet*. 40:1204–1210. doi:10.1038/ng.219.

Di Paolo, G., and P. De Camilli. 2006. Phosphoinositides in cell regulation and membrane dynamics. *Nature*. 443:651–657. doi:10.1038/nature05185.

Doerks, T., M. Strauss, M. Brendel, and P. Bork. 2000. GRAM, a novel domain in glucosyltransferases, myotubularins and other putative membrane-associated proteins. *Trends in Biochemical Sciences*. 25:483–485.

Du, X., J. Kumar, C. Ferguson, T.A. Schulz, Y.S. Ong, W. Hong, W.A. Prinz, R.G. Parton, A.J. Brown, and H. Yang. 2011. A role for oxysterol-binding protein-related protein 5 in endosomal cholesterol trafficking. *The Journal of Cell Biology*. 192:121–135. doi:10.1083/jcb.201004142.

Dyson, M.R. 2010. Selection of soluble protein expression constructs: the experimental determination of protein domain boundaries. *Biochem. Soc. Trans.* 38:908–913. doi:10.1042/BST0380908.

Ejsing, C.S., J.L. Sampaio, V. Surendranath, E. Duchoslav, K. Ekroos, R.W. Klemm, K. Simons, and A. Shevchenko. 2009. Global analysis of the yeast lipidome by quantitative shotgun mass spectrometry. *Proc. Natl. Acad. Sci. U.S.A.* 106:2136–2141. doi:10.1073/pnas.0811700106.

Elbaz-Alon, Y., E. Rosenfeld-Gur, V. Shinder, A.H. Futerman, T. Geiger, and M. Schuldiner. 2014. A dynamic interface between vacuoles and mitochondria in yeast. *Developmental Cell*. 30:95–102. doi:10.1016/j.devcel.2014.06.007.

Elbaz-Alon, Y., M. Eisenberg-Bord, V. Shinder, S.B. Stiller, E. Shimoni, N. Wiedemann, T. Geiger, and M. Schuldiner. 2015. Lam6 Regulates the Extent of Contacts between Organelles. *Cell Rep*. 12:7–14. doi:10.1016/j.celrep.2015.06.022.

Epstein, S., C.L. Kirkpatrick, G.A. Castillon, M. Muñiz, I. Riezman, F.P.A. David, C.B. Wollheim, and H. Riezman. 2012. Activation of the unfolded protein response pathway causes ceramide accumulation in yeast and INS-1E insulinoma cells. *J. Lipid Res.* 53:412–420. doi:10.1194/jlr.M022186.

Ermishkin, L.N., K.M. Kasumov, and V.M. Potzeluyev. 1976. Single ionic channels induced in lipid bilayers by polyene antibiotics amphotericin B and nystatine. *Nature*. 262:698–699.

Fadok, V.A., D.R. Voelker, P.A. Campbell, J.J. Cohen, D.L. Bratton, and P.M. Henson. 1992. Exposure of phosphatidylserine on the surface of apoptotic lymphocytes triggers specific recognition and removal by macrophages. *J. Immunol.* 148:2207–2216.

Fagone, P., and S. Jackowski. 2009. Membrane phospholipid synthesis and endoplasmic reticulum function. *The Journal of Lipid Research*. 50 Suppl:S311–6. doi:10.1194/jlr.R800049-JLR200.

Fairn, G.D., N.L. Schieber, N. Ariotti, S. Murphy, L. Kuerschner, R.I. Webb, S. Grinstein, and R.G. Parton. 2011. High-resolution mapping reveals topologically distinct cellular pools of phosphatidylserine. *The Journal of Cell Biology*. 194:257–275. doi:10.1083/jcb.201012028.

Fernández, C., and G. Wider. 2003. TROSY in NMR studies of the structure and function of large biological macromolecules. *Curr. Opin. Struct. Biol.* 13:570–580.

Fernández-Busnadiego, R., Y. Saheki, and P. De Camilli. 2015. Three-dimensional architecture of extended synaptotagmin-mediated endoplasmic reticulum-plasma membrane contact sites. *Proc. Natl. Acad. Sci. U.S.A.* 112:E2004–13. doi:10.1073/pnas.1503191112.

Field, F.J., E. Born, S. Murthy, and S.N. Mathur. 1998. Transport of cholesterol from the endoplasmic reticulum to the plasma membrane is constitutive in CaCo-2 cells and differs from the transport of plasma membrane cholesterol to the endoplasmic reticulum. *The Journal of Lipid Research*. 39:333–343.

Frechin, M., T. Stoeger, S. Daetwyler, C. Gehin, N. Battich, E.-M. Damm, L. Stergiou, H. Riezman, and L. Pelkmans. 2015. Cell-intrinsic adaptation of lipid composition to local crowding drives social behaviour. *Nature*. 523:88–91. doi:10.1038/nature14429.

Friedman, J.R., A. Mourier, J. Yamada, J.M. McCaffery, and J. Nunnari. 2015. MICOS coordinates with respiratory complexes and lipids to establish mitochondrial inner membrane architecture. *Elife*. 4:621. doi:10.7554/eLife.07739.

Fröhlich, F., R. Christiano, D.K. Olson, A. Alcazar-Roman, P. DeCamilli, and T.C. Walther. 2014. A Role for Eisosomes in Maintenance of Plasma Membrane Phosphoinositide Levels. *Mol. Biol. Cell*. doi:10.1091/mbc.E13-11-0639.

Fu, S., L. Yang, P. Li, O. Hofmann, L. Dicker, W. Hide, X. Lin, S.M. Watkins, A.R. Ivanov, and G.S. Hotamisligil. 2011. Aberrant lipid metabolism disrupts calcium homeostasis causing liver endoplasmic reticulum stress in obesity. *Nature*. 473:528–531. doi:10.1038/nature09968.

Funato, K., and H. Riezman. 2001. Vesicular and nonvesicular transport of ceramide from ER to the Golgi apparatus in yeast. *The Journal of Cell Biology*. 155:949–960. doi:10.1083/jcb.200105033.

Futerman, A.H., and G. van Meer. 2004. The cell biology of lysosomal storage disorders. *Nat Rev Mol Cell Biol*. 5:554–565. doi:10.1038/nrm1423.

Garner, K., A.N. Hunt, G. Koster, P. Somerharju, E. Groves, M. Li, P. Raghu, R. Holic, and S. Cockcroft. 2012. Phosphatidylinositol transfer protein, cytoplasmic 1 (PITPNC1) binds and transfers phosphatidic acid. *Journal of Biological Chemistry*. 287:32263–32276. doi:10.1074/jbc.M112.375840.

Gatta, A.T., L.H. Wong, Y.Y. Sere, D.M. Calderón-Noreña, S. Cockcroft, A.K. Menon, and T.P. Levine. 2015. A new family of StART domain proteins at membrane contact sites has a role in ER-PM sterol transport. *Elife*. 4:e07253. doi:10.7554/eLife.07253.

Gavin, A.-C., M. Bösche, R. Krause, P. Grandi, M. Marzioch, A. Bauer, J. Schultz, J.M. Rick, A.-M. Michon, C.-M. Cruciat, M. Remor, C. Höfert, M. Schelder, M. Brajenovic, H. Ruffner, A. Merino, K. Klein, M. Hudak, D. Dickson, T. Rudi, V. Gnau, A. Bauch, S. Bastuck, B. Huhse, C. Leutwein, M.-A. Heurtier, R.R. Copley, A. Edelmann, E. Querfurth, V. Rybin, G. Drewes, M. Raida, T. Bouwmeester, P. Bork, B. Séraphin, B. Kuster, G. Neubauer, and G. Superti-Furga. 2002. Functional organization of the yeast proteome by systematic analysis of protein complexes. *Nature*. 415:141–147. doi:10.1038/415141a.

Georgiev, A.G., D.P. Sullivan, M.C. Kersting, J.S. Dittman, C.T. Beh, and A.K. Menon. 2011. Osh proteins regulate membrane sterol organization but are not required for sterol movement between the ER and PM. *Traffic*. 12:1341–1355. doi:10.1111/j.1600-0854.2011.01234.x.

Ghaemmaghami, S., W.-K. Huh, K. Bower, R.W. Howson, A. Belle, N. Dephoure, E.K. O'Shea, and J.S. Weissman. 2003. Global analysis of protein expression in yeast. *Nature*. 425:737–741. doi:10.1038/nature02046.

Gietz, R.D., and R.H. Schiestl. 2007. Frozen competent yeast cells that can be transformed with high efficiency using the LiAc/SS carrier DNA/PEG method. *Nat Protoc*. 2:1–4. doi:10.1038/nprot.2007.17.

Giordano, F., Y. Saheki, O. Idevall-Hagren, S.F. Colombo, M. Pirruccello, I. Milosevic, E.O. Gracheva,

S.N. Bagriantsev, N. Borgese, and P. De Camilli. 2013. PI(4,5)P(2)-dependent and Ca(2+)-regulated ER-PM interactions mediated by the extended synaptotagmins. *Cell*. 153:1494–1509. doi:10.1016/j.cell.2013.05.026.

Gnamusch, E., C. Kalaus, C. Hrastnik, F. Paltauf, and G. Daum. 1992. Transport of phospholipids between subcellular membranes of wild-type yeast cells and of the phosphatidylinositol transfer protein-deficient strain Saccharomyces cerevisiae sec 14. *Biochim. Biophys. Acta*. 1111:120–126.

Goldstein, J.L., and M.S. Brown. 2015. A century of cholesterol and coronaries: from plaques to genes to statins. *Cell*. 161:161–172. doi:10.1016/j.cell.2015.01.036.

Golovanov, A.P., G.M. Hautbergue, S.A. Wilson, and L.-Y. Lian. 2004. A Simple Method for Improving Protein Solubility and Long-Term Stability. *J. Am. Chem. Soc.* 126:8933–8939. doi:10.1021/ja049297h.

Graham, T.R., and S.D. Emr. 1991. Compartmental organization of Golgi-specific protein modification and vacuolar protein sorting events defined in a yeast sec18 (NSF) mutant. *The Journal of Cell Biology*. 114:207–218.

Graham, T.R., P.A. Scott, and S.D. Emr. 1993. Brefeldin A reversibly blocks early but not late protein transport steps in the yeast secretory pathway. *EMBO J.* 12:869–877.

Gray, K.C., D.S. Palacios, I. Dailey, M.M. Endo, B.E. Uno, B.C. Wilcock, and M.D. Burke. 2012. Amphotericin primarily kills yeast by simply binding ergosterol. *Proc. Natl. Acad. Sci. U.S.A.* 109:2234–2239. doi:10.1073/pnas.1117280109.

Gräslund, S., P. Nordlund, J. Weigelt, J. Bray, O. Gileadi, S. Knapp, U. Oppermann, C. Arrowsmith, R. Hui, J. Ming, S. dhe-Paganon, H.-W. Park, A. Savchenko, A. Yee, A. Edwards, R. Vincentelli, C. Cambillau, R. Kim, S.-H. Kim, Z. Rao, Y. Shi, T.C. Terwilliger, C.-Y. Kim, L.-W. Hung, G.S. Waldo, Y. Peleg, S. Albeck, T. Unger, O. Dym, J. Prilusky, J.L. Sussman, R.C. Stevens, S.A. Lesley, I.A. Wilson, A. Joachimiak, F. Collart, I. Dementieva, M.I. Donnelly, W.H. Eschenfeldt, Y. Kim, L. Stols, R. Wu, M. Zhou, S.K. Burley, J.S. Emtage, J.M. Sauder, D. Thompson, K. Bain, J. Luz, T. Gheyi, F. Zhang, S. Atwell, S.C. Almo, J.B. Bonanno, A. Fiser, S. Swaminathan, F.W. Studier, M.R. Chance, A. Sali, T.B. Acton, R. Xiao, L. Zhao, L.C. Ma, J.F. Hunt, L. Tong, K. Cunningham, M. Inouye, S. Anderson, H. Janjua, R. Shastry, C.K. Ho, D. Wang, H. Wang, M. Jiang, G.T. Montelione, D.I. Stuart, R.J. Owens, S. Daenke, A. Schütz, U. Heinemann, S. Yokoyama, K. Büssow, and K.C. Gunsalus. 2008. Protein production and purification. *Nature Methods*. 5:135–146. doi:10.1038/nmeth.f.202.

Grieve, A.G., and C. Rabouille. 2011. Golgi bypass: skirting around the heart of classical secretion. *Cold Spring Harb Perspect Biol*. 3:a005298–a005298. doi:10.1101/cshperspect.a005298.

Grinstein, S. 2010. Imaging signal transduction during phagocytosis: phospholipids, surface charge, and electrostatic interactions. *Am. J. Physiol., Cell Physiol.* 299:C876–81. doi:10.1152/ajpcell.00342.2010.

Gruszecki, W.I., R. Luchowski, M. Gagoś, M. Arczewska, P. Sarkar, M. Hereć, B. Myśliwa-Kurdziel, K. Strzałka, I. Gryczynski, and Z. Gryczynski. 2009. Molecular organization of antifungal antibiotic amphotericin B in lipid monolayers studied by means of Fluorescence Lifetime Imaging Microscopy. *Biophys. Chem.* 143:95–101. doi:10.1016/j.bpc.2009.04.008.

Grzesiek, S., and A. Bax. 1993. Amino acid type determination in the sequential assignment procedure of uniformly 13C/15N-enriched proteins. *J. Biomol. NMR*. 3:185–204.

Guan, X.L., C.M. Souza, H. Pichler, G. Dewhurst, O. Schaad, K. Kajiwara, H. Wakabayashi, T. Ivanova, G.A. Castillon, M. Piccolis, F. Abe, R. Loewith, K. Funato, M.R. Wenk, and H. Riezman. 2009. Functional interactions between sphingolipids and sterols in biological membranes regulating cell physiology. *Mol. Biol. Cell*. 20:2083–2095. doi:10.1091/mbc.E08-11-1126.

Guan, X.L., I. Riezman, M.R. Wenk, and H. Riezman. 2010. Yeast lipid analysis and quantification by mass spectrometry. *Meth. Enzymol.* 470:369–391. doi:10.1016/S0076-6879(10)70015-X.

Guarani, V., E.M. McNeill, J.A. Paulo, E.L. Huttlin, F. Fröhlich, S.P. Gygi, D. Van Vactor, and J.W. Harper. 2015. QIL1 is a novel mitochondrial protein required for MICOS complex stability and cristae morphology. *Elife*. 4:40. doi:10.7554/eLife.06265.

Guindon, S., and O. Gascuel. 2003. A simple, fast, and accurate algorithm to estimate large phylogenies by maximum likelihood. *Syst. Biol.* 52:696–704.

Hammond, G.R.V., M.J. Fischer, K.E. Anderson, J. Holdich, A. Koteci, T. Balla, and R.F. Irvine. 2012. PI4P and PI(4,5)P2 are essential but independent lipid determinants of membrane identity. *Science*. 337:727–730. doi:10.1126/science.1222483.

Hanada, K., K. Kumagai, S. Yasuda, Y. Miura, M. Kawano, M. Fukasawa, and M. Nishijima. 2003. Molecular machinery for non-vesicular trafficking of ceramide. *Nature*. 426:803–809. doi:10.1038/nature02188.

Hannun, Y.A., and L.M. Obeid. 2008. Principles of bioactive lipid signalling: lessons from sphingolipids. *Nat Rev Mol Cell Biol*. 9:139–150. doi:10.1038/nrm2329.

Harlan, J.E., P.J. Hajduk, H.S. Yoon, and S.W. Fesik. 1994. Pleckstrin homology domains bind to phosphatidylinositol-4,5-bisphosphate. *Nature*. 371:168–170. doi:10.1038/371168a0.

Harner, M., C. Körner, D. Walther, D. Mokranjac, J. Kaesmacher, U. Welsch, J. Griffith, M. Mann, F. Reggiori, and W. Neupert. 2011. The mitochondrial contact site complex, a determinant of mitochondrial architecture. *EMBO J.* 30:4356–4370. doi:10.1038/emboj.2011.379.

Henne, W.M. 2016. Organelle remodeling at membrane contact sites. *Journal of Structural Biology*. doi:10.1016/j.jsb.2016.05.003.

Henne, W.M., J. Liou, and S.D. Emr. 2015a. Molecular mechanisms of inter-organelle ER-PM contact sites. *Current Opinion in Cell Biology*. 35:123–130. doi:10.1016/j.ceb.2015.05.001.

Henne, W.M., L. Zhu, Z. Balogi, C. Stefan, J.A. Pleiss, and S.D. Emr. 2015b. Mdm1/Snx13 is a novel ER-endolysosomal interorganelle tethering protein. *The Journal of Cell Biology*. 210:541–551. doi:10.1083/jcb.201503088.

Henry, S.A., S.D. Kohlwein, and G.M. Carman. 2012. Metabolism and regulation of glycerolipids in the yeast Saccharomyces cerevisiae. *Genetics*. 190:317–349. doi:10.1534/genetics.111.130286.

Hillenmeyer, M.E., E. Fung, J. Wildenhain, S.E. Pierce, S. Hoon, W. Lee, M. Proctor, R.P. St Onge, M. Tyers, D. Koller, R.B. Altman, R.W. Davis, C. Nislow, and G. Giaever. 2008. The Chemical Genomic Portrait of Yeast: Uncovering a Phenotype for All Genes. *Science*. 320:362–365. doi:10.1126/science.1150021.

Hirata, Y., M. Brotto, N. Weisleder, Y. Chu, P. Lin, X. Zhao, A. Thornton, S. Komazaki, H. Takeshima, J. Ma, and Z. Pan. 2006. Uncoupling store-operated Ca2+ entry and altered Ca2+ release from sarcoplasmic reticulum through silencing of junctophilin genes. *Biophys. J.* 90:4418–4427. doi:10.1529/biophysj.105.076570.

Holic, R., Z. Šimová, T. Ashlin, V. Pevala, K. Poloncová, D. Tahotná, E. Kutejová, S. Cockcroft, and P. Griač. 2014. Phosphatidylinositol binding of Saccharomyces cerevisiae Pdr16p represents an essential feature of this lipid transfer protein to provide protection against azole antifungals. *BBA - Molecular and Cell Biology of Lipids*. 1841:1483–1490. doi:10.1016/j.bbalip.2014.07.014.

Holland, W.L., and S.A. Summers. 2008. Sphingolipids, insulin resistance, and metabolic disease: new insights from in vivo manipulation of sphingolipid metabolism. *Endocr. Rev.* 29:381–402. doi:10.1210/er.2007-0025.

Holthuis, J.C., T. Pomorski, R.J. Raggers, H. Sprong, and G. van Meer. 2001. The organizing potential of sphingolipids in intracellular membrane transport. *Physiol. Rev.* 81:1689–1723.

Holthuis, J.C.M., and A.K. Menon. 2014. Lipid landscapes and pipelines in membrane homeostasis. *Nature*. 510:48–57. doi:10.1038/nature13474.

Holthuis, J.C.M., and T.P. Levine. 2005. Lipid traffic: floppy drives and a superhighway. *Nat Rev Mol Cell Biol*. 6:209–220. doi:10.1038/nrm1591.

Hoppins, S., S.R. Collins, A. Cassidy-Stone, E. Hummel, R.M. Devay, L.L. Lackner, B. Westermann, M. Schuldiner, J.S. Weissman, and J. Nunnari. 2011. A mitochondrial-focused genetic interaction map reveals a scaffold-like complex required for inner membrane organization in mitochondria. *The Journal of Cell Biology*. 195:323–340. doi:10.1083/jcb.201107053.

Hotamisligil, G.S. 2006. Inflammation and metabolic disorders. *Nature*. 444:860–867. doi:10.1038/nature05485.

Hönscher, C., M. Mari, K. Auffarth, M. Bohnert, J. Griffith, W. Geerts, M. van der Laan, M. Cabrera, F. Reggiori, and C. Ungermann. 2014. Cellular metabolism regulates contact sites between vacuoles and mitochondria. *Developmental Cell*. 30:86–94. doi:10.1016/j.devcel.2014.06.006.

Huh, W.-K., J.V. Falvo, L.C. Gerke, A.S. Carroll, R.W. Howson, J.S. Weissman, and E.K. O'Shea. 2003. Global analysis of protein localization in budding yeast. *Nature*. 425:686–691. doi:10.1038/nature02026.

Huta, B.P., M.R. Mehlenbacher, Y. Nie, X. Lai, C. Zubieta, F. Bou-Abdallah, and R.P. Doyle. 2016. The Lysosomal Protein Saposin B Binds Chloroquine. *ChemMedChem*. 11:277–282. doi:10.1002/cmdc.201500494.

Huttlin, E.L., L. Ting, R.J. Bruckner, F. Gebreab, M.P. Gygi, J. Szpyt, S. Tam, G. Zarraga, G. Colby, K. Baltier, R. Dong, V. Guarani, L.P. Vaites, A. Ordureau, R. Rad, B.K. Erickson, M. Wühr, J. Chick, B. Zhai, D. Kolippakkam, J. Mintseris, R.A. Obar, T. Harris, S. Artavanis-Tsakonas, M.E. Sowa, P. De Camilli, J.A. Paulo, J.W. Harper, and S.P. Gygi. 2015. The BioPlex Network: A Systematic Exploration of the Human Interactome. *Cell*. 162:425–440. doi:10.1016/j.cell.2015.06.043.

Idevall-Hagren, O., A. Lü, B. Xie, and P. De Camilli. 2015. Triggered Ca2+ influx is required for extended synaptotagmin 1-induced ER-plasma membrane tethering. *EMBO J.* 34:2291–2305.

doi:10.15252/embj.201591565.

Ikura, M., L.E. Kay, and A. Bax. 1990. A novel approach for sequential assignment of 1H, 13C, and 15N spectra of proteins: heteronuclear triple-resonance three-dimensional NMR spectroscopy. Application to calmodulin. *Biochemistry*. 29:4659–4667.

Im, Y.J., A.J. Davis, I.Y. Perera, E. Johannes, N.S. Allen, and W.F. Boss. 2007. The N-terminal membrane occupation and recognition nexus domain of Arabidopsis phosphatidylinositol phosphate kinase 1 regulates enzyme activity. *J. Biol. Chem.* 282:5443–5452. doi:10.1074/jbc.M611342200.

Im, Y.J., S. Raychaudhuri, W.A. Prinz, and J.H. Hurley. 2005. Structural mechanism for sterol sensing and transport by OSBP-related proteins. *Nat Cell Biol*. 437:154–158. doi:10.1038/nature03923.

Inda, M.E., M. Vandenbranden, A. Fernández, D. de Mendoza, J.-M. Ruysschaert, and L.E. Cybulski. 2014. A lipid-mediated conformational switch modulates the thermosensing activity of DesK. *Proc. Natl. Acad. Sci. U.S.A.* 111:3579–3584. doi:10.1073/pnas.1317147111.

Infante, R.E., M.L. Wang, A. Radhakrishnan, H.J. Kwon, M.S. Brown, and J.L. Goldstein. 2008. NPC2 facilitates bidirectional transfer of cholesterol between NPC1 and lipid bilayers, a step in cholesterol egress from lysosomes. *Proc. Natl. Acad. Sci. U.S.A.* 105:15287–15292. doi:10.1073/pnas.0807328105.

Jeener, J., B.H. Meier, P. Bachmann, and R.R. Ernst. 1979. Investigation of exchange processes by two-dimensional NMR spectroscopy. *J. Chem. Phys.* 71:4546–9. doi:10.1063/1.438208.

Jousset, H., M. Frieden, and N. Demaurex. 2007. STIM1 knockdown reveals that store-operated Ca2+ channels located close to sarco/endoplasmic Ca2+ ATPases (SERCA) pumps silently refill the endoplasmic reticulum. *J. Biol. Chem.* 282:11456–11464. doi:10.1074/jbc.M609551200.

Kaiser, C.A., and R. Schekman. 1990. Distinct sets of SEC genes govern transport vesicle formation and fusion early in the secretory pathway. *Cell*. 61:723–733.

Kanno, K., M.K. Wu, E.F. Scapa, S.L. Roderick, and D.E. Cohen. 2007. Structure and function of phosphatidylcholine transfer protein (PC-TP)/StarD2. *Biochim. Biophys. Acta*. 1771:654–662. doi:10.1016/j.bbalip.2007.04.003.

Kaplan, M.R., and R.D. Simoni. 1985a. Intracellular transport of phosphatidylcholine to the plasma membrane. *The Journal of Cell Biology*. 101:441–445.

Kaplan, M.R., and R.D. Simoni. 1985b. Transport of cholesterol from the endoplasmic reticulum to the plasma membrane. *The Journal of Cell Biology*. 101:446–453.

Kay, J.G., M. Koivusalo, X. Ma, T. Wohland, and S. Grinstein. 2012. Phosphatidylserine dynamics in cellular membranes. *Mol. Biol. Cell*. 23:2198–2212. doi:10.1091/mbc.E11-11-0936.

Kay, L.E., G.M. Clore, A. Bax, and A.M. Gronenborn. 1990. Four-dimensional heteronuclear triple-resonance NMR spectroscopy of interleukin-1 beta in solution. *Science*. 249:411–414.

Keinan, O., A. Kedan, N. Gavert, M. Selitrennik, S. Kim, T. Karn, S. Becker, and S. Lev. 2014. The lipid-transfer protein Nir2 enhances epithelial-mesenchymal transition and facilitates breast cancer metastasis. *Journal of Cell Science*. 127:4740–4749. doi:10.1242/jcs.155721.

Kellis, M., B.W. Birren, and E.S. Lander. 2004. Proof and evolutionary analysis of ancient genome duplication in the yeast Saccharomyces cerevisiae. *Nature*. 428:617–624. doi:10.1038/nature02424.

Khafif, M., L. Cottret, C. Balagué, and S. Raffaele. 2014. Identification and phylogenetic analyses of VASt, an uncharacterized protein domain associated with lipid-binding domains in Eukaryotes. *BMC Bioinformatics*. 15:222–12. doi:10.1186/1471-2105-15-222.

Kim, Y.J., M.-L. Guzman-Hernandez, and T. Balla. 2011. A highly dynamic ER-derived phosphatidylinositol-synthesizing organelle supplies phosphoinositides to cellular membranes. *Developmental Cell*. 21:813–824. doi:10.1016/j.devcel.2011.09.005.

Kim, Y.J., M.-L. Guzman-Hernandez, E. Wisniewski, and T. Balla. 2015. Phosphatidylinositol-Phosphatidic Acid Exchange by Nir2 at ER-PM Contact Sites Maintains Phosphoinositide Signaling Competence. *Developmental Cell*. 33:549–561. doi:10.1016/j.devcel.2015.04.028.

Kim, Y.J., M.-L. Guzman-Hernandez, E. Wisniewski, N. Echeverria, and T. Balla. 2016. Phosphatidylinositol and phosphatidic acid transport between the ER and plasma membrane during PLC activation requires the Nir2 protein. *Biochem. Soc. Trans.* 44:197–201. doi:10.1042/BST20150187.

Kinch, L.N., and N.V. Grishin. 2002. Evolution of protein structures and functions. *Curr. Opin. Struct. Biol.* 12:400–408.

Kippenberger, S., S. Loitsch, M. Guschel, J. Müller, Y. Knies, R. Kaufmann, and A. Bernd. 2005. Mechanical stretch stimulates protein kinase B/Akt phosphorylation in epidermal cells via

angiotensin II type 1 receptor and epidermal growth factor receptor. *J. Biol. Chem.* 280:3060–3067. doi:10.1074/jbc.M409590200.

Klose, C., M.A. Surma, M.J. Gerl, F. Meyenhofer, A. Shevchenko, and K. Simons. 2012. Flexibility of a eukaryotic lipidome--insights from yeast lipidomics. *PLoS ONE*. 7:e35063. doi:10.1371/journal.pone.0035063.

Kopec, K.O., V. Alva, and A.N. Lupas. 2010. Homology of SMP domains to the TULIP superfamily of lipid-binding proteins provides a structural basis for lipid exchange between ER and mitochondria. *Bioinformatics*. 26:1927–1931. doi:10.1093/bioinformatics/btq326.

Kopec, K.O., V. Alva, and A.N. Lupas. 2011. Bioinformatics of the TULIP domain superfamily. *Biochem. Soc. Trans.* 39:1033–1038. doi:10.1042/BST0391033.

Kornmann, B., D.S. Currle, J.J. Collins, M. Schuldiner, J. Nunnari, J.S. Weissman, and P. Walter. 2009. An ER-mitochondria tethering complex revealed by a synthetic biology screen. *Science*. 325:477–481. doi:10.1126/science.1175088.

Kreishman-Deitrick, M., C. Egile, D.W. Hoyt, J.J. Ford, R. Li, and M.K. Rosen. 2003. NMR analysis of methyl groups at 100-500 kDa: model systems and Arp2/3 complex. *Biochemistry*. 42:8579–8586. doi:10.1021/bi034536j.

Krishnarjuna, B., G. Jaipuria, A. Thakur, P. D'Silva, and H.S. Atreya. 2011. Amino acid selective unlabeling for sequence specific resonance assignments in proteins. *J. Biomol. NMR*. 49:39–51. doi:10.1007/s10858-010-9459-z.

Krogh, A., B. Larsson, G. von Heijne, and E.L. Sonnhammer. 2001. Predicting transmembrane protein topology with a hidden Markov model: application to complete genomes. *J. Mol. Biol.* 305:567–580. doi:10.1006/jmbi.2000.4315.

Kudo, N., K. Kumagai, N. Tomishige, T. Yamaji, S. Wakatsuki, M. Nishijima, K. Hanada, and R. Kato. 2008. Structural basis for specific lipid recognition by CERT responsible for nonvesicular trafficking of ceramide. *Proc. Natl. Acad. Sci. U.S.A.* 105:488–493. doi:10.1073/pnas.0709191105.

Kulak, N.A., G. Pichler, I. Paron, N. Nagaraj, and M. Mann. 2014. Minimal, encapsulated proteomic-sample processing applied to copy-number estimation in eukaryotic cells. *Nature Methods*. 11:319–324. doi:10.1038/nmeth.2834.

Kwon, H.J., L. Abi-Mosleh, M.L. Wang, J. Deisenhofer, J.L. Goldstein, M.S. Brown, and R.E. Infante. 2009. Structure of N-Terminal Domain of NPC1 Reveals Distinct Subdomains for Binding and Transfer of Cholesterol. *Cell*. 137:1213–1224. doi:10.1016/j.cell.2009.03.049.

Lackner, M.R., S.J. Nurrish, and J.M. Kaplan. 1999. Facilitation of synaptic transmission by EGL-30 Gqalpha and EGL-8 PLCbeta: DAG binding to UNC-13 is required to stimulate acetylcholine release. *Neuron*. 24:335–346.

Lang, A.B., A.T. John Peter, P. Walter, and B. Kornmann. 2015. ER-mitochondrial junctions can be bypassed by dominant mutations in the endosomal protein Vps13. *J. Cell Biol.* 210:883–890. doi:10.1083/jcb.201502105.

Lee, I., and W. Hong. 2006. Diverse membrane-associated proteins contain a novel SMP domain. *The FASEB Journal*. 20:202–206. doi:10.1096/fj.05-4581hyp.

Lee, J.-Y., L.N. Kinch, D.M. Borek, J. Wang, J. Wang, I.L. Urbatsch, X.-S. Xie, N.V. Grishin, J.C. Cohen, Z. Otwinowski, H.H. Hobbs, and D.M. Rosenbaum. 2016. Crystal structure of the human sterol transporter ABCG5/ABCG8. *Nature*. 533:561–564. doi:10.1038/nature17666.

Lesage, P., X. Yang, and M. Carlson. 1994. Analysis of the SIP3 protein identified in a two-hybrid screen for interaction with the SNF1 protein kinase. *Nucleic Acids Res.* 22:597–603.

Lev, S. 2010. Non-vesicular lipid transport bylipid-transfer proteins and beyond. *Nat Rev Mol Cell Biol*. 11:739–750. doi:10.1038/nrm2971.

Levine, T. 2004. Short-range intracellular trafficking of small molecules across endoplasmic reticulum junctions. *Trends in Cell Biology*. 14:483–490. doi:10.1016/j.tcb.2004.07.017.

Levine, T., and C. Loewen. 2006. Inter-organelle membrane contact sites: through a glass, darkly. *Current Opinion in Cell Biology*. 18:371–378. doi:10.1016/j.ceb.2006.06.011.

Levine, T.P., and S. Munro. 2001. Dual targeting of Osh1p, a yeast homologue of oxysterol-binding protein, to both the Golgi and the nucleus-vacuole junction. *Mol. Biol. Cell*. 12:1633–1644.

Levine, T.P., and S. Patel. 2016. Signalling at membrane contact sites: two membranes come together to handle second messengers. *Current Opinion in Cell Biology*. 39:77–83. doi:10.1016/j.ceb.2016.02.011.

Levine, T.P., C.A. Wiggins, and S. Munro. 2000. Inositol phosphorylceramide synthase is located in the Golgi apparatus of Saccharomyces cerevisiae. *Mol. Biol. Cell*. 11:2267–2281.

Li, Y., and W.A. Prinz. 2004. ATP-binding cassette (ABC) transporters mediate nonvesicular, raft-

modulated sterol movement from the plasma membrane to the endoplasmic reticulum. *J. Biol. Chem.* 279:45226–45234. doi:10.1074/jbc.M407600200.

Liou, J., M.L. Kim, W.D. Heo, J.T. Jones, J.W. Myers, J.E. Ferrell, and T. Meyer. 2005. STIM is a Ca2+ sensor essential for Ca2+-store-depletion-triggered Ca2+ influx. *Curr. Biol.* 15:1235–1241. doi:10.1016/j.cub.2005.05.055.

Liscum, L., R.M. Ruggiero, and J.R. Faust. 1989. The intracellular transport of low density lipoprotein-derived cholesterol is defective in Niemann-Pick type C fibroblasts. *The Journal of Cell Biology*. 108:1625–1636.

Liu, R., P. Lu, J.W.K. Chu, and F.J. Sharom. 2008. Characterization of Fluorescent Sterol Binding to Purified Human NPC1. *J. Biol. Chem.* 284:1840–1852. doi:10.1074/jbc.M803741200.

Liu, X., and N.D. Ridgway. 2014. Characterization of the sterol and phosphatidylinositol 4-phosphate binding properties of Golgi-associated OSBP-related protein 9 (ORP9). *PLoS ONE*. 9:e108368. doi:10.1371/journal.pone.0108368.

Loewen, C.J.R. 2012. Lipids as conductors in the orchestra of life. *F1000 Biol Rep*. 4:4. doi:10.3410/B4-4.

Loewen, C.J.R., A. Roy, and T.P. Levine. 2003. A conserved ER targeting motif in three families of lipid binding proteins and in Opi1p binds VAP. *EMBO J.* 22:2025–2035. doi:10.1093/emboj/cdg201.

Loewen, C.J.R., B.P. Young, S. Tavassoli, and T.P. Levine. 2007. Inheritance of cortical ER in yeast is required for normal septin organization. *The Journal of Cell Biology*. 179:467–483. doi:10.1083/jcb.200708205.

Loewen, C.J.R., M.L. Gaspar, S.A. Jesch, C. Delon, N.T. Ktistakis, S.A. Henry, and T.P. Levine. 2004. Phospholipid metabolism regulated by a transcription factor sensing phosphatidic acid. *Science*. 304:1644–1647. doi:10.1126/science.1096083.

Lohman, D.C., F. Forouhar, E.T. Beebe, M.S. Stefely, C.E. Minogue, A. Ulbrich, J.A. Stefely, S. Sukumar, M. Luna-Sánchez, A. Jochem, S. Lew, J. Seetharaman, R. Xiao, H. Wang, M.S. Westphall, R.L. Wrobel, J.K. Everett, J.C. Mitchell, L.C. López, J.J. Coon, L. Tong, and D.J. Pagliarini. 2014. Mitochondrial COQ9 is a lipid-binding protein that associates with COQ7 to enable coenzyme Q biosynthesis. *Proc. Natl. Acad. Sci. U.S.A.* 111:E4697–705. doi:10.1073/pnas.1413128111.

Loura, L.M.S., and M. Prieto. 2011. FRET in Membrane Biophysics: An Overview. *Front Physiol*. 2:82. doi:10.3389/fphys.2011.00082.

Loura, L.M.S., M. Prieto, and F. Fernandes. 2010. Quantification of protein-lipid selectivity using FRET. *Eur. Biophys. J.* 39:565–578. doi:10.1007/s00249-010-0580-4.

Lüthy, R., J.U. Bowie, and D. Eisenberg. 1992. Assessment of protein models with three-dimensional profiles. *Nature*. 356:83–85. doi:10.1038/356083a0.

Lykidis, A. 2007. Comparative genomics and evolution of eukaryotic phospholipid biosynthesis. *Progress in Lipid Research*. 46:171–199. doi:10.1016/j.plipres.2007.03.003.

Ma, H., Y. Lou, W.H. Lin, and H.W. Xue. 2006. MORN motifs in plant PIPKs are involved in the regulation of subcellular localization and phospholipid binding. *Cell Res.* 16:466–478. doi:10.1038/sj.cr.7310058.

Maeda, K., K. Anand, A. Chiapparino, A. Kumar, M. Poletto, M. Kaksonen, and A.-C. Gavin. 2013. Interactome map uncovers phosphatidylserine transport by oxysterol-binding proteins. *Nature*. 1–8. doi:10.1038/nature12430.

Malinauskas, T., A.R. Aricescu, W. Lu, C. Siebold, and E.Y. Jones. 2011. Modular mechanism of Wnt signaling inhibition by Wnt inhibitory factor 1. *Nat Struct Mol Biol*. 18:886–893. doi:10.1038/nsmb.2081.

Malinina, L., M.L. Malakhova, A. Teplov, R.E. Brown, and D.J. Patel. 2004. Structural basis for glycosphingolipid transfer specificity. *Nature*. 430:1048–1053. doi:10.1038/nature02856.

Malsburg, von der, K., J.M. Müller, M. Bohnert, S. Oeljeklaus, P. Kwiatkowska, T. Becker, A. Loniewska-Lwowska, S. Wiese, S. Rao, D. Milenkovic, D.P. Hutu, R.M. Zerbes, A. Schulze-Specking, H.E. Meyer, J.-C. Martinou, S. Rospert, P. Rehling, C. Meisinger, M. Veenhuis, B. Warscheid, I.J. van der Klei, N. Pfanner, A. Chacinska, and M. van der Laan. 2011. Dual role of mitofilin in mitochondrial membrane organization and protein biogenesis. *Developmental Cell*. 21:694–707. doi:10.1016/j.devcel.2011.08.026.

Manford, A.G., C.J. Stefan, H.L. Yuan, J.A. MacGurn, and S.D. Emr. 2012. ER-to-Plasma Membrane Tethering Proteins Regulate Cell Signaling and ER Morphology. *Developmental Cell*. 23:1129–1140. doi:10.1016/j.devcel.2012.11.004.

Marchler-Bauer, A., M.K. Derbyshire, N.R. Gonzales, S. Lu, F. Chitsaz, L.Y. Geer, R.C. Geer, J. He, M. Gwadz, D.I. Hurwitz, C.J. Lanczycki, F. Lu, G.H. Marchler, J.S. Song, N. Thanki, Z. Wang, R.A.

Yamashita, D. Zhang, C. Zheng, and S.H. Bryant. 2015. CDD: NCBI's conserved domain database. *Nucleic Acids Res.* 43:D222–6. doi:10.1093/nar/gku1221.

Marion, D., P.C. Driscoll, L.E. Kay, P.T. Wingfield, A. Bax, A.M. Gronenborn, and G.M. Clore. 1989. Overcoming the overlap problem in the assignment of 1H NMR spectra of larger proteins by use of three-dimensional heteronuclear 1H-15N Hartmann-Hahn-multiple quantum coherence and nuclear Overhauser-multiple quantum coherence spectroscopy: application to interleukin 1 beta. *Biochemistry*. 28:6150–6156.

Maxfield, F.R., and D. Wüstner. 2012. Analysis of Cholesterol Trafficking with Fluorescent Probes. *In* Methods in Cell Biology. Elsevier. 367–393.

Maxfield, F.R., and M. Mondal. 2006. Sterol and lipid trafficking in mammalian cells. *Biochem. Soc. Trans.* 34:335–339. doi:10.1042/BST0340335.

McIntosh, L.P., and F.W. Dahlquist. 1990. Biosynthetic incorporation of 15N and 13C for assignment and interpretation of nuclear magnetic resonance spectra of proteins. *Q. Rev. Biophys.* 23:1–38.

McLean, L.R., and M.C. Phillips. 1984. Kinetics of phosphatidylcholine and lysophosphatidylcholine exchange between unilamellar vesicles. *Biochemistry*. 23:4624–4630.

McMahon, H.T., and J.L. Gallop. 2005. Membrane curvature and mechanisms of dynamic cell membrane remodelling. *Nature*. 438:590–596. doi:10.1038/nature04396.

Mesa-Arango, A.C., N. Trevijano-Contador, E. Román, R. Sánchez-Fresneda, C. Casas, E. Herrero, J.C. Argüelles, J. Pla, M. Cuenca-Estrella, and O. Zaragoza. 2014. The production of reactive oxygen species is a universal action mechanism of Amphotericin B against pathogenic yeasts and contributes to the fungicidal effect of this drug. *Antimicrobial Agents and Chemotherapy*. 58:6627–6638. doi:10.1128/AAC.03570-14.

Mesmin, B., J. Bigay, J.M. von Filseck, S. Lacas-Gervais, G. Drin, and B. Antonny. 2013. A Four-Step Cycle Driven by PI(4)P Hydrolysis Directs Sterol/PI(4)P Exchange by the ER-Golgi Tether OSBP. *Cell*. 155:830–843. doi:10.1016/j.cell.2013.09.056.

Mesmin, B., N.H. Pipalia, F.W. Lund, T.F. Ramlall, A. Sokolov, D. Eliezer, and F.R. Maxfield. 2011. STARD4 abundance regulates sterol transport and sensing. *Mol. Biol. Cell*. 22:4004–4015. doi:10.1091/mbc.E11-04-0372.

Messerle, B.A., G. Wider, G. Otting, C. Weber, and K. Wüthrich. 1989. Solvent suppression using a spin lock in 2D and 3D NMR spectroscopy with H2O solutions. *Journal of Magnetic Resonance (1969)*. 85:608–613. doi:10.1016/0022-2364(89)90252-7.

Michaud, M., V. Gros, M. Tardif, S. Brugière, M. Ferro, W.A. Prinz, A. Toulmay, J. Mathur, M. Wozny, D. Falconet, E. Maréchal, M.A. Block, and J. Jouhet. 2016. AtMic60 Is Involved in Plant Mitochondria Lipid Trafficking and Is Part of a Large Complex. *Curr. Biol.* 26:627–639. doi:10.1016/j.cub.2016.01.011.

Mikitova, V., and T.P. Levine. 2012. Analysis of the key elements of FFAT-like motifs identifies new proteins that potentially bind VAP on the ER, including two AKAPs and FAPP2. *PLoS ONE*. 7:e30455. doi:10.1371/journal.pone.0030455.

Miliara, X., J.A. Garnett, T. Tatsuta, F. Abid Ali, H. Baldie, I. Pérez-Dorado, P. Simpson, E. Yague, T. Langer, and S. Matthews. 2015. Structural insight into the TRIAP1/PRELI-like domain family of mitochondrial phospholipid transfer complexes. *EMBO reports*. 16:824–835. doi:10.15252/embr.201540229.

Min, S.-W., W.-P. Chang, and T.C. Südhof. 2007. E-Syts, a family of membranous Ca2+-sensor proteins with multiple C2 domains. *Proc. Natl. Acad. Sci. U.S.A.* 104:3823–3828. doi:10.1073/pnas.0611725104.

Mitra, K., I. Ubarretxena-Belandia, T. Taguchi, G. Warren, and D.M. Engelman. 2004. Modulation of the bilayer thickness of exocytic pathway membranes by membrane proteins rather than cholesterol. *Proc. Natl. Acad. Sci. U.S.A.* 101:4083–4088. doi:10.1073/pnas.0307332101.

Mohankumar, K.M., D.S. Currle, E. White, N. Boulos, J. Dapper, C. Eden, B. Nimmervoll, R. Thiruvenkatam, M. Connelly, T.A. Kranenburg, G. Neale, S. Olsen, Y.-D. Wang, D. Finkelstein, K. Wright, K. Gupta, D.W. Ellison, A.O. Thomas, and R.J. Gilbertson. 2015. An in vivo screen identifies ependymoma oncogenes and tumor-suppressor genes. *Nat Genet*. 47:878–887. doi:10.1038/ng.3323.

Monk, B.C., and A. Goffeau. 2008. Outwitting Multidrug Resistance to Antifungals. *Science*. 321:367–369. doi:10.1126/science.1159746.

Montefusco, D.J., N. Matmati, and Y.A. Hannun. 2014. The yeast sphingolipid signaling landscape. *Chem. Phys. Lipids*. 177:26–40. doi:10.1016/j.chemphyslip.2013.10.006.

Montigny, C., J. Lyons, P. Champeil, P. Nissen, and G. Lenoir. 2015. On the molecular mechanism of flippase- and scramblase-mediated phospholipid transport. *Biochim. Biophys. Acta*.

doi:10.1016/j.bbalip.2015.12.020.

Mor, V., A. Rella, A.M. Farnoud, A. Singh, M. Munshi, A. Bryan, S. Naseem, J.B. Konopka, I. Ojima, E. Bullesbach, A. Ashbaugh, M.J. Linke, M. Cushion, M. Collins, H.K. Ananthula, L. Sallans, P.B. Desai, N.P. Wiederhold, A.W. Fothergill, W.R. Kirkpatrick, T. Patterson, L.H. Wong, S. Sinha, G. Giaever, C. Nislow, P. Flaherty, X. Pan, G.V. Cesar, P. de Melo Tavares, S. Frases, K. Miranda, M.L. Rodrigues, C. Luberto, L. Nimrichter, and M. Del Poeta. 2015. Identification of a New Class of Antifungals Targeting the Synthesis of Fungal Sphingolipids. *MBio*. 6:e00647. doi:10.1128/mBio.00647-15.

Mora-Duarte, J., R. Betts, C. Rotstein, A.L. Colombo, L. Thompson-Moya, J. Smietana, R. Lupinacci, C. Sable, N. Kartsonis, J. Perfect, Caspofungin Invasive Candidiasis Study Group. 2002. Comparison of caspofungin and amphotericin B for invasive candidiasis. *N. Engl. J. Med.* 347:2020–2029. doi:10.1056/NEJMoa021585.

Moser von Filseck, J., A. Čopič, V. Delfosse, S. Vanni, C.L. Jackson, W. Bourguet, and G. Drin. 2015a. INTRACELLULAR TRANSPORT. Phosphatidylserine transport by ORP/Osh proteins is driven by phosphatidylinositol 4-phosphate. *Science*. 349:432–436. doi:10.1126/science.aab1346.

Moser von Filseck, J., S. Vanni, B. Mesmin, B. Antonny, and G. Drin. 2015b. A phosphatidylinositol-4-phosphate powered exchange mechanism to create a lipid gradient between membranes. *Nat Commun*. 6:6671. doi:10.1038/ncomms7671.

Mount, D.W. 2004. Bioinformatics. CSHL Press. 1 pp.

Mouri, R., K. Konoki, N. Matsumori, T. Oishi, and M. Murata. 2008. Complex formation of amphotericin B in sterol-containing membranes as evidenced by surface plasmon resonance. *Biochemistry*. 47:7807–7815. doi:10.1021/bi800334p.

Möbius, W., E. van Donselaar, Y. Ohno-Iwashita, Y. Shimada, H.F.G. Heijnen, J.W. Slot, and H.J. Geuze. 2003. Recycling compartments and the internal vesicles of multivesicular bodies harbor most of the cholesterol found in the endocytic pathway. *Traffic*. 4:222–231.

Muir, A., F.M. Roelants, G. Timmons, K.L. Leskoske, and J. Thorner. 2015. Down-regulation of TORC2-Ypk1 signaling promotes MAPK-independent survival under hyperosmotic stress. *Elife*. 4:12. doi:10.7554/eLife.09336.

Muir, A., S. Ramachandran, F.M. Roelants, G. Timmons, and J. Thorner. 2014. TORC2-dependent protein kinase Ypk1 phosphorylates ceramide synthase to stimulate synthesis of complex sphingolipids. *Elife*. 3:944. doi:10.7554/eLife.03779.

Mukherjee, S., X. Zha, I. Tabas, and F.R. Maxfield. 1998. Cholesterol distribution in living cells: fluorescence imaging using dehydroergosterol as a fluorescent cholesterol analog. *Biophys. J.* 75:1915–1925. doi:10.1016/S0006-3495(98)77632-5.

Munro, S. 2003. Lipid rafts: elusive or illusive? *Cell*. 115:377–388.

Murley, A., R.D. Sarsam, A. Toulmay, J. Yamada, W.A. Prinz, and J. Nunnari. 2015. Ltc1 is an ER-localized sterol transporter and a component of ER-mitochondria and ER-vacuole contacts. *The Journal of Cell Biology*. 209:539–548. doi:10.1083/jcb.201502033.

Murphy, S.E., and T.P. Levine. 2016. VAP, a Versatile Access Point for the Endoplasmic Reticulum: Review and analysis of FFAT-like motifs in the VAPome. *Biochim. Biophys. Acta*. doi:10.1016/j.bbalip.2016.02.009.

Müller, A., R.M. MacCallum, and M.J.E. Sternberg. 2002. Structural characterization of the human proteome. *Genome Res.* 12:1625–1641. doi:10.1101/gr.221202.

Müller, P., and A. Herrmann. 2002. Rapid transbilayer movement of spin-labeled steroids in human erythrocytes and in liposomes. *Biophys. J.* 82:1418–1428. doi:10.1016/S0006-3495(02)75496-9.

Nagiec, M.M., E.E. Nagiec, J.A. Baltisberger, G.B. Wells, R.L. Lester, and R.C. Dickson. 1997. Sphingolipid synthesis as a target for antifungal drugs. Complementation of the inositol phosphorylceramide synthase defect in a mutant strain of Saccharomyces cerevisiae by the AUR1 gene. *J. Biol. Chem.* 272:9809–9817.

Nakase, M., M. Tani, T. Morita, H.K. Kitamoto, J. Kashiwazaki, T. Nakamura, A. Hosomi, N. Tanaka, and K. Takegawa. 2010. Mannosylinositol phosphorylceramide is a major sphingolipid component and is required for proper localization of plasma-membrane proteins in Schizosaccharomyces pombe. *Journal of Cell Science*. 123:1578–1587. doi:10.1242/jcs.059139.

Nguyen, T.T., A. Lewandowska, J.-Y. Choi, D.F. Markgraf, M. Junker, M. Bilgin, C.S. Ejsing, D.R. Voelker, T.A. Rapoport, and J.M. Shaw. 2012. Gem1 and ERMES do not directly affect phosphatidylserine transport from ER to mitochondria or mitochondrial inheritance. *Traffic*. 13:880–890. doi:10.1111/j.1600-0854.2012.01352.x.

Nietlispach, D., Y. Ito, and E.D. Laue. 2002. A novel approach for the sequential backbone assignment of larger proteins: selective intra-HNCA and DQ-HNCA. *J. Am. Chem. Soc.* 124:11199–11207.

Niles, B.J., and T. Powers. 2012. Plasma membrane proteins Slm1 and Slm2 mediate activation of the AGC kinase Ypk1 by TORC2 and sphingolipids in S. cerevisiae. *Cell Cycle*. 11:3745–3749. doi:10.4161/cc.21752.

Novick, P., C. Field, and R. Schekman. 1980. Identification of 23 complementation groups required for post-translational events in the yeast secretory pathway. *Cell*. 21:205–215.

Odabasi, Z., A. Karaalp, H. Cermik, J. Mohr, E.T. Tigen, M. Koc, and V. Korten. 2009. Reduction of amphotericin B-induced renal tubular apoptosis by N-acetylcysteine. *Antimicrobial Agents and Chemotherapy*. 53:3100–3102. doi:10.1128/AAC.00001-09.

Ohsaki, Y., M. Suzuki, and T. Fujimoto. 2014. Open questions in lipid droplet biology. *Chem. Biol.* 21:86–96. doi:10.1016/j.chembiol.2013.08.009.

Olkkonen, V.M. 2015. OSBP-Related Protein Family in Lipid Transport Over Membrane Contact Sites. *Lipid Insights*. 8:1–9. doi:10.4137/LPI.S31726.

Orr-Weaver, T.L., J.W. Szostak, and R.J. Rothstein. 1983. Genetic applications of yeast transformation with linear and gapped plasmids. *Meth. Enzymol.* 101:228–245.

Oura, M., T.H. Sternberg, and E.T. Wright. 1955. A new antifungal antibiotic, amphotericin B. *Antibiot Annu*. 3:566–573.

Pagano, R.E. 1990. Lipid traffic in eukaryotic cells: mechanisms for intracellular transport and organelle-specific enrichment of lipids. *Current Opinion in Cell Biology*. 2:652–663.

Palacios, D.S., I. Dailey, D.M. Siebert, B.C. Wilcock, and M.D. Burke. 2011. Synthesis-enabled functional group deletions reveal key underpinnings of amphotericin B ion channel and antifungal activities. *Proc. Natl. Acad. Sci. U.S.A.* 108:6733–6738. doi:10.1073/pnas.1015023108.

Palacios, D.S., T.M. Anderson, and M.D. Burke. 2007. A Post-PKS Oxidation of the Amphotericin B Skeleton Predicted to be Critical for Channel Formation Is Not Required for Potent Antifungal Activity. *J. Am. Chem. Soc.* 129:13804–13805. doi:10.1021/ja075739o.

Panavas, T., C. Sanders, and T.R. Butt. 2009. SUMO fusion technology for enhanced protein production in prokaryotic and eukaryotic expression systems. *Methods Mol. Biol.* 497:303–317. doi:10.1007/978-1-59745-566-4_20.

Panchenko, A.R. 2003. Finding weak similarities between proteins by sequence profile comparison. *Nucleic Acids Res.* 31:683–689.

Park, C.Y., P.J. Hoover, F.M. Mullins, P. Bachhawat, E.D. Covington, S. Raunser, T. Walz, K.C. Garcia, R.E. Dolmetsch, and R.S. Lewis. 2009. STIM1 clusters and activates CRAC channels via direct binding of a cytosolic domain to Orai1. *Cell*. 136:876–890. doi:10.1016/j.cell.2009.02.014.

Park, E., J.-F. Ménétret, J.C. Gumbart, S.J. Ludtke, W. Li, A. Whynot, T.A. Rapoport, and C.W. Akey. 2014. Structure of the SecY channel during initiation of protein translocation. *Nature*. 506:102–106. doi:10.1038/nature12720.

Peretti, D., N. Dahan, E. Shimoni, K. Hirschberg, and S. Lev. 2008. Coordinated lipid transfer between the endoplasmic reticulum and the Golgi complex requires the VAP proteins and is essential for Golgi-mediated transport. *Mol. Biol. Cell*. 19:3871–3884. doi:10.1091/mbc.E08-05-0498.

Pernas, L., and L. Scorrano. 2016. Mito-Morphosis: Mitochondrial Fusion, Fission, and Cristae Remodeling as Key Mediators of Cellular Function. *Annu. Rev. Physiol.* 78:505–531. doi:10.1146/annurev-physiol-021115-105011.

Pervushin, K., R. Riek, G. Wider, and K. Wüthrich. 1997. Attenuated T2 relaxation by mutual cancellation of dipole-dipole coupling and chemical shift anisotropy indicates an avenue to NMR structures of very large biological macromolecules in solution. *Proc. Natl. Acad. Sci. U.S.A*. 94:12366–12371.

Petkovic, M., A. Jemaiel, F. Daste, C.G. Specht, I. Izeddin, D. Vorkel, J.-M. Verbavatz, X. Darzacq, A. Triller, K.H. Pfenninger, D. Tareste, C.L. Jackson, and T. Galli. 2014. The SNARE Sec22b has a non-fusogenic function in plasma membrane expansion. *Nat Cell Biol*. doi:10.1038/ncb2937.

Pfenninger, K.H. 2009. Plasma membrane expansion: a neuron's Herculean task. *Nat Rev Neurosci*. 10:251–261. doi:10.1038/nrn2593.

Phillips, A.J., I. Sudbery, and M. Ramsdale. 2003. Apoptosis induced by environmental stresses and amphotericin B in Candida albicans. *Proc. Natl. Acad. Sci. U.S.A.* 100:14327–14332. doi:10.1073/pnas.2332326100.

Phillips, M.J., and G.K. Voeltz. 2015. Structure and function of ER membrane contact sites with other organelles. *Nat Rev Mol Cell Biol*. doi:10.1038/nrm.2015.8.

Platt, F.M. 2014. Sphingolipid lysosomal storage disorders. *Nature*. 510:68–75. doi:10.1038/nature13476.

Porter, K.R., and G.E. Palade. 1957. Studies on the endoplasmic reticulum. III. Its form and distribution in striated muscle cells. *J Biophys Biochem Cytol*. 3:269–300.

Pozniakovsky, A.I., D.A. Knorre, O.V. Markova, A.A. Hyman, V.P. Skulachev, and F.F. Severin. 2005. Role of mitochondria in the pheromone- and amiodarone-induced programmed death of yeast. *The Journal of Cell Biology*. 168:257–269. doi:10.1083/jcb.200408145.

Prinz, W.A. 2014. Bridging the gap: Membrane contact sites in signaling, metabolism, and organelle dynamics. *The Journal of Cell Biology*. 205:759–769. doi:10.1083/jcb.201401126.

Radhakrishnan, A., J.L. Goldstein, J.G. McDonald, and M.S. Brown. 2008. Switch-like control of SREBP-2 transport triggered by small changes in ER cholesterol: a delicate balance. *Cell Metab.* 8:512–521. doi:10.1016/j.cmet.2008.10.008.

Raiborg, C., E.M. Wenzel, N.M. Pedersen, H. Olsvik, K.O. Schink, S.W. Schultz, M. Vietri, V. Nisi, C. Bucci, A. Brech, T. Johansen, and H. Stenmark. 2015. Repeated ER-endosome contacts promote endosome translocation and neurite outgrowth. *Nature*. 520:234–238. doi:10.1038/nature14359.

Ramachandran, G.N., C. Ramakrishnan, and V. Sasisekharan. 1963. Stereochemistry of polypeptide chain configurations. *J. Mol. Biol.* 7:95–99.

Raychaudhuri, S., Y.J. Im, J.H. Hurley, and W.A. Prinz. 2006. Nonvesicular sterol movement from plasma membrane to ER requires oxysterol-binding protein-related proteins and phosphoinositides. *The Journal of Cell Biology*. 173:107–119. doi:10.1083/jcb.200510084.

Reinisch, K.M., and P. De Camilli. 2015. SMP-domain proteins at membrane contact sites: Structure and function. *Biochim. Biophys. Acta*. doi:10.1016/j.bbalip.2015.12.003.

Rhee, J.S., A. Betz, S. Pyott, K. Reim, F. Varoqueaux, I. Augustin, D. Hesse, T.C. Südhof, M. Takahashi, C. Rosenmund, and N. Brose. 2002. Beta phorbol ester- and diacylglycerol-induced augmentation of transmitter release is mediated by Munc13s and not by PKCs. *Cell*. 108:121–133.

Ridgway, N.D., P.A. Dawson, Y.K. Ho, M.S. Brown, and J.L. Goldstein. 1992. Translocation of oxysterol binding protein to Golgi apparatus triggered by ligand binding. *The Journal of Cell Biology*. 116:307–319.

Riezman, H. 2006. Organization and functions of sphingolipid biosynthesis in yeast. *Biochem. Soc. Trans.* 34:367–369. doi:10.1042/BST0340367.

Rocha, N., C. Kuijl, R. van der Kant, L. Janssen, D. Houben, H. Janssen, W. Zwart, and J. Neefjes. 2009. Cholesterol sensor ORP1L contacts the ER protein VAP to control Rab7-RILP-p150 Glued and late endosome positioning. *The Journal of Cell Biology*. 185:1209–1225. doi:10.1083/jcb.200811005.

Roelants, F.M., D.K. Breslow, A. Muir, J.S. Weissman, and J. Thorner. 2011. Protein kinase Ypk1 phosphorylates regulatory proteins Orm1 and Orm2 to control sphingolipid homeostasis in Saccharomyces cerevisiae. *Proc. Natl. Acad. Sci. U.S.A.* 108:19222–19227. doi:10.1073/pnas.1116948108.

Roy, A., A. Kucukural, and Y. Zhang. 2010. I-TASSER: a unified platform for automated protein structure and function prediction. *Nat Protoc*. 5:725–738. doi:10.1038/nprot.2010.5.

Rychlewski, L., B. Zhang, and A. Godzik. 1998. Fold and function predictions for Mycoplasma genitalium proteins. *Fold Des*. 3:229–238. doi:10.1016/S1359-0278(98)00034-0.

Sacchettini, J.C., J.I. Gordon, and L.J. Banaszak. 1989. Crystal structure of rat intestinal fatty-acid-binding protein. Refinement and analysis of the Escherichia coli-derived protein with bound palmitate. *J. Mol. Biol.* 208:327–339. doi:10.1016/0022-2836(89)90392-6.

Saheki, Y., X. Bian, C.M. Schauder, Y. Sawaki, M.A. Surma, C. Klose, F. Pincet, K.M. Reinisch, and P. De Camilli. 2016. Control of plasma membrane lipid homeostasis by the extended synaptotagmins. *Nat Cell Biol*. doi:10.1038/ncb3339.

Sali, A., and T.L. Blundell. 1993. Comparative protein modelling by satisfaction of spatial restraints. *J. Mol. Biol.* 234:779–815. doi:10.1006/jmbi.1993.1626.

Santos, A.X.S., and H. Riezman. 2012. Yeast as a model system for studying lipid homeostasis and function. *FEBS Letters*. 586:2858–2867. doi:10.1016/j.febslet.2012.07.033.

Sanyal, A.J. 2005. Mechanisms of Disease: pathogenesis of nonalcoholic fatty liver disease. *Nat Clin Pract Gastroenterol Hepatol*. 2:46–53. doi:10.1038/ncpgasthep0084.

Sanyal, S., and A.K. Menon. 2009. Flipping lipids: why an“ what”s the reason for? *ACS Chem. Biol.* 4:895–909. doi:10.1021/cb900163d.

Sattler, M., J. Schleucher, and C. Griesinger. 1999. Heteronuclear multidimensional NMR experiments for the structure determination of proteins in solution employing pulsed field gradients. *Progress in Nuclear Magnetic Resonance Spectroscopy*. 34:93–158. doi:10.1016/S0079-6565(98)00025-9.

Schaaf, G., E.A. Ortlund, K.R. Tyeryar, C.J. Mousley, K.E. Ile, T.A. Garrett, J. Ren, M.J. Woolls, C.R.H. Raetz, M.R. Redinbo, and V.A. Bankaitis. 2008. Functional Anatomy of Phospholipid Binding and Regulation of Phosphoinositide Homeostasis by Proteins of the Sec14 Superfamily. *Molecular*

Cell. 29:191–206. doi:10.1016/j.molcel.2007.11.026.

Schauder, C.M., X. Wu, Y. Saheki, P. Narayanaswamy, F. Torta, M.R. Wenk, P. De Camilli, and K.M. Reinisch. 2014. Structure of a lipid-bound extended synaptotagmin indicates a role in lipid transfer. *Nature*. 510:552–555. doi:10.1038/nature13269.

Schneiter, R., B. Brügger, R. Sandhoff, G. Zellnig, A. Leber, M. Lampl, K. Athenstaedt, C. Hrastnik, S. Eder, G. Daum, F. Paltauf, F.T. Wieland, and S.D. Kohlwein. 1999. Electrospray ionization tandem mass spectrometry (ESI-MS/MS) analysis of the lipid molecular species composition of yeast subcellular membranes reveals acyl chain-based sorting/remodeling of distinct molecular species en route to the plasma membrane. *The Journal of Cell Biology*. 146:741–754.

Schrick, K., M. Bruno, A. Khosla, P.N. Cox, S.A. Marlatt, R.A. Roque, H.C. Nguyen, C. He, M.P. Snyder, D. Singh, and G. Yadav. 2014. Shared functions of plant and mammalian StAR-related lipid transfer (START) domains in modulating transcription factor activity. *BMC Biol.* 12:70. doi:10.1186/s12915-014-0070-8.

Schroeder, F., P. Butko, G. Nemecz, and T.J. Scallen. 1990. Interaction of fluorescent delta 5,7,9(11),22-ergostatetraen-3 beta-ol with sterol carrier protein-2. *J. Biol. Chem.* 265:151–157.

Schulz, T.A., M.G. Choi, S. Raychaudhuri, J.A. Mears, R. Ghirlando, J.E. Hinshaw, and W.A. Prinz. 2009. Lipid-regulated sterol transfer between closely apposed membranes by oxysterol-binding protein homologues. *The Journal of Cell Biology*. 187:889–903. doi:10.1083/jcb.200905007.

Seibel, N.M., J. Eljouni, M.M. Nalaskowski, and W. Hampe. 2007. Nuclear localization of enhanced green fluorescent protein homomultimers. *Anal. Biochem.* 368:95–99. doi:10.1016/j.ab.2007.05.025.

Ségui, B., V. Allen-Baume, and S. Cockcroft. 2002. Phosphatidylinositol transfer protein beta displays minimal sphingomyelin transfer activity and is not required for biosynthesis and trafficking of sphingomyelin. *Biochem. J.* 366:23–34. doi:10.1042/BJ20020317.

Sharma, S., M. Alfatah, V.K. Bari, Y. Rawal, S. Paul, and K. Ganesan. 2014. Sphingolipid biosynthetic pathway genes FEN1 and SUR4 modulate amphotericin B resistance. *Antimicrobial Agents and Chemotherapy*. 58:2409–2414. doi:10.1128/AAC.02130-13.

Sharpe, H.J., T.J. Stevens, and S. Munro. 2010. A comprehensive comparison of transmembrane domains reveals organelle-specific properties. *Cell*. 142:158–169. doi:10.1016/j.cell.2010.05.037.

Shi, J., T.L. Blundell, and K. Mizuguchi. 2001. FUGUE: sequence-structure homology recognition using environment-specific substitution tables and structure-dependent gap penalties. *J. Mol. Biol.* 310:243–257. doi:10.1006/jmbi.2001.4762.

Shibata, Y., G.K. Voeltz, and T.A. Rapoport. 2006. Rough Sheets and Smooth Tubules. *Cell*. 126:435–439. doi:10.1016/j.cell.2006.07.019.

Sikorski, R.S., and P. Hieter. 1989. A system of shuttle vectors and yeast host strains designed for efficient manipulation of DNA in Saccharomyces cerevisiae. *Genetics*. 122:19–27.

Simanshu, D.K., R.K. Kamlekar, D.S. Wijesinghe, X. Zou, X. Zhai, S.K. Mishra, J.G. Molotkovsky, L. Malinina, E.H. Hinchcliffe, C.E. Chalfant, R.E. Brown, and D.J. Patel. 2013. Non-vesicular trafficking by a ceramide-1-phosphate transfer protein regulates eicosanoids. *Nature*. 500:463–467. doi:10.1038/nature12332.

Singh, M.V., and P.A. Weil. 2002. A method for plasmid purification directly from yeast. *Anal. Biochem.* 307:13–17.

Skehel, P.A., K.C. Martin, E.R. Kandel, and D. Bartsch. 1995. A VAMP-binding protein from Aplysia required for neurotransmitter release. *Science*. 269:1580–1583.

Skinner, S.P., B.T. Goult, R.H. Fogh, W. Boucher, T.J. Stevens, E.D. Laue, and G.W. Vuister. 2015. Structure calculation, refinement and validation using CcpNmr Analysis. *Acta Crystallogr. D Biol. Crystallogr.* 71:154–161. doi:10.1107/S1399004714026662.

Sleight, R.G., and R.E. Pagano. 1983. Rapid appearance of newly synthesized phosphatidylethanolamine at the plasma membrane. *J. Biol. Chem.* 258:9050–9058.

Slotte, J.P. 2013. Biological functions of sphingomyelins. *Progress in Lipid Research*. 52:424–437. doi:10.1016/j.plipres.2013.05.001.

Soding, J. 2005. Protein homology detection by HMM-HMM comparison. *Bioinformatics*. 21:951–960. doi:10.1093/bioinformatics/bti125.

Soding, J., A. Biegert, and A.N. Lupas. 2005. The HHpred interactive server for protein homology detection and structure prediction. *Nucleic Acids Res.* 33:W244–W248. doi:10.1093/nar/gki408.

Sokolov, S., D. Knorre, E. Smirnova, O. Markova, A. Pozniakovsky, V. Skulachev, and F. Severin. 2006. Ysp2 mediates death of yeast induced by amiodarone or intracellular acidification. *Biochimica et Biophysica Acta (BBA) - Bioenergetics*. 1757:1366–1370. doi:10.1016/j.bbabio.2006.07.005.

Steck, T.L., J. Ye, and Y. Lange. 2002. Probing red cell membrane cholesterol movement with cyclodextrin. *Biophys. J.* 83:2118–2125. doi:10.1016/S0006-3495(02)73972-6.

Stefan, C.J., A.G. Manford, D. Baird, J. Yamada-Hanff, Y. Mao, and S.D. Emr. 2011. Osh Proteins Regulate Phosphoinositide Metabolismat ER-Plasma Membrane Contact Sites. *Cell*. 144:389–401. doi:10.1016/j.cell.2010.12.034.

Stevens, B.J., and J.G. White. 1979. Computer reconstruction of mitochondria from yeast. *Meth. Enzymol.* 56:718–728.

Stoica, R., K.J. De Vos, S. Paillusson, S. Mueller, R.M. Sancho, K.-F. Lau, G. Vizcay-Barrena, W.-L. Lin, Y.-F. Xu, J. Lewis, D.W. Dickson, L. Petrucelli, J.C. Mitchell, C.E. Shaw, and C.C.J. Miller. 2014. ER-mitochondria associations are regulated by the VAPB-PTPIP51 interaction and are disrupted by ALS/FTD-associated TDP-43. *Nat Commun*. 5:3996. doi:10.1038/ncomms4996.

Sullivan, D.P., A.G. Georgiev, and A.K. Menon. 2009. Tritium suicide selection identifies proteins involved in the uptake and intracellular transport of sterols in Saccharomyces cerevisiae. 8:161–169. doi:10.1128/EC.00135-08.

Sullivan, D.P., H. Ohvo-Rekilä, N.A. Baumann, C.T. Beh, and A.K. Menon. 2006. Sterol trafficking between the endoplasmic reticulum and plasma membrane in yeast. *Biochem. Soc. Trans.* 34:356–358. doi:10.1042/BST0340356.

Suzuki, J., E. Imanishi, and S. Nagata. 2014. Exposure of phosphatidylserine by Xk-related protein family members during apoptosis. *J. Biol. Chem.* 289:30257–30267. doi:10.1074/jbc.M114.583419.

Takamori, S., M. Holt, K. Stenius, E.A. Lemke, M. Grønborg, D. Riedel, H. Urlaub, S. Schenck, B. Brügger, P. Ringler, S.A. Müller, B. Rammner, F. Gräter, J.S. Hub, B.L. De Groot, G. Mieskes, Y. Moriyama, J. Klingauf, H. Grubmüller, J. Heuser, F. Wieland, and R. Jahn. 2006. Molecular anatomy of a trafficking organelle. *Cell*. 127:831–846. doi:10.1016/j.cell.2006.10.030.

Takeshima, H., M. Hoshijima, and L.-S. Song. 2015. Ca^{2+} microdomains organized by junctophilins. *Cell Calcium*. 58:349–356. doi:10.1016/j.ceca.2015.01.007.

Takeshima, H., S. Komazaki, M. Nishi, M. Iino, and K. Kangawa. 2000. Junctophilins: a novel family of junctional membrane complex proteins. *Molecular Cell*. 6:11–22.

Tall, A. 1995. Plasma lipid transfer proteins. *Annu. Rev. Biochem.* 64:235–257. doi:10.1146/annurev.bi.64.070195.001315.

Tang, F., Y. Peng, J.J. Nau, E.J. Kauffman, and L.S. Weisman. 2006. Vac8p, an armadillo repeat protein, coordinates vacuole inheritance with multiple vacuolar processes. *Traffic*. 7:1368–1377. doi:10.1111/j.1600-0854.2006.00458.x.

Tatsuta, T., M. Scharwey, and T. Langer. 2014. Mitochondrial lipid trafficking. *Trends in Cell Biology*. 24:44–52. doi:10.1016/j.tcb.2013.07.011.

Tavassoli, S., J.T. Chao, B.P. Young, R.C. Cox, W.A. Prinz, A.I.P.M. de Kroon, and C.J.R. Loewen. 2013. Plasma membrane--endoplasmic reticulum contact sites regulate phosphatidylcholine synthesis. *EMBO reports*. 14:434–440. doi:10.1038/embor.2013.36.

Teale, F.W., and G. Weber. 1957. Ultraviolet fluorescence of the aromatic amino acids. *Biochem. J.* 65:476–482.

Thiam, A.R., R.V. Farese, and T.C. Walther. 2013. The biophysics and cell biology of lipid droplets. *Nat Rev Mol Cell Biol*. 14:775–786. doi:10.1038/nrm3699.

Thorsell, A.-G., W.H. Lee, C. Persson, M.I. Siponen, M. Nilsson, R.D. Busam, T. Kotenyova, H. Schüler, and L. Lehtiö. 2011. Comparative Structural Analysis of Lipid Binding START Domains. *PLoS ONE*. 6:e19521. doi:10.1371/journal.pone.0019521.

Tilley, S.J., A. Skippen, J. Murray-Rust, P.M. Swigart, A. Stewart, C.P. Morgan, S. Cockcroft, and N.Q. McDonald. 2004. Structure-function analysis of human [corrected] phosphatidylinositol transfer protein alpha bound to phosphatidylinositol. *Structure*. 12:317–326. doi:10.1016/j.str.2004.01.013.

Tkach, J.M., A. Yimit, A.Y. Lee, M. Riffle, M. Costanzo, D. Jaschob, J.A. Hendry, J. Ou, J. Moffat, C. Boone, T.N. Davis, C. Nislow, and G.W. Brown. 2012. Dissecting DNA damage response pathways by analysing protein localization and abundance changes during DNA replication stress. *Nat Cell Biol*. 14:966–976. doi:10.1038/ncb2549.

Tonelli, A. 2014. Non-Stoichiometric Polymer-Cyclodextrin Inclusion Compounds: Constraints Placed on Un-Included Chain Portions Tethered at Both Ends and Their Relation to Polymer Brushes. *Polymers*. 6:2166–2185. doi:10.3390/polym6082166.

Tong, J., H. Yang, H. Yang, S.H. Eom, and Y.J. Im. 2013. Structure of Osh3 reveals a conserved mode of phosphoinositide binding in oxysterol-binding proteins. *Structure*. 21:1203–1213. doi:10.1016/j.str.2013.05.007.

Tong, Y., Y. Sun, X. Tian, T. Zhou, H. Wang, T. Zhang, R. Zhan, L. Zhao, B. Kuerban, Z. Li, Q. Wang,

Y. Jin, D. Fan, X. Guo, H. Han, S. Qin, and D. Chui. 2015. Phospholipid transfer protein (PLTP) deficiency accelerates memory dysfunction through altering amyloid precursor protein (APP) processing in a mouse model of Alzheimer's disease. *Hum. Mol. Genet.* 24:5388–5403. doi:10.1093/hmg/ddv262.

Toulmay, A., and W.A. Prinz. 2012. A conserved membrane-binding domain targets proteins to organelle contact sites. *Journal of Cell Science*. 125:49–58. doi:10.1242/jcs.085118.

Tsujishita, Y., and J.H. Hurley. 2000. Structure and lipid transport mechanism of a StAR-related domain. *Nat. Struct. Biol.* 7:408–414. doi:10.1038/75192.

Tugarinov, V., V. Kanelis, and L.E. Kay. 2006. Isotope labeling strategies for the study of high-molecular-weight proteins by solution NMR spectroscopy. *Nat Protoc*. 1:749–754. doi:10.1038/nprot.2006.101.

Uetz, P., L. Giot, G. Cagney, T.A. Mansfield, R.S. Judson, J.R. Knight, D. Lockshon, V. Narayan, M. Srinivasan, P. Pochart, A. Qureshi-Emili, Y. Li, B. Godwin, D. Conover, T. Kalbfleisch, G. Vijayadamodar, M. Yang, M. Johnston, S. Fields, and J.M. Rothberg. 2000. A comprehensive analysis of protein-protein interactions in Saccharomyces cerevisiae. *Nature*. 403:623–627. doi:10.1038/35001009.

Uhlén, M., L. Fagerberg, B.M. Hallström, C. Lindskog, P. Oksvold, A. Mardinoglu, Å. Sivertsson, C. Kampf, E. Sjöstedt, A. Asplund, I. Olsson, K. Edlund, E. Lundberg, S. Navani, C.A.-K. Szigyarto, J. Odeberg, D. Djureinovic, J.O. Takanen, S. Hober, T. Alm, P.-H. Edqvist, H. Berling, H. Tegel, J. Mulder, J. Rockberg, P. Nilsson, J.M. Schwenk, M. Hamsten, K. von Feilitzen, M. Forsberg, L. Persson, F. Johansson, M. Zwahlen, G. von Heijne, J. Nielsen, and F. Pontén. 2015. Proteomics. Tissue-based map of the human proteome. *Science*. 347:1260419. doi:10.1126/science.1260419.

Urbani, L., and R.D. Simoni. 1990. Cholesterol and vesicular stomatitis virus G protein take separate routes from the endoplasmic reticulum to the plasma membrane. *J. Biol. Chem.* 265:1919–1923.

van der Kant, R., A. Fish, L. Janssen, H. Janssen, S. Krom, N. Ho, T. Brummelkamp, J. Carette, N. Rocha, and J. Neefjes. 2013. Late endosomal transport and tethering are coupled processes controlled by RILP and the cholesterol sensor ORP1L. *Journal of Cell Science*. 126:3462–3474. doi:10.1242/jcs.129270.

van Meer, G., D.R. Voelker, and G.W. Feigenson. 2008. Membrane lipids: Where they are and how they behave. *Nat Rev Mol Cell Biol*. 9:112–124. doi:10.1038/nrm2330.

Vanni, S., L. Vamparys, R. Gautier, G. Drin, C. Etchebest, P.F.J. Fuchs, and B. Antonny. 2013. Amphipathic lipid packing sensor motifs: probing bilayer defects with hydrophobic residues. *Biophys. J.* 104:575–584. doi:10.1016/j.bpj.2012.11.3837.

Varbiro, G., A. Toth, A. Tapodi, B. Veres, B. Sumegi, and F. Gallyas. 2003. Concentration dependent mitochondrial effect of amiodarone. *Biochem. Pharmacol.* 65:1115–1128.

Vassilev, B., H. Sihto, S. Li, M. Hölttä-Vuori, J. Ilola, J. Lundin, J. Isola, P.-L. Kellokumpu-Lehtinen, H. Joensuu, and E. Ikonen. 2015. Elevated Levels of StAR-Related Lipid Transfer Protein 3 Alter Cholesterol Balance and Adhesiveness of Breast Cancer CellsPotential Mechanisms Contributing to Progression of HER2-Positive Breast Cancers. *The American Journal of Pathology*. 185:987–1000. doi:10.1016/j.ajpath.2014.12.018.

Vincent, B.M., A.K. Lancaster, R. Scherz-Shouval, L. Whitesell, and S. Lindquist. 2013. Fitness trade-offs restrict the evolution of resistance to amphotericin B. *PLoS Biol.* 11:e1001692. doi:10.1371/journal.pbio.1001692.

Vitner, E.B., F.M. Platt, and A.H. Futerman. 2010. Common and uncommon pathogenic cascades in lysosomal storage diseases. *J. Biol. Chem.* 285:20423–20427. doi:10.1074/jbc.R110.134452.

Voelker, D.R. 2009. Genetic and Biochemical Analysis of Non-Vesicular Lipid Traffic. *Annu. Rev. Biochem.* 78:827–856. doi:10.1146/annurev.biochem.78.081307.112144.

Volmer, A.A., A.M. Szpilman, and E.M. Carreira. 2010. Synthesis and biological evaluation of amphotericin B derivatives. *Nat. Prod. Rep.* 27:1329. doi:10.1039/b820743g.

Wach, A., A. Brachat, R. Pöhlmann, and P. Philippsen. 1994. New heterologous modules for classical or PCR-based gene disruptions in Saccharomyces cerevisiae. *Yeast*. 10:1793–1808.

Walev, I., S.C. Bhakdi, F. Hofmann, N. Djonder, A. Valeva, K. Aktories, and S. Bhakdi. 2001. Delivery of proteins into living cells by reversible membrane permeabilization with streptolysin-O. *Proc. Natl. Acad. Sci. U.S.A.* 98:3185–3190. doi:10.1073/pnas.051429498.

Walsh, C.M., M. Chvanov, L.P. Haynes, O.H. Petersen, A.V. Tepikin, and R.D. Burgoyne. 2010. Role of phosphoinositides in STIM1 dynamics and store-operated calcium entry. *Biochem. J.* 425:159–168. doi:10.1042/BJ20090884.

Walther, T.C., and R.V. Farese. 2012. Lipid droplets and cellular lipid metabolism. *Annu. Rev. Biochem.* 81:687–714. doi:10.1146/annurev-biochem-061009-102430.

Walther, T.C., J.H. Brickner, P.S. Aguilar, S. Bernales, C. Pantoja, and P. Walter. 2006. Eisosomes mark static sites of endocytosis. *Nature*. 439:998–1003. doi:10.1038/nature04472.

Wang, Y., X. Deng, S. Mancarella, E. Hendron, S. Eguchi, J. Soboloff, X.D. Tang, and D.L. Gill. 2010. The calcium store sensor, STIM1, reciprocally controls Orai and CaV1.2 channels. *Science*. 330:105–109. doi:10.1126/science.1191086.

Waterhouse, A.M., J.B. Procter, D.M.A. Martin, M. Clamp, and G.J. Barton. 2009. Jalview Version 2--a multiple sequence alignment editor and analysis workbench. *Bioinformatics*. 25:1189–1191. doi:10.1093/bioinformatics/btp033.

Webb, B., and A. Sali. 2014. Comparative Protein Structure Modeling Using MODELLER. *Curr Protoc Bioinformatics*. 47:5.6.1–32. doi:10.1002/0471250953.bi0506s47.

Weber-Boyvat, M., H. Kentala, J. Peränen, and V.M. Olkkonen. 2015. Ligand-dependent localization and function of ORP-VAP complexes at membrane contact sites. *Cell. Mol. Life Sci.* 72:1967–1987. doi:10.1007/s00018-014-1786-x.

Welscher, te, Y.M., L. Jones, M.R. van Leeuwen, J. Dijksterhuis, B. de Kruijff, G. Eitzen, and E. Breukink. 2010. Natamycin Inhibits Vacuole Fusion at the Priming Phase via a Specific Interaction with Ergosterol. *Antimicrobial Agents and Chemotherapy*. 54:2618–2625. doi:10.1128/AAC.01794-09.

Wenk, M.R. 2010. Lipidomics: new tools and applications. *Cell*. 143:888–895. doi:10.1016/j.cell.2010.11.033.

West, M., N. Zurek, A. Hoenger, and G.K. Voeltz. 2011. A 3D analysis of yeast ER structure reveals how ER domains are organized by membrane curvature. *The Journal of Cell Biology*. 193:333–346. doi:10.1083/jcb.201011039.

Wilcox, L.J., D.A. Balderes, B. Wharton, A.H. Tinkelenberg, G. Rao, and S.L. Sturley. 2002. Transcriptional profiling identifies two members of the ATP-binding cassette transporter superfamily required for sterol uptake in yeast. *J. Biol. Chem.* 277:32466–32472. doi:10.1074/jbc.M204707200.

Wilson, D.W., C.A. Wilcox, G.C. Flynn, E. Chen, W.J. Kuang, W.J. Henzel, M.R. Block, A. Ullrich, and J.E. Rothman. 1989. A fusion protein required for vesicle-mediated transport in both mammalian cells and yeast. *Nature*. 339:355–359. doi:10.1038/339355a0.

Wirtz, K.W., and D.B. Zilversmit. 1968. Exchange of phospholipids between liver mitochondria and microsomes in vitro. *J. Biol. Chem.* 243:3596–3602.

Wolf, W., A. Kilic, B. Schrul, H. Lorenz, B. Schwappach, and M. Seedorf. 2012. Yeast Ist2 recruits the endoplasmic reticulum to the plasma membrane and creates a ribosome-free membrane microcompartment. *PLoS ONE*. 7:e39703. doi:10.1371/journal.pone.0039703.

Wong, L.H., and T.P. Levine. 2016. Lipid transfer proteins do their thing anchored at membrane contact sites… but what is their thing? *Biochem. Soc. Trans.* 44:517–527. doi:10.1042/BST20150275.

Woo, J.S., S. Srikanth, M. Nishi, P. Ping, H. Takeshima, and Y. Gwack. 2016. Junctophilin-4, a component of the endoplasmic reticulum-plasma membrane junctions, regulates Ca2+ dynamics in T cells. *Proc. Natl. Acad. Sci. U.S.A.* 113:2762–2767. doi:10.1073/pnas.1524229113.

Wu, C.-H., S.-C. Lee, and C.-W. Wang. 2011. Viral protein targeting to the cortical endoplasmic reticulum is required for cell-cell spreading in plants. *The Journal of Cell Biology*. 193:521–535. doi:10.1083/jcb.201006023.

Wu, M.M., J. Buchanan, R.M. Luik, and R.S. Lewis. 2006. Ca2+ store depletion causes STIM1 to accumulate in ER regions closely associated with the plasma membrane. *The Journal of Cell Biology*. 174:803–813. doi:10.1083/jcb.200604014.

Wu, S.Y., X. Yang, K.M. Gharpure, H. Hatakeyama, M. Egli, M.H. McGuire, A.S. Nagaraja, T.M. Miyake, R. Rupaimoole, C.V. Pecot, M. Taylor, S. Pradeep, M. Sierant, C. Rodriguez-Aguayo, H.J. Choi, R.A. Previs, G.N. Armaiz-Pena, L. Huang, C. Martinez, T. Hassell, C. Ivan, V. Sehgal, R. Singhania, H.-D. Han, C. Su, J.H. Kim, H.J. Dalton, C. Kovvali, K. Keyomarsi, N.A.J. McMillan, W.W. Overwijk, J. Liu, J.-S. Lee, K.A. Baggerly, G. Lopez-Berestein, P.T. Ram, B. Nawrot, and A.K. Sood. 2014. 2'-OMe-phosphorodithioate-modified siRNAs show increased loading into the RISC complex and enhanced anti-tumour activity. *Nat Commun*. 5:3459. doi:10.1038/ncomms4459.

Wüthrich, K., G. Wider, G. Wagner, and W. Braun. 1982. Sequential resonance assignments as a basis for determination of spatial protein structures by high resolution proton nuclear magnetic resonance. *J. Mol. Biol.* 155:311–319.

Xu, S., B. Benoff, H.-L. Liou, P. Lobel, and A.M. Stock. 2007. Structural basis of sterol binding by NPC2, a lysosomal protein deficient in Niemann-Pick type C2 disease. *J. Biol. Chem.* 282:23525–23531. doi:10.1074/jbc.M703848200.

Xu, W., J. Wang, J.E. Rothman, and F. Pincet. 2015. Accelerating SNARE-Mediated Membrane Fusion by DNA-Lipid Tethers. *Angew. Chem. Int. Ed. Engl.* 54:14388–14392. doi:10.1002/anie.201506844.

Yadav, S., K. Garner, P. Georgiev, M. Li, E. Gomez-Espinosa, A. Panda, S. Mathre, H. Okkenhaug, S. Cockcroft, and P. Raghu. 2015. RDGBα, a PtdIns-PtdOH transfer protein, regulates G-protein-coupled PtdIns(4,5)P2 signalling during Drosophila phototransduction. *Journal of Cell Science*. 128:3330–3344. doi:10.1242/jcs.173476.

Yan, R., D. Xu, J. Yang, S. Walker, and Y. Zhang. 2013. A comparative assessment and analysis of 20 representative sequence alignment methods for protein structure prediction. *Sci Rep*. 3:2619. doi:10.1038/srep02619.

Yeung, T., G.E. Gilbert, J. Shi, J. Silvius, A. Kapus, and S. Grinstein. 2008. Membrane phosphatidylserine regulates surface charge and protein localization. *Science*. 319:210–213. doi:10.1126/science.1152066.

Yona, G., and M. Levitt. 2002. Within the twilight zone: a sensitive profile-profile comparison tool based on information theory. *J. Mol. Biol.* 315:1257–1275. doi:10.1006/jmbi.2001.5293.

Yoo, J.-S., B.D. Moyer, S. Bannykh, H.-M. Yoo, J.R. Riordan, and W.E. Balch. 2002. Non-conventional trafficking of the cystic fibrosis transmembrane conductance regulator through the early secretory pathway. *J. Biol. Chem.* 277:11401–11409. doi:10.1074/jbc.M110263200.

Young, B.P., J.J.H. Shin, R. Orij, J.T. Chao, S.C. Li, X.L. Guan, A. Khong, E. Jan, M.R. Wenk, W.A. Prinz, G.J. Smits, and C.J.R. Loewen. 2010. Phosphatidic acid is a pH biosensor that links membrane biogenesis to metabolism. *Science*. 329:1085–1088. doi:10.1126/science.1191026.

Yu, H., Y. Liu, D.R. Gulbranson, A. Paine, S.S. Rathore, and J. Shen. 2016. Extended synaptotagmins are Ca2+-dependent lipid transfer proteins at membrane contact sites. *Proc. Natl. Acad. Sci. U.S.A.* 201517259. doi:10.1073/pnas.1517259113.

Yu, J.W., J.M. Mendrola, A. Audhya, S. Singh, D. Keleti, D.B. DeWald, D. Murray, S.D. Emr, and M.A. Lemmon. 2004. Genome-wide analysis of membrane targeting by S. cerevisiae pleckstrin homology domains. *Molecular Cell*. 13:677–688.

Zaman, S., S.I. Lippman, X. Zhao, and J.R. Broach. 2008. How Saccharomyces responds to nutrients. *Annu. Rev. Genet.* 42:27–81. doi:10.1146/annurev.genet.41.110306.130206.

Zhou, Y., P. Srinivasan, S. Razavi, S. Seymour, P. Meraner, A. Gudlur, P.B. Stathopulos, M. Ikura, A. Rao, and P.G. Hogan. 2013. Initial activation of STIM1, the regulator of store-operated calcium entry. *Nat Struct Mol Biol*. 20:973–981. doi:10.1038/nsmb.2625.